AGE AND ORIGIN OF THE TURNAGAIN ALASKAN-TYPE INTRUSION AND ASSOCIATED NI-SULPHIDE MINERALIZATION, NORTH-CENTRAL BRITISH COLUMBIA, CANADA

by

J. ERIK SCHEEL

B.Sc.H. University of Alberta, 2004

A THESIS SUBMITTED FOR PARTIAL FULFILMENT

OF THE REQUIREMENTS FOR THE DEGREE OF

MASTER OF SCIENCE

in

THE FACULTY OF GRADUATE STUDIES

(GEOLOGICAL SCIENCES)

THE UNIVERSITY OF BRITISH COLUMBIA

May 2007

© J. Erik Scheel, 2007

ABSTRACT

The Turnagain Alaskan-type intrusion in north-central British Columbia consists of ultramafic to dioritic rocks and contains significant magmatic sulphide mineralization. The age of the intrusion is constrained by U-Pb and Ar-Ar geochronology to be 190±1 Ma and the minimum depositional age of the youngest host rocks (volcanic wacke) is 301 Ma. Whole rock Nd isotopic compositions are characteristic of Paleozoic arc-derived mafic rocks in the northern Canadian Cordillera ($\varepsilon_{Nd(190)}$ = +4 to +6), but indicative of variable crustal contamination in some samples ($\varepsilon_{Nd(190)}$ = +2 down to -3.3). The age and tectonic characteristics of the Turnagain intrusion and its host rocks constrain the terrane it intrudes to be either Yukon-Tanana or Quesnellia, but not Ancestral North America. The Turnagain parent magmas were hydrous, arc-derived, in equilibrium with mantle peridotite, and ankaramitic. Cross-cutting and geochemical relationships define the crystallization and emplacement sequence of the Turnagain intrusion to be: dunite (~Fo_{91}) → wehrlite (~Fo_{87}) → olivine clinopyroxenite (~Fo_{85}, $Mg\#_{cpx}$ = 0.92) → hornblende clinopyroxenite ($Mg\#_{cpx}$ = 0.81, $Mg\#_{hbl}$ = 0.65) → hornblendite ($Mg\#_{hbl}$ = 0.60) → diorite. Mineral and whole-rock geochemistry indicate that all ultramafic lithologies are genetically related and relative depletion in the HFSE, specifically Nb and Ta, are consistent with an arc mantle source for the parent magmas. Variations in spinel chemistry in the Turnagain intrusion are mainly a function of post-crystallization re-equilibration and oxidation. Primary (unmodified) chromite compositions, observed in chromitite samples, are Cr-rich (Cr/(Cr+Al) = 0.86-0.90) and Fe^{3+}-poor ($Fe^{3+}/(Fe^{3+}+Cr+Al)<0.1$), indicating their crystallization from a magma with relatively low fO_2 ($\Delta FMQ < 0$), which is substantially lower than for other Alaskan-type intrusions. At these relatively reduced conditions, S was dissolved as sulphide (S^{2-}) rather than sulphate (SO_4^{2-}). Sulphur ($\delta^{34}S$ = -9.7 to +1.4‰) and lead isotopic compositions of sulphide from the ultramafic rocks indicate that upper crustal sulphur and lead were added to the parent magmas by assimilation of graphitic, pyritic metasedimentary inclusions ($\delta^{34}S$ = -17.9‰), which are found only in the sulphide-mineralized zones. Thus, addition of crustal carbon and sulphur reduced the Turnagain magmas and increased total S, which lead to early sulphide saturation.

TABLE OF CONTENTS

ABSTRACT ii
TABLE OF CONTENTS iii
LIST OF TABLES vi
LIST OF FIGURES vii
LIST OF APPENDICES ix
ACKNOWLEDGEMENTS x

CHAPTER 1: GEOLOGICAL CONTEXT AND EXPLORATION HISTORY OF THE TURNAGAIN ALASKAN-TYPE INTRUSION, NORTH-CENTRAL BRITISH COLUMBIA 1

1.1 INTRODUCTION 2
1.2 EXPLORATION HISTORY OF THE TURNAGAIN INTRUSION 5
1.3 OVERVIEW OF THE THESIS 6
1.4 REFERENCES 9

CHAPTER 2: GEOCHRONOLOGY OF THE TURNAGAIN ALASKAN-TYPE INTRUSION, NORTH-CENTRAL BRITISH COLUMBIA, WITH IMPLICATIONS FOR THE TECTONIC EVOLUTION OF THE NORTHERN CANADIAN CORDILLERA 12

2.1 INTRODUCTION 13
2.2 GEOLOGICAL SETTING OF THE TURNAGAIN INTRUSION 14
2.3 GEOLOGY OF THE TURNAGAIN INTRUSION 19
2.4 SAMPLE DESCRIPTIONS AND ANALYTICAL TECHNIQUES 21
2.4.1 U-Pb zircon/titanite 21
2.4.2 Ar-Ar phlogopite/amphibole 24
2.4.3 Neodymium isotopes 25
2.5 RESULTS 26
2.5.1 U-Pb geochronology 26
2.5.1.1 Mela-diorite 26
2.5.1.2 Leuco-diorite 27
2.5.1.3 Volcanic wacke 30
2.5.1.4 Hornblendite 30
2.5.2 Ar-Ar geochronology 32
2.5.2.1 Hornblendite 32
2.5.2.2 Wehrlite 32
2.5.3 Rare earth elements and Nd isotopes 36
2.6 DISCUSSION 36
2.6.1 Age and source of the Turnagain intrusion 36

2.6.2 Age comparison with other Alaskan-type intrusions 43
2.6.3 Tectonic implications for northern British Columbia 47
2.7 CONCLUSION 49
2.8 ACKNOWLEDGEMENTS 50
2.9 REFERENCES 51

CHAPTER 3: CHROMITE CHEMISTRY OF THE TURNAGAIN INTRUSION, NORTHERN BRITISH COLUMBIA, AND THE REDOX STATES OF ALASKAN-TYPE PARENTAL MAGMAS 58

3.1 INTRODUCTION 59
3.2 REGIONAL GEOLOGY 60
3.3 GEOLOGY AND SPINEL CONTENT OF THE TURNAGAIN INTRUSION 60
3.3.1 Dunite 62
3.3.2 Wehrlite 65
3.3.3 Olivine clinopyroxenite 65
3.3.4 Hornblende clinopyroxenite and hornblendite 67
3.4 ANALYTICAL TECHNIQUES 67
3.5 RESULTS 69
3.5.1 Chromitite 72
3.5.2 Dunite 72
3.5.3 Wehrlite 72
3.5.4 Olivine clinopyroxenite 75
3.4.1 Hornblende clinopyroxenite 75
3.6 DISCUSSION 77
3.6.1 Primary spinel compositions 77
3.6.2 Reequilibration trends 79
3.6.3 Compositional effects of serpentinization on spinel chemistry 80
3.6.4 Implications for the redox state of the Turnagain intrusion 80
3.7 CONCLUSIONS 83
3.8 ACKNOWLEDGEMENTS 84
3.9 REFERENCES 85

CHAPTER 4: PETROLOGY AND METALLOGENY OF TURNAGAIN ALASKAN-TYPE INTRUSION AND ITS ASSOCIATED NI-SULPHIDE MINERALIZATION 89

4.1 INTRODUCTION 90
4.2 GEOLOGY OF THE TURNAGAIN INTRUSION 91
4.2.1 Regional geology 91
4.2.2 Ultramafic rocks 94
4.2.2.1 Dunite and chromitite 94
4.2.2.2 Wehrlite 99

4.2.2.3 Olivine clinopyroxenite and clinopyroxenite 100
4.2.2.4 Hornblende clinopyroxenite 101
4.2.2.5 Hornblendite 102
4.2.3 Other rocks 102
4.2.3.1 Diorite 102
4.2.3.2 Hornfels 103
4.2.4 Sulphide 103
4.2.5 Inclusions 106

4.3 ANALYTICAL TECHNIQUES 107

4.3.1 Mineral chemistry 107
4.3.2 Major and trace elements 110
4.3.3 Platinum group elements 118
4.3.4 Sulphur isotopes - sulphide 121
4.3.5 Lead isotopes - sulphide 121

4.4 RESULTS 125

4.4.1 Olivine chemistry 125
4.4.2 Clinopyroxene chemistry 127
4.4.3 Amphibole and biotite chemistry 127
4.4.4 Major and trace element chemistry 129
4.4.4.1 High-Mg olivine-rich rocks 129
4.4.4.2 Intermediate-Mg clinopyroxene-rich rocks 133
4.4.4.3 Hornblendites 133
4.4.4.4 Dioritic rocks 134
4.4.5 Platinum group elements 134
4.4.6 Sulphur isotopic compositions 137
4.4.7 Lead isotopic compositions 137

4.5 DISCUSSION 137

4.5.1 Parent magma characteristics 137
4.5.2 Sequence of crystallization 140
4.5.3 Implications for associated volcanic rocks 141
4.5.4 Origin of sulphide mineralization in the Turnagain intrusion 142
4.5.5 Petrogenesis the Turnagain intrusion and associated Ni-sulphide mineralization 144

4.6 CONCLUSIONS 145

4.7 ACKNOWLEDGEMENTS 147

4.8 REFERENCES 148

CHAPTER 5: SUMMARY AND CONCLUSIONS 153

5.1 SUMMARY AND CONCLUSIONS 154

5.2 REFERENCES 157

LIST OF TABLES

Table 2.1: U-Pb TIMS analytical data from zircon and titanite grains separated from samples from the Turnagain intrusion 28

Table 2.2: $^{40}Ar/^{39}Ar$ step-heating results of mineral separates from ultramafic rocks of the Turnagain intrusion 34

Table 2.3: Major (wt. % oxide) and trace element abundances (ppm) in whole rock samples from the Turnagain intrusion 37

Table 2.4: Nd isotopic compositions of whole rock samples from the Turnagain intrusion 39

Table 2.5: Ages of Alaskan-type intrusions in B.C. and Alaska 44

Table 3.1: Representative spinel compositions from spinel-bearing ultramafic rocks of the Turnagain intrusion 70

Table 4.1: Representative olivine compositions from olivine-bearing ultramafic lithologies in the Turnagain intrusion 111

Table 4.2: Representative clinopyroxene compositions from clinopyroxene-bearing ultramafic lithologies in the Turnagain intrusion 113

Table 4.3: Amphibole compositions from ultramafic rocks of the Turnagain intrusion 115

Table 4.4: Biotite compositions from biotite-bearing ultramafic lithologies in the Turnagain intrusion... 117

Table 4.5: Major (wt. % oxide) trace element abundances (ppm) in mafic-ultramafic rocks of the Turnagain intrusion 119

Table 4.6: PGE concentrations of representative ultramafic rocks from the Turnagain intrusion 122

Table 4.7: Sulphur isotopic compositions of sulphide from the Turnagain intrusion and surrounding lithologies 123

Table 4.8: Pb isotopic compositions of selected sulphide fractions from the Turnagain intrusion and surrounding lithologies 124

LIST OF FIGURES

Figure 1.1: Simplified geological map of the Turnagain Alaskan-type intrusion, modified from Clark (1975) 3

Figure 2.1: Terrane map of British Columbia, modified from Colpron & Nelson (2004) 15

Figure 2.2: Regional geological map of the area immediately surrounding the Turnagain intrusion, extracted and modified from Massey et al. (2005) 16

Figure 2.3: Geologic map of the Turnagain intrusion 18

Figure 2.4: Photomicrographs of zircon and titanite separates from the Turnagain intrusion 22

Figure 2.5: Concordia plots for U-Pb data from analyzed zircon fractions for diorite samples from the Turnagain intrusion 29

Figure 2.6: Concordia plots for U-Pb data from analyzed zircon fractions from a volcanic wacke sample from the Turnagain intrusion (04ES-00-07-02) 31

Figure 2.7: Concordia plots for U-Pb data from analyzed titanite fractions separated from a hornblendite dike (04ES-00-07-04) in the northwestern region of the Turnagain intrusion. 33

Figure 2.8: $^{40}Ar/^{39}Ar$ incremental-heating age spectra and $^{40}Ar/^{39}Ar$ inverse isochron diagrams for mineral separates from the Turnagain intrusion. 35

Figure 2.9: Chondrite-normalized rare earth element diagram for whole rock samples from the Turnagain intrusion, and whole rock samples from Erdmer *et al.* (2005) 38

Figure 2.10: Nd isotopic geochemistry of whole rock samples from the Turnagain intrusion 40

Figure 2.11: Ages of Alaskan-type intrusions in B.C. and Alaska 45

Figure 3.1: Simplified geological map of the Turnagain Alaskan-type intrusion 61

Figure 3.2: Photographs of chromitite in outcrop from the Turnagain intrusion 63

Figure 3.3. Photomicrographs of chromite textures from chromitite and dunite 64

Figure 3.4: Photomicrographs of chromite textures from wehrlite and olivine clinopyroxenite in the Turnagain intrusion 66

Figure 3.5: Photomicrographs of magnetite textures from sample DDH04-47-7-49, a hornblende clinopyroxenite from the western zone of the Turnagain intrusion 68

Figure 3.6: Chromite compositional ternary diagrams, represented by sample number 73

Figure 3.7: Binary plots of spinel compositions from the Turnagain intrusion. A) divalent vs. trivalent cation plot. B) Fe# vs. Cr/Cr+Al. 74

Figure 3.8: Binary plots of spinel compositions from the Turnagain intrusion. A) $Fe^{3+}/(Fe^{3+}+Cr+Al)$ vs. TiO_2. B) Ti vs. V. 76

Figure 3.9: Expanded trivalent cation (Fe^{3+}-Cr-Al) plot of Turnagain spinel compositions, focusing on those compositions nearest end-member chromite 78

Figure 3.10: Expanded trivalent cation (Fe^{3+}-Cr-Al) plot of Turnagain spinel compositions with the data density maxima for other Alaskan-type intrusions from Barnes & Roeder (2001) 82

Figure 4.1: Geological map of the Turnagain intrusion showing sample locations chosen for whole rock geochemistry and sulphide sulphur and lead isotopic compositions 92

Figure 4.2: Photographs of dunite exposures in the Turnagain intrusion 93

Figure 4.3a: Photographs of outcrop-scale features from olivine cumulate lithologies in the Turnagain intrusion. 95

Figure 4.3b: Photographs of outcrop-scale features in olivine-clinopyroxene cumulate lithologies in the Turnagain intrusion. 96

Figure 4.4a: Photomicrographs (transmitted light, crossed-polars) of silicate mineral textures in the Turnagain intrusion from dunite and wehrlite 97

Figure 4.4b: Photomicrographs (transmitted light, crossed-polars) of silicate mineral textures in the Turnagain intrusion from olivine clinopyroxenite, hornblendite, and diorite 98

Figure 4.5: Photomicrographs of sulphide textures in the Turnagain intrusion 105

Figure 4.6: Photographs of sedimentary xenoliths in NQ size drillcore from the Turnagain intrusion 108

Figure 4.7: Olivine mineral chemistry 126

Figure 4.8: Clinopyroxene mineral chemistry 128

Figure 4.9: Select major element oxides and Mg# vs. MgO for whole rock samples and mineral analyses from the Turnagain intrusion 130

Figure 4.10: Compatible trace element geochemistry vs. MgO 131

Figure 4.11: Chondrite-normalized rare earth element diagrams for whole rocks from the Turnagain intrusion and whole rock samples from Erdmer *et al.* (2006) 132

Figure 4.12: PGE compositional variations for whole rocks from the Turnagain intrusion 135

Figure 4.13: Primitive-mantle normalized platinum group element diagrams for whole rocks from the Turnagain intrusion 136

Figure 4.14: Sulphur isotopic composition of sulphide vs. lithology in the Turnagain intrusion 138

Figure 4.15: Lead isotopic compositions ($^{206}Pb/^{204}Pb$ vs. $^{207}Pb/^{204}Pb$) of sulphide from the Turnagain intrusion 139

Figure 4.16: The effects of oxygen fugacity on sulphur speciation and saturation, after Jugo *et al.* (2004; 2005) 143

LIST OF APPENDICES

Appendix I: Spinel compositions from spinel-bearing ultramafic rocks of the Turnagain intrusion 160

Appendix II: Olivine compositions from olivine-bearing ultramafic rocks of the Turnagain intrusion 179

Appendix III: Clinopyroxene compositions from clinopyroxene-bearing ultramafic lithologies of the Turnagain intrusion 189

Appendix IV: Garnet compositions from a serpentine vein in dunite from the Turnagain intrusion 195

Appendix V: List of X-ray lines and mineral standards for EPMA 196

Appendix VI: Blind duplicate analyses from whole-rock geochemical samples 198

Appendix VII: Clinopyroxene compositions from clinopyroxene-bearing ultramafic lithologies of the Turnagain intrusion 200

ACKNOWLEDGEMENTS

There are many people who have contributed in some part to the development and completion of this thesis. I would never have written this thesis without the advice and support of my supervisors James Scoates and Graham Nixon, who have taught me so much since I first arrived at UBC. James was always willing to answer questions that I had about everything thesis-related or otherwise, regardless of his own workload. James also spent significant amounts of time editing various draft sections of this thesis, and for that I am extremely grateful. Graham introduced me to the Turnagain property and imparted his experiences of working on Alaskan-type intrusions on me with skill and precision. He must also be thanked for helping me set-up necessary field gear, maps, air photographs, and lodging when I visited him in Victoria. Rich Friedman, Janet Gabites, Bruno Kieffer, Thomas Ullrich, and Mati Raudsepp are thanked for their analytical work and advice during the research phase of this thesis. Also Rich Friedman, Dominique Weis, and Jim Mortensen of the PCIGR are thanked for consultations during data interpretation and the implications thereof. I also thank Andrew Greene, Caroline Emmanuelle-Morisset, and Robin Mackie for sharing their thoughts on ultramafic rocks with me.

Hard Creek Nickel Corporation, its president Mark Jarvis, and its past and present employees Tony Hitchins, Chris Baldys, Bruce Northcote, and Leslie Young are all thanked for the ideas, support, and seasonal employment during the duration of this thesis as well as for funding the research project. Other past and present Hard Creek Nickel employees, including Jeff Kyba, Tyler Kuhn, Mark Greenhalgh, and Greg Ross, must also be thanked for making summer work a great experience. Jim and Sharon Reed at Pacific Western Helicopters must be thanked for transport during the numerous summers spent in the Turnagain camp. Thanks to John Schussler, the first driller on the Turnagain property and former owner of DJ Drilling, for lodging in Boulder City in 2004 and 2005.

Finally, I like to thank my family for their help and support during the last 7 years of my academic career. I would like to thank Tom Chacko, Bob Luth, Larry Heaman, Sarah Gleeson, and Jeremy Richards at the University of Alberta for helping me find my calling in geology, and for making the undergraduate program there one of the best in the continent. Many thanks to all my friends at UBC and in Vancouver, because without them I would not have made it this far.

CHAPTER 1

GEOLOGICAL CONTEXT AND EXPLORATION HISTORY OF THE TURNAGAIN ALASKAN-TYPE INTRUSION, NORTH-CENTRAL BRITISH COLUMBIA

1.1 INTRODUCTION

This study focuses on the Turnagain Alaskan-type mafic-ultramafic intrusion, which is located 70 km east of Dease Lake, British Columbia, Canada. The Turnagain intrusion is a 24 km^2 pluton that is dominantly composed of ultramafic cumulate rocks and minor dioritic phases and that contains appreciable nickeliferrous sulphide mineralization (Figure 1.1). Globally, Alaskan-type intrusions are characteristically sulphide-poor and no other intrusion found to date contains significant concentrations of magmatic Ni-bearing sulphide. The main goal of this thesis is to assess the origin and petrogenesis of the Turnagain intrusion and to constrain the mechamism of sulphide mineralization by combined field mapping and drillcore logging, geochemistry (mineral chemistry, major and trace elements, Nd-S-Pb isotopes) and geochronology (U-Pb, Ar-Ar).

The Turnagain intrusion is situated within greenschist facies metasedimentary rocks currently assigned to the Ancestral North American miogeocline (Gabrielse, 1998). The intrusion is entirely fault-bounded on all margins, and is situated 1.5 km northeast of the Kutcho Fault, which is a major tectonic structure separating the miogeocline to the east from felsic plutons and mafic volcanics of the Quesnel accreted terrane to the west. The term "Alaskan-type," synonymous with "Uralian-type", "Uralian-Alaskan-type", and "zoned ultramafic", was first used by Taylor & Noble (1960) and Noble & Taylor (1960) and originally referred to mafic-ultramafic intrusions found in the Alaskan Panhandle and in the Ural Mountains, Russia (e.g. Duke Island, Irvine, 1962; Nizhnii-Tagil, Krause *et al.*, 2006). These two belts, along with other occurrences of Alaskan-type intrusions, are typically found in paleo-arc environments. The subduction zone or arc setting of these intrusions has been qualified in a large number of studies (e.g. Irvine, 1974; Tistl *et al.*, 1994; Green *et al.*, 2004; Batanova *et al.*, 2005) by association with other arc rocks, mineralogy, and geochemistry. Despite the fact that many more of these bodies have been found throughout the world, the term "Alaskan-type" is still retained. "Zoned ultramafic" refers to the observation that many of these intrusions are zoned from the core outwards, from more mafic (or ultramafic) to less mafic rocks. This zonation can be perfectly concentric, or completely absent, and is a common, although not a diagnostic, trait of Alaskan-type intrusions. It has long been known that Alaskan-type intrusions can be spatially associated with basaltic volcanic rocks (Findlay, 1969; Irvine, 1974), and a genetic link between Alaskan-type intrusions and arc-derived ankaramitic/picritic magmas and lavas has recently been established (Mossman *et al.*, 2000).

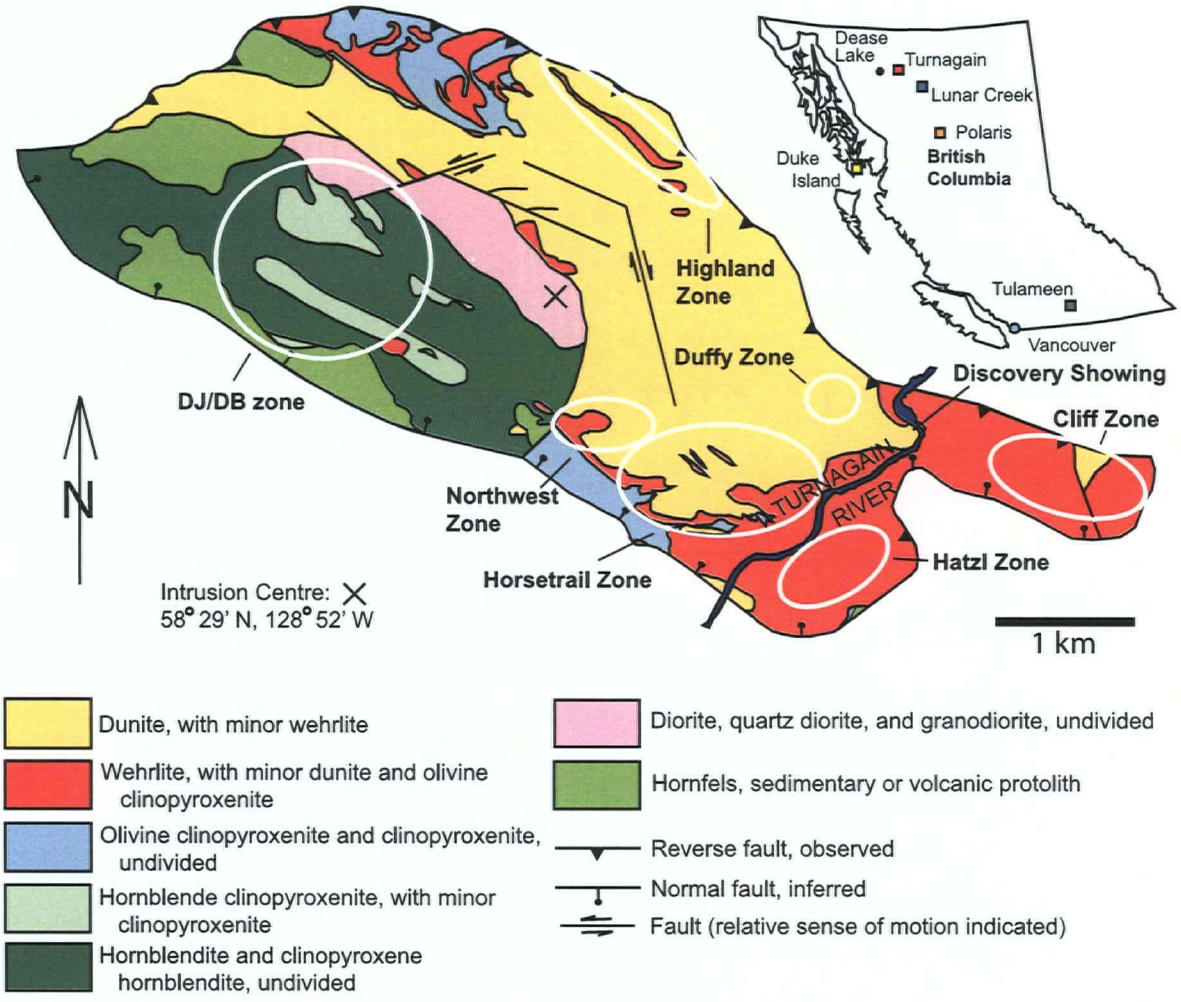

Figure 1.1: Simplified geological map of the Turnagain Alaskan-type intrusion, with its location in British Columbia shown as an inset in the upper right corner (also indicated are the locations of other major Alaskan-type intrusions in B.C. and Alaska), modified from Clark (1975). The lithologies of the intrusion are shown in the legend; some units are composites (e.g. olivine clinopyroxenite and clinopyroxenite). The intrusion is entirely fault-bounded, and the large area of hornblende-rich lithologies with associated felsic rocks in the west is mostly interpreted from both airborne and ground geophysics, as well as information from drill holes. Major mineralized zones are indicated with white ovals, as is the Discovery Showing. The DJ/DB zone is a hydrothermal Pt-Pd zone, whereas all other zones contain Ni-sulphide mineralization.

Arc-derived ankaramites are composed of olivine- and clinopyroxene-porphyritic basalt containing groundmass amphibole and plagioclase. Ankaramite dikes, typically found cross-cutting certain Alaskan-type intrusions (e.g. Greenhills, Spandler *et al.*, 2003), are commonly zoned from the interior to the margin, suggesting that the observed zonation in Alaskan-type intrusions may be the result of common petrogenetic processes. The mineralogy and crystallization sequence of ankaramite and Alaskan-type intrusions is also nearly identical and the chemical signatures of both rock types indicates their common origin from the mantle (e.g. Green *et al.*, 2004).

The defining characteristic of Alaskan-type intrusions is their mineralogy. Their typical order of crystallization is olivine+chromite → diopside → magnetite → hornblende+calcic plagioclase. Chromite is an early (high temperature) crystallizing phase in Alaskan-type intrusions and typically ceases to crystallize shortly after clinopyroxene saturation (Irvine, 1965). In general, mafic-ultramafic intrusions rarely contain primary magmatic hornblende, but primary hornblende is a common mineral in evolved rocks within many Alaskan-type intrusions. Orthopyroxene is typically absent, save a few isolated examples (e.g. Salt Chuck, Alaska, Loney & Himmelberg, 1992; Gabbro Akarem, Egypt, Helmy & El Mahalawi, 2003), indicating that the parental magmas to these bodies were silica-undersaturated (Irvine, 1965). Plagioclase is generally absent as an early cumulus phase, and crystallizes after clinopyroxene or hornblende. The suppression of early plagioclase crystallization is due to the relatively high water contents of the magmas as elevated water contents in silicate magmas are known to suppress the crystallization of plagioclase to low temperatures (e.g. Irvine, 1965; Gaetani *et al.*, 1993). The presence of small amounts of primary phlogopite in the most ultramafic parts of intrusions is also a diagnostic feature, and may reflect the alkaline to subalkaline chemical characteristics of primitive Alaskan-type magmas (Findlay, 1969; Irvine, 1974; Nixon *et al.*, 1997).

Many intrusions have lode and associated placer Pt (± Pd) mineral deposits (e.g. Tulameen, B.C., Findlay, 1969; Alto Condoto, Columbia, Tistl, 1994; Nizhnii Tagil, Russia, Johan, 2002) and they are commonly explored for platinum-group metals (PGM). The majority of these PGM are found in chromitite as Pt_3Fe (isoferroplatinum) (e.g. Nixon *et al.*, 1990; Johan *et al.*, 2000), however there are also occurrences of Os-Ir alloys (e.g. Garuti *et al.*, 2003) and possible alloys, such as Pt_2CuFe (tulameenite, Nixon *et al.*, 1990), of hydrothermal origin. Two Alaskan-type intrusions contain significant sulphide (Salt Chuck and Turnagain),

each with a distinctive sulphide mineralogy and lithologic association. The Salt Chuck intrusion contains Pd-rich, bornite-bearing clinopyroxenite and gabbro (Loney & Himmelberg, 1992). In contrast, the Turnagain intrusion contains disseminated to semi-massive pyrrhotite and pentlandite with minor secondary phases, but also contains a late-stage, hydrothermal Pt-Pd zone associated with a Cu soil geochemical anomaly (Figure 1.1).

Thirty-five of the 39 known Alaskan-type intrusions (e.g. Duke Island; Irvine, 1962) in southeastern Alaska occur in a 560 km long by 50 km wide belt (Taylor, 1967). The other four occurrences (e.g. Salt Chuck; Loney *et al.*, 1987) are to the west of this belt, are older, and have different petrological characteristics (e.g. more plagioclase, trace orthopyroxene). Similar large belts occur in the Ural Mountains (15 large bodies; Taylor, 1967; Krause, 2006), which is approximately 1000 km long and 60 km wide; the Kamchatka Peninsula, Far East Russia (Batanova *et al.*, 2005; and references therein), which contains over 20 Alaskan-type intrusions; and British Columbia, which has 9 known occurrences (e.g. Tulameen; Findlay, 1969; Turnagain; Clark, 1980; Nixon *et al.*, 1997). Alaskan-type intrusions in Columbia and Ecuador (Tistl, 1994; Tistl *et al.*, 1994) may belong to a larger belt that currently remains unconstrained and relatively unexplored. A tectonically dismembered belt that existed prior to the Miocene opening of the Sea of Japan has been proposed to link Alaskan-type intrusions in Japan, northeastern China, and Far East Russia (Ishiwatari & Ichiyama, 2004). There are also a number of other Alaskan-type intrusions that occur as either single intrusions (e.g. Papua New Guinea; Johan *et al.*, 2000; Greenhills; Mossman *et al.*, 2000) or as small groups of intrusions (e.g. Fifield, Australia; Johan, 2002).

1.2 EXPLORATION HISTORY OF THE TURNAGAIN INTRUSION

Sulphide mineralization in the Turnagain intrusion was discovered along the banks of the Turnagain River ca. 1956, and this semi-massive sulphide showing has henceforth been called the Discovery showing (Figure 1.1). Falconbridge Nickel Mines Ltd., interested in the nickel potential of the semi-massive sulphide, owned and explored the Turnagain property between 1966 and 1973 and drilled the major sulphide showings (Northwest, Horsetrail, Fishing Rock, Discovery, Hatzl; Figure 1) with small, portable "packsack" drills. Airborne magnetic surveys were also flown across the entire intrusion. A Ph.D. thesis on the geology and petrography of the intrusion was completed by Tom Clark in 1975 at Queens University (Clark, 1975), followed by several publications derived from the thesis (Clark, 1978; Clark,

1980). Interest in the platinum-group element (PGE) potential of Alaskan-type intrusions in British Columbia during the 1980s resulted in significant government survey mapping and associated geochemical studies (especially PGE) of these intrusions across the province (Nixon *et al.*, 1989; 1990; 1997).

Interest in the nickel potential of the intrusion was renewed when Bren-Mar Ltd. acquired the property in 1996 (Bren-Mar Ltd. became Canadian Metals Exploration Ltd. in 2002, and then became Hard Creek Nickel Corp. in 2004). Contour-defined and grid soil sampling was conducted over the entire intrusion to constrain existing nickel targets and to find covered targets (the intrusion is only ~30% exposed). A zone of hydrothermal Pt-Pd-Cu mineralization was discovered as a result of extensive soil sampling in the summer of 2004. Sulphide mineralogical and chemical studies have been carried out by Dr. Harry Kucha at the University of Krakow, Poland (Hard Creek Nickel internal reports), and are ongoing. Recent air photographs, and airborne and ground geophysics (magnetic, electromagnetic), were acquired in late 2005. To date, Hard Creek Nickel Corp. has drilled ~50 km of BQ and NQ drillcore in ~170 holes, and has outlined a Ni resource of 429 Mt (measured and indicated) containing 0.17% sulphide Ni (see http://www.hardcreeknickel.com).

The author spent 8 weeks in the summer of 2004 at the Turnagain property as part of his field work, during which time detailed mapping and sampling of outcrops within and around the Turnagain intrusion were conducted. In the summer of 2005, the author conducted two weeks of drillcore sampling from the Turnagain intrusion for sulphides of various textures and tenors, and sulphide from the wallrocks where the contact had been penetrated by drilling. The author also sampled for chromitite and whole-rock geochemical samples. For the remainder of the summer, the author was involved in the summer exploration program of Hard Creek Nickel Corp., which involved logging core and in-fill mapping. The current map of the Turnagain intrusion, based on the map of Clark (1975), was created as a joint effort by the author and Bruce Northcote (formerly of Hard Creek Nickel Corp.).

1.3 OVERVIEW OF THESIS

There are three complimentary studies on the Turnagain intrusion presented in this thesis. Prior to this study, there was no geochronological data for the Turnagain intrusion, nor were there any whole rock trace element or isotopic compositions. The main objectives of this thesis were 1) to determine the age and tectonic significance of the intrusion and its host rocks, 2) to

characterize the lithologies and magmatic evolution of the Turnagain intrusion using mineral and whole rock chemistry, and 3) to ultimately constrain the origin of the anomalous sulphide mineralization in the intrusion. Chapters 2, 3, and 4 were prepared in manuscript format for submission to appropriate scientific journals, and as such they contain some similar introductory figures and geologic backgrounds, although only information relevant to each specific study is reported in each chapter.

Chapter 2 describes the geochronology and tectonic setting of the Turnagain intrusion. The age of the intrusion is determined by the dating of four ultramafic and mafic samples using both U-Pb and Ar-Ar geochronological techniques. A fifth sample, representing the stratigraphically-highest wallrocks to the Turnagain intrusion, was also dated using detrital zircon U-Pb geochronology. The Nd isotopic compositions of eight whole rock samples were determined to help constrain the source of the Turnagain intrusion and to ascertain the relative degree of crustal contamination. Additionally, available age data from other Alaskan-type intrusions in B.C. and southeastern Alaska were compiled in an effort to constrain the temporal evolution of their respective arc systems. The results from this study place important constraints on the source of the Turnagain intrusion, terrane assessment, and the temporal evolution of the host rocks to the intrusion. Mineral separation (zircon, titanite, phlogopite, hornblende) was performed by the author, Rich Friedman, Hai Lin, and Tom Ullrich at UBC. Gwen Williams, Bruno Keiffer, and Jane Barling were responsible for aquiring the Nd isotopic compositions (sample dissolution, column chemistry, and mass spectrometry), and U-Pb and Ar-Ar goechonologic analyses were carried out by Rich Friedman and Tom Ullrich, respectively.

Chapter 3 documents the chemistry of chromite in the Turnagain intrusion with emphasis on the origin and significance of compositional variations. Spinel grains from sixteen samples were analyzed by electron microprobe (a total of 320 point analyses). From these analyses, a primary spinel composition for the Turnagain intrusion has been defined. The intrasample chemical trends present in the analyzed chromite grains are used to discriminate reequilibration with olivine, clinopyroxene, interstitial liquid, and the effects of oxidizing and serpentinizing fluids. Establishment of primary chromite compositions also provides constraints on the relative oxygen fugacity of the parental magmas, which is critical for understanding the origin of the nickeliferrous sulphide mineralization in the Turnagain

intrusion. All analytical work was carried out by the author with supervision by Mati Raudsepp.

Chapter 4 involves a detailed petrological study of the ultramafic and mafic rocks in the Turnagain intrusion based on silicate mineral chemistry, whole rock major/trace element geochemistry, platinum-group element chemistry, and sulphur and lead isotopes of sulphides. The forsterite contents of olivine confirm the primitive nature of the Turnagain parent magmas (up to $Fo_{92.5}$ in olivine that has not reequilibrated with chromitite) and the Ni contents of olivine provide a clear signal of sulphide liquid saturation during formation of some of the dunites, wehrlites, and olivine clinopyroxenites. The major element geochemistry of 23 whole rock samples was used in tandem with olivine, clinopyroxene, and amphibole mineral chemistry to constrain the chemical relationships of whole rock samples relative to their mineralogy. These results have important implications for the crystallization sequence and emplacement history of the magmas that formed the Turnagain intrusion. Trace element chemistry from the whole rock suite further constrains the genetic relationship between all lithologies present in the Turnagain intrusion and allows for recognition of an arc affinity. Twenty-seven sulphur isotopic compositions and 14 lead isotopic compositions of sulphide separates from hand samples and drillcore samples are used evaluate the extent of crustal contamination involved in sulphide saturation in the Turnagain intrusion, which is important for understanding the formation of nickeliferrous magmatic sulphide deposits in Alaskan-type intrusions. All microprobe analyses were carried out by the auther under the supervision of Mati Raudsepp at UBC. The author also produced the sulphide separates for Pb and S isotopic anaysis, and Janet Gabites at UBC processed the sulphides for chemistry and perfomed the Pb-isotopic analyses.

Finally, the appendices contain the full datasets for spinel, olivine, clinopyroxene, and garnet microprobe analyses, the X-ray lines and standards for all microprobe analyses, and the comparison between whole rock geochemical samples and respective blind duplicates. Additionally, the UTM coordinates for all samples relevant to this thesis are listed in the final appendix.

1.4 REFERENCES

Batanova, V.G., Pertsev, A.N., Kamenetsky, V.S., Ariskin, A.A., Mochalov, A.G., & Sobolev, A.V. (2005). Crustal evolution of island-arc ultramafic magma: Galmoenan pyroxenite-dunite plutonic complex, Koryak Highland (Far East Russia). *Journal of Petrology* **46**, 1345-1366

Clark, T. (1975). Geology of an ultramafic complex on the Turnagain River, northwestern British Columbia. Unpublished Ph.D. dissertation, *Queens University*, 453p

Clark, T. (1978). Oxide minerals in the Turnagain ultramafic complex, northwestern British Columbia. *Canadian Journal of Earth Sciences* **15** (12), 1893-1903

Clark, T. (1980). Petrology of the Turnagain ultramafic complex, northwestern British Columbia. *Canadian Journal of Earth Sciences* **17**, 744-757

Findlay, D.C. (1969). Origin of the Tulameen ultramafic-gabbro complex, southern British Columbia. *Canadian Journal of Earth Sciences* **6**, 399-425

Gabrielse, H. (1998). Geology of Cry Lake and Dease Lake map areas, north-central British Columbia; *Geological Survey of Canada*, Bulletin **504**, 147p

Gaetani, G.A., Grove, T.L., Bryan, W.B. (1993). The influence of water on the petrogenesis of subduction-related igneous rocks. *Nature* **365**, 332-334

Garuti, G., Pushkarew, E.V., Zaccarini, F., Cabella, R., and Anikina, E. (2003). Chromite composition and platinum-group mineral assemblage in the Uktus Uralian-Alaskan-type complex (Central Urals, Russia). *Mineralium Deposita* **38**, 312-326

Green, D.H., Schmidt, M.W., & Hibberson, W.O. (2004). Island-arc ankaramites: Primitive melts from fluxed refractory lherzolitic mantle. *Journal of Petrology* **45**, 391-403

Helmy, H.M., El Mahallawi, M.M. (2003). Gabbro Akarem mafic-ultramafic complex, Eastern Desert, Egypt: A late Precambrian analogue of Alaskan-type complexes. *Mineralogy and Petrology* **77**, 85-108

Irvine, T.N. (1962). Mineralogy and petrology of the ultramafic complex at Duke Island, S.E. Alaska. *American Mineralogist* **47**, 193

Irvine, T.N. (1965). Chromian spinel as a petrogenetic indicator. Part 1. Theory. *Canadian Journal of Earth Sciences* **2**, 648-672

Irvine, T.N. (1974). Petrology of the Duke Island ultramafic complex, southeastern Alaska. *Geological Society of America – Memoir* **138**, 240p

Ishiwatari, A., & Ichiyama, Y. (2004). Alaskan-type plutons and ultramafic lavas in Far East Russia, northeast China, and Japan. *International Geology Review* **46**, 316-331

Johan, Z., Slansky, E., & Kelly, D.A. (2000). Platinum nuggets from the Kompiam area, Enga Province, Papua New Guinea: Evidence for an Alaskan-type complex. *Mineralogy and Petrology* **68**, 159-176

Johan, Z. (2002). Alaskan-types complexes and their platinum-group element mineralization. *In*: Cabri, L.J. (ed.) *The Geology, Geochemistry, Mineralogy and Mineral Beneficiation of Platinum-Group Elements*. Canadian Institute of Mining, Metallurgy and Petroleum, Special Volume **54**, 669-719

Krause, J., Brügmann, G.E., Pushkarev, E.V. (2007). Accessory and rock forming minerals monitoring the evolution of zoned mafic-ultramafic complexes in the Central Ural Mountains. *Lithos* **95**, 19-42

Loney, R.A., Himmelberg, G.R., Shaw, N.B. (1987). Salt Chuck palladium-bearing ultramafic body, Prince of Wales Island. *U.S. Geological Survey Circular Report* **C 0998**, 126-127

Loney, R.A., Himmelberg, G.R. (1992). Petrogenesis of the Pd-rich intrusion at Salt Chuck, Prince of Wales Island: An Early Paleozoic Alaskan-type ultramafic body. *Canadian Mineralogist* **30**, 1005-1022

Mossman, D.J., Coombs, D.S., Kawachi, Y., & Reay, A. (2000). High-Mg arc ankaramitic dikes, Greenhills Complex, Southland, New Zealand. *Canadian Mineralogist* **38**, 191-216

Nixon, G.T., Ash, C.H., Connelly, J.N., Case, G. (1989). Geology and noble metal geochemistry of the Turnagain ultramafic complex, northern British Columbia. *B.C. Ministry of Energy, Mines, and Petroleum Resources*, Open File 1989-18

Nixon, G.T., Cabri, L.J., & Laflamme, J.H.G. (1990). Platinum-group-element mineralization in lode and placer deposits associated with the Tulameen Alaskan-type complex, British Columbia. *Canadian Mineralogist* **28**, 503-535

Nixon, G.T., Hammack, J.L., Ash, C.H., Cabri, L.J., Case, G., Connelly, J.N., Heaman, L.M., Laflamme, J.H.G., Nuttall, C., Paterson, W.P.E., & Wong, R.H. (1997). Geology and platinum-group-element mineralization of Alaskan-type ultramafic-mafic complexes in British Columbia. *B.C. Ministry of Employment and Investment,* Bulletin **93**, 141p

Noble, J.A., & Taylor, H.P., Jr. (1960). Correlation of the ultramafic complexes of southeastern Alaska with those of other parts of North America and the World. *21st International Geological Progress Report* **Part XIII**, 188-197

Spandler, C.J., Arculus, R.J., Eggins, S.M., Maurogenes, J.A., Price, R.C., & Reay, A.J. (2003). Petrogenesis of the Greenhills Complex, Southland, New Zealand: Magmatic differentiation and cumulate formation at the roots of a Permian island-arc volcano. *Contributions to Mineralogy and Petrology* **144**, 703-721

Taylor, H.P., Jr., & Noble, J.A. (1960). Origin of the ultramafic complexes in southeastern Alaska. *21st International Geological Progress Report* **Part XIII**, 175-187

Taylor, H.P., Jr. (1967). The zoned ultramafic complexes of southeastern Alaska. *In*: Wyllie, P.J. (ed.) *Ultramafic and Related Rocks.* New York: John Wiley and Sons, 97-121

Tistl, M. (1994). Geochemistry of platinum-group elements of the zoned ultramafic Alto Condoto complex, northwest Columbia. *Economic Geology* **89**, 158-167

Tistl, M., Burgath, K.P., Hoehndorf, A., Kreuzer, H., Munox, R., & Salinas, R. (1994). Origin and emplacement of Tertiary ultramafic complexes in northwest Columbia: Evidence from geochemistry and K-Ar, Sm-Nd, and Rb-Sr isotopes. *Earth and Planetary Science Letters* **126**, 41-59

CHAPTER 2

GEOCHRONOLOGY OF THE TURNAGAIN ALASKAN-TYPE INTRUSION, NORTH-CENTRAL BRITISH COLUMBIA, WITH IMPLICATIONS FOR THE TECTONIC EVOLUTION OF THE NORTHERN CANADIAN CORDILLERA

2.1 INTRODUCTION

Alaskan-type intrusions, synonymous with Uralian-type and zoned ultramafic intrusions (e.g. Taylor & Noble, 1960), are predominantly composed of ultramafic cumulate rocks (e.g. dunite, wehrlite, hornblendite) with minor dioritic phases. The majority of Alaskan-type intrusions occur within paleo-arcs (e.g. Quesnel terrane, B.C., Nixon *et al.*, 1997; Alexander terrane, Alaska, Himmelberg & Loney, 1995) that are island or continental in nature, and a few occur in cratonic environments (e.g. Kondyor Complex, Russia, Johan, 2002). A number of Alaskan-type intrusions have been studied with respect to their platinum-group-element potential in lode and associated placer deposits (e.g. Ural Mountains, Russia, Garuti *et al.*, 2003). In general, few precise ages of crystallization are available for Alaskan-type intrusions, which is critical for understanding their tectonic setting and proposed relationships to contemporaneous intrusive rocks or volcanic sequences.

The Turnagain intrusion, situated in north-central British Columbia, is distinct from other Alaskan-type intrusions in that it contains unusually high, and perhaps economic, concentrations of Ni-sulphide mineralization. The current resource estimate (measured and indicated) is 428 Mt grading 0.17% Ni (http://www.hardcreeknickel.com). The age and tectonic history of the Turnagain intrusion, as well as the origin of the magmas, are important for understanding the evolution of the northern Canadian Cordillera. Nixon (1998) proposed two contrasting interpretations for the tectonic setting of the Turnagain intrusion. The first interpretation is that the Turnagain intrusion was emplaced into miogeoclinal metasedimentary rocks of Ancestral North America in a subduction zone environment. The second interpretation is that the Turnagain intrusion lies within a series of northeast-verging imbricated thrusts. This study presents new U-Pb and Ar-Ar geochronologic data, coupled with whole-rock Nd isotopic compositions, to constrain the age and origin of the Turnagain intrusion and its host rocks. Determining the precise age of crystallization of ultramafic rocks in Alaskan-type intrusions is typically difficult as abundances of U-bearing (e.g. zircon, baddeleyite) accessory minerals are relatively low to absent, and primary K-bearing (e.g. biotite, feldspar) phases tend to be altered. The results from this study have implications for the significance of Alaskan-type intrusions and tectonic evolution of a portion of the northern Canadian Cordillera.

2.2 GEOLOGICAL SETTING OF THE TURNAGAIN INTRUSION

The Turnagain Alaskan-type intrusion is located approximately 70 km east of the town of Dease Lake, in north-central British Columbia (Figure 2.1). The intrusion is fault-bounded and proximal to the Kutcho Fault, which is a major tectonic structure that is interpreted to separate intrusive and volcanic sequences of the accreted Quesnel terrane from passive margin sedimentary rocks and post-accretionary Cretaceous granitoids of Ancestral North America (Gabrielse, 1998). The Quesnel terrane is part of the Intermontane Belt, a composite of terranes that extend south into Washington State and north into Yukon Territory (Figure 2.1). Seven Alaskan-type intrusions have been identified in the Quesnel terrane, including the Polaris intrusion and the Tulameen intrusion, which is the largest Alaskan-type intrusion in the world and is associated with concentrations of placer platinum-group metals in both lode and placer occurrences (Findlay, 1963; Nixon *et al.*, 1990) (Figure 2.1). The Tulameen is one of the three precisely dated (U-Pb zircon) Alaskan-type intrusions in B.C. (Rublee, 1994; Nixon *et al.*, 1997). The Alaskan-type intrusions of Quesnellia are typically associated with dioritic plutons of Triassic-Jurassic age and mafic volcanics, specifically the Late Triassic Takla, Nicola, and Stuhini groups. These mafic volcanics have been considered to be genetically associated with Alaskan-type intrusions (e.g. Findlay, 1969; Irvine, 1974; Nixon *et al.*, 1997), and the Turnagain intrusion is 20 km northwest of an exposure of Takla volcanics (Figure 2.2), although their genetic association with the intrusion remains to be evaluated. Numerous Alaskan-type intrusions of Cretaceous age occur within the Alexander terrane in southeastern Alaska, including the Duke Island intrusion (Irvine, 1967; Irvine, 1974; Loney & Himmelberg, 1992). Four other intrusions located to the west of the Cretaceous intrusions are Paleozoic in age and include the Salt Chuck intrusion, which exhibits extensive Pd-enriched Cu-sulphide mineralization at a major lithological boundary (Loney *et al.*, 1987; Loney & Himmelberg, 1992; Watkinson & Melling, 1992).

Pelagic sedimentary rocks of the Road River and Earn Groups (~Ordivician-Mississippian) were mapped by Gabrielse (1998) to occur along the northern and eastern edges of the Turnagain intrusion (Figure 2.2). The Road River and Earn Groups have been interpreted to represent ocean basin sediments deposited on the margin of Ancestral North America (Gabrielse, 1998; Erdmer *et al.*, 2005). The lithologically diverse Road River Formation in the McDame locality has a type thickness of 95 m (Gabrielse, 1998) and varies from a lower member of black, graptolitic, locally calcareous shale, a middle member of

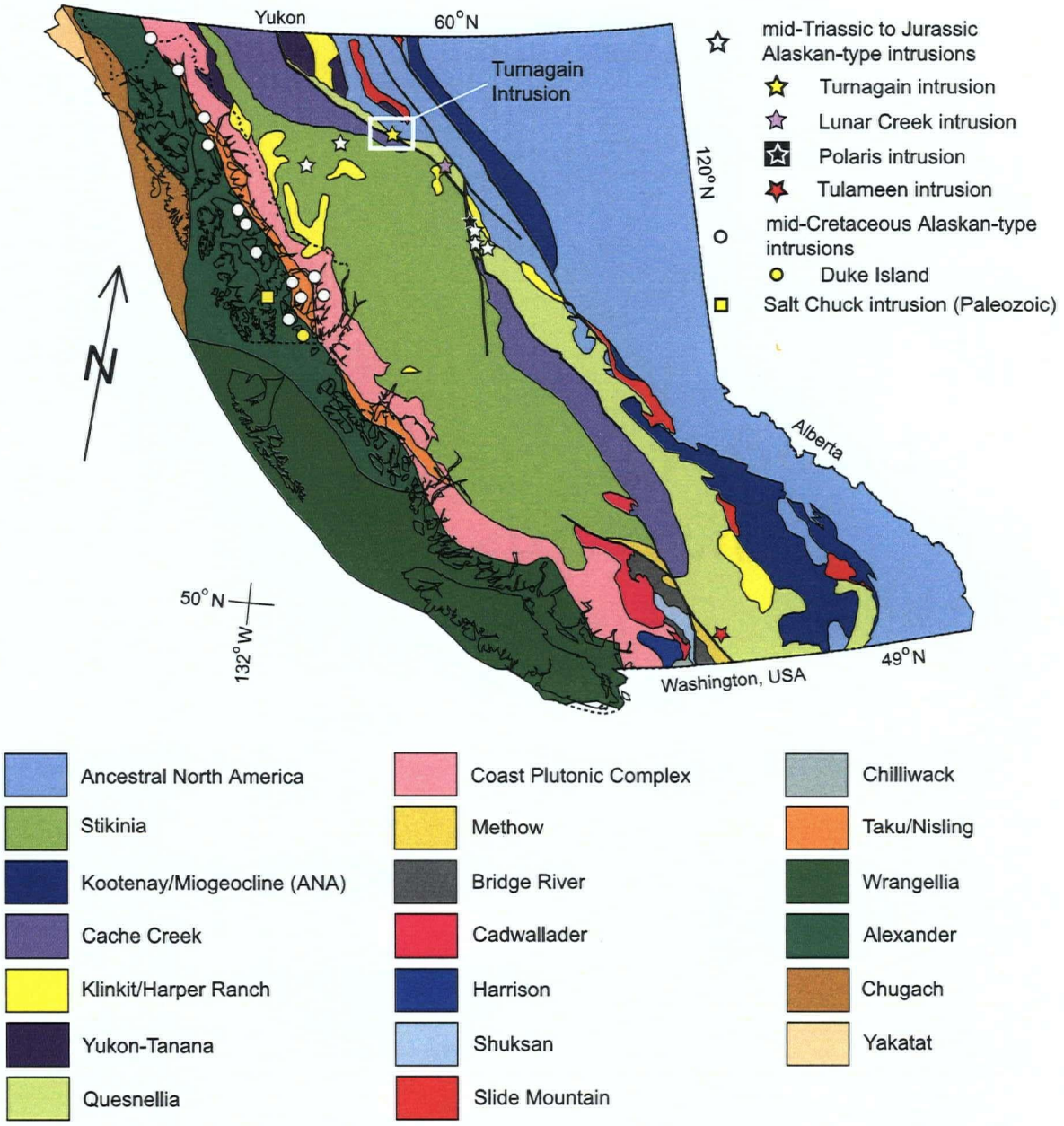

Figure 2.1: Terrane map of British Columbia, modified from Colpron & Nelson (2004), showing the locations of the major Alaskan-type intrusions in British Columbia and southeastern Alaska. The region outlined by the white box is the area displayed in Figure 2.2. Note that the Turnagain intrusion is situated on the western edge of Ancestral North America.

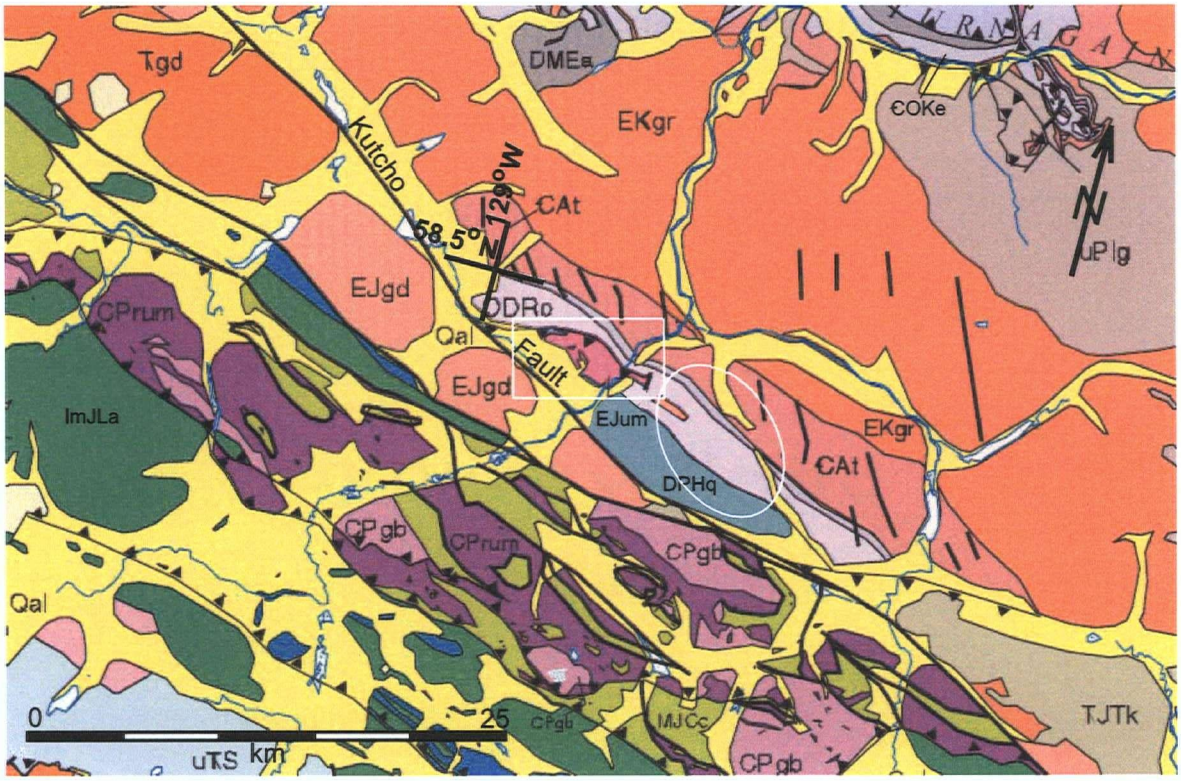

Ancestral North America

DPHq	**Nizi Formation**
DMEa	Earn Group
ODRo	**Road River Group**
€OKe	**Kechika Group**
€At	**Atan Group**
uPIg	Ingenika Group
	Quaternary Cover

Cache Creek

CPgb	Carboniferous to Permian gabbro
CPrum	Carboniferous to Permian ultramafic complexes
MJCc	Cache Creek Complex

Stikinia

uTrS	Stuhini Group, Mosley and Mount Moore Formations
PJKu	Kutcho Formation, Sillika Assemblage
ImJLa	Laberge Group
MJdg	monzodiorite

Quesnellia

TrJTk	Takla Group
Trgd	Triassic granodiorite
EJum	**Turnagain Alaskan-type ultramafic intrusion**
EJgd	Eaglehead Pluton and equivalents

Late Intrusive/Extrusive rocks

EKgr	Cassiar Batholith: granitoid
LTQT	Tuya Formation

Figure 2.2: Regional geological setting of the area immediately surrounding the Turnagain intrusion, extracted and modified after Massey *et al.* (2005). Note that the western, northern, and eastern margins of the Turnagain intrusion are flanked by the Road River/Earn groups. The Kutcho Fault separates Ancestral North America from Quesnellia and Cache Creek. The white box represents the study area (shown in more detail in Figure 2.3) and the white oval represents the general study area of Erdmer *et al.* (2005).

laminated dolomite, and an upper member of calcareous siltstone and shale. The entire package ranges in biostratigraphic age from Early Ordivician to Middle Silurian (Gabrielse, 1998). The Earn Group also exhibits extreme lithological diversity depending on where it is observed. In general, the Earn Group is a darkly coloured slate to siltstone that is locally pyritic and ranges in thickness from 50 to 1000 m in northern B.C. (Gabrielse, 1998). It is has been biostratigraphically dated to be Devonian to Mississippian in age. However, the age of the phyllite to the north and east of the Turnagain intrusion has not been determined and is currently assigned to the undivided Road River and Earn Groups based on lithological similarities with these two sedimentary packages (Gabrielse, 1998). Constrastingly, the Sandpile, Ramhorn, and McDame formations, which are observed between the Road River Formation and the Earn Group elsewhere in B.C., are not observed in the vicinity of the Turnagain intrusion. Due to these discrepancies, the greenschist-facies pelagic sediments proximal to the Turnagain intrusion are referred to as "graphitic phyllite" in this manuscript.

Graphitic pre-Devonian sediments are also associated with the Yukon-Tanana terrane (Mortensen, 1992; Simard *et al.*, 2003; Nelson & Friedman, 2004) and have been observed stratigraphically below the Lay Range Assemblage (Ferri & Melville, 1990), which is a volcano-sedimentary, arc-derived, package of rocks observed in Quesnellia. The graphitic phyllite to the north and east of the Turnagain intrusion, possibly part of the Road River Formation and Earn Groups, is composed of unfossiliferous, graphitic, and pyritic slates and phyllites containing interbeds of tuff, calcareous phyllite, and rare quartzite (Gabrielse, 1998; Erdmer *et al.*, 2005; Scheel *et al.*, 2005). The graphitic phyllite is typically recessive-weathering and crops out along the Turnagain River to the north and southeast of the intrusion, as well as in alpine areas to the east of the Turnagain River (Figure 2.2). These rocks generally have a steeply-dipping cleavage and may be complexly folded (Erdmer *et al.*, 2005; Scheel *et al.*, 2005). The graphitic phyllites, and a metasedimentary inclusion in the northwestern part of the Turnagain intrusion (Figure 2.3), commonly contain 1 cm to 1 m-thick quartz veins that do not cross-cut the Turnagain intrusion.

The few exposures of the metasedimentary unit to the south of the Turnagain intrusion have been interpreted by Massey *et al.* (2005) as the Nizi Formation, and referred to by Gabrielse (1998) as "uncorrelative". These metasediments are a grey-green, banded wacke, and appear similar to the hornfelsed unit that crops out in the northwestern portion of the intrusion (Figure 2.3). This unit (herein referred to as volcanic wacke) is described by Erdmer

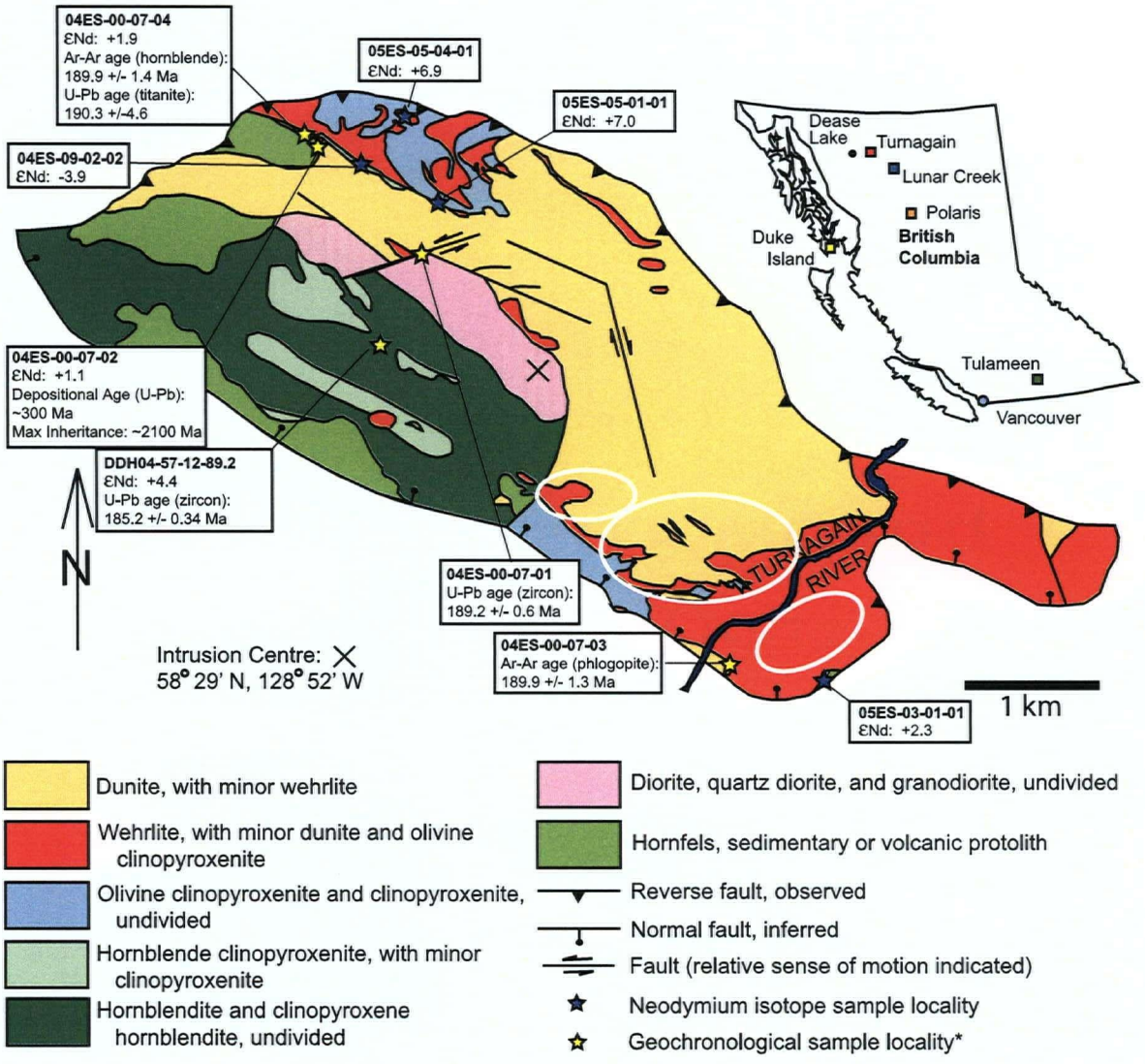

Figure 2.3: Generalized geologic map of the Turnagain intrusion, modified after Clark (1975). Note that some lithological units are composites at this scale. The inset in the upper right corner shows the location of the Turnagain intrusion in British Columbia, as well as other major Alaskan-type intrusions. The main nickeliferous sulphide zones are marked with white ovals (from west to east: Northwest Zone, Horsetrail Zone, Hatzl Zone). The geochronological sample localities are marked as yellow stars and U-Pb and Ar-Ar ages, and initial ε_{Nd} values (for geochronological samples) are indicated as yellow stars. Other whole rock sample localities for Nd isotopic compositions are marked as blue stars.

et al. (2005) as a "tuffeaceous phyllite with minor wacke" and is observed to conformably overlie "Road River" strata. However, Gabrielse (1998) proposed that this metasedimentary unit was separated from "Road River" strata by a fault. A westward extension of this fault was postulated to merge into the north-bounding and east-bounding faults bounding the Turnagain intrusion, creating a small nappe. Because of the inferred ages of the volcanic wacke and the Turnagain intrusion (both considered to be Late Triassic), Gabrielse (1998) associated this apparently "fault-bounded" package of rocks with the Quesnel terrane. However, recent geochronological studies of Erdmer *et al.* (2005) indicate that the metasedimentary package, coupled with its conformable nature to the underlying graphitic phyllites, is Mississippian in age. The graphitic phyllite is also observed to be intruded by an Early Jurassic "granodiorite" pluton (Erdmer *et al.*, 2005), a relationship that is not observed in "bona fide" Ancestral North American lithologies (J.K. Mortensen, pers. comm., 2006). Additionally, relatively small (0.5-20 m) inclusions of metamorphosed graphitic phyllite (containing graphite, quartz, and pyrrhotite bands) and volcanic wacke are observed in drillcore from the sulphide-mineralized zones within the Turnagain intrusion.

2.3 GEOLOGY OF THE TURNAGAIN INTRUSION

The 3.5 km x 8 km Turnagain Alaskan-type intrusion was the subject of a Ph.D. dissertation by Tom Clark (1975) and subsequent publications (Clark, 1978; 1980). It is a crudely zoned mafic-ultramafic pluton that ranges from dunite to a hornblende-rich diorite in the west-central portion (Figure 2.3). The central dunite is considered to represent the base of the intrusion, whereas the hornblende-rich central portion of the intrusion is considered to represent part of the roof zone. Dunite in the Turnagain intrusion contains Mg-rich cumulus olivine (Fo_{89}-Fo_{93}) (Chapter 4), disseminated cumulus chromite, minor intercumulus clinopyroxene and rare interstitial phlogopite. Local accumulations of chromite are observed as thin layers, rare beds, pods, schleiren, and wispy concentrations (see Chapter 3). In many Alaskan-type intrusions, these chromitites are prospective for platinum-group element mineralization. Wehrlite in the Turnagain intrusion occurs as either olivine cumulates or olivine-clinopyroxene cumulates (olivine: Fo_{85} to Fo_{90}). Disseminated sulphide reaches ~0.5 vol.% in most lithologies of the Turnagain intrusion. In the sulphide-mineralized Horsetrail Zone (Figure 2.3), both dunite and wehrlite can contain significant abundances of sulphide (typically 5 vol.%, but up to 50 vol.% locally). Olivine clinopyroxenite is a relatively uncommon lithology and is typically an

olivine-clinopyroxene cumulate with olivine compositions ranging from Fo_{83} to Fo_{89}. Hornblende clinopyroxenite with local cumulus magnetite is rarely exposed and is typically observed in drillcore from the east-central part of the intrusion. Hornblende clinopyroxenite is typically composed of cumulus clinopyroxene and intercumulus amphibole; as such it commonly grades into clinopyroxene hornblendite and *vice versa*. Hornblendite is a recessive lithology and is also rarely exposed. A fine-grained (<1 mm) hornblendite dike, 30 to 50 cm in width, in the northwestern part of the intrusion (Figure 2.3) contains abundant igneous amphibole (magnesiohastingsite) and accessory titanite.

The crystallization sequence of the Turnagain intrusion, from dunite → wehrlite → olivine clinopyroxenite → hornblende clinopyroxenite → hornblendite → diorite, is constrained by cross-cutting and gradational contact relationships, as well as by systematic mineral and whole rock geochemical trends (see Chapter 4). The intrusion is fault-bounded on its northern and eastern margins margins (observed on surface, in drillcore, and inferred from aeromagnetic data) against graphitic phyllite and on its western and southern margins by volcanic wacke. The entire intrusion is interpreted to represent a small klippe, however based on the results of this study and others (Chapters 3 and 4), this klippe was not significantly displaced.

The metasedimentary rocks in the northwest (Figure 2.3) are relatively coarse-grained (~1-2 mm) compared to similar rocks south of the Turnagain intrusion (<1 mm). The metasedimentary inclusion in the northwest is composed of hornfelsed volcanic wacke that contains abundant detrital zircon. The volcanic wacke appears to represent an inclusion of wallrock within the Turnagain intrusion in contrast to the lower-grade, finer-grained, metasediments observed to the south of the intrusion. This inclusion does not appear to be fault-bounded, but is in igneous contact with the ultramafic lithologies. Small pods (1-5 cm wide) of amphibole-bearing two-mica granite, interpreted as partial melt, were observed by the author in this inclusion, but not in the metasedimentary rocks to the south.

Melanocratic to leucocratic dioritic rocks in the Turnagain intrusion have gradational contacts with, or cross-cut, ultramafic rocks and represent the youngest intrusive phases. Dioritic rocks are the only zircon-bearing lithology present in the Turnagain intrusion. The largest diorite occurrence is located in the central part of the intrusion (Figure 2.3). The margins of this pluton are melanocratic (85 vol.% amphibole, 14 vol.% plagioclase) and fine- to medium-grained (1-5 mm grain sizes), whereas the central part of the pluton (as observed

from surface exposures) is dominantly composed of plagioclase and quartz. Texturally and mineralogically similar mafic diorite is also observed in drillcore as 4 cm to 1 m-wide dikes that intrude the hornblende-rich central portion of the intrusion and the adjacent dunite to the east. Leucocratic diorite dikes, predominantly composed of plagioclase and quartz, are commonly found cross-cutting the hornblende-bearing lithologies, however these felsic dikes are rarely found cutting ultramafic rocks elsewhere in the intrusion.

2.4 SAMPLE DESCRIPTIONS AND ANALYTICAL TECHNIQUES

2.4.1 U-Pb Zircon/Titanite

Four samples were selected for U-Pb geochronology (see sample locations on Figure 2.3). Zircon ($ZrSiO_4$) was separated from three samples (04ES-00-07-01, DDH04-57-12, 04ES-00-07-02) and titanite ($CaTiSiO_5$) from a fourth sample (04ES-00-07-04). Sample 04ES-00-07-01 is a green-black, medium-grained diorite with relatively abundant (10-15 vol.%) large plagioclase crystals (subsequently referred to as mela-diorite) and occurs at the north-central margin of the large felsic body. At this location no ultramafic inclusions in the diorite were observed, however a similar lithology intersected in NQ drillcore in the north-central part of the intrusion locally contains abundant (10-70 vol.%) ultramafic xenoliths. Sample DDH04-57-12 is a green-and-white, coarse-grained hornblende diorite with 20 vol.% euhedral amphibole (3 cm long), and 1 cm-wide euhedral plagioclase (subsequently referred to as leuco-diorite). The sample was obtained from NQ drillcore from the west-central part of the Turnagain intrusion (see Figure 4.6: G,H, Chapter 4). The interval from which this sample was taken is gradational into hornblendite over a distance of 10 cm. Sample 04ES-00-07-02 is a hornfelsed volcanic wacke (epidote + plagioclase ± amphibole ± biotite ± quartz) from the northwestern part of the intrusion, and based on contact relationships (intruded by hornblendite) and degree of metamorphism (the mineral assemblage is indicative of epidote-amphibole hornfels facies) it is interpreted to represent an inclusion of wallrock. Sample 04ES-00-07-04 is a black, fine-grained equigranular hornblendite dike (~30 cm wide) that contains accessory titanite (1-2 vol.%), abundant wall-rock inclusions, and intruded rocks equivalent to the previous sample (volcanic wacke) (Figure 2.3). The morphologies of some of the zircon and titanite separates are exhibited in Figure 2.4.

All sample preparation, geochemical separation and mass spectrometry were done at the Pacific Centre for Isotopic and Geochemical Research in the Department of Earth and

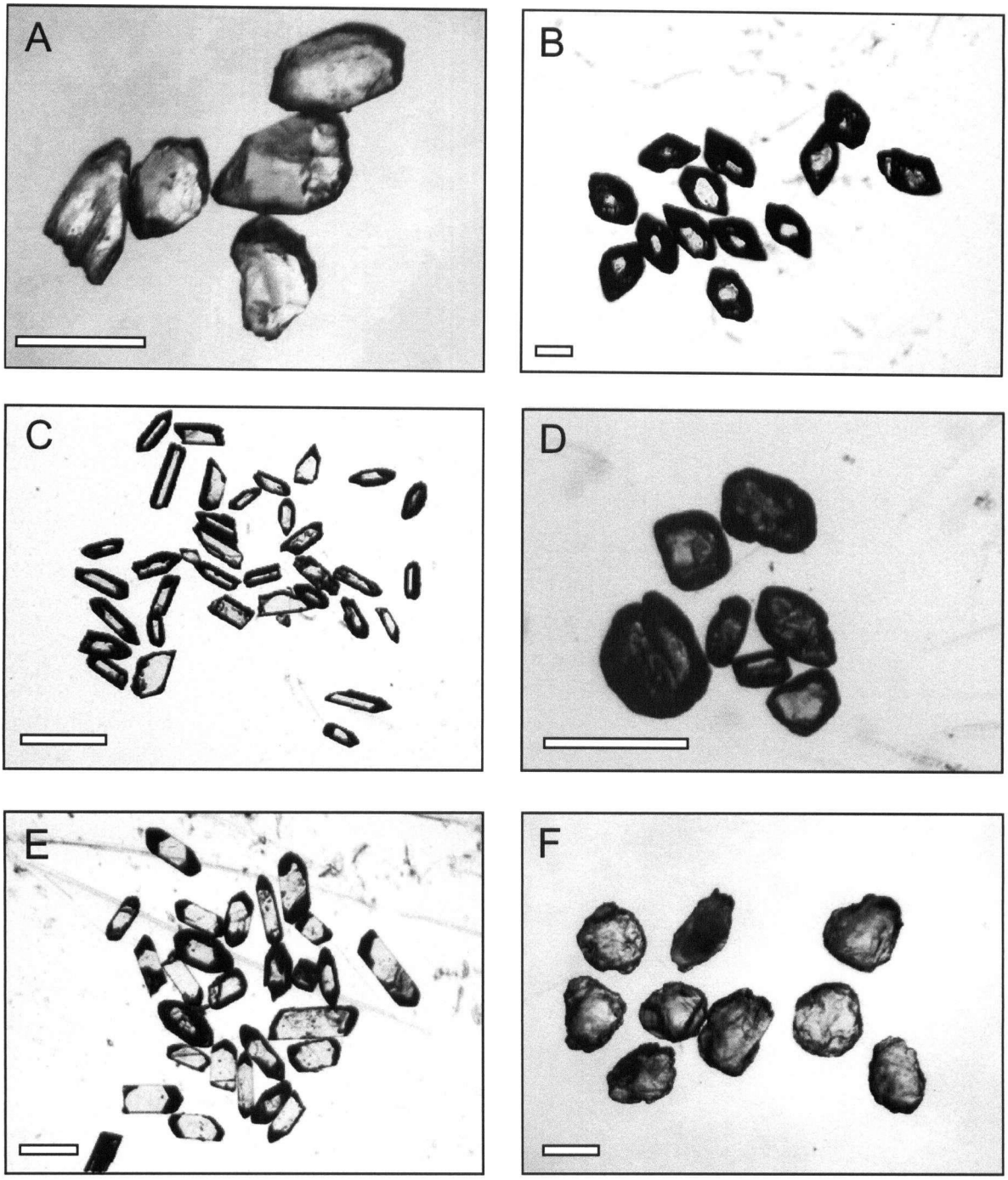

Figure 2.4: Photomicrographs of zircon and titanite separates from the Turnagain intrusion. The scale bar in each photo is 200 μm. A) Mela-diorite (04ES-00-07-01); large, clear, broken grains, one of which is fraction F. B) Mela-diorite (04ES-00-07-01), fraction A; large equant, slightly elongate zircon grains. Note their similar size. C) Mela-diorite (04ES-00-07-01), fraction D; large zircon laths, some with minute inclusions. D) Leuco-diorite (DDH04-57-12), fraction H; slightly rounded, broken, prismatic grains of medium size. E) Volcanic wacke (04ES-00-07-02), fractions D, F, G (pre-separation); intermediate zircon laths, clear and relatively inclusion-free. F) Hornblendite (04ES-00-07-04); colourless to slightly yellow titanite grains.

Ocean Sciences, University of British Columbia. Zircon and titanite were separated from the rocks using conventional crushing, grinding, and Wilfley table techniques. Final concentration incorporated the use of heavy liquids and a magnetic separator. Zircon and titanite fractions were selected for analysis based on magnetic susceptibility, grain quality, size, and morphology. Using the technique of Krogh (1982), all zircon fractions were air-abraded prior to dissolution to minimize the effects of post-crystallization Pb-loss. Titanite grains were dissolved on a hotplate in 7 mL screwtop PFA beakers for at least 48 hours at ~130°C. Zircon grains were dissolved in sub-boiled 48% HF and 14 M HNO_3 (ratio of ~10:1, respectively) in the presence of a mixed $^{233-235}U$-^{205}Pb tracer for 40 hours at 240°C in 300 μL PTFE or PFA microcapsules contained in high-pressure vessels (Parr™ acid digestion vessels with 125 mL PTFE liners). Sample solutions were then dried to salts at ~130°C. Zircon residues were redissolved in ~100 μL of sub-boiled 3.1 M HCl for 12 hours at 210°C in high-pressure vessels and titanite residues were redissolved on a hotplate in ~1 mL of sub-boiled 6.2 M HCl in the same 7 mL screwtop PFA beakers for at least 24 hours at ~130°C. Titanite solutions were again dried to salts and were again redissolved on a hotplate, in the same beakers, in 1 mL of sub-boiled 3.1 M HCl at ~130°C for at least 24 hours. For zircon fractions of about 10 μg or less, 3.1 M HCl was transferred to 7 mL PFA beakers, dried to a small droplet after addition of 2 μL of 1 M phosphoric acid (H_3PO_4), and loaded directly onto Re filaments for analysis, as described below (referred to as the "no chemistry" method). For larger fractions of both minerals, separation and purification of Pb and U employed ion exchange column techniques modified slightly from those described by Parrish *et al.* (1987). Pb and U were sequentially eluted into a single beaker; U from titanite solutions was purified by passing through columns a second time. Elutants were dried in 7 mL screwtop PFA beakers on a hotplate at ~120°C in the presence of 2 μL of ultrapure 1 M H_3PO_4. Samples were then loaded on single, degassed zone-refined Re filaments in 5 μL of a silica gel ($SiCl_4$) phosphoric acid emitter. Isotopic ratios were measured using a modified single collector VG-54R thermal ionization mass spectrometer equipped with an analogue Daly photomultiplier. Measurements were done in peak-switching mode on the Daly detector. Analytical blanks were <1 pg for U and for 1-3 pg Pb for the "no chemistry" fractions. For dissolved zircon and titanite that passed through ion exchange columns, a blank of 2-10 pg Pb was used. Pb isotopic ratios were corrected for fractionation of 0.32-0.37 %/amu, based on replicate analyses of the NBS-982 Pb standard reference material and the values recommended by Thirlwall (2000), and U

fractionation was determined directly on individual runs using the $^{233-235}U$ tracer. Reported precisions for Pb/U and Pb/Pb dates were determined by numerically propagating all analytical uncertainties through the entire age calculation using the technique of Roddick (1987). Standard concordia diagrams were constructed and regression intercepts calculated with Isoplot 3.09 (Ludwig, 2003). Unless otherwise noted, all errors are quoted at the 2σ level.

2.4.2 Ar-Ar Phlogopite/Amphibole

Two samples (04ES-00-07-03, 04ES-00-07-04) were selected for Ar-Ar geochronology. Sample 04ES-00-07-03, a black, medium-grained wehrlite located in the far southeastern corner of the Turnagain intrusion (Figure 2.3), was chosen because it contained 1-2 vol.% interstitial phlogopite. Amphibole was separated from sample 04ES-00-07-04, the hornblendite dike described above. The samples were crushed using a steel jaw crusher and sieved to obtain fragments ranging in size from 0.25 to 1.0 mm. The sieved fractions were washed in deionized water and then air-dried at room temperature after magnetite and metallic crusher fragments were removed with a hand magnet. The amphibole and phlogopite separates were hand-picked using a binocular microscope, wrapped in aluminum foil and stacked in an irradiation capsule with similar-aged samples, neutron flux monitors (Fish Canyon Tuff sanidine, 28.02 Ma; Renne *et al.*, 1998), optical grade CaF_2 and potassium glass. The samples were irradiated with cadmium shielding on April 25-27, 2005 at the McMaster Nuclear Reactor in Hamilton, Ontario, for 84 MWH, with a neutron flux of approximately $3x10^{16}$ neutrons/cm^2. Total fusion analyses (n=72) of 21 neutron flux monitor positions produced errors of <0.5% in the J value. The samples were analyzed on June 3 and 6, 2005, at the Pacific Centre for Isotopic and Geochemical Research, University of British Columbia. Using a defocused beam of a 10W CO_2 laser (New Wave Research MIR10), the mineral separates were step-heated at incrementally higher powers until fused. A VG5400 mass spectrometer, equipped with an ion-counting electron multiplier, analyzed the gas evolved from each step. All measurements were corrected for mass discrimination, mass spectrometer sensitivity, total system blank, radioactive decay during and subsequent to irradiation, and interfering Ar from atmospheric contamination and the irradiation of Ca, Cl and K. Isotope production ratios were: $(^{40}Ar/^{39}Ar)_K$=0.0005±0.00006, $(^{37}Ar/^{39}Ar)_{Ca}$=1048±0.9, $(^{36}Ar/^{39}Ar)_{Ca}$=0.3542±0.0008, Ca/K=1.83±0.01($^{37}Ar_{Ca}/^{39}Ar_K$).

The plateau and correlation ages were calculated using Isoplot 3.09 (Ludwig, 2003). Errors are quoted at the 2σ (95% confidence) level and are propagated from all sources except mass spectrometer sensitivity and age of the flux monitor. The best statistically-justified plateau and plateau ages for both samples were picked based on the following criteria: (1) three or more contiguous steps comprising more than 50% of the ^{39}Ar; (2) a probability of fit of the weighted mean age greater than 5%; (3) a slope of the error-weighted line through the plateau ages equals zero at 5% confidence; (4) the ages of the two outermost steps on a plateau are not significantly different from the weighted-mean plateau age (at 1.8σ six or more steps only); and (5) the outermost two steps on either side of a plateau must not have non-zero slopes with the same sign (at 1.8σ nine or more steps only).

2.4.3 Neodymium Isotopes

A total of eight samples were selected for neodymium isotopic composition measurements and were chosen to reflect the lithological range of the Turnagain intrusion. Dunites were excluded from analysis due to their extremely low Nd concentrations (<0.1-0.4 ppm). Samarium and neodymium concentrations, as well as major elements and other incompatible trace elements, were determined by ICP-MS at Activation Laboratories Ltd. (Actlabs) in Ancaster, Ontario (see complete analytical techniques description in Chapter 4). The accuracy of the suite of elements analyzed was determined by the use of USGS reference materials ranging in composition from basalt to granite and by various in-house standard materials. Relative standard deviations from three duplicated analyses are typically less than 5% for most elements. Low concentrations of Sm and Nd in one duplicate (sample 05ES-05-06-01, a hornblende clinopyroxenite) resulted in higher standard deviations; however when concentrations of Sm and Nd are an order of magnitude higher than their respective detection limits (04ES-00-07-04) the standard deviation drops to below 5% relative.

The Nd isotopic compositions of samples from the Turnagain intrusion were measured at the Pacific Centre for Isotopic and Geochemical Research, University of British Columbia. The volcanic wacke and leuco-diorite samples (04ES-00-07-02 and DDH04-57-12, respectively) were digested in Teflon bombs enclosed in metallic bombs (modified Krogh design) and placed for 120 hrs in $HF\text{-}HNO_3\text{-}HClO_4$ (7:1:1) and 24 hrs in HCl in an oven at 190°C. All other samples were dissolved in Savillex™ and subject to the above digestion procedure. The Nd isotopic ratios were measured using a Thermo Finnigan Triton-TI thermal

ionization mass spectrometer (TIMS) in static mode with relay matrix rotation. The measured composition of each sample is the average of 125-130 separate analyses. The La Jolla Nd standard was measured once giving a value of $^{143}Nd/^{144}Nd = 0.511858 \pm 0.000008$ (2σ) and the Rennes Nd standard was measured 48 times within one week giving a mean value of $^{143}Nd/^{144}Nd = 0.511960 \pm 0.000008$ (2σ). The Nd isotopic compositions of procedural duplicates of three samples (04ES-09-02-02, 05ES-05-06-02, 04ES-00-07-02) are within the 2σ error (less than 0.001% relative). All measurements were corrected using $^{146}Nd/^{144}Nd = 0.7219$ for internal mass fractionation. The USGS GSP-2 reference material was also analyzed for its Nd isotopic composition, and the results are within the 2σ analytical error of previously reported results (Weis *et al.*, 2006).

2.5 RESULTS

Three dates from two ultramafic samples (wehrlite and hornblendite) were obtained from the Turnagain intrusion using Ar-Ar and U-Pb geochronological techniques. The two Ar-Ar samples are from opposite corners of the intrusion (~8 km apart) (Figure 2.3). Additional U-Pb (zircon) dates were determined from a mela-diorite, a leuco-diorite, and the hosted volcanic wacke inclusion. Neodymium isotopic compositions were analyzed from the three geochronological samples, and five additional ultramafic samples.

2.5.1 U-Pb Geochronology

2.5.1.1 04ES-00-07-01 – Mela-diorite

The mela-diorite was sampled from the north-central margin of the large dioritic body that intruded, and/or is gradational with, the central part of the Turnagain intrusion (Figure 2.3). The margin of the diorite is hornblende-rich, locally resembling hornblendite elsewhere in the Turnagain intrusion. However, this hornblende-rich outer phase grades inwardly to a more felsic diorite over a distance of ~100 m on surface. The presence of euhedral (cumulus) plagioclase (~1 cm in diameter) helps discriminate this lithology from feldspathic hornblendite elsewhere in the Turnagain intrusion. The least magnetic fraction of sample 04ES-00-07-01 yielded abundant (>500) zircon grains typically 150-250 μm in length. The zircon grains exhibit either equant (3:1 to 2:1) (Figure 2.4B) or lath (length/width 6:1 to 4:1) (Figure 2.4C) morphology and range in colour from clear to pale yellow. A distinct population of grains exhibit inherited cores (not analyzed), some of which are metamict. Each analyzed fraction

contained 2-18 grains with the exception of Fraction F (Figure 2.4A), which is represented by a single grain of zircon. Uranium concentrations range from 123-283 ppm and Th/U ratios from 0.32 to 0.79 (Table 2.1). The U-Pb data from the analyzed fractions yield similar $^{206}Pb/^{238}U$ ages, ranging from 186.3±0.4 Ma to 189.2±0.6 Ma, the latter of which (Fraction B, seven 75-100 μm equant grains) has the highest $^{206}Pb/^{238}U$ and $^{207}Pb/^{235}U$ and is interpreted to be the minimum age of crystallization of the mela-diorite. Each of the error ellipses (2σ) for each of the five fractions overlap concordia (Figure 2.5A), however their distribution suggests that zircon from all fractions may have undergone Pb-loss. A free-fit discordia line through all fractions (MSWD =0.17) yields an upper intercept with concordia of 190.5±6.6 Ma (and a poorly constrained lower intercept of 705±2500 Ma) (Figure 2.5A). Alternatively, a fixed regression (lower intercept at 0 Ma) yields an older upper intercept of 199.2±6.6 Ma. Neither the upper intercept age of 190.5 +6.6/-1.9 Ma from the free-fit regression (lower error combined with the error of the oldest fraction), nor the fixed regression age of 199.2±6.6 Ma are considered to represent the true crystallization age of the mela-diorite, because the calculated upper intercept ages have relatively large 2σ errors due to the relatively small dispersion of points along the fitted discordia lines. The better constrained minimum age of 189.2±0.6 Ma of fraction B is interpreted to be the minimum age of the Turnagain intrusion. These results are consistent with the Ar-Ar geochronological results (see below).

2.5.1.2 DDH04-57-12 – Leuco-diorite

This sample, taken from a drillhole in the south-central portion of the intrusion (Figure 2.3), is a coarse-grained leucocratic hornblende diorite composed of euhedral, cumulus plagioclase and amphibole. Multiple 10-50 cm-wide lithological variations were observed in drillcore along the 9 m-thick interval (e.g. amphibole-rich phases, quartz-rich phases). Fewer than 200 zircon grains, 20-200 μm in length, were present in the least magnetic fraction. Broken lath (length/width 2:1 to 1.5:1) and some intact lath (length/width 4:1 to 3:1) morphologies are exhibited by most zircon grains, and all grains are generally colourless (Figure 2.4). Of the four fractions analyzed, two were single grains (Fractions B and F), whereas fractions E and H (Figure 2.4D) contained 2 and 7 grains, respectively. Uranium concentrations range from 183-582 ppm and Th/U ratios range from 0.17 to 0.39 (Table 2.1). The U-Pb data from the four analyzed fractions are concordant and yield similar $^{206}Pb/^{238}U$ dates from 183.6±0.6 to

Table 2.1: U-Pb TIMS analytical data from zircon and titanite grains separated from samples from the Turnagain intrusion

Fraction[1]	Wt (mg)	U[2] (ppm)	Pb*[3] (ppm)	$^{206}Pb/^{204}Pb$[4]	Pb[5] (pg)	Th/U[6]	Isotopic ratios (1σ,%)[7] $^{206}Pb/^{238}U$	$^{207}Pb/^{235}U$	$^{207}Pb/^{206}Pb$	Apparent ages (2σ,Ma)[7] $^{206}Pb/^{238}U$	$^{207}Pb/^{235}U$	$^{207}Pb/^{206}Pb$	discordance to origin (%)
04ES-00-07-01 - mela-diorite													
A, 2	35	229	6.8	4179	3.5	0.41	0.02946 (0.08)	0.2036 (0.24)	0.05011 (0.21)	187.2 (0.3)	188.1 (0.8)	200.2 (9.5)	6.6
B, 7	32	145	4.2	1557	5.5	0.28	0.02979 (0.17)	0.2058 (0.63)	0.05012 (0.58)	189.2 (0.6)	190.1 (2.2)	201 (27)	5.7
C, 18	38	123	3.7	3324	3.1	0.40	0.02965 (0.11)	0.2045 (0.34)	0.05002 (0.31)	188.4 (0.4)	188.9 (1.2)	196 (14)	4.0
D, 5	19	254	8.3	2207	4.0	0.79	0.02932 (0.11)	0.2029 (0.42)	0.05020 (0.38)	186.3 (0.4)	187.6 (1.4)	204 (18)	8.9
F, 1	41	283	8.3	1580	13.6	0.32	0.02961 (0.14)	0.2038 (0.57)	0.04992 (0.53)	188.1 (0.5)	188.3 (2.0)	191 (24/25)	1.7
DDH04-57-12-89 - leuco-diorite													
B*, 1	9	183	5.0	1248	2.4	0.17	0.02890 (0.16)	0.1984 (0.72)	0.04979 (0.67)	183.6 (0.6)	183.7 (2.4)	185 (31/32)	0.8
E*, 2	3	276	7.9	379	4.1	0.30	0.02921 (0.32)	0.2022 (2.20)	0.05020 (2.1)	185.6 (1.2)	187.0 (7.5)	204 (93/98)	9.3
F, 1	14	213	6.0	422	13.9	0.26	0.02911 (0.17)	0.1998 (1.94)	0.04979 (1.86)	185.0 (0.6)	185.0 (6.6)	185 (84/89)	0.0
H, 7	17	582	17.2	1520	11.9	0.39	0.02915 (0.09)	0.2004 (0.23)	0.04986 (0.18)	185.2 (0.3)	185.5 (0.8)	188.4 (8.3)	1.7
04ES00-07-04 - hornblendite dike													
T1, 20	188	8.7	0.5	45.4	112	3.90	0.02983 (1.75)	0.2108 (7.2)	0.05124 (6.32)	189.5 (6.6)	194 (25)	252 (267/320)	25.0
T2, 20	156	9.4	0.5	46.4	97.2	3.20	0.03009 (1.68)	0.2163 (7.61)	0.05216 (6.77)	191.1 (6.3)	199 (28)	292 (283/343)	35.1
04ES-00-07-02 - volcanic wacke													
A, 2	25	202	62.4	23000	4.0	0.35	0.29220 (0.11)	5.2136 (0.15)	0.12941 (0.07)	1652.5 (3.3)	1854.5 (2.5)	2089.9 (2.5)	23.7
B, 5	30	152	11.2	5004	4.0	0.31	0.07265 (0.16)	0.7948 (0.18)	0.07935 (0.16)	452.1 (1.4)	593.9 (1.6)	1180.9 (6.2)	63.9
C, 5	5	175	14.6	580	7.5	0.51	0.07845 (0.30)	0.9486 (0.50)	0.07845 (0.30)	486.9 (2.8)	677.4 (5.0)	1375.7 (16.3)	67.0
D, 3	13	97.1	15.6	891	3.5	0.34	0.03863 (0.20)	0.2805 (0.80)	0.03863 (0.20)	244.4 (1.0)	251.0 (3.5)	314 (33/34)	22.6
E, 12	8	260	16.9	1316	6.1	0.46	0.06179 (0.22)	0.6855 (0.32)	0.08046 (0.24)	386.5 (1.6)	530.1 (2.7)	1208.2 (9.4)	70.0
F, 2	12	113	5.5	364	11.6	0.40	0.04786 (0.21)	0.3450 (2.29)	0.05228 (2.18)	301.4 (1.2)	301 (12)	298 (97/103)	-1.3
G*, 5	4	271	13.1	776	4.2	0.41	0.04750 (0.26)	0.3533 (0.26)	0.05395 (1.17)	299.1 (1.5)	307.2 (6.7)	369 (52/54)	19.3
H, 4	11	132	11.2	539	13.9	0.37	0.08063 (0.19)	1.3242 (0.62)	0.11911 (0.54)	499.9 (1.9)	856.4 (7.2)	1943 (19)	77.1

[1] All zircon grains selected for analysis were air-abraded prior to dissolution. Fraction ID (capital letter) followed by the number of grains: T1, T2 for titanite fractions. Asterisk after fraction name signifies no chemistry samples.

[2] U blank correction of 1 pf ± 20%; U fractionation corrections were measured for each run with a double ^{233}U-^{235}U spike.

[3] Radiogenic Pb.

[4] Measured ratio corrected for spike and Pb fractionation of 0.0028-0.0033/Amu ± 20% (Daly collector), which was determined by repeated analysis of NBS 982 Pb standard reference material throughout the course of this study.

[5] Total common Pb in analysis based on blank isotopic composition.

[6] Model Th/U derived from radiogenic ^{208}Pb and the $^{207}Pb/^{206}Pb$ age of fraction.

[7] Blank and common Pb corrected; Pb procedural blanks were ~2 pg (zircon), 14 pg (titanite) and U, 1 pg for zircon and titanite. Common Pb compositions are based on Stacey-Kramer model Pb at the interpreted age or the $^{207}Pb/^{206}Pb$ age of the rock (Stacy and Kramers, 1975).

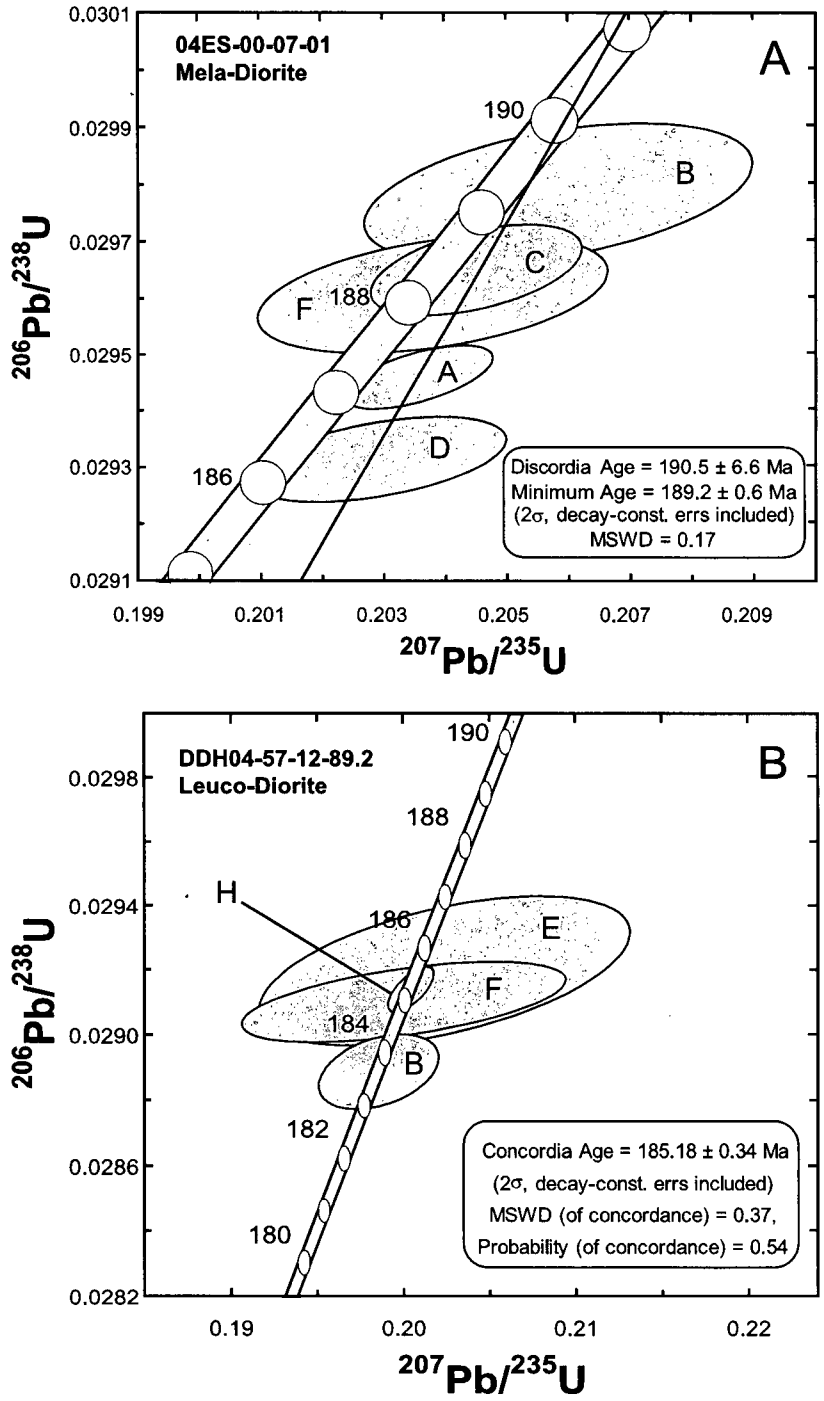

Figure 2.5: Concordia plots for U-Pb data from analyzed zircon fractions for diorite samples from the Turnagain intrusion. Each ellipse (2σ error) represents the analysis of a single fraction; all fractions are labelled. A) Sample 04ES-00-07-01, a mela-diorite proximal to the ultramafic lithologies in the centre of the intrusion. B) Sample DDH04-57-12, leuco-diorite, sampled from a plagioclase-rich horizon in the hornblende-rich central region of the Turnagain intrusion. The shaded gray band is the decay constant error envelope of the concordia curve.

185.6±1.2 Ma. The age of the oldest fraction (fraction H, 185.6±1.2 Ma), is interpreted as the minimum age of crystallization of the leuco-diorite (Figure 2.5B).

2.5.1.3 04ES-00-07-02 – Volcanic Wacke

To constrain the age of the host rocks, the volcanic wacke was sampled from the hornfelsed sedimentary unit in the northwestern portion of the intrusion (Figure 2.3), within 50 m of the hornblendite dike (04ES-00-07-04). Zircon in the least magnetic fraction is relatively abundant (>300 grains) and ranges in colour from colourless to pale yellow to dark red-brown. Three distinct zircon morphologies are present in this sample: (1) large lath-shaped fragments (aspect ratio 1.5:1), some >200 μm wide, (2) smaller laths (~200 μm long, aspect ratio of 4:1) (Figure 2.4E) commonly containing fluid inclusions and inherited cores, and (3) sub-equant grains (aspect ratio 2:1) ranging from <50 μm to ~200 μm in diameter, the largest of which are commonly dark in colour. A total of eight fractions were analyzed comprising 2-12 zircon grains per fraction. Uranium concentrations range from 97-260 ppm, with a range of Th/U ratios between 0.31 and 0.51 (Table 2.1). The U-Pb data from these analyzed fractions yield an extremely large range of $^{206}Pb/^{238}U$ dates (244 Ma to 1652 Ma, Figure 2.6A). The results from two fractions (F and G) plot on or near concordia at ~300 Ma. Fraction F is concordant with a $^{206}Pb/^{238}U$ age of 301.4±1.2 Ma (Figure 2.6B), which is interpreted to be the maximum depositional age of the volcanic wacke. Fraction D has a significantly younger $^{206}Pb/^{238}U$ age (244 Ma) and is discordant, which is attributed to Pb-loss from ~300 Ma. Fraction A (not shown on Figure 2.6) is highly discordant with a $^{206}Pb/^{238}U$ age of 1652 Ma and a $^{207}Pb/^{206}Pb$ age of ~2090 Ma. The old $^{207}Pb/^{206}Pb$ ages of fractions A, B, C, and E indicate the presence of Early Proterozoic zircon grains in the source of the volcanic wacke. A regression line through the discordant and concordant grains (not including fraction D) has an upper intercept with concordia of ~2100 Ma, which is considered to be the average age of inheritance in the analyzed fractions.

2.5.1.4 04ES-00-07-04 – Hornblendite

The fine-grained hornblendite was sampled from a 30 cm-wide dike that intrudes the volcanic wacke in the northwestern part of the Turnagain intrusion discussed above (Figure 2.3). The heavy mineral separate yielded abundant (>100 grains) colourless to pale yellow to pale brown titanite grains (Figure 2.4F). Most grains are anhedral and equant, with an aspect ratio of ~1:1.

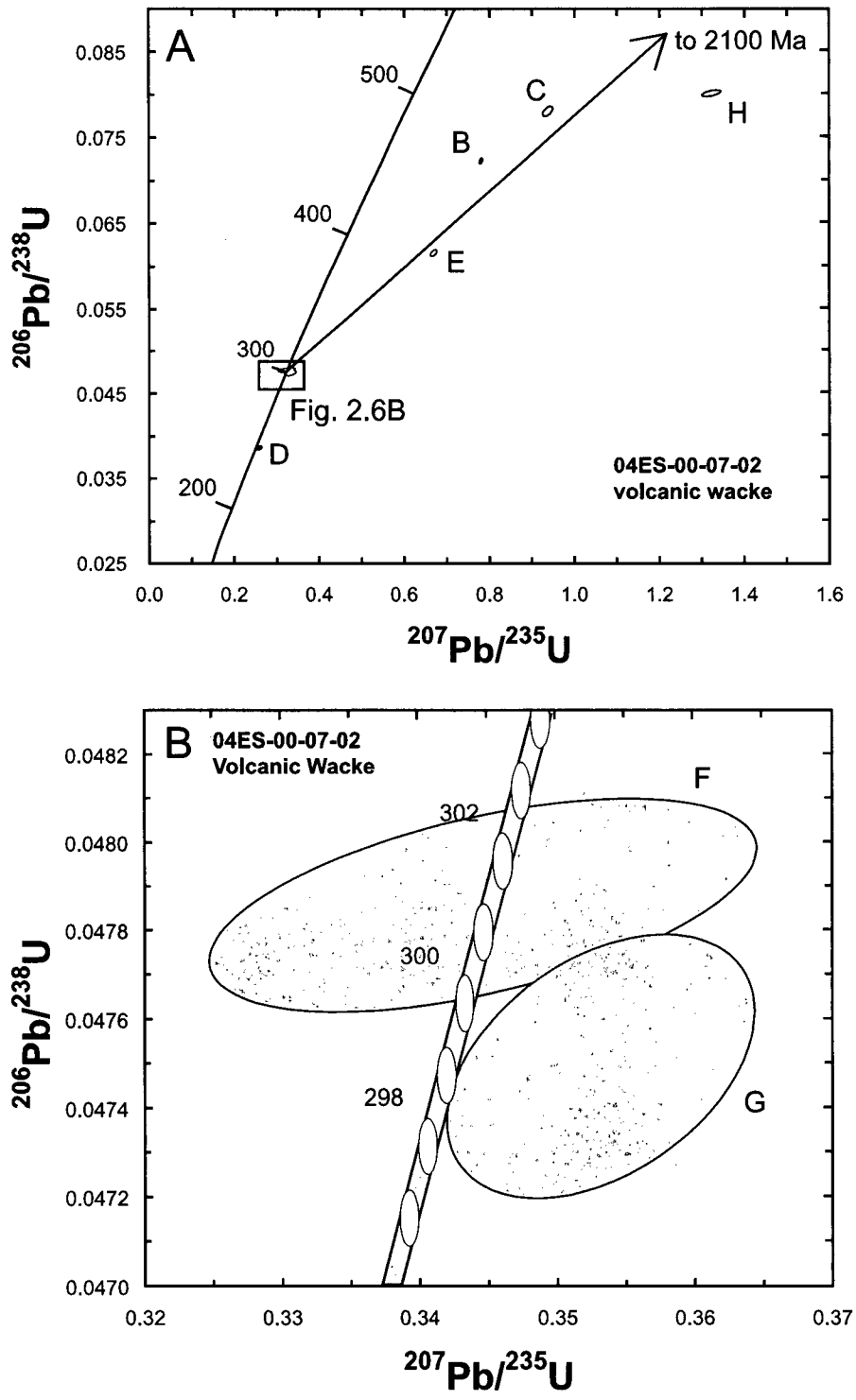

Figure 2.6: Concordia plots for U-Pb data from analyzed zircon fractions from a volcanic wacke sample from the northwestern part of the Turnagain intrusion (04ES-00-07-02). All fractions are labelled. A) All analyzed zircon grains except fraction A (7 fractions, n=36 grains). The discordia line has a lower intercept of ~300 Ma and an upper intercept of ~2.1 Ga. B) Expanded view showing the concordant to nearly concordant results at ~300 Ma (fractions F and G). The shaded gray band is the decay constant error envelope of the concordia curve.

Both of the analyzed fractions contained 20 titanite grains each. U contents range from 7 to 9.4 ppm, with Th/U ratios of ~3.9 (Table 2.1). The U-Pb data of the two titanite fractions are concordant and the $^{206}Pb/^{238}U$ ages are 189.5 Ma and 191.1 Ma, respectively. The weighted mean of these two concordant and statistically identical results is 190.3 ± 4.6 Ma (Figure 2.7), which is interpreted to represent the minimum crystallization age of the hornblendite when the rock cooled through the closure temperature to Pb diffusion in titanite (see Discussion).

2.5.2 Ar-Ar Geochronology

2.5.2.1 04ES-00-07-04 – Hornblendite

This sample, also dated by the U-Pb (titanite) method as documented above, yielded abundant, dark brown to black, low-K (Ca/K =10-32), amphibole crystals. The amount of ^{40}Ar is extremely high in the grain edge (up to 94%), however the range in ^{40}Ar in the core of the grain is small (1.6-4.2%) (Table 2.2). The first eight heating steps (155 Ma to 1279 Ma, 6% of total Ar released) yield a distorted initial age spectrum, however a well-defined plateau (189.3±1.4 Ma) is observed for the remainder of the heating steps (94% of all Ar released) (Figure 2.8A). A similar total gas age of 190.1±1.4 Ma was also obtained. The inverse isochron age is 190.7±2.3 Ma (MSWD =0.14) (Figure 2.8B). The Ar-Ar results for this amphibole separate are consistent with the U-Pb (titanite) age of 190.3±4.6 Ma. The plateau age obtained above is considered to represent the minimum age of the hornblendite dike when the rock cooled through the closure temperature to Ar diffusion in hornblende (see Discussion).

2.5.2.2 04ES-00-07-03 - Wehrlite

This sample comes from an outcrop in the far southeastern part of the Turnagain intrusion, in the southern portion of the Hatzl Zone (Figure 2.3). Although phlogopite is not abundant in this sample (<2 vol.%), there were sufficient grains for Ar-Ar analysis. Phlogopite from this sample, which has high-K interiors (Ca/K between 0.2-2), displays a large range in ^{40}Ar (3.4-94.9%) relative to 04ES-00-07-04 (Table 2.2), but the flat plateau step analyses have a smaller range in ^{40}Ar (3.7-48.9%). The age range in this sample is somewhat smaller than the previous sample (36-220 Ma), with a younger total gas age of 181±1 Ma. The plateau age of 189.9±1.3 Ma (Figure 2.8C), which represents 56% of all argon released during step heating analysis, is in agreement with the inverse isochron age of 190.2±1.8 Ma (MSWD =1.17, Figure 2.8D).

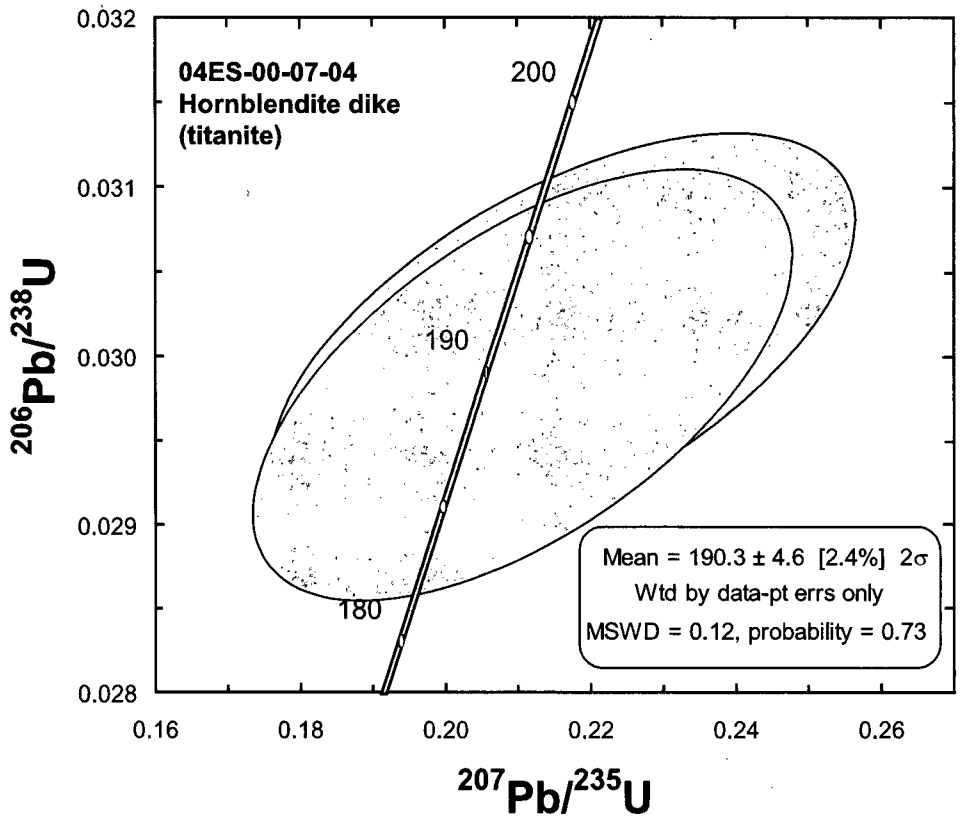

Figure 2.7: Concordia plot for U-Pb data from analyzed titanite fractions separated from a hornblendite dike (04ES-00-07-04) in the northwestern region of the Turnagain intrusion. Each ellipse (2σ error) represents the analysis of a single fraction. The results from the two analyzed fractions are concordant and nearly identical and the age is calculated from the weighted mean of their $^{206}Pb/^{238}U$ ages. The shaded gray band is the decay constant error envelope of the concordia curve.

Table 2.2: 40Ar/39Ar step-heating results of mineral separates from ultramafic rocks of the Turnagain intrusion

Laser Power (%)	$^{40}Ar/^{39}Ar$	2σ	$^{38}Ar/^{39}Ar$	2σ	$^{37}Ar/^{39}Ar$	2σ	$^{36}Ar/^{39}Ar$	2σ	$^{40}Ar^*/^{39}Ar$	2σ	$\%^{40}Ar^*$	Age (Ma)	2σ	Ca/K	Cl/K	$f^{39}Ar$
04ES-00-07-03 - wehrlite (phlogopite separate)																
J = 0.009579±0.000012																
Volume ^{39}ArK = 681.36																
Integrated Date = 181.08±0.99																
2	167.703	0.020	0.122	0.081	0.736	0.034	0.546	0.036	8.559	5.177	94.91	142.2	82.7	7.40	0.001	0.46
2.2	20.646	0.012	0.027	0.099	0.277	0.022	0.064	0.036	2.121	0.652	89.74	36.3	11.0	2.78	0	2.89
2.4	14.667	0.013	0.021	0.049	0.122	0.022	0.037	0.038	3.852	0.427	73.78	65.4	7.1	1.22	0	4.49
2.6	11.511	0.012	0.018	0.073	0.070	0.030	0.019	0.055	5.897	0.322	48.87	99.1	5.3	0.700	0	3.95
2.8	13.320	0.015	0.014	0.066	0.034	0.040	0.007	0.085	11.413	0.251	14.52	187.2	3.9	0.343	0	9.38
3	12.567	0.016	0.013	0.046	0.028	0.024	0.003	0.064	11.664	0.199	7.40	191.1	3.1	0.284	0	10.96
3.2	12.982	0.006	0.014	0.046	0.022	0.029	0.005	0.067	11.603	0.123	10.83	190.1	1.9	0.218	0	11.84
3.4	12.007	0.005	0.013	0.040	0.019	0.023	0.002	0.097	11.586	0.070	3.73	189.9	1.1	0.194	0	24.26
3.5	12.698	0.005	0.013	0.039	0.019	0.031	0.002	0.088	12.294	0.073	3.41	200.8	1.1	0.195	0	19.59
3.6	13.514	0.006	0.012	0.056	0.025	0.028	0.002	0.219	13.025	0.142	3.85	212.1	2.2	0.258	0	7.89
3.8	14.475	0.008	0.014	0.062	0.074	0.020	0.007	0.152	12.445	0.336	14.23	203.2	5.2	0.754	0	3.27
4.1	17.217	0.012	0.015	0.207	0.120	0.054	0.013	0.245	13.599	0.934	21.21	220.9	14.3	1.22	0	1.02
04ES-00-07-04 - hornblendite (amphibole separate)																
J = 0.009575±0.000012																
Volume ^{39}ArK = 510.3																
Integrated Date = 190.92±1.36																
2	1833.924	0.054	1.161	0.080	2.692	0.069	5.916	0.059	107.792	41.445	94.15	1279	352.3	23.8	0.01	0.06
2.2	697.442	0.038	0.481	0.137	2.625	0.059	2.140	0.051	73.620	22.806	89.50	962.5	223.8	23.2	0.016	0.09
2.4	262.083	0.054	0.190	0.112	2.984	0.060	0.812	0.069	25.934	10.879	90.16	400.2	150.5	26.4	0.006	0.16
2.6	99.042	0.019	0.085	0.223	2.069	0.056	0.304	0.086	10.938	7.627	89.00	179.7	119.3	18.3	0.003	0.26
2.8	62.693	0.027	0.055	0.199	1.794	0.035	0.190	0.069	7.632	3.653	87.87	127.2	58.8	15.9	0.001	0.44
3	50.628	0.015	0.026	0.477	1.414	0.039	0.133	0.055	12.213	2.122	75.96	199.5	32.8	12.5	-0.003	0.55
3.2	36.948	0.016	0.032	0.106	1.220	0.030	0.091	0.038	10.733	0.967	71.05	176.5	15.2	10.8	0	0.8
3.4	23.810	0.011	0.026	0.102	1.762	0.021	0.051	0.052	9.376	0.788	60.77	155.1	12.5	15.6	0	1.15
3.6	15.387	0.011	0.020	0.098	3.645	0.018	0.019	0.083	10.787	0.488	30.28	177.3	7.7	32.3	0.001	2.64
3.8	12.730	0.017	0.019	0.030	3.316	0.019	0.007	0.067	11.490	0.252	10.22	188.3	3.9	29.4	0.001	14.32
4	11.959	0.009	0.018	0.043	3.832	0.015	0.005	0.105	11.522	0.194	4.20	188.8	3.0	33.6	0.001	9.35
4.3	11.887	0.012	0.018	0.036	3.520	0.016	0.004	0.053	11.589	0.157	3.04	189.8	2.4	30.9	0.001	15.5
4.6	11.814	0.010	0.018	0.034	3.346	0.015	0.004	0.106	11.560	0.175	2.67	189.4	2.7	29.3	0.001	14.04
4.9	11.809	0.011	0.017	0.043	3.146	0.015	0.004	0.079	11.650	0.151	1.85	190.8	2.3	27.6	0.001	16.28
5.2	11.783	0.012	0.018	0.033	3.262	0.016	0.004	0.095	11.652	0.170	1.63	190.8	2.7	28.6	0.001	15.93
5.8	11.973	0.008	0.018	0.058	3.459	0.015	0.005	0.120	11.610	0.188	3.55	190.2	2.9	30.3	0.001	8.44

Measured values of $^{40}Ar/^{39}Ar$, $^{38}Ar/^{39}Ar$, $^{37}Ar/^{39}Ar$, and $^{40}Ar^*/^{39}Ar$ are shown for each increment of step-heating.
All errors are absolute
*Indicates atmospheric argon
Volumes are 1E-13 cm^3 NPT

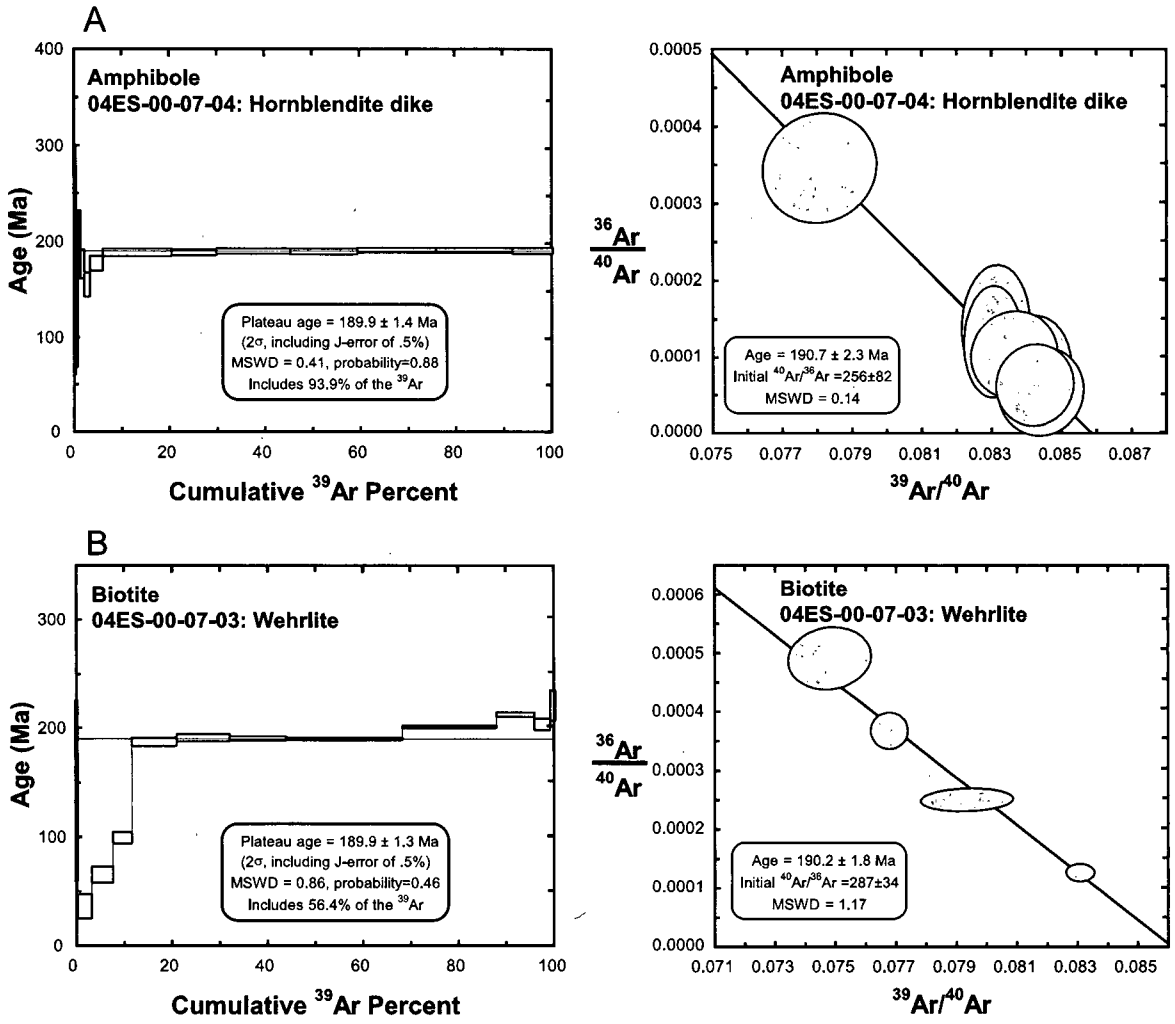

Figure 2.8: $^{40}Ar/^{39}Ar$ incremental-heating age spectra and $^{40}Ar/^{39}Ar$ inverse isochron diagrams for mineral separates from the Turnagain intrusion. A) Results for amphibole separated from a hornblendite dike (04ES-00-07-04) sampled from the northwestern part of the intrusion. B) Results for phlogopite separated from a wehrlite (04ES-00-07-03) sampled in the southeastern part of the Turnagain intrusion (southern Hatzl Zone).

The plateau age obtained above is considered to represent the minimum crystallization age of the wehrlite when the rock cooled through the closure temperature to Ar diffusion in phlogopite (see Discussion).

2.5.3 Rare Earth Elements and Nd Isotopes

The Sm-Nd isotopic compositions of eight whole rock samples from the Turnagain intrusion were determined in this study. With respect to rare earth element (REE) concentrations (Table 2.3), the samples have broadly subparallel chondrite-normalized patterns with prominent LREE-depletion for the ultramafic rocks (Figure 2.9A). The leuco-diorite and the volcanic wacke exhibit distinctive LREE-enriched chondrite-normalized patterns (Figure 2.9B). The volcanic wacke, as well as the samples of Erdmer *et al.* (2005), fall within or bracket the REE range established for the Lay Range Assemblage (Ferri, 1997) and Klinkit Group (Simard *et al.*, 2003) (Figure 2.9B). $(La/Yb)_{cn}$ values in ultramafic rocks range from 0.27-2.0, with the volcanic wacke and hornblende diorite samples exhibiting $(La/Yb)_{cn}$ values of 3.9 and 1.9, respectively. The samples analyzed for Nd isotopes (Table 2.4) show a wide range of concentrations (Sm = 0.6-6 ppm, Nd = 1.3-18.5 ppm), variable Sm/Nd values (0.33-0.45), a wide range in $^{143}Nd/^{144}Nd$ (measured) from 0.512440 to 0.512997, and do not exhibit an isochron relationship (Figure 2.10A). The majority of Turnagain samples have $\varepsilon_{Nd(190)}$ values between +1.9 and +5.9 (05ES-05-04-01), whereas one sample (hornblende clinopyroxenite) exhibits a moderately negative $\varepsilon_{Nd(190)}$ at -3.4 (Figure 2.10B).

2.6 DISCUSSION

2.6.1 Age and Source of the Turnagain Intrusion

The Turnagain intrusion is a composite mafic-ultramafic pluton that contains a range of lithologies from dunite to diorite (plagioclase + amphibole). Field relationships, and mineral and whole rock geochemistry (see Chapter 4) indicate the following general crystallization sequence: dunite → wehrlite → olivine clinopyroxenite → hornblende clinopyroxenite → hornblendite → diorite. The Ar-Ar phlogopite date from the wehrlite (189.9±1.3 Ma) from the mineralized Hatzl Zone and the Ar-Ar hornblende date from the hornblendite (189.9±1.4 Ma) from the northwestern part of the Turnagain intrusion are identical within error and represent the ages of closure to Ar diffusion (i.e. cooling ages) at ~450°C (phlogopite) and ~575°C (hornblende) (closure temperatures from Hodges, 2003; and references therein). Titanite from

Table 2.3: Major (wt. % oxide) and trace (ppm) element abundances in whole rock samples from the Turnagain intrusion

Rock Type:	Olivine Cpxite	Cpxite	Cpxite	Hbl Cpxite	Hblite	Hblite	Wacke	Diorite
Sample Prefix:	05ES	05ES	05ES	04ES	05ES	04ES	04ES	DDH04
Sample #:	05-01-01	05-04-01	03-01-02	09-02-02	05-06-02	00-07-04	00-07-02	57-12-89.2
Oxides (wt. %)								
SiO_2	51.23	48.99	49.04	47.14	38.53	41.93	49.67	53.56
TiO_2	0.20	0.38	0.29	0.75	2.32	2.16	0.80	0.29
Al_2O_3	1.05	2.21	2.07	4.20	12.06	12.21	16.19	20.82
Fe_2O_3*	7.45	7.65	8.55	11.64	15.51	14.30	10.01	4.14
MgO	22.45	18.65	20.30	16.46	12.99	11.95	4.86	3.60
MnO	0.13	0.15	0.19	0.16	0.21	0.26	0.20	0.09
CaO	17.26	19.12	15.25	16.04	13.85	11.62	9.82	7.68
Na_2O	0.17	0.20	0.17	0.63	0.67	0.78	3.57	6.02
K_2O	0.10	0.08	0.11	0.40	0.32	0.89	1.86	1.17
P_2O_5			0.03	0.14	0.01	0.31	0.37	0.19
LOI		2.20	3.37	2.35	3.31	2.80	1.88	2.12
Total	99.34	99.65	99.36	99.92	99.78	99.20	99.23	99.68
S	0.42	0.04	0.33	1.08	0.14	0.35	0.31	0.10
Mg #:	0.857	0.829	0.825	0.737	0.624	0.624	0.491	0.633
Trace Elements (ppm)								
Co	98	59	56	151	85	66	30	15
Cr	3200	1480	2690	1320	38	404	79	11
Cu	292	292	47	249	133	84	101	12
Ni	511	173	56	130	132	136	20	9
Sc	55.4	68.1	41.8	68.8	69.3	73.7	36.1	12.9
V	81	147	265	343	645	492	291	110
Zn	18	20	57	49	69	99	74	29
Rb				3		12.0	28	11
Ba	1	12	36	35	69	422	700	1980
Th			0.29	0.17	0.10	0.36	1.54	0.07
U			0.16	0.08	0.06	0.12	0.21	0.09
Ta				0.1		0.2	0.3	0.1
Nb		0.3	0.5	1.8	1.6	3.9	4.1	2.3
La	0.19	0.52	1.56	4.47	2.11	6.61	10.50	1.50
Ce	0.8	2.0	3.8	14.5	7.0	20.5	21.6	3.4
Pb		5		13	34	36	12	5
Pr	0.18	0.41	0.64	2.57	1.40	3.35	2.65	0.52
Sr	35	71	60	62	336	284	949	2808
Nd	1.33	2.64	3.60	12.60	8.64	18.25	11.60	2.62
Zr	2	7	12	14	30	49	38	17
Hf		0.3	0.4	0.7	1.3	2.1	1.4	0.7
Sm	0.60	1.04	1.16	3.69	3.26	5.95	2.99	0.80
Eu	0.204	0.318	0.277	0.928	1.310	1.845	1.020	0.386
Gd	0.80	1.31	1.36	3.62	4.10	7.18	3.21	0.86
Tb	0.15	0.25	0.25	0.63	0.76	1.33	0.56	0.15
Dy	0.92	1.57	1.56	3.49	4.74	7.91	3.42	0.95
Ho	0.18	0.31	0.31	0.65	0.97	1.62	0.70	0.19
Er	0.49	0.86	0.90	1.84	2.79	4.54	2.13	0.57
Tm	0.07	0.12	0.13	0.26	0.39	0.65	0.31	0.09
Yb	0.44	0.74	0.81	1.49	2.25	3.82	1.82	0.53
Lu	0.053	0.100	0.108	0.193	0.310	0.530	0.287	0.073
Y	5	10	8	19	28	42	19	4

Note: Blank entries represent values that were below detection limits.
Abbreviated rock types: cpxite (clinopyroxenite), hblite (hornblendite)
Mg# = Mg/(Mg+Fe) assuming all iron as Fe^{2+}

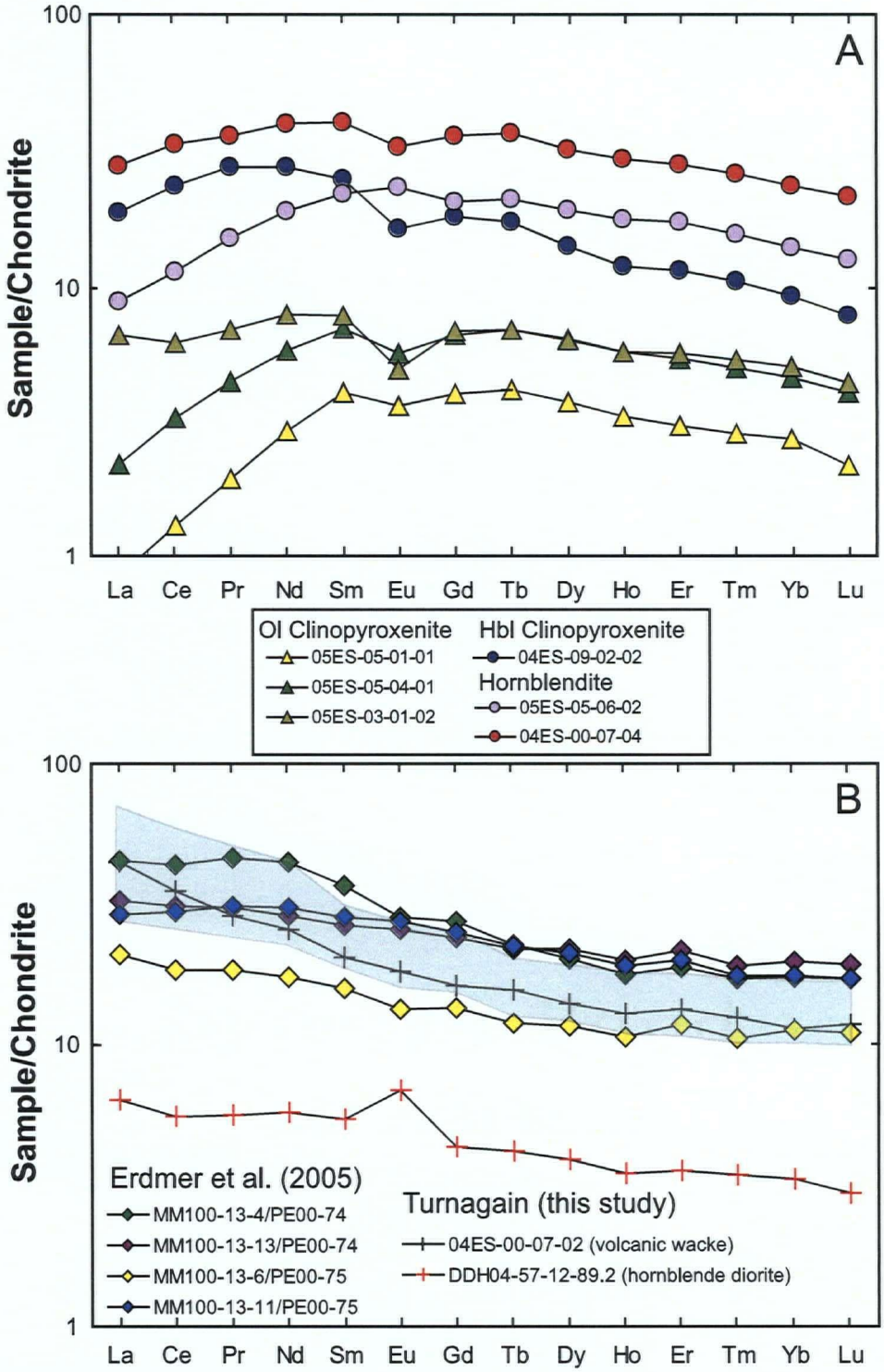

Figure 2.9: Chondrite-normalized rare earth element diagrams for whole rock samples from the Turnagain intrusion, and whole rock samples of mafic to intermediate volcanics from Erdmer *et al.* (2005) for comparison (normalizing values from McDonough & Sun, 1995). Note the wide range in concentrations of the rare earth elements from olivine clinopyroxenite to hornblendite, the broadly sub-parallel patterns with prominent LREE-depletion for the ultramafic rocks, and the distinctive LREE-enriched pattern for the hornblende diorite and the volcanic wacke. Note also that the volcanic wacke and the Erdmer *et al.* (2005) samples plot in or near the range of the Lay Range Assemblage (after Ferri, 1997).

Table 2.4: Nd isotopic compositions of whole-rock samples from the Turnagain intrusion

Sample No.	Rock Type	Sm (ppm)	Nd (ppm)	$^{143}Nd/^{144}Nd$	2σ	$^{147}Sm/^{144}Nd$	$^{143}Nd/^{144}Nd$ (190 Ma)	ε_{Nd} (0)	ε_{Nd} (190 Ma)	T_{CHUR} (Ma)	T_{DM} (Ma)
05ES-05-01-01	clinopyroxenite	0.175	0.41	0.512997	0.000008	0.2581	0.512676	7.0	5.5	891	-
05ES-05-04-01	clinopyroxenite	1.04	2.64	0.512993	0.000010	0.2382	0.512697	6.9	5.9	1300	-
05ES-03-01-02	clinopyroxenite	1.16	3.60	0.512754	0.000008	0.1948	0.512511	2.3	2.3	-	3175
04ES-09-02-02A (a)	hbl clinopyroxenite	3.69	12.6	0.512442	0.000005	0.1770	0.512222	-3.8	-3.3	1522	2924
04ES-09-02-02A (b)	hbl clinopyroxenite	3.69	12.6	0.512438	0.000007	0.1770	0.512218	-3.9	-3.4	1557	2942
05ES-05-06-02 (a)	hornblendite	3.26	8.64	0.512892	0.000004	0.2281	0.512608	4.9	4.2	1225	-
05ES-05-06-02 (b)	hornblendite	3.26	8.64	0.512900	0.000004	0.2281	0.512617	5.1	4.4	1266	-
04ES-00-07-04	hornblendite	5.95	18.3	0.512738	0.000005	0.1971	0.512493	1.9	1.9	-	3751
DDH04-57-12-89.2	diorite	0.800	2.62	0.512865	0.000007	0.1846	0.512641	4.4	4.8	-	1490
04ES-00-07-02 (a)	volcanic wacke	2.99	11.6	0.512693	0.000008	0.1558	0.512499	1.1	2.1	-	1202
04ES-00-07-02 (b)	volcanic wacke	2.99	11.6	0.512695	0.000006	0.1558	0.512501	1.1	2.1	-	1197
GSP-2 (n=14)	reference			0.511374	0.000011						

Hornblende has been abbrieviated to hbl
Concentrations of Sm and Nd were measured by ICP-MS
T_{CHUR} and T_{DM} ages with hyphens represent either negative ages or unreasonably large ages

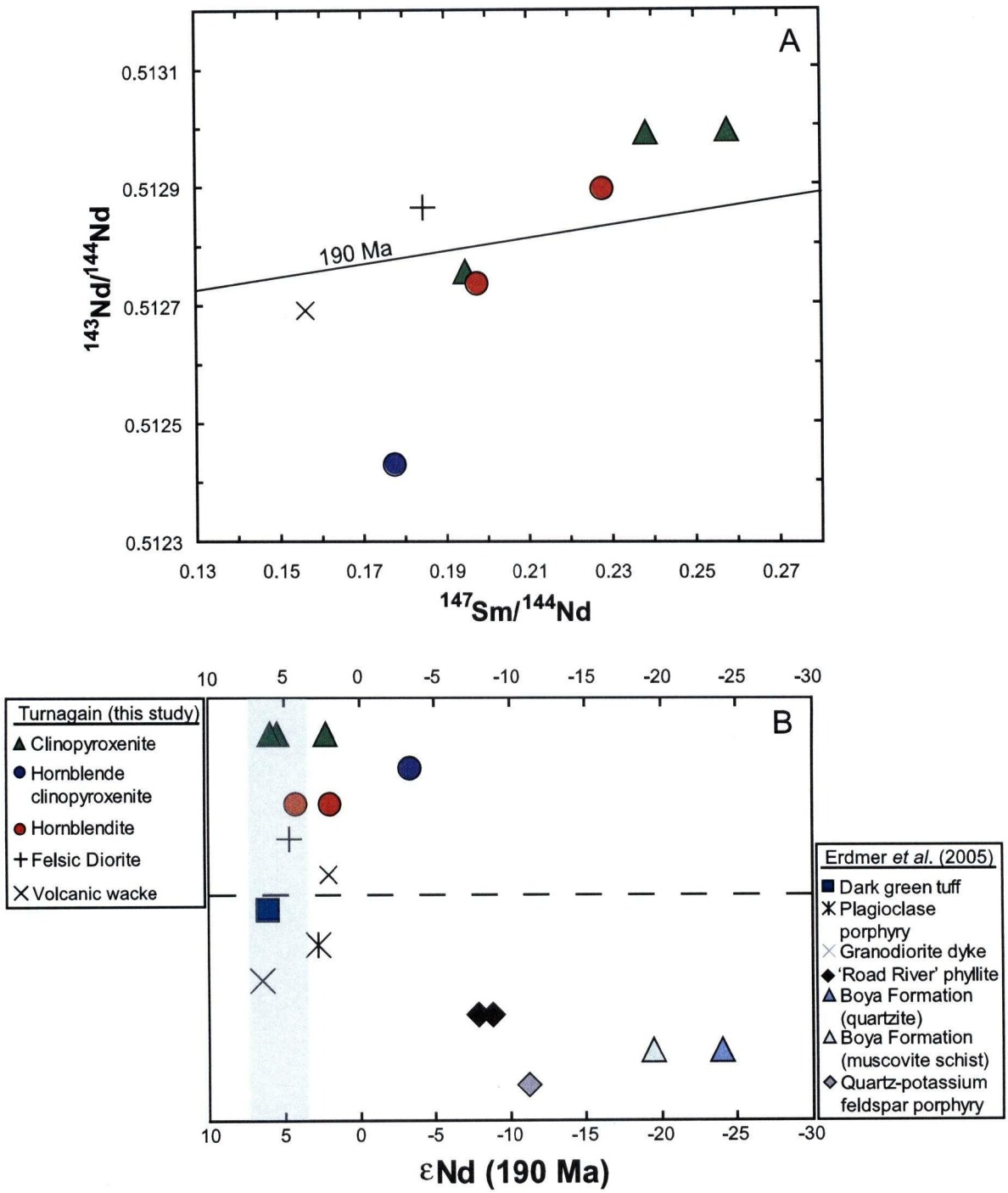

Figure 2.10: Nd isotopic geochemistry of whole-rock samples from the Turnagain intrusion. A) $^{143}Nd/^{144}Nd$ vs. $^{147}Sm/^{144}Nd$ with a 190 Ma reference isochron. Symbol size is greater than the 2σ error for each analysis. B) Initial ε_{Nd} vs. rock type. The upper portion of the diagram illustrates the range in initial ε_{Nd} in Turnagain lithologies and the lower portion shows results from Erdmer *et al.* (2005), recalculated at 190 Ma, for samples collected ~10 km southeast of the Turnagain intrusion. The light blue field represents the range of ε_{Nd} for mafic volcanic rocks from Yukon-Tanana (from Piercey *et al.*, 2006).

the same hornblendite sample yields a date of 190.3±4.6 Ma (Figure 2.7), which represents the time of closure to Pb diffusion in titanite (~650°C) (Cherniak, 1993; Frost *et al.*, 2000). All three dates from the ultramafic rocks of the Turnagain intrusion are identical within error and correspond to a range of closure temperatures for the respective minerals and isotopic systems from 650°C down to 450°C, which is consistent with relatively rapid cooling of the Turnagain intrusion following emplacement and crystallization. Based on these three dates, the age of crystallization and cooling of ultramafic rocks from the Turnagain intrusion is 189.9±0.9 Ma (n=3, weighted mean age, 2σ).

The mela-diorite sample (04ES-00-07-01) exhibits gradational contacts with hornblendite, but intrudes dunite (Figure 2.3). The closure temperature for Pb diffusion in zircon is >900°C (Cherniak & Watson, 2000), which is likely to be higher than the temperature of the fractionated hydrous melt from which the zircon in this sample precipitated; thus the U-Pb zircon date for this sample can be interpreted as a crystallization age. As noted previously, all analyzed zircon in this sample appears to have lost Pb since the time of crystallization. Based on the oldest least discordant fraction (Fraction B), the mela-diorite has a minimum crystallization age of 189.2±0.6 Ma (Figure 2.5A), which is identical within error to the weighted mean Ar-Ar (phlogopite, hornblende) and U-Pb (titanite) age noted above. The absolute crystallization age of the Turnagain intrusion is inferred to be 189.4±0.5 Ma based on a weighted mean of Fraction B from the mela-diorite and the Ar-Ar and U-Pb titanite ages referred to above.

The 185.2±0.3 Ma U-Pb zircon age of the leuco-diorite (DDH-04-57-12-89) is approximately 4.5 million years younger than the crystallization age of the Turnagain intrusion established above. This younger age can be interpreted as (1) the true crystallization age of the leuco-diorite, thus implying an extended period of magmatism in the formation of the Turnagain intrusion; or (2) a function of Pb loss from zircon in this sample. Field and petrographic relations suggest that the leuco-diorite is an integral part of the 190 Ma ultramafic and mafic rocks of the Turnagain intrusion. The first interpretation is consistent with the observation that late dioritic dikes are a common feature of many Alaskan-type intrusions (e.g. Lunar Creek; Nixon *et al.*, 1997). In addition, a diorite to granodiorite composite pluton ~5 km to the east-southeast of the Turnagain intrusion (Figure 2.2), a body considered to be a small ultramafic 'Ring Complex' genetically related to the Turnagain intrusion (Clark, 1975), was recently dated by Erdmer *et al.* (2005) at 187.5±2.9 Ma (U-Pb zircon). This age overlaps both

the ages of the leuco-diorite and the ultramafic rocks of the Turnagain intrusion. The composite Ring Complex is described by Erdmer *et al.* (2005) as a "medium-grained hornblende granodiorite to tonalite-diorite," which suggests that it may be a similar lithology to the mela-diorite of the Turnagain intrusion. The date of the granodiorite is a lower intercept age with concordia based on three of the five analyzed fractions (see Fig. 5 of Erdmer *et al.*, 2005). However, the oldest analyzed fraction (not used in the above regression) is concordant and yields a $^{206}Pb/^{238}U$ age of 192.4±0.8 Ma, thus it is possible that this hornblende granodiorite may be several million years older that its proposed crystallization age of 187.5±2.9 Ma. The second interpretation of the age of the leuco-diorite from the Turnagain intrusion – Pb-loss from zircon after crystallization at ca. 190 Ma – is based on the observation of Pb-loss in all zircon fractions from the mela-diorite (sample 04ES-00-07-01) and the field and petrographic characteristics of the leuco-diorite sample. The hornblende diorite contains coarse (up to 1 cm in width) euhedral crystals of plagioclase and amphibole, interpreted to be cumulus phases that crystallized from an evolved plagioclase-amphibole-saturated magma late in the crystallization history of the Turnagain intrusion. The drillcore from which the sample was collected contains 9 metres of alternating plagioclase-rich and amphibole-rich bands, perhaps representing a layered sequence of cumulate rocks. These observations require the leuco-diorite to have crystallized at the same time as the other dated samples, thus the obtained age of 185.2±0.3 Ma is most likely a function of Pb-loss from zircon following crysallization.

The Mg-rich olivine ($Fo_{92.5}$) of some Turnagain dunites indicate that the Turnagain magmas equilibrated with peridotitic mantle (with respect to major elements). However, the Nd isotopic composition of all lithologies in the Turnagain intrusion ($\varepsilon_{Nd(190)}$= +5.9 to -3.3) indicates that the intrusion was variably contaminated with continental crust (depleted mantle $\varepsilon_{Nd(190Ma)}$ = +9 to +10; DePaolo & Wasserburg, 1976). The most positive $\varepsilon_{Nd(190)}$ results are consistent with the range observed in Paleozoic mafic volcanic rocks in Yukon-Tanana (Piercey *et al.*, 2006). The Nd isotopic compositions of the graphitic phyllite (Erdmer *et al.*, 2005) and the volcanic wacke (this study) both indicate (respectively) their origin from, and contamination with, continental crust (Figure 2.10). The variable $\varepsilon_{Nd(190)}$ of the analyzed ultramafic samples may reflect heterogeneous assimilation of the volcanic wacke and the graphitic phyllite, both of which are found as partially digested inclusions in the Turnagain intrusion.

2.6.2 Age Comparison with other Alaskan-type Intrusions

The mineralogy and mineral compositions of Alaskan-type intrusions suggest that they form from relatively hydrous, alkalic to subalkalic, primitive picritic/ankaramitic magmas (Irvine, 1974; Hernandez, 2000; Mossman *et al.*, 2000; Spandler *et al.*, 2003; Green *et al.*, 2004; Batanova *et al.*, 2005) in arc settings. The ages of Alaskan-type intrusions, therefore, are important for understanding the temporal evolution of arc systems. This is particularly relevant to the Cordilleran orogeny of B.C., Yukon, and southeastern Alaska, which consists of numerous accreted allochthonous and parautochthonous terranes (e.g. Monger *et al.*, 1982; Schermer *et al.*, 1984; Gabrielse & Yorath, 1991; Colpron *et al.*, 2006) (Figure 2.1). The published and reported ages of Alaskan-type intrusions in B.C. and southeastern Alaska are compiled in Table 2.5 and shown with respect to terranes in Figure 2.11. Of the 9 known Alaskan-type intrusions in B.C. and 39 in southeastern Alaska, only 12 have been dated; mostly by the K-Ar method during the 1960s. Prior to this study, the only precise U-Pb zircon ages of Alaskan-type intrusions in B.C. and Alaska were reported by Saleeby (1992), Rubin & Saleeby (1992), Rublee (1994), and Nixon *et al.* (1997) (Duke Island, Union Bay, Tulameen, and Lunar Creek+Polaris, respectively). There are two important observations that can be made regarding the age distribution of Alaskan-type intrusions (see Figure 2.1 for terrane locations). Firstly, there are four age groups: ~435-400 Ma, ~240-205 Ma, ~195-185 Ma, and ~125-100 Ma. The oldest (Silurian-Devonian) and youngest (Cretaceous) age groups are found in the Alexander terrane, whereas the intermediate age groups (Triassic-Jurassic) are found in Stikinia and Quesnellia (Figure 2.1). Secondly, the ~240-205 Ma intrusions are observed in both Stikinia and Quesnellia, whereas the ~195-185 Ma intrusions are found only in Quesnellia.

Alaskan-type intrusions in B.C. and southeastern Alaska also exhibit an age distribution relative to their host rocks. The oldest group of intrusions (Salt Chuck, Dall Island, and Sukkwan Island) intrude older gabbroic plutons as well as the Descon Formation (lower Paleozoic metavolcanic and metasedimentary rocks; e.g. Rubin & Saleeby, 1992), which is unconformably overlain by the Gravina (Upper Jurassic-Lower Cretaceous metavolcanic and metasedimentary rocks) and Alva (upper Paleozoic-lower Mesozoic metabasalt, marble, and argillite) sequences. The youngest age group is also dominantly hosted by the Descon Formation, however the Union Bay intrusion is hosted by the overlying Gravina sequence (Rubin & Saleeby, 1992). This implies that the youngest age group of intrusions were

Table 2.5: Compilation of isotopic dates for Alaskan-type intrusions in British Columbia and southeastern Alask

Terrane	Intrusion	Rock Type	Method (Mineral)	Age (Ma)	Uncertainty (2σ)	Host Lithology	Reference
Quesnellia	*Turnagain*	Wehrlite	Ar-Ar (phlogopite)	189.9	1.3	"Road River" phyllite,	This study
		Hornblendite dike	Ar-Ar (hornblende)	189.9	1.4	Lay Range Assemblage	
		Hornblendite dike	U-Pb (titanite)	190.3	4.6		
		Mela-diorite	U-Pb (zircon)	189.2	0.6		
		Leuco-diorite	U-Pb (zircon)	185.2	0.3		
	Ring Complex[1]	diorite	U-Pb (zircon)	187.5	2.9	"Road River" phyllite	Erdmer *et al.*, 2005
	Lunar Creek	K-spar pegmatite	U-Pb (zircon)	237	2	Takla Group	Nixon *et al.*, 1997
		Cross-cutting dike	K-Ar (hornblende)	190	8		Gabrielse *et al.*, 1980
		Cross-cutting dike	K-Ar (hornblende)	182	13		Gabrielse *et al.*, 1980
	Wrede Creek	Hornblende pegmatite	K-Ar (hornblende)	219	20	Takla Group	Wong *et al.*, 1985
		Hornblende pegmatite	K-Ar (hornblende)	225	16		
	Johansson Lake	Coase hornblendite	K-Ar (hornblende)	232	13	Takla Group	Stevens *et al.*, 1982
	Polaris	Qtz-hbl-plag pegmatite	U-Pb (zircon)	186	2	Lay Range Assemblage	Nixon *et al.*, 1997
		Peridotite	K-Ar (biotite)	167	9		Wanless *et al.*, 1968
		Peridotite	K-Ar (hornblende)	156	15		Wanless *et al.*, 1968
	Tulameen	Syenodiorite	U-Pb (zircon)	209.9	4.7	Nicola Group	Rublee, 1994
		Hornblende clinopyroxenite	K-Ar (hornblende)	208	*20		Nixon *et al.*, 1997 -refs therein
		Hornblende clinopyroxenite	Ar-Ar (hornblende)	196	*15		Nixon *et al.*, 1997 -refs therein
Stikinia	*Gnat Lakes*	Hornblendite	K-Ar (hornblende)	230	10	Stuhini Group	Stevens *et al.*, 1982
		Hornblende clinopyroxenite	K-Ar (hornblende)	227	14		
Alexander	*Duke Island*	Gabbro	U-Pb (zircon)	109.5	1.5	Descon Formation	Saleeby, 1992
		Hornblendite	Ar-Ar (hornblende)	118.5	10		Meen *et al.*, 1991
	Union Bay	Gabbro pod in hornblendite	U-Pb (zircon)	101.9	0.6[2]	Gravina Sequence	Rubin & Saleeby, 1992
	Salt Chuck	Biotite clinopyroxenite	K-Ar (biotite)	429	11	Descon Formation	Loney *et al.*, 1987
	Dall Island[3]			401.1	*20	Descon Formation	Himmelberg & Loney, 1995 -refs therein
	Sukkwan Island[3]			440.5	*20	Descon Formation	Himmelberg & Loney, 1995 -refs therein

[1] The Ring Complex, originally described by Clark (1975), was interpreted to be ultramafic in nature (based on aeromagnetic results). However subsequent mapping by Erdmer *et al.*, 2005, and the principal author, showed that the Ring Complex is a diorite pluton that intruded phyllites of the Road River Group. See Discussion for details

[2] Conservative estimate of error on $^{206}Pb/^{238}U$ age

[3] Age of intrusion derived from a personally communicated age to the refered authors, such that no specific data are available

* These uncertainties are conservative estimates - no uncertainties are given by the original authors

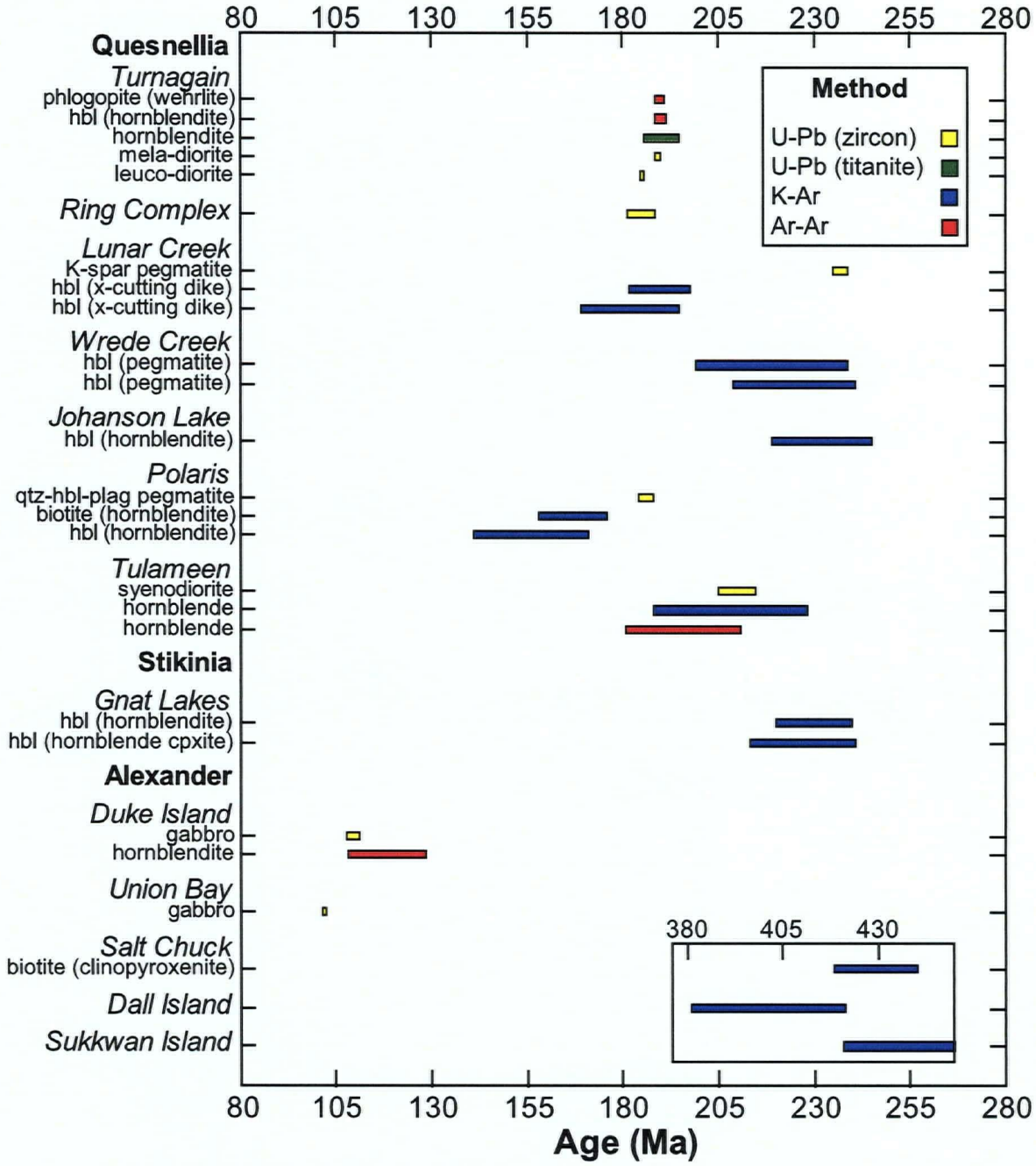

Figure 2.11: Compilation of ages of Alaskan-type intrusions in B.C. and southeastern Alaska arranged from north to south (top to bottom) with each bar representing the age with its associated analytical uncertainty (2σ), its dating method and mineral dated. References for the above ages are found in Table 2.5.

emplaced through both the Descon Formation and the Gravina sequence, and that a second arc was built upon a preexisting, extinct, arc. The Triassic intrusions (~240-205 Ma) are typically hosted in the Takla (Monger, 1977) and Nicola (e.g. Shau, 1970) Groups, which are Triassic packages of volcanic rocks that occur in Quesnellia and Stikinia (Dostal *et al.*, 1999). The Gnat Lakes Alaskan-type intrusion, however, is hosted in the Stuhini Group in Stikina, and Stuhini Group, Takla Group, and Nicola Group are considered to be coeval (Dostal *et al.*, 1999). The Jurassic (~195-185 Ma) group of intrusions is represented by the Polaris and Turnagain intrusions, which have similar crystallization ages (186±2 Ma, 190±1 Ma, respectively) and host rocks. The Polaris intrusion is hosted in the Lay Range Assemblage, which has been correlated with the Harper Ranch Subterrane and the Klinkit Group (e.g. Ferri, 1997) and is proximal to the Upper Proterozoic Ingenika Group, whereas the Turnagain is hosted by graphitic phyllites (possibly the Road River Formation and Earn Group) and volcanic wacke that possibly correlates to the Lay Range Assemblage (see next section).

The apparent 10 million year gap, based on the few reliable U-Pb dates, between the Late to Middle Triassic and Early Jurassic intrusions may be related to (1) a period of quiescence in arc magmatism, or (2) an artifact of the lack of geochronological data. Monger & Church (1977) constrain the biostratigraphic age of the Takla Group from late Carnian to early Norian (~220 to 230 Ma using the time scale of Okulitch, 1999). In addition, a Late Triassic angular unconformity with the overlying Early Jurassic Rossland Group, a package of volcanic rocks (with lateral facies changes gradational with limestone and epiclastic rocks) that are texturally and mineralogically similar to the Nicola Group, is observed in southern Quesnellia (Beatty *et al.*, 2006). This succession is inferred to represent the uplift and erosion of the Nicola Group followed by eastward-shifted renewed arc magmatism (overlying Rossland Group) at ~195 Ma (Parrish and Monger, 1992). The older biostratigraphic age of the Takla Group, in comparison to the Late Triassic Alaskan-type intrusions, may indicate that its top has been removed by erosion. The youngest Alaskan-type intrusions, found at the easternmost extent of Quesnellia (Figure 2.1), may corroborate the eastward shift of arc magmatism in Quesnellia during the Early Jurassic. However, the number of precisely-dated Alaskan-type intrusions in B.C. is small (n=4). The apparent time gap may therefore simply be related to the lack of dated Alaskan-type intrusions in B.C. A 185-212 Ma plutonic suite does occur in the Yukon-Tanana terrane (Mortensen, 1992), with whole-rock compositions similar to the Takla Group (Nelson *et al.*, 2006). Some plutons contain ultramafic rocks with Alaskan-

type-like lithologies but have not yet been defined as Alaskan-type bodies *per se* (J.K. Mortensen, pers. comm., 2007). There is also an absence of preserved Late Triassic or Early Jurassic volcanic rocks, but there is no apparent age gap of early Mesozoic plutonic rocks in Yukon-Tanana – presumably the basement to Quesnellia (Nelson *et al.*, 2006).

2.6.3 Tectonic Implications for Northern British Columbia

The combined ages, host lithologies, and Nd isotopic compositions of the Turnagain intrusion have implications for its tectonic setting and relation to the accreted terranes of the Canadian Cordillera. The two major host lithologies, graphitic phyllite and latest Pennsylvanian/earliest Permian volcanic wacke, are both found as inclusions in the Turnagain intrusion and appear to represent the host rocks to this fault-bounded intrusion. Based on limited fossil biochronology, the age of the Road River Formation *sensu stricto* is Early Ordivician to Middle Silurian elsewhere in B.C., and the overlying the Earn Group is Upper Devonian to Mississippian (Gabrielse, 1998). The undivided Road River and Earn Groups (as mapped by Gabrielse (1998) in the study area) are conformably overlain by volcanic and volcanosedimentary rocks that contain abundant Proterozoic inherited zircon (Figure 2.6A) and are intruded at their base by a 337 Ma porphyritic dike (Erdmer *et al.*, 2005). A gradational contact (interbedded over 5-10 m) between the graphitic phyllite and the volcanic wacke was observed in drillcore in late 2006. The age of the phyllite is uncertain, as only a few poorly preserved graptolites have been found in the Dease Lake map area (Gabrielse, 1998; and references therein).

Accreted terranes within the Canadian Cordillera, specifically the Quesnel, Stikine, and Yukon-Tanana terranes, have recently been argued to be genetically related (Nelson *et al.*, 2006), partially based on lithological similarities. For example, Alaskan-type intrusions are known in Stikinia and Quesnellia, and recent unpublished findings indicate their probable presence in Yukon-Tanana (J. Nelson, pers. comm., 2007). The association between carbonaceous phyllite and overlying volcanic/volcano-sedimentary rocks has been documented in both Quesnellia and Yukon-Tanana (Ferri & Melville, 1990; Mortensen, 1992; Ferri, 1997; Simard *et al.*, 2003; Nelson & Friedman, 2004). In Quesnellia, such volcanic-volcaniclastic rocks have been included either in the Mississippian-Permian Lay Range Assemblage or the Devonian-Middle Permian Harper Ranch Subterrane (Ferri & Melville, 1990; Ferri, 1997; Dostal *et al.*, 1999). The Lay Range Assemblage (Ferri, 1997) contains (1) a Middle Mississippian-late Middle Pennsylvanian Lower Sedimentary division, consisting

predominantly of argillite and siltstone with lesser limestone, tuff, and volcanic sandstones; and (2) an Early Permian Upper Mafic Tuff division, consisting of a variety of tuffs, agglomerates, and lavas flows. The Lay Range Assemblage is considered correlative with the Middle Mississippian-Early Permian Klinkit Group in Yukon-Tanana (Simard *et al.*, 2003; Nelson & Friedman, 2004). The Klinkit Group has been observed to tectonically overlie a succession of phyllites, grits, and tuffs of the Devonian-Middle Permian Swift River succession (Simard *et al.*, 2003; Nelson & Friedman, 2004), while the base of the Lay Range Assemblage has been observed in central B.C. by Ferri & Melville (1990) to conformably overlie carbonaceous phyllite. The base of the Harper Ranch Subterrane has not been observed (Dostal *et al.*, 1999). Other similarities between Yukon-Tanana and Quesnellia possibly include a shared Ancestral North America basement source. Erdmer *et al.* (2002) documented 313-1058 Ma detrital zircon in sedimentary rocks of the Quesnellian Nicola Horst in south-central B.C. and Untershutz *et al.* (2002) documented a mixture of primitive and evolved Nd isotopic compositions in Triassic sandstones overlying the Lay Range Assemblage. Ferri (1997) documented inherited Proterozoic zircon in Permian tuffs and lavas from the Upper Mafic Tuff division of the Lay Range Assemblage. In summary, the "Earn Group"/Snowcap Assemblage is overlain by the Klinkit Group/Lay Range Assemblage/Harper Ranch Subterrane, all of which contain detrital zircon of Proterozoic age. The Turnagain intrusion is the first documented Alaskan-type intrusion to be hosted in both Lay Range-equivalent rocks and older graphitic phyllite.

The ~300 Ma volcanic wacke, with inherited Proterozoic zircons and trace element characteristics (REE) similar to samples of the Lay Range Assemblage and the Klinkit Group (Ferri, 1997; Simard *et al.*, 2003 - Figure 9A) (Figure 2.9B), is likely a northern equivalent of the Lay Range Assemblage. The "Road River" phyllite, as assigned by Gabrielse (1998), is conformably overlain by the Lay Range Assemblage and therefore constitutes part of the same crustal block. The conformable nature of these two rock packages is broadly consistent with the first interpreted tectonic setting of the Turnagain intrusion of Nixon (1998) as outlined in the introduction, however this lithological succession cannot be part of Ancestral North America. These lithologies are intruded by the Turnagain Alaskan-type intrusion, a composite mafic-ultramafic pluton of arc affinity (see Chapter 4). No conclusive terrane assignment can be made based on the presence of Lay Range Assemblage-equivalent rocks, on the presence of an Early Jurassic arc-derived intrusion, or on the presence of Precambrian inheritance. The

results of this study demonstrate that the succession of Cambrian(?) to Permian sedimentary rocks in this part of northern B.C., intruded by the Turnagain intrusion and the Ring Complex, was at the locus of arc magmatism during the Early Jurassic. If the assignment of the graphitic phyllite to the Road River/Earn Groups (Gabrielse, 1998) is correct, then the conclusions of Erdmer *et al.* (2005) – that an Early Jurassic subduction zone existed beneath Ancestral North America – are correct. However, if the graphitic phyllites are in fact part of the Snowcap assemblage or equivalents, then the lithologies around the study area are part of Yukon-Tanana or Quesnellia.

2.7 CONCLUSION

The principal results from this geochronological study of the Turnagain Alaskan-type intrusion and host rocks in north-central British Columbia are 1) the crystallization age of mafic and ultramafic phases in the Turnagain intrusion, as determined by U-Pb (zircon, titanite) and Ar-Ar (phlogopite, amphibole) geochronometry, is 190±1 Ma, 2) the range of whole rock Nd isotopic compositions from the Turnagain intrusion is $\varepsilon_{Nd(190)}$ = +6 to +2 with a hornblende clinopyroxenite sample extending to $\varepsilon_{Nd(190)}$ = -3, indicating variable amounts of crustal contamination of mantle-derived parental magmas in an arc setting, 3) the minimum depositional age of the youngest host rocks to the Turnagain intrusion is 301 Ma (U-Pb zircon), or latest Pennsylvanian-earliest Permian, and 4) the hosting volcanic wacke in the study area, based on its age, REE geochemistry, and lithological similarities with other rocks in B.C. and Yukon, is equivalent to the Lay Range Assemblage, which is considered to be the basement to the Quesnellia terrane. The Turnagain intrusion, which intrudes the volcanic wacke and graphitic phyllite, is indicative of the presence of an Early Jurassic subduction zone in the study area and constrains the terrane assessment of the study area to be either Quesnellia or Yukon-Tanana. The association of other Alaskan-type intrusions in Quesnellia with the Lay Range Assemblage/Harper Ranch Subterrane is well-established, and may indicate the presence of unidentified Alaskan-type intrusions in the Klinkit Group of Yukon-Tanana, which would further support the proposed genetic relationships between Yukon-Tanana and Quesnellia.

2.8 ACKNOWLEDGEMENTS

We would like to thank a number of individuals at the Pacific Centre for Isotopic and Geochemical Research, University of British Columbia, Vancouver: Rich Friedman for U-Pb TIMS chemistry and analyses, and his continuous input into data interpretation for this manuscript; Tom Ullrich for Ar-Ar analyses; Gwen Williams and Bruno Keiffer for sample preparation, digestion, and Nd isotopic analyses; and Dominique Weis for assistance in the interpretation of the Nd isotopic results. Jim Mortensen, Luke Baranek, and Reza Tafti are thanked for sharing their opinions and ideas concerning northern B.C. tectonics, and Katrin Breitsprecher for her helpful comments on this manuscript. The authors are grateful to Hard Creek Nickel Corp. for continued field support for this project and to Jim Reed of Pacific Western Helicopters for his exemplary logistical support in the field. Special thanks to Tony Hitchins, Bruce Northcote, Chris Baldys, and Mark Jarvis (President) of Hard Creek Nickel Corp. for their generous support and interactions throughout the period of the principal author's M.Sc. thesis at UBC. Funding for this project was provided by a research grant from Hard Creek Nickel Corp. (formerly Canadian Metals Exploration Ltd.).

2.9 REFERENCES

Batanova, V.G., Pertsev, A.N., Kamenetsky, V.S., Ariskin, A.A., Mochalov, A.G., & Sobolev, A.V. (2005). Crustal evolution of island-arc ultramafic magma: Galmoenan pyroxenite–dunite plutonic complex, Koryak Highland (Far East Russia). *Journal of Petrology* **46**, 1345-1366

Beatty, T.W., Orchard, M.J., & Mustard, P.S. (2006). Geology and tectonic history of the Quesnel terrane, in the area of Kamloops, British Columbia. *In*: Colpron, M., and Nelson, J.L. (ed.) Paleozoic Evolution and Metallogeny of Pericratonic Terranes at the Ancient Pacific Margin of North America. *Geological Association of Canada*, Special Paper **45**, 483-504

Cherniak, D.J. (1993). Lead diffusion in titanite and preliminary results of the effects of radiation damage on Pb transport. *Chemical Geology* **110**, 177-194

Cherniak, D.J., Watson, E.B. (2000). Pb diffusion in zircon. *Chemical Geology* **172**, 5-24

Clark, T. (1975). Geology of an ultramafic complex on the Turnagain River, northwestern B.C.; unpublished PhD dissertation, *Queens University*, 454p.

Clark, T. (1978). Oxide minerals in the Turnagain ultramafic complex, northwestern British Columbia. *Canadian Journal of Earth Sciences* **15**, 1893-1903

Clark, T. (1980). Petrology of the Turnagain ultramafic complex, northwestern British Columbia. *Canadian Journal of Earth Sciences* **17**, 744-757

Colpron, M., and Nelson, J.L. (2004). Cordilleran terranes revisited; the dossier on some long-suspected relationships. *Abstracts with Programs - Geological Society of America* **36**, 271

Colpron, M., Nelson, J.L., & Murphy, D.C. (2006). A tectonostratigraphic framework for the pericratonic terranes of the northern Canadian Cordillera. *In*: Colpron, M., and Nelson, J.L. (ed.) Paleozoic Evolution and Metallogeny of Pericratonic Terranes at the Ancient Pacific Margin of North America. *Geological Association of Canada*, Special Paper **45**, 1-23

DePaolo, D.J., Wasserburg, G.J. (1976). Nd isotopic variations and petrogenetic models. *Geophysical Research Letters* **3**, 249-252

Dostal, J., Gale, V., & Church, B.N. (1999). Upper Triassic Takla Group volcanic rocks, Stikine Terrane, north-central British Columbia: geochemistry, petrogenesis, and tectonic implications. *Canadian Journal of Earth Sciences* **36**, 1483-1494

Erdmer, P., Moore, J.M., Heaman, L., Thompson, R.I., Daughtry, K.L., & Creaser, R.A. (2002). Extending the ancient margin outboard in the Canadian Cordillera: Record of Proterozoic crust and Paleocene regional metamorphism in the Nicola horst, southeastern British Columbia. *Canadian Journal of Earth Sciences* **39**, 1605-1623

Erdmer, P., Mihalynuk, M.G., Gabrielse, H., Heaman, L.M., & Creaser, R.A. (2005). Mississippian volcanic assemblage conformably overlying Cordilleran miogeoclinal strata, Turnagain River area, northern British Columbia, is not part of an accreted terrane. *Canadian Journal of Earth Sciences* **42**, 1449-1465

Ferri, F., & Melville, D.M. (1990). Geology between Nina Lake and Otilinka River, North-Central British Columbia (93N/15, 94C/2). *Geological Fieldwork 1989, B.C. Ministry of Energy, Mines, and Petroleum Resources*. Paper **1990-1**, 101-114

Ferri, F. (1997). Nina Creek Group and Lay Range Assemblage, north-central British Columbia: remnants of late Paleozoic oceanic and arc terranes. *Canadian Journal of Earth Sciences* **34**, 854-874

Findlay, D.C. (1963). Petrology of the Tulameen ultramafic complex, Yale District, British Columbia; unpublished PhD dissertation, *Queens University*, 431p

Findlay, D.C. (1969). Origin of the Tulameen ultramafic-gabbro complex, southern British Columbia. *Canadian Journal of Earth Sciences* **6**, 399-425

Frost, B.R., Chamberlain, K.R., & Schumacher, J.C. (2000). Sphene (titanite): phase relations and role as a geochronometer. *Chemical Geology* **172**, 131-148

Gabrielse, H.,Wanless, R.K., Armstrong, R.L., & Erdman, L.R. (1980). Isotopic dating of Early Jurassic volcanism and plutonism in north-central British Columba. *Geological Survey of Canada*, Paper **80-1A**, 27-32

Gabrielse, H., & Yorath, C.J. (1991). Tectonic synthesis. *In* Geology of the Cordilleran Orogen in Cananda. *Edited by* H. Gabrielse and C.J. Yorath. Geological Survey of Canada, Geology of Canada **4**, 677-705

Gabrielse, H. (1998). Geology of Cry Lake and Dease Lake map areas, north-central British Columbia; *Geological Survey of Canada*, Bulletin **504**, 147p

Garuti, G., Pushkarew, E.V., Zaccarini, F., Cabella, R., & Anikina, E. (2003). Chromite composition and platinum-group mineral assemblage in the Uktus Uralian-Alaskan-type complex (Central Urals, Russia). *Mineralium Deposita* **38**, 312-326

Green, D.H., Schmidt, M.W., & Hibberson, W.O. (2004). Island-arc ankaramites: primitive melts from fluxed refractory lherzolitic mantle. *Journal of Petrology* **45**, 391-403

Himmelberg, G.R. & Loney, R.A. (1995). Characteristics and petrogenesis of Alaskan-type ultramafic-mafic intrusions, southeastern Alaska. *United States Geological Survey Professional Paper*, Report **P 1564**, 47p

Hernandez, L.E.O. (2000). An arc ankaramite occurrence in central Mexico. *Revista Mexicana de Ciencias Geológicas* **17**, 34-44

Hodges, K.V. (2003). Geochronology and thermochronology in orogenic systems. *Treatise on Geochemistry* **3**, 263-292

Irvine, T.N. (1974). Petrology of the Duke Island ultramafic complex, southeastern Alaska. *Geological Society of America – Memoir* **138**, 240p

Johan, Z. (2002). Alaskan-types complexes and their platinum-group element mineralization. *In*: Cabri, L.J. (ed.) The Geology, Geochemistry, Mineralogy and Mineral Beneficiation of Platinum-Group Elements. *Canadian Institute of Mining, Metallurgy and Petroleum*, Special Volume **54**, 669-719

Krogh, T.E (1982). Improved accuracy of U-Pb zircon ages by the creation of more concordant systems using an air abrasion technique. *Geochimica et Cosmochimica Acta* **46**, 637-649.

Loney, R.A., Himmelberg, G.R., & Shaw, N.B. (1987). Salt Chuck palladium-bearing ultramafic body, Prince of Wales Island. *U.S. Geological Survey Circular*, Report **C 0998**, 126-127

Loney, R.A., & Himmelberg, G.R. (1992). Petrogenesis of the Pd-rich intrusion at Salt Chuck, Prince of Wales Island: An Early Paleozoic Alaskan-type ultramafic body. *Canadian Mineralogist* **30**, 1005-1022

Ludwig, K.R (2003). Isoplot 3.09. A Geochronological Toolkit for Microsoft Excel. Berkeley Geochronology Center, Special Publication No. **4**

Massey, N.M.D., MacIntyre, D.G., Desjardins, P.J., & Cooney, R.T. (2005). Geology of British Columbia. *B.C. Geological Survey*, Geoscience Map 2005-3, scale 1:1,000,000

McDonough, W.F., & Sun, S.-S. (1995). The composition of the Earth. *Chemical Geology* **120**, 223-253

Meen, J.K., Ross, D.K., & Elthon, D. (1991). Gabbros and ultramafic rocks of Duke Island, southeastern Alaska; differences and similarities of mafic magmas during arc evolution. *EOS - Transactions, American Geophysical Union* **72**, 293

Monger, J.W.H. (1977). The Triassic Takla Group in McConnell Creek map-area, North-central British Columbia. *Paper - Geological Survey of Canada* **76-29**, 45 p.

Monger, J.W.H., & Church, B.N. (1977). Revised stratigraphy of the Takla Group, North-central British Columbia. *Canadian Journal of Earth Sciences* **14**, 318-326

Monger, J.W.H., Price, R.A., & Tempelman-Kluit, D.J. (1982). Tectonic accretion and the origin of the two major metamorphic and plutonic belts in the Canadian Cordillera. *Geology* **10**, 70-75

Mortensen, J.K. (1992). Pre-Mid-Mesozoic tectonic evolution of the Yukon-Tanana Terrane, Yukon and Alaska. *Tectonics* **11**, 806-180

Mossman, D.J., Coombs, D.S., Kawachi, Y., & Reay, A. (2000). High-Mg arc ankaramitic dikes, Greenhills Complex, Southland, New Zealand. *Canadian Mineralogist* **38**, 191-216

Nelson, J.L., & Friedman, R. (2004). Superimposed Quesnel (late Paleozoic-Jurassic) and Yukon-Tanana (Devonian –Mississippian) arc assemblages, Cassiar Mountains, northern British Columbia: field, U-Pb, and igneous petrochemical evidence. *Canadian Journal of Earth Sciences* **41**, 1201-1235

Nelson, J.L., Colpron, M., Piercey, S.J., Dusel-Bacon, C., Murphy, D.C., & Roots, C.F. (2006). Paleozoic tectonic and metallogenetic evolution of pericratonic terranes in Yukon, northern British Columbia and eastern Alaska. *In*: Colpron, M., and Nelson, J.L. (ed.) Paleozoic Evolution and Metallogeny of Pericratonic Terranes at the Ancient Pacific Pargin of North America. *Geological Association of Canada*, Special Paper **45**, 323-260

Nixon, G.T., Cabri, L.J., & Laflamme, J.H.G. (1990). Platinum-group-element mineralization in lode and placer deposits associated with the Tulameen Alaskan-type complex, British Columbia. *Canadian Mineralogist* **28**, 503-535

Nixon, G.T., Hammack, J.L., Ash, C.H., Cabri, L.J., Case, G., Connelly, J.N., Heaman, L.M., Laflamme, J.H.G., Nuttall, C., Paterson, W.P.E., & Wong, R.H. (1997). Geology and platinum-group-element mineralization of Alaskan-type ultramafic-mafic complexes in British Columbia. *B.C. Ministry of Employment and Investment.* Bulletin **93**, 141p

Nixon, G.T. (1998). Ni-Cu sulphide mineralization in the Turnagain Alaskan-type complex: A unique magmatic environment. *Geological Fieldwork 1997, B.C. Ministry of Energy, Mines, and Petroleum Resources*, Paper **1998-1**, 18-1 - 18-11

Okulitch, A.V. (1999). Geological time chart. *Geological Survey of Canada* Open-File Report **3040**

Parrish, R., Roddick, J.C., Loveridge, W.D., & Sullivan, R.W. (1987). Uranium-lead analytical techniques at the geochronology laboratory, Geological Survey of Canada. *In* Radiogenic Age and Isotopic Studies, Report 1, Geological Survey of Canada, Paper **87-2**, 3-7

Parrish, R.R, & Monger, J.W.H. (1992). New U-Pb dates from southwestern British Columbia. *Paper - Geological Survey of Canada*, Report **91-02**, 87-108

Piercey, S.J., Nelson, J.-A.L., Dusel-Bacon, C., Simard, R.-L., Roots, C.F. (2006). Paleozoic magmatism and crustal recycling along the Ancient Pacific Margin of North America, northern Cordillera. *In*: Colpron, M., and Nelson, J.L. (ed.) Paleozoic Evolution and Metallogeny of Pericratonic Terranes at the Ancient Pacific Margin of North America. *Geological Association of Canada*, Special Paper **45**, 281-322

Renne, P.R., Swisher, C.C., III, Deino, A.L., Karner, D.B., Owens, T. & DePaolo, D.J. (1998). Intercalibration of standards, absolute ages and uncertainties in $^{40}Ar/^{39}Ar$ dating. *Chemical Geology* **145,** 117-152

Roddick, J.C. (1987). Generalized numerical error analysis with application to geochronology and thermodynamics. *Geochimica et Cosmochimica Acta* **51**, 2129-2135.

Rubin, C.M., & Saleeby, J.B. (1992). Tectonic history of the eastern edge of the Alexander Terrance, southeastern Alaska. *Tectonics* **11**, 586-602

Rublee, V.J. (1994). Chemical petrology, mineralogy, and structure of the Tulameen complex, Princeton area, British Columbia. Unpublished M.Sc. dissertation, *University of Ottawa*, Ottawa, Ontario, 183p

Saleeby, J.B. (1992). Age and tectonic setting of the Duke Island ultramafic intrusion, southeast Alaska. *Canadian Journal of Earth Sciences* **29**, 506-522

Schau, M. (1970). Stratigraphy and structure of the type area of the upper Triassic Nicola group in south-central British Columbia. *Special Paper - Geological Association of Canada* **6**,123-135

Scheel, J.E., Nixon, G.T., & Scoates, J.S. (2005). New observations on the Turnagain Alaskan-type ultramafic intrusive suite and associated Ni-Cu-PGE mineralization. *Geological Fieldwork 2004, B.C. Ministry of Energy, Mines, and Petroleum Resources*. Paper **2005-1**, 167-176

Schermer, E.R., Howell, D.G., & Jones, D.L. (1984). The origin of allochthonous terranes. *Annual Review of Earth and Planetary Sciences* **12**, 107-131

Simard, R-L., Dostal, J., & Roots, C.F. (2003). Development of late Paleozoic volcanic arcs in the Canadian Cordillera: an example from the Klinkit Group, northern British Columbia and southern Yukon. *Canadian Journal of Earth Sciences* **40**, 907-924

Spandler, C.J., Arculus, R.J., Eggins, S.M., Mavrogenes, J.A., Price, R.C., & Reay, A.J. (2003). Petrogenesis of the Greenhills Complex, Southland, New Zealand: Magmatic differentiation and cumulate formation at the roots of a Permian island-arc volcano. *Contributions to Mineralogy and Petrology* **144**, 703-721

Stacey, J.S., & Kramers, J.D. (1975). Approximation of terrestrial lead isotope evolution by a two-stage model. *Earth and Planetary Science Letters* **26**, 207-221

Stevens, R.D., Delabia, R.N., & Lachance, G.R. (1982). Age determinations and geological studies; K-Ar isotopic ages, Report 16. *Geological Survey of Canada*, Paper **82-2**, 56p

Taylor, H.P., Jr., & Noble, J.A. (1960). Origin of the ultramafic complexes in southeastern Alaska. *21st International Geological Progress Report* **Part 13**, 175-187

Thirlwall, M.F. (2000). Inter-laboratory and other errors in Pb isotope analyses investigated using a ^{207}Pb-^{204}Pb double spike. *Chemical Geology* **163**, 299–322.

Unterschutz, J.L.E., Creaser, R.A., Erdmer, P., Thompson, R.I., & Daughtry, K.L. (2002). North American margin origin of Quesnel terrane strata in the southern Canadian cordillera: inferences from geochemical and Nd isotopic characteristics of Triassic metasedimentary rocks. *Geological Society of America Bulletin* **114**, 462-475

Wanless, R.K., Stevens, R.D., Lachance, G.R., & Edmonds, C.M. (1968). Age determinations and geologic studies, K-Ar isotopic ages, Report 8. *Geological Survey of Canada*, Paper **67-2A**, 141p

Watkinson, D.H., & Melling, D.R. (1992). Hydrothermal origin of platinum-group mineralization in low-temperature copper sulphide-rich assemblages, Salt Chuck intrusion, Alaska. *Economic Geology* **87**, 175-184

Weis, D., Kieffer, B., Maerschalk, C., Barling, J. de Jong, J., Williams, G.A., Hanano, D., Pretorious, W., Mattielli, N., Scoates, J.S., Goolaerts, A., Friedman, R.M., & Mahoney, J.B. (2006). High-precision isotopic characterization of USGS reference materials by TIMS and MC-ICP-MS. *Geochemistry Geophysics Geosystems* **7** (8), Q08006, doi:10.1029/2006GC001283

Wong, R.H., Godwin, C.I., & McTaggart, K.C. (1985). 1977-Geology, K/Ar dates, and associated sulphide mineralization of Wrede Creek zoned ultramafic complex (94D/9E). *Geology in British Columbia*, 1977-1981, 148-155

CHAPTER 3

CHROMITE CHEMISTRY OF THE TURNAGAIN INTRUSION, NORTHERN BRITISH COLUMBIA, AND THE REDOX STATES OF ALASKAN-TYPE PARENTAL MAGMAS

3.1 INTRODUCTION

Chromian spinel, or chromite ($FeCr_2O_4$ with minor amounts of Mg, Al, and Fe^{3+} substitution), is found as an accessory mineral in a wide variety of mafic and ultramafic rocks (e.g. Barnes & Roeder, 2001). It crystallizes from magmas that are broadly basaltic in composition and is typically one of the earliest phases to saturate in a mafic melt (e.g. Roeder, 1994). The abundance of chromite in many ultramafic and mafic rocks is generally low (1 vol.%), although large accumulations called chromitite do occur in a number of layered mafic-ultramafic intrusions (e.g. Roach *et al.*, 1998), ophiolites, and Alaskan-type intrusions (e.g. Garuti *et al.*, 2003; Krause *et al.*, 2006) worldwide. The composition of chromite is extremely sensitive to its environment of formation as well as post-magmatic processes and thus can be a powerful petrogenetic indicator in petrologic studies (e.g. Irvine, 1965; Irvine, 1967; Dick & Bullen, 1984; Roeder & Campbell, 1985; Sack & Ghiorso, 1991; Scowen *et al.*, 1991; Poustovetov & Roeder, 2000; Power *et al.*, 2000). Variations in chromite compositions may record changes in magma compositions and types of co-precipitating phases (Roeder, 1994), oxygen fugacity (e.g. Poustovetov & Roeder, 2000), pressure (e.g. Roeder & Reynolds, 1991), and may also record the effects of sub-solidus re-equilibration and serpentinization (e.g. Roeder & Campbell, 1985).

A recent compilation of chromite compositions from mafic-ultramafic rocks worldwide (Barnes & Roeder, 2001) includes only seven referenced sources of data for Alaskan-type intrusions. These intrusions are typically composed of ultramafic cumulate rocks, consisting of Mg-rich olivine, clinopyroxene, amphibole ± plagioclase, and they may be crudely to concentrically zoned. Alaskan-type intrusions occur mostly in subduction zone settings and are proposed to have formed from relatively water-rich magmas (Himmelberg & Loney, 1995; Mossman *et al.*, 2000; Johan, 2002; Spandler *et al.*, 2003; Ishiwatari & Ichiyama, 2004; Green *et al.*, 2004; Batanova *et al.*, 2005). Chromite is a common accessory mineral and is typically disseminated in the most magnesian lithologies (dunite and wehrlite). The earlier chromite compositional study of Clark (1978) provided a good basis for this study, which provides an overview of spinel compositions from the Turnagain Alaskan-type intrusion in northwestern British Columbia (Canada) with the aims of 1) significantly increasing the spinel compositional database for Alaskan-type intrusions, 2) assessing the crystallization sequence and subsequent chemical modifications during cooling and serpentinization using chromite compositional variability and, importantly, 3) constraining the relative oxygen fugacity of the

parental magmas for the Turnagain intrusion. The Turnagain Alaskan-type intrusion is unusual in that it contains zones with significant Ni-sulphide mineralization (428 Mt – measured and indicated – @ 0.17% sulphide Ni; http://www.hardcreeknickel.com). Given the proposed arc setting for Alaskan-type intrusions, they are considered to form from relatively oxidized parental magmas (ΔFMQ = +1 to +3.5, e.g. Carmichael, 1991; Parkinson & Arculus, 1999) with sulphur dissolved as sulphate (SO_4^{2-}) rather than sulphide (S^{2-}) (Jugo *et al.*, 2004) and have thus traditionally been considered unfavourable environments for nickeliferrous ore deposits.

3.2 REGIONAL GEOLOGY

Numerous Alaskan-type intrusions in British Columbia occur within the Mesozoic Quesnel accreted arc terrane, including the Tulameen (Findlay, 1969), Polaris (Foster, 1974), Lunar Creek, Wrede Creek, Johansson Lake (Nixon *et al.*, 1997), and Turnagain (Clark, 1975; 1978; 1980; Nixon, 1998) intrusions. The Turnagain intrusion is located in northwestern B.C., approximately 70 km east of Dease Lake, to the east of the Kutcho Fault, which is a regional strike-slip fault that represents the terrane boundary between Ancestral North America to the north and Quesnellia to the south (Gabrielse, 1998). The 24 km^2 Turnagain intrusion is completely fault-bounded, and during the Early Jurassic was thrust onto graphitic and pyritic phyllites currently assigned to the undivided Ordivician-Devonian Road River Formation/Earn Group, a deep marine facies of paleo-passive margin sedimentary units of Ancestral North America (Gabrielse, 1998). Conformably overlying the phyllite is a Devonian-Mississippian volcanic to sedimentary unit (Erdmer *et al.*, 2005) that may be correlative to the Lay Range Assemblage (see Chapter 2). The crystallization age of the Turnagain intrusion is constrained to be 190 Ma using U-Pb and Ar-Ar geochronological techniques (see Chapter 2).

3.3 GEOLOGY AND SPINEL CONTENT OF THE TURNAGAIN INTRUSION

Rocks of the Turnagain intrusion are predominantly ultramafic cumulate rocks with associated late dioritic phases and intrusions (Figure 3.1). The 3.5 km x 8.5 km Turnagain intrusion is elongate in a NW-SE direction and the apparent thickness of the intrusion is estimated at approximately 450 m based on inverse modeling of gravity data (C. Baldys, pers. comm., 2005). Exposures of the intrusion are limited to the northern and northeastern areas, which are above treeline, and near the Ni-mineralized zones (the Horsetrail Zone and satellite zones) in

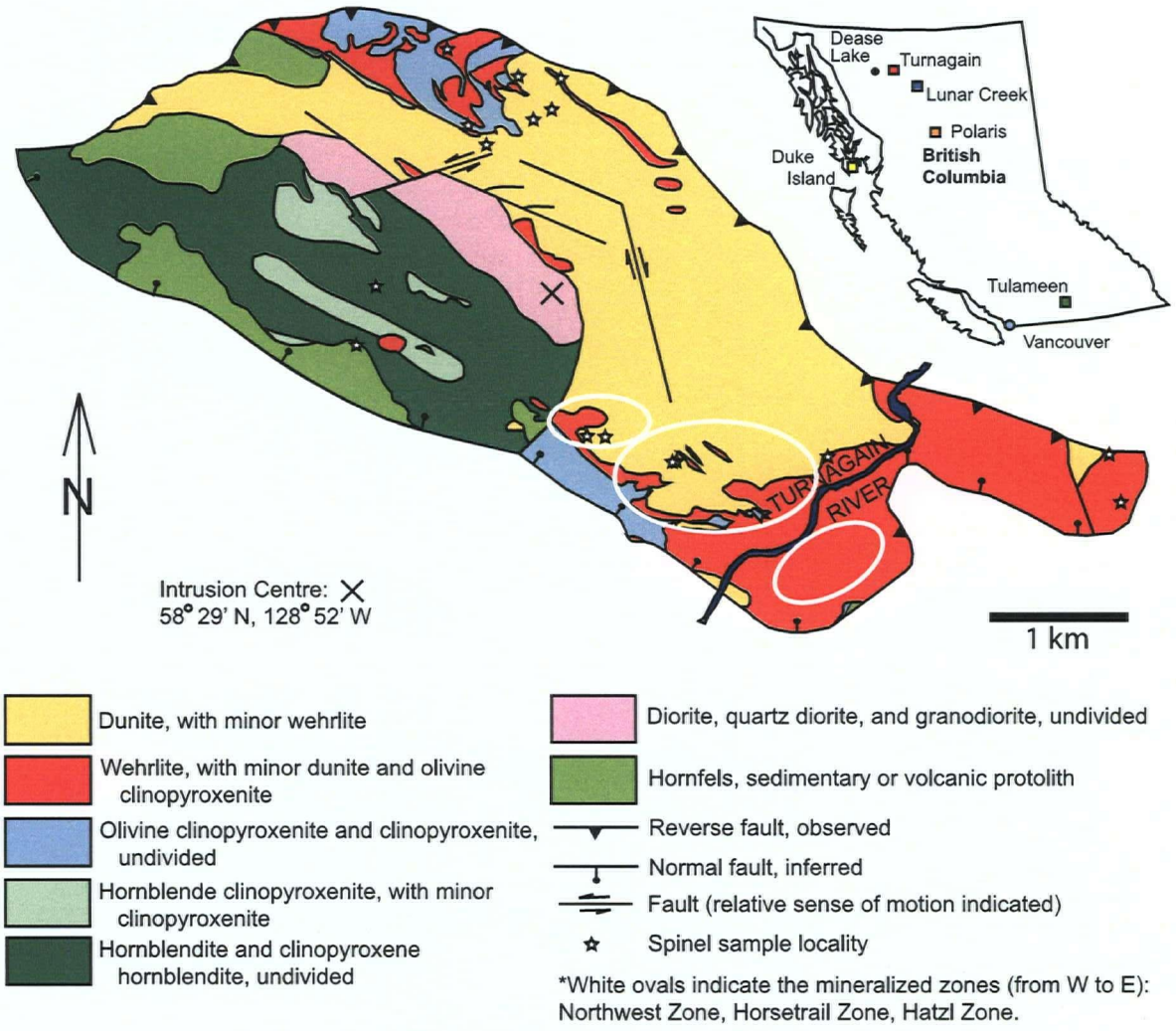

Figure 3.1: Simplified geological map of the Turnagain Alaskan-type intrusion, modified from Clark (1975), with its location in British Columbia shown as an inset in the upper right corner (also indicated are the locations of other major Alaskan-type intrusions in B.C. and Alaska). The lithologies of the intrusion are shown in the legend; some units are composites (e.g. olivine clinopyroxenite and clinopyroxenite). The intrusion is entirely fault-bounded, and the large area of hornblende-rich lithologies with associated felsic rocks in the west is mostly interpreted from both airborne and ground geophysics, as well as information from drill holes. The Ni-sulphide-mineralized zones (Horsetrail and satellite zones) are outlined in white ovals. Sample locations with spinel chemistry discussed in this paper are indicated as white stars.

the southeastern part of the intrusion, both northwest and southeast of the Turnagain River (Figure 3.1). Chromite is common in the more magnesian olivine-rich cumulates and magnetite is typical of the more evolved, clinopyroxene/hornblende-bearing lithologies that comprise the west-central portion of the intrusion. This part is considered to represent the roof of the intrusion and contains porphyritic, megacrystic, and pegmatoidal textured rocks and appears to intrude the underlying olivine cumulate rocks based on an interpretation of aeromagnetic data and diamond drill hole results (courtesy of Hard Creek Nickel Corp.). In the section below, the typical abundances and textures of spinel in rocks of the Turnagain intrusion are described.

3.3.1 Dunite

Dunite, the most abundant rock type in the Turnagain intrusion, is primarily composed of cumulus olivine and chromite with minor interstitial clinopyroxene (<10 vol.%) and rare phlogopite (0-1 vol.%). Equigranular olivine is typical of most dunite; however, local post-crystallization deformation has produced dunite with porphyroclastic textures. Olivine grain-size ranges from 2 mm in fine-grained equigranular dunite to 10 mm in porphyroclastic dunite. Kink bands, observed as discrete undulatory extinction bands in individual olivine grains, and irregular grain boundaries are also observed. Serpentinization of olivine in dunite is common, ranging from none to nearly complete, although the average amount of serpentinization is ~10%. Secondary magnetite is common between olivine grains.

Chromite in dunite can be found as chromitite schleiren, pods, lamellae, and rarely as layers (max. 5 cm thick) (Figure 3.2). Chromite grain sizes are typically the largest in chromitite (up to 3 mm) and slightly smaller in dunite (up to 2 mm), and grain shapes are equigranular to euhedral (Figure 3.3; A and B). Olivine may be encased within chromitite, but more commonly olivine grains are only partially surrounded by chromite and are present near the edge of the chromitite. Dunite typically contains up to 4 vol.% disseminated euhedral to subhedral chromite (Figure 3.3 C) both included within olivine and along grain boundaries between olivine crystals, although 2 vol.% is the typical abundance. Secondary alteration has resulted in the formation of magnetite rims (~30 μm thick) as overgrowths on chromite, and in some cases a 'ferritchromit' rim (Cr-rich magnetite) has been produced (Figure 3.3D). Ferritchromit, with no directly defined composition (e.g. Kanaris-Sotiriou *et al.*, 1978; Zakrzewski, 1989; Takashi & Adachi, 1995), is a term broadly used for Cr- and Al-rich

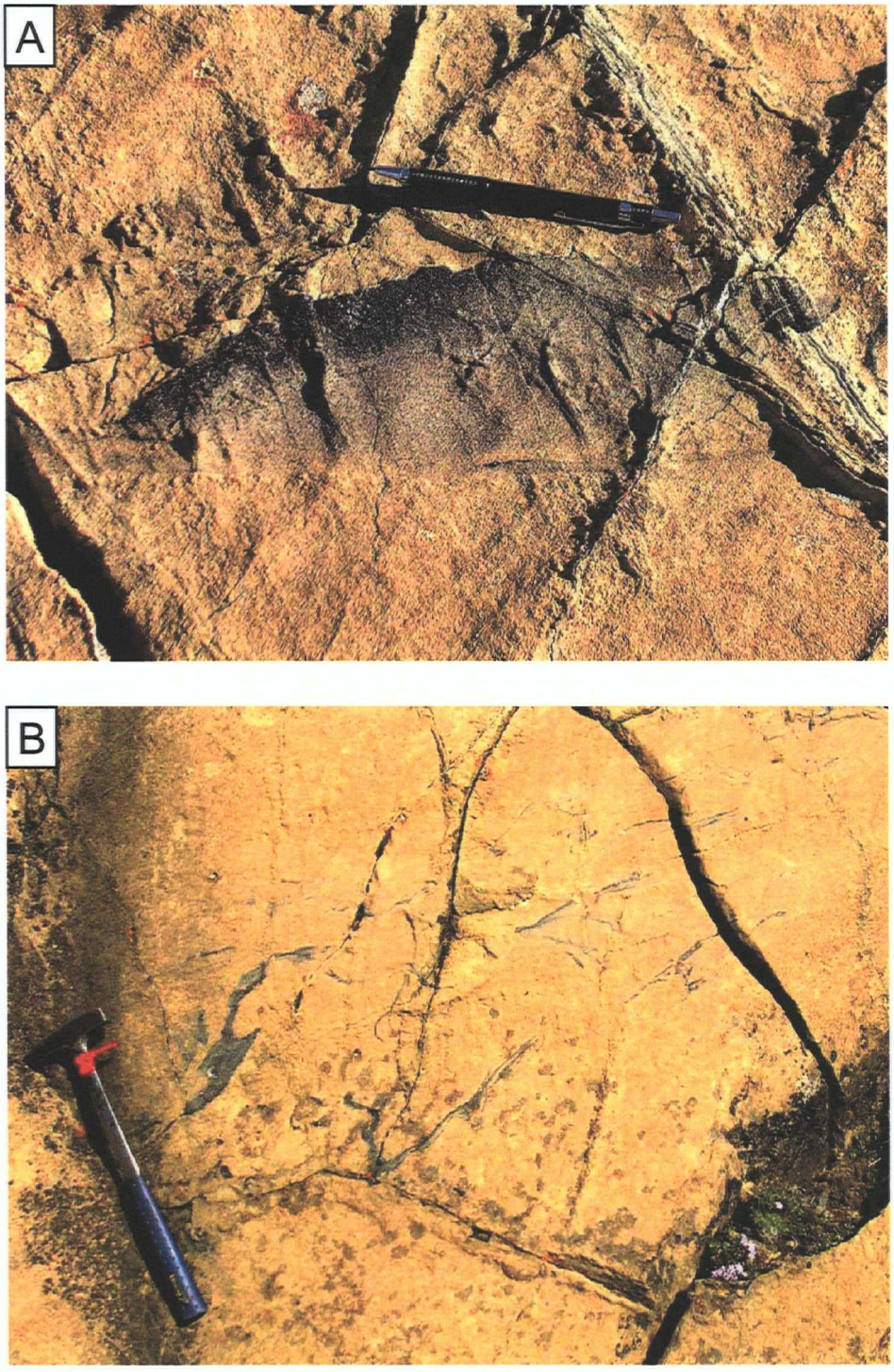

Figure 3.2: Photographs of chromitite in outcrop from the north-central portion of the Turnagain intrusion. A) Chromitite schleiren, grading into dunite towards the lower part of the photograph. Cross-cutting veins are filled with serpentine minerals. Pencil is approximately 12 cm long. B) Numerous chromitite schleiren, which may represent disrupted layers, within dunite. Hammer is approximately 50 cm long.

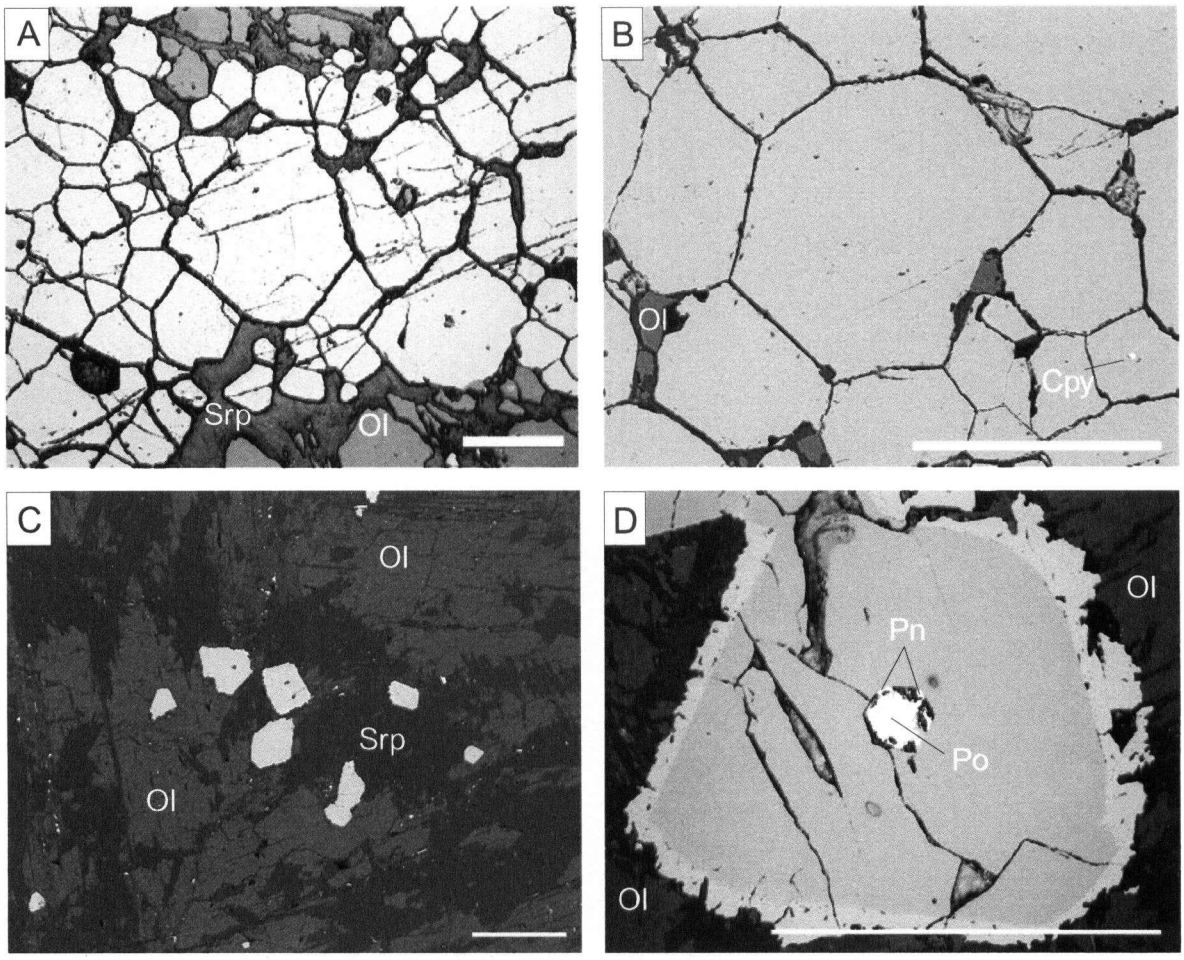

Figure 3.3: Photomicrographs of chromite textures from chromitite and dunite in the Turnagain intrusion. The white scale bar on each photo is 200 μm in length. A) Reflected light, sample 05ES-01-01-01, cluster 5. The large central chromite grain lies within a thin chromitite seam enclosed in dunite consisting of olivine (Ol) and secondary serpentine (Srp). Note the polygonal shapes of the chromite grains. B) BSE (backscattered electron) image, sample 05ES-01-01-01, cluster 4. Massive chromitite showing equigranular grain shapes produced during slow cooling and recrystallization. A small chalcopyrite (Cpy) inclusion is found in a chromite grain in the bottom right of the photograph. C) BSE image, sample 04ES-10-05-01, cluster 2. This cluster, within a partially serpentinized dunite, shows the primary euhedral nature of the chromite grains as well as the initial development of a thin magnetite rim (bright material on edge of grains). D) Reflected light, sample 04ES-08-01-01. Note the sulphide inclusion in the centre of a chromite grain. The inclusion originally consisted of an immiscible sulphide liquid that crystallized into pyrrhotite (Po) and pentlandite (Pn); note that the habit of the sulphide inclusion is determined by its host chromite grain. The distinct rim around the chromite grain is `ferritchromit' produced during serpentinization.

magnetite, or Fe^{3+}-rich chromite, rims observed on cumulus chromite (and rarely as entire grains) in serpentinized ultramafic rocks, which appear to be overgrowths rather than alteration products (Roeder *et al.*, 2001). The thickness of these rims appears to depend on factors such as position with respect to olivine, clinopyroxene, and degree of serpentinization. Since clinopyroxene is only rarely affected by serpentinization, chromite grains within or partially encased by clinopyroxene typically do not show secondary overgrowths/rims.

3.3.2 Wehrlite

Cumulus olivine and interstitial clinopyroxene are the dominant phases in wehrlite from the Turnagain intrusion; however, rare cumulus diopsidic clinopyroxene may occur. Olivine grain size is comparable to that in dunite (2 mm), although equigranular textures are less common and only occur in clinopyroxene-poor rocks. Olivine contained, either partially or entirely, within large clinopyroxene oikocrysts is typically rounded. Porphyroclastic textures are rarely observed in wehrlite, and clinopyroxene is typically interstitial to olivine porphyroclasts and neoblasts. Cumulus clinopyroxene is commonly finer grained than neighbouring olivine, with grain sizes ranging from 75 μm in diameter up to 2 mm in some samples. Serpentine minerals replace only olivine in wehrlites, and secondary magnetite is common along silicate grain boundaries.

Chromite, typically ~150 μm in diameter, in wehrlite is ubiquitous, is always disseminated, and is less abundant than in dunite (Figure 3.4; A and B). Wehrlite-hosted chromite grains are typically concentrated in specific areas, or clusters, and chromite grains in wehrlite tend to exhibit subhedral and anhedral habits. The majority of chromite grains are included in olivine or along olivine-olivine or olivine-clinpyroxene grain boundaries, with rare examples included in interstitial clinopyroxene. Magnetite and ferritchromit rims are as common in wehrlite as those described in dunite.

3.3.3 Olivine Clinopyroxenite

This lithology is typically composed of variable amounts of cumulus olivine and clinopyroxene, although a few samples contain significant oikocrystic clinopyroxene (Figure 3.4C). This latter type of olivine clinopyroxenite commonly contains more chromite than olivine clinopyroxenite where both the silicate minerals are cumulus (see Discussion). Olivine grain size (~1 mm) is significantly smaller compared to olivine in wehrlite and dunite and

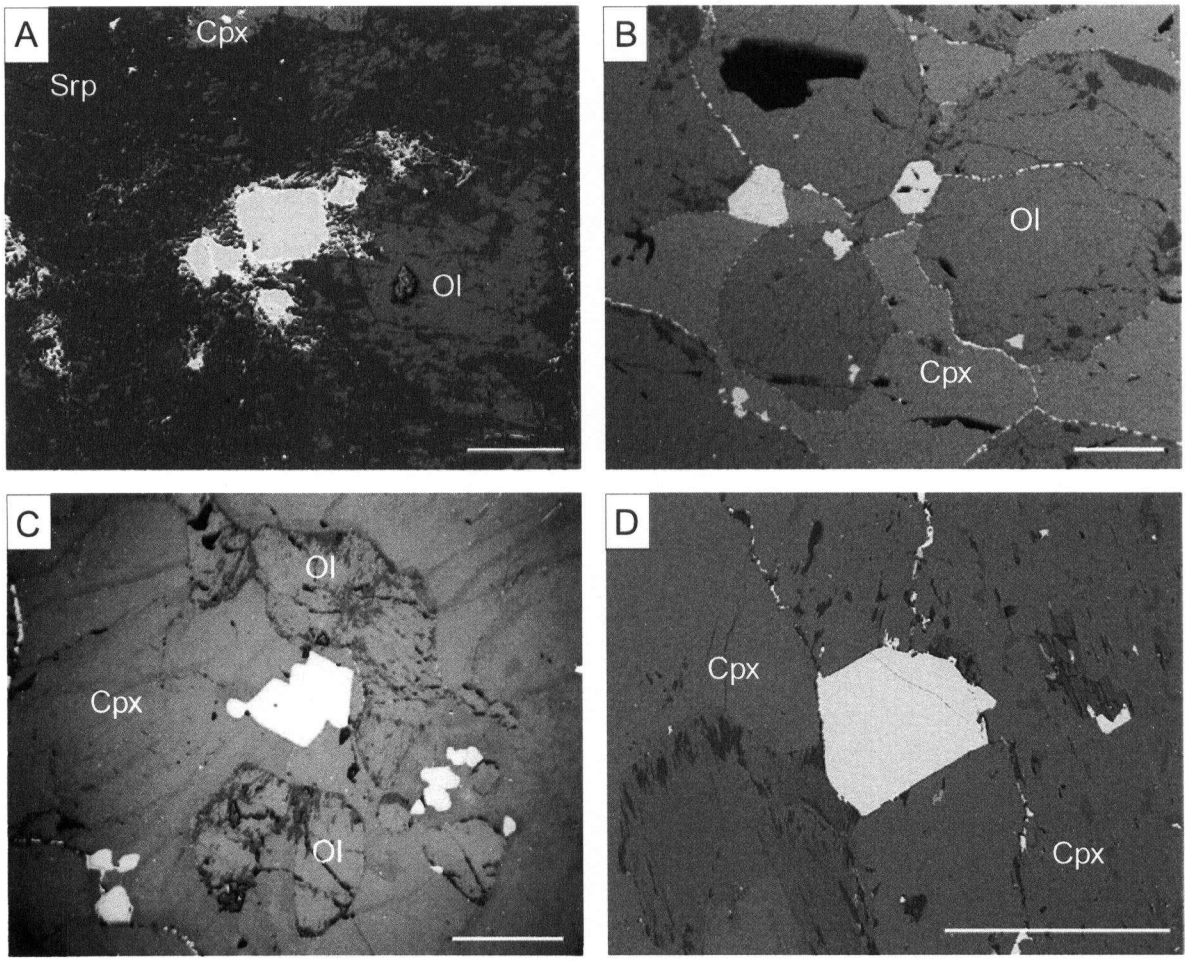

Figure 3.4: Photomicrographs of chromite textures from wehrlite and olivine clinopyroxenite in the Turnagain intrusion. The scale bar on each photo is 200 μm in length. A) BSE image, sample 04ES-10-06-01, cluster 5. This strongly serpentinized wehrlite contains few chromite grains and those present show well-developed magnetite/ ferritchromit rims, as well as a magnetite aureole (localized, very fine-grained magnetite). B) BSE image, sample 04ES-15-01-05, cluster 1. Small, euhedral chromite grains between cumulus olivine grains with little to no magnetite rim. Note the presence of fine-grained magnetite along grain boundaries between cumulus minerals and within fractures. C) Reflected light, sample 04ES-01-04-01, cluster 5. Cumulus olivine with abundant interstitial clinopyroxene (olivine clinopyroxenite). D) BSE image, sample 05ES-05-01-01, cluster 7. This grain is one of only two grains found in the entire thin section, which is a common feature of many Alaskan-type olivine clinopyroxenites. This small chromite grain is entirely encased within cumulus clinopyroxene.

clinopyroxene grains reach up to 15 mm across. The size of the two cumulus silicate phases in olivine clinopyroxenite appears to be directly proportional to their modal abundance (i.e. an olivine clinopyroxenite with 60 vol.% clinopyroxene will generally have an equigranular texture, whereas an olivine clinopyroxenite with 90 vol.% clinopyroxene will have significantly larger clinopyroxene and very small olivine). Olivine in olivine-poor clinopyroxenite is typically strongly serpentinized.

Chromite in olivine clinopyroxenite is typically found as inclusions within cumulus clinopyroxene or olivine, is never interstitial to the silicate minerals, and rarely contains secondary magnetite rims (Figure 3.4; C, D). Grain sizes are typically small, around 150 μm, and chromite is commonly euhedral (Figure 3.4D). Chromite abundance is significantly reduced (<0.5 vol.%) compared to wehrlite. Chromite in olivine clinopyroxenite with intercumulus clinopyroxene, or clinopyroxene oikocrysts, is commonly very similar in texture and size to chromite found in both dunite and wehrlite.

3.3.4 Hornblende Clinopyroxenite and Hornblendite

Hornblende clinopyroxenite and hornblendite occur in two distinct settings within the Turnagain intrusion. The first setting is as fine-grained dikes that are interpreted to represent evolved magma compositions. Some of these hornblendite dikes intrude a pendant of wallrock in the northwestern part of the intrusion (Figure 3.1). Hornblende-bearing rocks, some of which are cumulate, also occur in the west-central portion of the intrusion. Hornblendite dikes commonly contain subhedral ilmenite, whereas hornblende-rich lithologies of the western portion of the Turnagain intrusion typically contain primary magnetite (Figure 3.5). Although its occurrence is limited, magnetite may be found as local accumulations in hornblende-clinopyroxene-rich lithologies with grains reaching up to 1 cm across. Magnetite is typically much larger than chromite (about 5 times larger), and is subhedral to anhedral. Some grains appear intergrown (Figure 3.5B) and ilmenite oxy-exsolution is common.

3.4 ANALYTICAL TECHNIQUES

The spinel content of each sample, textural relationships to other phases, and relative degree of alteration were carefully scrutinized using both transmitted and reflected light microscopy prior to analysis. Samples were selected to represent the various rock types found in the Turnagain intrusion and the range of spinel morphologies and spinel-silicate associations

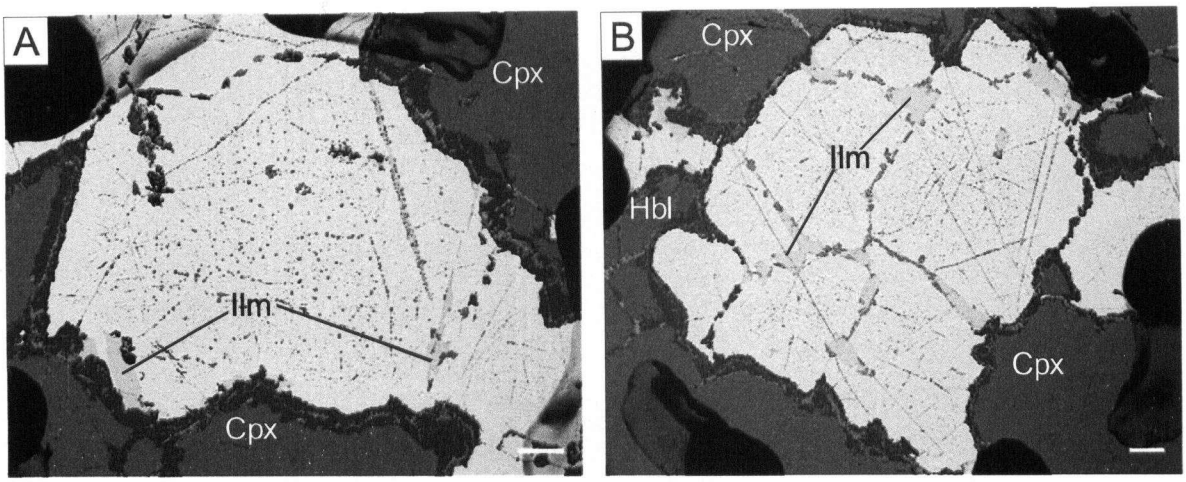

Figure 3.5: Photomicrographs of magnetite textures from sample DDH04-47-7-49, a hornblende clinopyroxenite from the western zone of the Turnagain intrusion. The scale bar on each photo is 200 μm in length. A) Cluster 3. This cluster contains large magnetite grains with oxy-exsolved lamellae of ilmenite (Ilm) and larger composite grains of ilmenite (internal and external) that are interpreted to represent granule exsolution. B) Cluster 7. Composite magnetite grain (at least 8 separate grains) with oxy-exsolved lamellae of ilmenite and larger composite granule exsolution blebs along grain boundaries.

described above. Some samples contained appreciable spinel, such that local accumulations of larger spinel grains were referred to as "clusters". Chromite grains from three different clusters were analyzed in each thin section.

A total of 16 samples were selected for microprobe analysis, carbon-coated, and documented using a Philips XL-30 scanning electron microscope at the University of British Columbia, Vancouver, BC. Quantitative analyses were carried out in wavelength-dispersion mode using a Cameca SX-50 electron microprobe with a beam diameter of 10 μm, an accelerating voltage of 15 keV, and a beam current of 20 nA with 20 s peak count-time and 10 s background count-time. The Ni contents of chromite grains from chromitite samples were analyzed using a fixed matrix, a beam diameter of 10 μm, an accelerating voltage of 15 keV, and a beam current of 200 nA with peak count-time extended to 100 s and a background time to 50 s. For the elements considered, the following standards, X-ray lines and crystals were used: synthetic rhodonite, Mn$K\alpha$, LIF; diopside, Ca$K\alpha$, PET, and Si$K\alpha$, TAP; synthetic spinel, Al$K\alpha$, TAP; synthetic fayalite, Fe$K\alpha$, LIF; synthetic magnesiochromite, Mg$K\alpha$, TAP, and Cr$K\alpha$, LIF; rutile, Ti$K\alpha$, PET; V metal, V$K\alpha$, PET; synthetic Ni_2SiO_4, Ni$K\alpha$, LIF. Data reduction of all analytical results was undertaken using the "PAP" $\phi(\rho Z)$ procedure of Pouchou & Pichoir (1985). Using the higher beam current and counting times for Ni as described above results in an analytical precision of <5% relative.

A total of 360 points were analyzed in this study, 25 of which were magnetite analyses. Individual grains, prior to analysis, had their selected point locations ordered from rim to core. In the case of grains on the edge of chromitite schlieren, the part of the grain closest to a neighbouring silicate was analyzed first, as opposed to the grain boundary in contact with other chromite. All spinels were assumed to be stoichiometric (Kamperman *et al.*, 1996) and cation abundances and ferrous/ferric iron were calculated using the method of Barnes and Roeder (2001). This method isolates Ti and V into an ulvöspinel component and is considered the most accurate calculation technique for cations in spinel-group minerals.

3.5 RESULTS

Table 3.1 contains representative chromite and magnetite analyses from the various ultramafic lithologies and the complete set of spinel analyses from this study are presented in Appendix I. Below, the variations in spinel chemistry are described for spinels from each of the major rock types of the Turnagain intrusion.

Table 3.1a: Representative spinel compositions from spinel-bearing ultramafic rocks of the Turnagain intrusion

Rock:	Chromitite			Dunite			Dunite			Dunite			Wehrlite		
Sample:	05ES-01-04-01			04ES-19-01-02			04ES-03-02-01			04ES-08-01-01			04ES-11-03-03		
Cluster:	6			2			5			2			4		
Grain Number:	1			1			1			1			2		
Style:	l. anh.			s. anh.			l. sub.			s. eu.			m. sub.		
Zone:	Core	Mid	Rim	Core	Mid	Rim	Core	Mid	Rim	Core	Mid	Rim	Core	Mid	Rim
Oxides (wt. %)															
SiO_2	0.00	0.00	0.00	0.02	0.06	0.03	0.02	0.01	0.08	0.03	0.03	0.05	0.00	0.00	0.01
TiO_2	0.22	0.28	0.22	0.79	0.94	0.76	0.47	0.51	0.02	0.52	0.54	0.53	1.35	1.28	1.26
Al_2O_3	5.94	5.81	5.07	8.98	8.99	8.73	6.72	5.72	0.02	7.35	7.28	7.47	10.23	10.26	10.47
Cr_2O_3	62.86	63.01	65.24	54.58	54.66	54.61	50.24	42.89	0.57	46.49	46.40	44.81	44.37	44.27	43.31
V_2O_3	0.05	0.01	0.02	0.10	0.14	0.18	0.07	0.08	0.02	0.07	0.09	0.06	0.32	0.30	0.30
Fe_2O_3	5.82	5.70	3.82	4.71	4.31	5.15	13.72	20.56	68.76	15.97	15.98	16.75	11.65	11.95	13.03
FeO	11.78	11.64	11.22	22.75	22.84	23.24	21.46	23.84	29.45	22.94	22.81	22.94	26.10	26.05	26.18
MnO	0.00	0.05	0.04	0.34	0.32	0.42	0.25	0.48	0.14	0.22	0.22	0.24	0.31	0.34	0.40
MgO	14.14	14.18	14.19	7.12	7.17	6.86	7.79	5.75	0.93	6.84	6.90	6.64	5.54	5.53	5.50
NiO	0.17	0.17	0.13	-	-	-	-	-	-	-	-	-	-	-	-
CaO	0.01	0.01	0.00	0.01	0.03	0.00	0.01	0.00	0.01	0.02	0.01	0.00	0.01	0.00	0.01
Total	100.99	100.85	99.96	99.42	99.46	99.99	100.74	99.84	99.99	100.46	100.26	99.48	99.87	99.97	100.45
Cations (p.f.u.)															
Ti	0.005	0.007	0.006	0.020	0.024	0.019	0.012	0.013	0.000	0.013	0.014	0.014	0.035	0.033	0.032
Cr	1.615	1.621	1.695	1.472	1.472	1.469	1.351	1.184	0.017	1.260	1.259	1.227	1.202	1.198	1.167
Al	0.228	0.223	0.196	0.361	0.361	0.350	0.270	0.234	0.001	0.297	0.295	0.305	0.413	0.414	0.420
V	0.001	0.000	0.000	0.002	0.003	0.004	0.002	0.002	0.000	0.002	0.002	0.001	0.007	0.007	0.007
Fe^{3+}*	0.142	0.140	0.094	0.121	0.110	0.132	0.351	0.550	1.977	0.412	0.413	0.436	0.300	0.308	0.334
Fe^{2+}*	0.320	0.317	0.308	0.649	0.651	0.661	0.610	0.701	0.941	0.657	0.655	0.664	0.748	0.746	0.746
Mn	0.000	0.001	0.001	0.010	0.009	0.012	0.007	0.015	0.005	0.006	0.006	0.007	0.009	0.010	0.012
Mg	0.685	0.688	0.695	0.362	0.364	0.348	0.395	0.298	0.053	0.349	0.353	0.343	0.283	0.282	0.279
Ni	0.004	0.004	0.004	-	-	-	-	-	-	-	-	-	-	-	-
Ca	0.000	0.000	0.000	0.000	0.001	0.000	0.000	0.000	0.000	0.001	0.000	0.000	0.000	0.000	0.000
Total	3.001	3.001	3.001	2.998	2.995	2.997	2.998	2.999	2.995	2.998	2.998	2.997	2.997	2.997	2.997
Trivalent End Members															
Cr/Σ3+	0.814	0.817	0.854	0.753	0.757	0.753	0.685	0.601	0.009	0.640	0.640	0.623	0.628	0.624	0.607
Al/Σ3+	0.115	0.112	0.099	0.185	0.186	0.179	0.137	0.119	0.000	0.151	0.150	0.155	0.216	0.216	0.219
Fe/Σ3+	0.072	0.070	0.048	0.062	0.057	0.068	0.178	0.280	0.991	0.209	0.210	0.222	0.157	0.160	0.174

Crystal textural style is abbreviated: euh. (euhedral), sub. (subhedral), anh. (anhedral), interg. (intergrown), irreg. (irregular); l. (large), m. (medium), s. (sm
Grain number refers to a particular grain within a cluster: most clusters have multiple grain
Note: Other phases (ol, cpx, hbl) were also analyzed on certain sections, such that Cluster refers to a specific location on each secti

Table 3.1b: Representative spinel compositions from spinel-bearing ultramafic rocks of the Turnagain intrusion

Rock:	Wehrlite			Wehrlite			Olivine Clinopyroxenite			Olivine Clinopyroxenite			Hornblende Clinopyroxenite		
Sample:	04ES-16-08-01			04ES-10-06-01			04ES-06-06-01			05ES-05-01-01			DDH04-47-7-49		
Cluster:	6			1			4.5			8			5		
Grain Number:	3			2			2			1			1		
Style:	s. eu.			m. anh.			m. anh.			s. eu.			l. anh.		
Zone:	Rim	Mid	Mid	Core	Mid	Rim	Core	Mid	Mid	Core	Mid	Rim	Core	Mid	Rim
Oxides (wt. %)															
SiO_2	0.01	0.03	0.04	0.00	0.03	0.03	0.02	0.00	0.01	0.03	0.00	0.03	0.03	0.03	0.03
TiO_2	1.03	1.05	1.01	0.89	0.94	0.11	1.02	0.98	0.84	2.51	2.48	2.42	3.27	3.11	0.35
Al_2O_3	7.99	7.85	8.01	11.86	12.00	0.03	8.35	8.61	8.25	4.64	4.44	4.18	2.27	0.95	0.16
Cr_2O_3	49.53	50.34	49.73	42.92	42.33	4.83	48.48	48.60	46.95	28.34	27.45	26.90	0.13	0.14	0.13
V_2O_3	0.08	0.08	0.08	0.16	0.20	0.00	0.22	0.24	0.25	0.11	0.08	0.07	0.46	0.45	0.73
Fe_2O_3	11.56	11.46	11.60	13.33	13.34	64.67	10.11	9.68	11.33	30.20	31.67	32.01	59.94	61.20	67.39
FeO	20.19	19.79	19.79	24.21	24.16	28.70	26.30	26.26	25.75	25.09	25.31	25.19	34.04	33.80	31.82
MnO	0.18	0.25	0.26	0.30	0.37	0.35	0.41	0.35	0.78	4.07	3.92	3.87	0.26	0.23	0.02
MgO	8.88	9.22	9.11	6.70	6.68	1.43	4.92	4.96	4.70	3.08	2.98	2.79	0.46	0.24	0.15
NiO	-	-	-	-	-	-	-	-	-	-	-	-	-	-	-
CaO	0.00	0.01	0.00	0.01	0.00	0.00	0.01	0.01	0.03	0.17	0.26	0.34	0.03	0.02	0.01
Total	99.45	100.09	99.64	100.39	100.05	100.17	99.85	99.69	98.90	98.24	98.60	97.80	100.90	100.17	100.78
Cations (p.f.u.)															
Ti	0.026	0.027	0.026	0.023	0.024	0.003	0.027	0.026	0.022	0.069	0.068	0.067	0.092	0.089	0.010
Cr	1.329	1.340	1.329	1.140	1.127	0.145	1.330	1.333	1.303	0.821	0.795	0.787	0.004	0.004	0.004
Al	0.320	0.311	0.319	0.470	0.476	0.002	0.342	0.352	0.341	0.200	0.192	0.182	0.100	0.043	0.007
V	0.002	0.002	0.002	0.004	0.005	0.000	0.005	0.005	0.006	0.003	0.002	0.002	0.011	0.011	0.018
Fe^{3+}*	0.295	0.290	0.295	0.337	0.338	1.846	0.264	0.253	0.299	0.833	0.873	0.891	1.687	1.751	1.929
Fe^{2+}*	0.573	0.557	0.560	0.680	0.681	0.910	0.763	0.762	0.756	0.769	0.775	0.779	1.064	1.074	1.012
Mn	0.005	0.007	0.007	0.009	0.011	0.011	0.012	0.010	0.023	0.126	0.122	0.121	0.008	0.008	0.001
Mg	0.449	0.463	0.459	0.336	0.335	0.081	0.255	0.257	0.246	0.168	0.163	0.154	0.026	0.014	0.008
Ni	-	-	-	-	-	-	-	-	-	-	-	-	-	-	-
Ca	0.000	0.000	0.000	0.000	0.000	0.000	0.000	0.000	0.001	0.007	0.010	0.014	0.001	0.001	0.001
Total	2.999	2.998	2.997	2.998	2.997	2.998	2.997	2.998	2.997	2.997	2.999	2.998	2.993	2.994	2.990
Trivalent End Members															
Cr/Σ3+	0.684	0.690	0.684	0.586	0.581	0.073	0.687	0.688	0.670	0.443	0.428	0.423	0.002	0.002	0.002
Al/Σ3+	0.164	0.160	0.164	0.241	0.245	0.001	0.176	0.182	0.176	0.108	0.103	0.098	0.056	0.024	0.004
Fe/Σ3+	0.152	0.150	0.152	0.173	0.174	0.926	0.136	0.130	0.154	0.449	0.469	0.479	0.942	0.974	0.994

Crystal textural style is abbreviated: euh. (euhedral), sub. (subhedral), anh. (anhedral), interg. (intergrown), irreg. (irregular); l. (large), m. (medium), s. (sma
Grain number refers to a particular grain within a cluster: most clusters have multiple grain
Note: Other phases (ol, cpx, hbl) were also analyzed on certain sections, such that Cluster refers to a specific location on each secti

3.5.1 Chromitite

Although volumetrically minor in the Turnagain intrusion, chromitite is petrologically important. Chromite grains from chromitites are characterized by the most Cr- and Mg-rich compositions of all lithologies (Cr_2O_3 = 59-67 wt.%, MgO = 10-14 wt.%) with correspondingly low TiO_2 (0.24-0.66 wt.%), V_2O_3 (0.01-0.34 wt.%), Al_2O_3 (4.60-7.14 wt.%), and Fe_2O_3 (3.82-6.88 wt.%) contents (Figures 3.6-3.7). Two samples (05ES-01-03-01 and 05ES-01-04-01) contain relatively Ni-rich chromite grains (NiO = 0.13-0.20 wt.%). All chromite analyses from chromitite are distinguished by $Fe^{3+}/(Fe^{3+}+Cr+Al)$ <0.1 (Figure 3.7A). There is no iron-enrichment trend present in the chromite analyses from chromitites indicating that their compositions likely record primary spinel compositions and that they have not been modified by subsolidus or post-magmatic processes (see Discussion).

3.5.2 Dunite

Chromite analyses from dunite span a relatively large range in composition (Cr_2O_3= 34-56 wt.%, TiO_2= 0.01-1.01 wt.%, FeO = 20-29 wt.%, Fe_2O_3 = 3.5-18.6 wt.%) compared to chromite from chromitites (Figure 3.6-3.7). With the exception of sample 04ES-19-01-02, spinel analyses from each dunite sample show an overall iron-enrichment trend (Figure 3.7A), which is a common feature of Alaskan-type intrusions (Barnes & Roeder, 2001). All Fe^{3+}-rich spinel compositions from dunite represent analyses of magnetite/ferritchromit rims around chromite grains and are associated with serpentine-group mineral replacement of olivine. Analyses of spinel grains from sample 04ES-19-01-02 have $Fe^{3+}/(Fe^{3+}+Cr+Al)$<0.1, similar to those from the chromitites described above.

3.5.3 Wehrlite

Similar to the dunite samples, chromite analyses from wehrlite in the Turnagain intrusion show a wide compositional range (Figures 3.6-3.7) and are relatively enriched in Al_2O_3 (7.5-15.4 wt.%), TiO_2 (0.7-1.8 wt.%) and Fe_2O_3 (10-18 wt.%). Magnetite and ferritchromit compositions, while rare, are nonetheless present and indicate that similar post-secondary process occurred in both wehrlite and dunite. Chromite analyses from one wehrlite sample (04ES-15-01-05) have markedly low $Fe^{3+}/(Fe^{3+}+Cr+Al)$ compared to the above wehrlites (Figure 3.6). The compositions of chromite from this sample have the lowest Fe_2O_3 (0.94-3.97 wt.%) of all spinel analyses from the Turnagain intrusion, and relatively low Cr/Cr+Al (0.68-

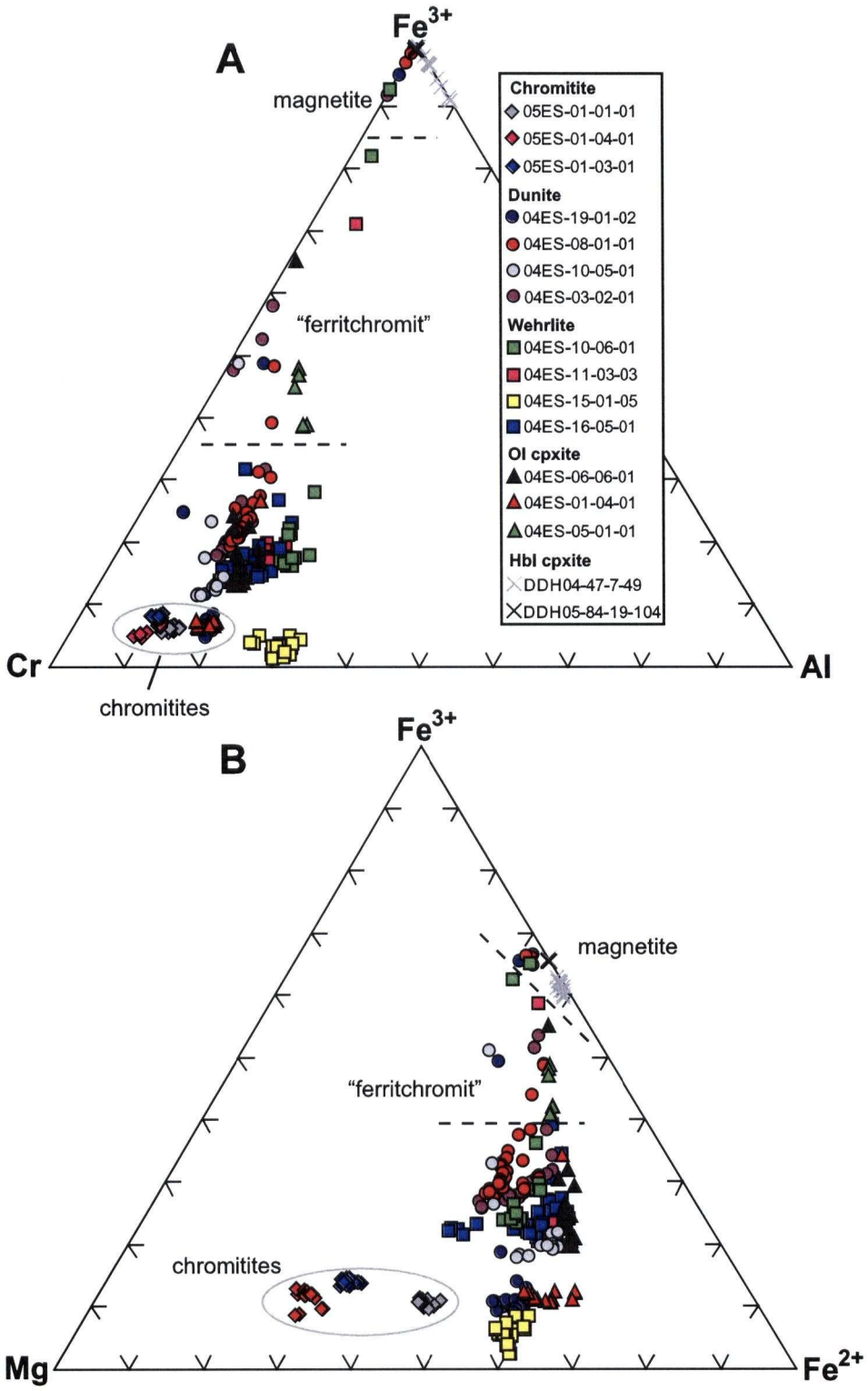

Figure 3.6: Chromite compositional ternary diagrams. A) Trivalent cation (Fe^{3+}-Cr-Al) plot of all Turnagain spinel compositions. All samples are represented by sample number. Chromites plot in the lower 40% of the diagram with the exception of magnetite rim analyses, which plot at or near the Fe^{3+} apex, and ferritchromit analyses, which plot in the intermediate part of the diagram. B) Ternary diagram (Mg-Fe^{2+}-Fe^{3+}) of all Turnagain spinel compositions.

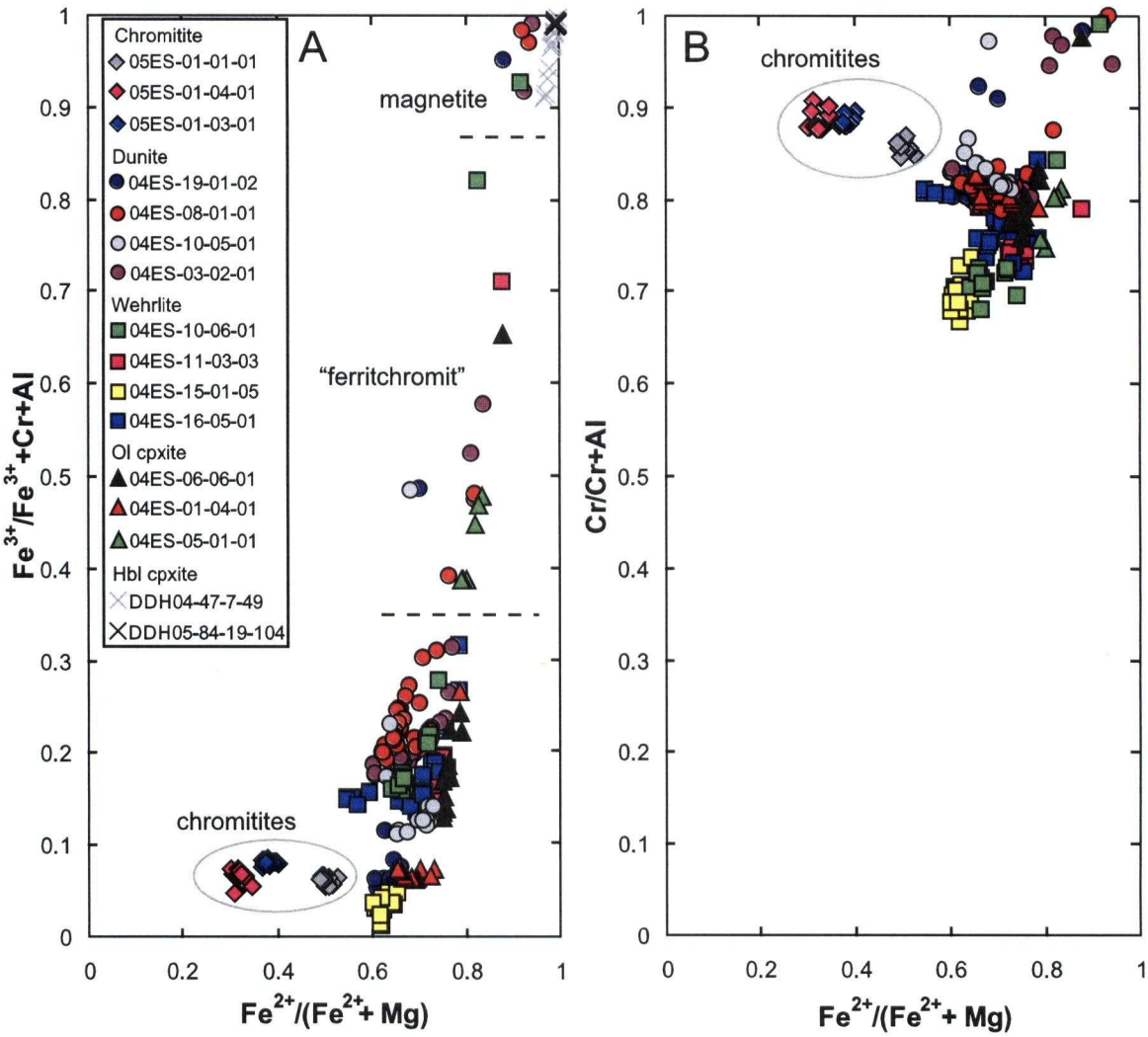

Figure 3.7: Binary plots of spinel compositions from the Turnagain intrusion represented by sample number. These plots are projections of the spinel prism (Irvine, 1965). A) $Fe^{2+}/(Fe^{2+}+Mg)$ (Fe#) vs. $Fe^{3+}/(Fe^{3+}+Cr+Al)$, or divalent vs. trivalent cation plot. A distinct Fe-enrichment trend exists for most Turnagain chromite compositions, a typical feature of Alaskan-type intrusions, with the exception of chromite grains from the chromitites and other chromite grains with $Fe^{3+}/(Fe^{3+}+Cr+Al)$ <0.1. B) Fe# vs. Cr/Cr+Al. Chromite grains from the chromitites have significantly lower $Fe^{2+}/(Fe^{2+}+Mg)$ compared to other spinel analyses. Magnetite analyses are not plotted due to their very low Cr and Mg contents.

0.73), high TiO_2 (1.1-2.5 wt.%), and high V_2O_3 (0.06-0.38 wt.%). In terms of their trivalent cation abundances (Figure 3.6A), chromite compositions from individual wehrlite samples, with the exception of the above sample, are characterized by intermediate sloping trends in terms of trivalent cations (decreasing Cr, increasing Fe^{3+} and Al). Chromite compositions from sample 04ES-15-01-05 plot in the field of the "Cr-Al trend" of Barnes and Roeder (2001) and likely reflect the effect of exchange with Al-bearing clinopyroxene (see Discussion).

3.5.4 Olivine Clinopyroxenite

Most olivine clinopyroxenite sampled in the Turnagain intrusion, and indeed in other Alaskan-type intrusions (Irvine, 1965), is devoid of chromite. A few samples of olivine clinopyroxenite from the Turnagain intrusion contain chromite, however the nature of the grains (small sizes, low abundances) appears to have allowed for more extensive subsolidus to post-magmatic compositional modifications compared to spinel grains from the previously described rock types. Chromite grains from olivine clinopyroxenite are relatively enriched in FeO (23-27 wt.%), Fe_2O_3 (9.7-17.2 wt.%), TiO_2 (0.9-2.1 wt.%) and V_2O_3 (0.22-0.54 wt.%), and depleted in Al_2O_3 (5.68-9.40 wt.%) compared to analyses from the other rock types. One notable exception is sample 04ES-01-04-01, where the spinel grains are characterized by $Fe^{3+}/(Fe^{3+}+Cr+Al)<0.1$ (Figure 3.7), and overlap with the analyses from the dunite sample 04ES-19-01-02. Spinel analyses from sample 05ES-05-01-01 are also distinct with high amounts of TiO_2 (2.5-3.2 wt.%) and $Fe^{3+}/(Fe^{3+}+Cr+Al)>0.4$ (Figure 3.7A, 3.8A), which indicates that all analyzed grains are ferritchromit in composition. This sample contains small (150 μm) chromite grains entirely encased within cumulus diopside (Figure 3.4H), thus the ferritchromit composition of the spinels in this sample is likely the result of subsolidus reequilibration with the hosting clinopyroxene. With respect to trivalent cations, chromite grains from olivine clinopyroxenite do not show the strong intrasample variations as seen in the dunites and wehrlites.

3.5.5 Hornblende Clinopyroxenite

In Alaskan-type intrusions, liquidus magnetite generally begins to crystallize after an extended period of clinopyroxene saturation and after the cessation of chromite crystallization. Chromite ceases to crystallize shortly after clinopyroxene saturation because Cr is compatible in clinopyroxene (e.g. Irvine, 1965; Findlay, 1969; Hill & Roeder, 1974; Clark, 1978). Analyses

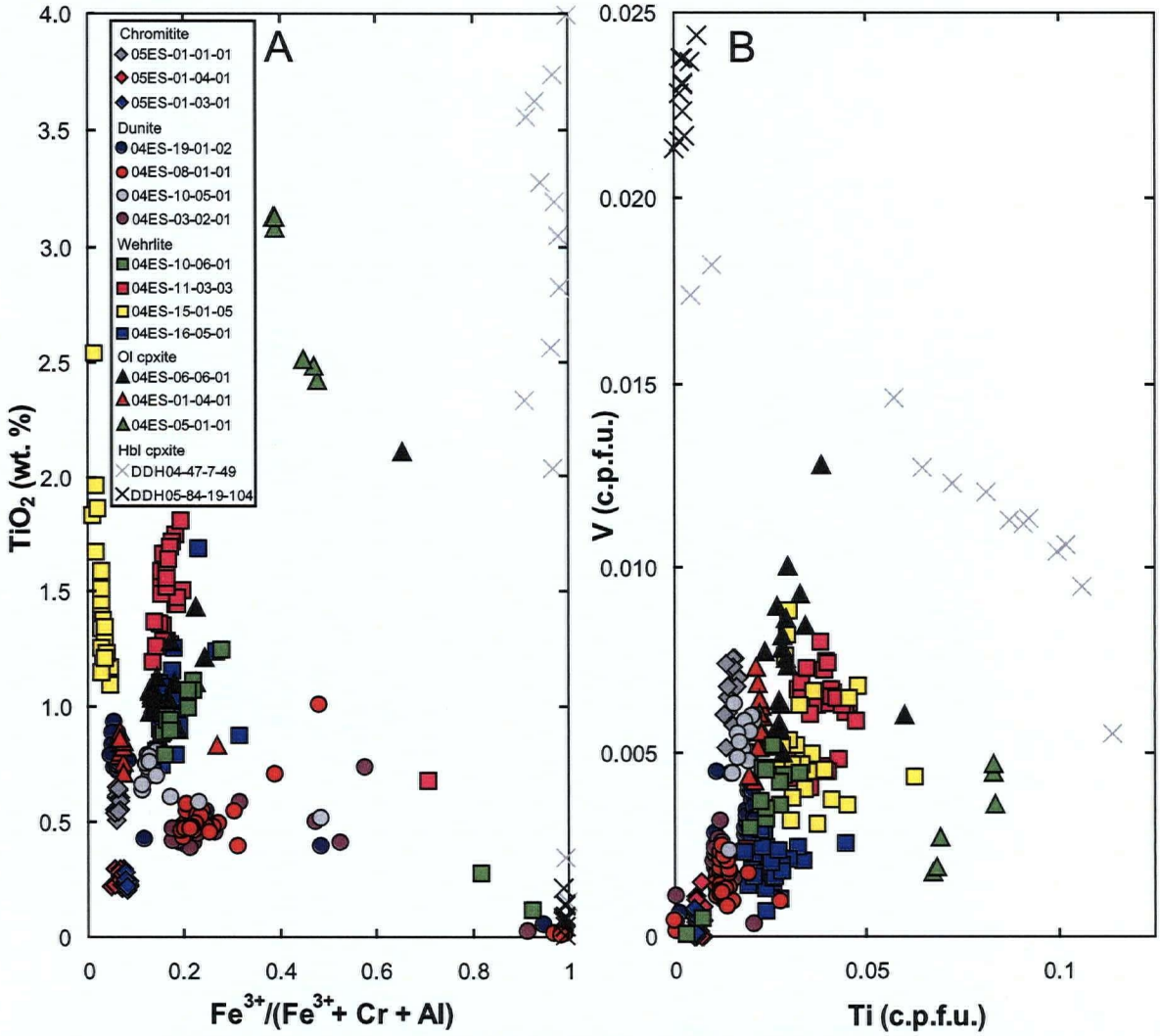

Figure 3.8: Binary plots of spinel compositions from the Turnagain intrusion. A) $Fe^{3+}/(Fe^{3+}+Cr+Al)$ vs. TiO_2. Spinel analyses from the Turnagain intrusion show a wide range of Ti contents. Note that both magnetite-bearing samples plot parallel to the Y-axis at almost constant Fe^{3+}#. Coupled increases (positive trends) are indicative of re-equilibration with interstitial melt, while increasing Fe^{3+} without increasing Ti is indicative of serpentinization. B) Ti vs. V. Most samples are characterized by nearly vertical trends with the exception of magnetite from DDH04-47-7-49. Note the V-enrichment of magnetite from sample DDH05-84-19-104.

of spinel from two cumulus magnetite-bearing hornblende clinopyroxenites, both from drillcore, show contrasting compositions. Spinel from sample DDH05-84-19 is nearly pure end-member magnetite (Fe_2O_3 = 67.1-67.8 wt.%, Cr_2O_3 = 0.37-0.60 wt.%, Al_2O_3 = 0.06-0.18 wt.%), whereas magnetite from sample DDH04-47-49 shows slight Al enrichment (Al_2O_3 = 0.12-3.77 wt.%) and relative V enrichment (V_2O_3 = 0.22-0.73 wt.%), and exhibits relatively high TiO_2 (0.15-4.0 wt.%) (Figure 3.8).

3.6 DISCUSSION

3.6.1 Primary Spinel Compositions

Although spinel is an extremely sensitive petrogenetic indicator in igneous rocks, the composition of primary spinel grains may be changed or reset by syn- and post-magmatic processes (e.g. Roeder & Campbell, 1985, Power *et al.*, 2000). In particular, reequilibration with interstitial melt and/or hosting silicate minerals and serpentinization can significantly change the composition of spinel (e.g. Roeder & Campbell, 1985; Sack & Ghiorso, 1991; Scowen *et al.*, 1991; Roeder, 1994; Melinni *et al.*, 2005). An important observation from this study is that spinel grains from chromitite schleiren, wisps, pods, and layers have the most Cr-rich, Al- and Fe^{3+}-poor, and lowest Fe# compositions in the Turnagain intrusion (Figures 3.6-3.7), suggesting that they represent primary or near primary compositions. Chromite grains in the chromitites did not significantly interact with the hosting olivine or interstitial melt and thus preserved the highest temperature spinel compositions that crystallized from the most primitive (highest MgO) magmas. Chromitite sample 05ES-01-04-01 contains chromite with the lowest Fe# (0.30-0.35) consistent with the primary nature of these grains. In Figure 3.9, chromite analyses from most of the dunite, wehrlite, and olivine clinopyroxenite samples plot along vectors that converge towards the field of each of the chromitite compositions, which indicates that the compositions closest to the chromitite field have undergone the least amount of re-equilibration. The proximity of dunite, wehrlite, and olivine clinopyroxenite chromite compositions to those from chromitite samples, coupled with the region of Cr-Al-Fe^{3+} space where sample-specific compositional vectors intersect, is consistent with derivation from a primary magma composition similar to that which precipitated the chromitites.

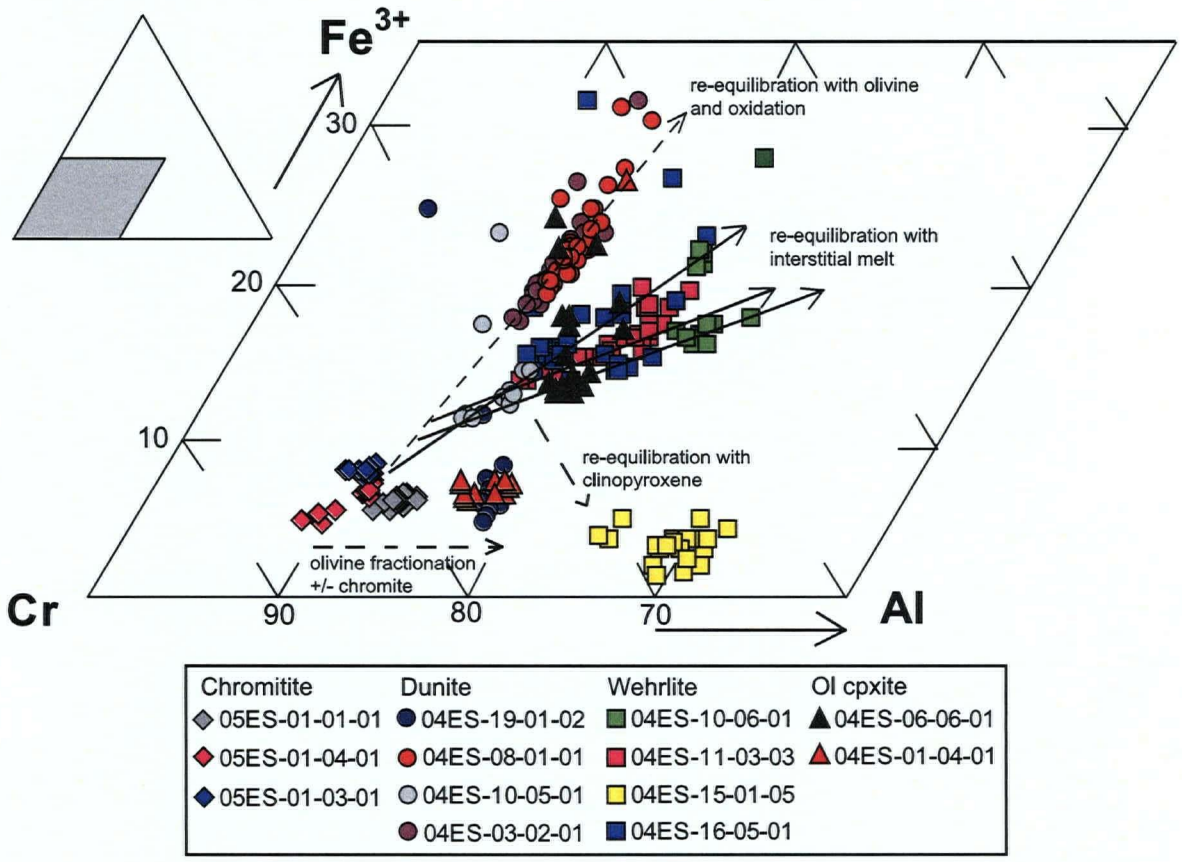

Figure 3.9: Trivalent cation (Fe^{3+}-Cr-Al) plot of Turnagain spinel compositions, focusing on those compositions nearest end-member chromite (inset in upper left shows entire ternary diagram). No rim compositions are plotted. Chromite grains from chromitites plot near the Cr-apex, whereas all compositions from wehrlites plot systematically to more Al-rich compositions than spinel grains from dunite. Note the wehrlite (04ES-15-01-05) and olivine clinopyroxenite (04ES-01-04-01) samples with anomalously low Fe^{3+} and high Al contents. Arrows indicate trends of spinel compositions from individual samples. Note the direction of trends (some arrows trend almost directly towards the Fe^{3+} apex, whereas others trend towards increased Al and Fe^{3+}), which explained by different reequilibration processes, and that all trends converge towards the area of the chromitite analyses.

3.6.2 Re-equilibration Trends

All chromite grains, except those from the chromitites, have undergone substantial compositional modification at high temperatures during cooling and interaction with evolved interstitial melt, enclosing silicates, or oxidizing fluids. The intersample change of chromite Fe# from chromitite to other lithologies at near-constant Fe^{3+}, as exhibited by specific samples in Figures 3.6, 3.7, and 3.9, is likely the result of olivine+chromite fractionation – olivine depletes the melt in Mg during crystallization and chromite depletes the melt in Cr such that co-precipitating chromite will have progressively higher Fe# and lower Cr/Al. The spinel trends with intermediate slopes on Figure 3.9, which contains only core and intermediate position analyses (no rims)mostly from wehrlite and olivine clinopyroxenite, converge towards the chromitite field and exhibit intrasample variations toward higher Al and Fe^{3+} with increasing Fe#. These trends can be explained by equilibration with evolved interstitial melt: the melt with which these chromite grains were in contact (either directly or by diffusion through olivine) was likely relatively rich in Ca, Al, Ti, and Fe^{3+}. Although the compositions of some samples in this trend may be related to their crystallization from a fractionated liquid, the dunite sample that parallels them did not and thus exhibits compositions related to re-equilibration with trapped melt. Chromite compositions with $Fe^{3+}/(Fe^{3+}+Cr+Al)>0.1$, which also exhibit an increase in Fe# (Figure 3.7), appear to have been modified by subsolidus re-equilibration with enclosing or enveloping olivine and by oxidizing fluids. The chromite compositions from dunites 04ES-03-02-01 and 04ES-08-01-01 overlap in the Cr-Al-Fe^{3+} ternary (Figure 3.9), extending parallel to the Cr-Fe^{3+} join but are distinct with respect to Fe# (Figure 3.7A). Most of the spinel grains in these two samples occur along olivine grain boundaries, not inside olivine, and the increase in $Fe^{3+}/(Cr+Al+Fe^{3+})$ can be attributed to oxidation by fluids that locally precipitated magnetite (but did not involve serpentinization). The increase of chromite Fe# is the result of the exchange of Fe^{2+} from olivine to chromite during cooling; the spinel grains from these two dunite samples do not show enrichments in Al or Ti, thus the trend towards lower Fe# is best explained by exchange with olivine, in the absence of interstitial melt. The unusual spinel compositions from wehrlite sample 04ES-15-01-05 and olivine clinopyroxenite sample 04ES-01-04-01 – relatively high Al/Cr and low Fe^{3+} – may be attributed to their silicate mineralogy. These samples contain cumulus olivine and chromite surrounded by 2 cm-diameter Cr-rich (see Chapter 4) clinopyroxene oikocrysts. The volume ratio of clinopyroxene to chromite is approximately 50:1, such that the significant

compositional changes exhibited by the chromite in these two samples is only weakly reflected in the hosting clinopyroxene.

3.6.3 Compositional Effects of Serpentinization on Spinel Chemistry

Magnetite and ferritchromit rims around chromite grains in many rocks from the Turnagain intrusion were formed during serpentinization. These rims, where wide enough to analyze with a 10 μm electron beam, exhibit compositions distinct from the primary spinel compositions in the chromitites and the high-temperature re-equilibrated compositions previously documented (Figure 3.9). The chromite analyses from dunite, wehrlite, and olivine clinopyroxenite samples that plot near the Fe^{3+} apex in Figure 3.6A are nearly pure magnetite in composition and likely reflect nucleation of magnetite around pre-existing chromite during serpentinization. Ferritchromit rims are recognized by individual spot analyses that plot further towards the Cr-Fe^{3+} join than their respective intrasample chemical trends (e.g. 04ES-10-05-01; Figure 3.9). These ferritchromit rims are characterized by lower Cr, slightly lower Al, and higher Fe^{3+} compared to other analyses and reflect the Fe-rich and Cr-poor nature of the serpentinizing fluids from which these rims formed. It is unclear whether ferritchromit rims are products of nucleation or reaction with serpentinizing fluids. However, some samples exhibit both ferritchromit and magnetite rims (e.g. 04ES-03-02-01), suggesting that ferritchromit represents a reaction product between magnetite-saturated serpentinizing fluids and chromite with a core-to-rim order of formation of chromite → ferritchromit → magnetite.

3.6.4 Implications for the Redox State of the Turnagain Intrusion

The low Fe^{3+} content of chromite grains from the chromitites in the Turnagain intrusion (Clark, 1978) is consistent with a low Fe^{3+}/Fe^{2+} ratio (i.e. relatively low oxygen fugacity) in the parental magma (e.g. Parkinson & Arculus, 1999). However, most Alaskan-type intrusions appear to have formed from relatively oxidized arc magmas, with calculated ΔFMQ (log units of oxygen relative to the fayalite-magnetite-quartz synthetic buffer) values between +1 to +3.5 (e.g. Ballhaus *et al.*, 1991; Carmichael, 1991; Rohrbach *et al.*, 2005). Under such oxidized conditions, sulphur will be dominantly dissolved as SO_2, SO_3, or SO_4^{2-} rather than sulphide (S^{2-}) and the magmas will not saturate in an immiscible sulphide liquid unless they are reduced to fO_2 values below FMQ (Jugo *et al.*, 2004; 2005). The presence of significant amounts of sulphide in the Turnagain intrusion indicates that the magmas achieved sulphide saturation and

therefore the oxygen fugacity was substantially lower than that typical for other Alaskan-type intrusions (e.g. Garuti *et al.*, 2003). In Figure 3.10, an expanded view of the Cr-Al-Fe^{3+} ternary, all chromite compositions from this study are plotted by lithology, with the data density maxima (50% and 90%) of chromite compositions from other Alaskan-type intrusions from Barnes & Roeder (2001). The majority of chromite compositions from the Turnagain intrusion lie to lower Fe^{3+} values than the established compositional fields. The compositions from chromitites contain significantly less Fe^{3+} than other chromite compositions and higher Cr/Al, which suggests that the chromitites crystallized from magmas with a lower oxygen fugacity than the parental magmas of other Alaskan-type intrusions. The low Fe^{3+} field for other Alaskan-type intrusions on Figure 3.10 may represent compositions that result from re-equilibration with clinopyroxene as observed in this study. Although not shown on Figure 3.10, chromite compositions from chromitite in the Turnagain intrusion plot well within the boninite field (see Barnes & Roeder, 2001), which may indicate that the magmas parental to the Turnagain intrusion also originated from a mantle previously depleted by partial melting. Decompression melting at back-arc ridges segregates Pt alloys in the residue (lithospheric mantle) which, if remelted by slab-derived fluids, would generate a Pt-rich basaltic melt (Kepezhinskas & Defant, 2001; Batanova *et al.*, 2005). The remelting of a Pt-enriched, previously depleted mantle, in a subduction zone setting may explain why many Alaskan-type intrusions are relatively enriched in Pt (Green *et al.*, 2004; Batanova *et al.*, 2005).

Inclusions of phyllite are observed in drillcore from the sulphide-mineralized zones of the Turnagain intrusion (Chapter 4) and reduction of the Turnagain parental magmas was likely achieved by the local assimilation of this graphitic, pyritic phyllite (Chapter 2 and 4). Assimilation of the pyrite-bearing phyllite also contributed additional S to the magma, thus increasing fS_2 and allowing for early sulphide saturation. The relatively reduced fO_2 of the Turnagain parental magmas not only lead to early sulphide saturation, but resulted in the crystallization of Fe^{3+}-poor chromite as represented by the chromitites. Chromite compositions from chromitites, therefore, may represent a possible reconnaissance exploration tool for assessing the relative redox state of parental magmas to ultramafic rocks where only olivine is co-crystallizing, and thus may be used as an indicator of the potential for magmatic sulphide mineralization in Alaskan-type intrusions.

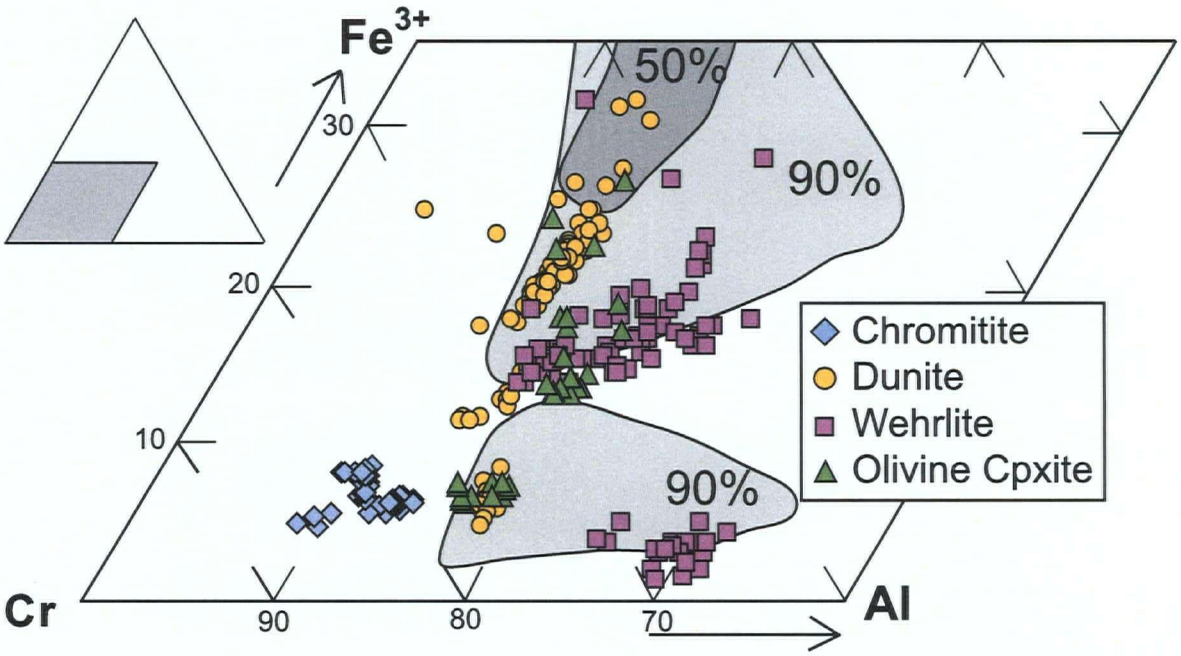

Figure 3.10: Trivalent cation (Fe^{3+}-Cr-Al) plot of Turnagain chromite compositions (inset in upper left shows entire ternary diagram). All samples are distinguished by lithology. Chromite compositions from the Turnagain intrusion are overlain by the data density maxima for other Alaskan-type intrusions from the compilation of Barnes & Roeder (2001). The 50% field is coloured dark grey (50% of all Alaskan-type spinel data plot within this field) and the 90% percent field is shaded light grey. In general the Turnagain spinel compositions have significantly lower Fe^{3+} and high Cr/(Cr+Al)relative to other Alaskan-type spinels, which is consistent with relatively low oxygen fugacity of the parental magmas of the Turnagain intrusion.

3.7 CONCLUSION

The principal results of this study on spinel compositions in ultramafic rocks from the Turnagain Alaskan-type intrusion are 1) primary spinel compositions are relatively Fe^{3+}-poor and Cr-rich compared to published results from other Alaskan-type intrusions, especially chromite from chromitite, 2) chromites from dunite, wehrlite and olivine clinopyroxenite exhibit intrasample trends that can be related to a variety of processes, including olivine fractionation, re-equilibration with interstitial melt, re-equilibration with coexisting silicate phases, oxidation, and serpentinization, 3) most intrasample re-equilibration trends can be interpolated to originate from the field of spinel compositions from chromitites, suggesting that all lithologies in the Turnagain intrusion crystallized from a similar parental magma, and 4) chromite compositions from chromitite are extremely Fe^{3+}-poor, indicating their crystallization from a magma characterized by a relatively low oxygen fugacity compared to other Alaskan-type intrusions. The reduced nature of the parental magmas, attributed to the assimilation of graphitic and pyritic country rocks, appears to have promoted local sulphide saturation. Therefore the Fe^{3+} content of chromite from chromitites may be used as a reconnaissance exploration tool for assessing the relative redox state and sulphide mineralization potential of Alaskan-type intrusions.

3.8 ACKNOWLEDGEMENTS

We would like to thank Mati Raudsepp at the University of British Columbia for use of the electron microprobe and support during the research phase of this manuscript, as well as Caroline-Emmanuelle Morisset at the Pacific Centre for Isotopic and Geochemical Research, University of British Columbia, for her input into this manuscript. The authors are grateful to Hard Creek Nickel Corp. for continued field support for this project and to Jim Reed of Pacific Western Helicopters for his exemplary logistical support in the field. Special thanks to Tony Hitchins, Bruce Northcote, Chris Baldys, and Mark Jarvis (President) of Hard Creek Nickel Corp. for their generous support and interactions throughout the period of the principal author's M.Sc. thesis at UBC. Funding for this project was provided by a research grant from Hard Creek Nickel Corp. (formerly Canadian Metals Exploration Ltd.).

3.9 REFERENCES

Ballhaus, C., Berry, R.F., & Green, D.H. (1991). High pressure experimental calibration of the olivine-orthopyroxene-spinel oxygen geobarometer: implications for the oxidation state of the upper mantle. *Contributions to Mineralogy and Petrology* **107** (1), 27-40

Barnes, S.J., & Roeder, P.L. (2001). The range of spinel compositions in terrestrial mafic and ultramafic rocks. *Journal of Petrology* **42** (12), 2279-2302

Batanova, V.G., Pertsev, A.N., Kamenetsky, V.S., Ariskin, A.A., Mochalov, A.G., & Sobolev, A.V. (2005). Crustal evolution of island-arc ultramafic magma: Galmoenan pyroxenite–dunite plutonic complex, Koryak Highland (Far East Russia). *Journal of Petrology* **46**, 1345-1366

Carmichael, I.S.E. (1991). The redox states of basic and silicic magmas: a reflection of their source regions? *Contributions to Mineralogy and Petrology* **106**, 129-141

Clark, T. (1975). Geology of an ultramafic complex on the Turnagain River, northwestern B.C.; unpublished PhD thesis, *Queen's University*, 454p.

Clark, T. (1978). Oxide minerals in the Turnagain ultramafic complex, northwestern British Columbia. *Canadian Journal of Earth Sciences* **15**, 1893-1903

Clark, T. (1980). Petrology of the Turnagain ultramafic complex, northwestern British Columbia. *Canadian Journal of Earth Sciences* **17**, 744-757

Dick, J.B., & Bullen, T. (1984). Chromian spinel as a petrogenetic indicator in abyssal and alpine-type peridotites and spatially associated lavas. *Contributions to Mineralogy and Petrology* **86**, 54-76

Erdmer, P., Mihalynuk, M.G., Gabrielse, H., Heaman, L.M., & Creaser, R.A. (2005). Mississippian volcanic assemblage conformably overlying Cordilleran miogeoclinal strata, Turnagain River area, northern British Columbia, is not part of an accreted terrane. *Canadian Journal of Earth Sciences* **42**, 1449-1465

Findlay, D.C. (1969). Origin of the Tulameen ultramafic-gabbro complex, southern British Columbia. *Canadian Journal of Earth Sciences* **6**, 399-425

Foster, F. (1974). History and origin of the Polaris ultramafic complex in the Aiken Lake area of north-central British Columbia; unpublished B.Sc. thesis, *University of British Columbia*, 66p.

Gabrielse, H. (1998). Geology of Cry Lake and Dease Lake map areas, north-central British Columbia; *Geological Survey of Canada*, Bulletin **504**, 147p

Garuti, G., Pushkarev, E.V., Zaccarini, F., Cabella, R., & Anikina, E. (2003). Chromite composition and platinum-group mineral assemblage in the Uktus Uralian-Alaskan-type complex (Central Urals, Russia). *Mineralium Deposita* **38**, 312-326

Green, D.H., Schmidt, M.W., & Hibberson, W.O. (2004). Island-arc ankaramites: primitive melts from fluxed refactory lherzolitic mantle. *Journal of Petrology* **45**, 391-403

Hill, R., & Roeder, P. (1974). The crystallization of spinel from basaltic liquid as a function of oxygen fugacity. *Journal of Geology* **82**, 709-729

Irvine, T.N. (1965). Chromian spinel as a petrogenetic indicator. Part I. Theory. *Canadian Journal of Earth Sciences* **2**, 648-672

Irvine, T.N. (1967). Chromian spinel as a petrogenetic indicator. Part II. Petrological applications. *Canadian Journal of Earth Sciences* **4**, 71-103

Jugo, P.J., Luth, R.W., & Richards, J.P. (2004). Experimental data on the speciation of sulfur as a function of oxygen fugacity in basaltic melts. *Geochimica et Cosmochimia Acta* **69** (2), 497-503

Jugo, P.J., Luth, R.W., & Richards, J.P. (2005). An experimental study of the sulfur content in basaltic melts saturated with immiscible sulfide or sulfate liquids at 1300°C and 1.0 GPa. *Journal of Petrology* **46** (4), 783-798

Kamenetsky, V.S., Crawford, A.J., & Meffre, S. (2001). Factors controlling chemistry of magmatic spinel: An empirical study of associated olivine, chrome-spinel and melt inclusion from primitive rocks. *Journal of Petrology* **42** (4), 655-671

Kamperman, M., Danyushevsky, L.V., Taylor, W.R., & Jablonski, W. (1996). Direct oxygen measurements of Cr-rich spinel: Implications for spinel stoichiometry. *American Mineralogist* **81**, 1186-1194

Kanaris-Sotiriou, R., Gibb, G.F., Carswell, D.A., & Curtis, C.D. (1978). Trace-element distribution and ore formation in vein-metasomatised peridotite at Kalskaret, near Tafjord, South Norway. *Contributions to Mineralogy and Petrology* **67**, 289-295

Kepezhinskas, P., & Defant, M.J. (2001). Nonchondritic Pt/Pd ratios in arc mantle xenoliths: Evidence for platinum enrichment in depleted island-arc mantle sources. *Geology* **29**, 851-854

Krause, J., Brügmann, G.E., Pushkarev, E.V. (2007). Accessory and rock forming minerals monitoring the evolution of zoned mafic-ultramafic complexes in the Central Ural Mountains. *Lithos* **95**, 19-42

Mellini, M., Rumori, C., & Viti, C. (2005). Hydrothermally reset magmatic spinels in retrograde serpentinites: formation of "ferritchromit" rims and chlorite aureoles. *Contributions to Mineralogy and Petrology* **149**, 266-275

Nixon, G.T., Hammack, J.L., Ash, C.H., Cabri, L.J., Case, G., Connelly, J.N., Heaman, L.M., Laflamme, J.H.G., Nuttall, C., Paterson, W.P.E., & Wong, R.H. (1997). Geology and platinum-group-element mineralization of Alaskan-type ultramafic-mafic complexes in British Columbia. *Geological Survey of British Columbia* Bulletin **93**, 141p.

Nixon, G.T. (1998). Ni-sulphide mineralization in the Turnagain Alaskan-type complex: A unique magmatic environment. *B.C. Ministry of Energy, Mines and Petroleum Resources* Paper **1998-1**, 18-1 – 18-12

Parkinson, I.J., & Arculus, R.J. (1999). The redox state of subduction zones: insights from arc-peridotites. *Chemical Geology* **160**, 409-423

Pouchou, J.L., & Pichoir, F. (1985): PAP $\phi(\rho Z)$ procedure for improved quantitative microanalysis. *Microbeam Analysis*, **1985**, 104-106.

Poustovetov, A.A., & Roeder, P.L. (2000). The distribution of chromium between basaltic melt and chromian spinel as an oxygen geobarometer. *Canadian Mineralogist* **39**, 309-317

Power, M.R., Pirrie, D., Anderson, J.C.Ø., & Wheeler, P.D. (2000). Testing the validity of chrome spinel as a provenance and petrogenetic indicator. *Geology* **28** (11), 1027-1030

Roach, T.A., Roeder, P.L., & Hulbert, L.J. (1998). Composition of chromite in the upper chromitite, Muskox layered intrusion, North West Territories. *Canadian Mineralogist* **36**, 117-135

Roeder, P.L., & Campbell, I.H. (1985). The effect of postcumulus reactions on composition of chrome-spinels from the Jimberlana intrusion. *Journal of Petrology* **26** (3), 763-786

Roeder, P.L., & Reynolds, I. (1991). Crystallization of chromite and chromium stability in basaltic melts. *Journal of Petrology* **32** (5), 909-934

Roeder, P.L. (1994). Chromite: from the fiery rain of chondrules to the Kilauea Iki lava lake. *Canadian Mineralogist* **32**, 729-746

Roeder, P.L., Poustovetov, A.A., & Oskarsson, N. (2001). Growth forms and composition of chromian spinel in MORB magma: diffusion-controlled crystallization of chromian spinel. *Canadian Mineralogist* **39**, 397-416

Rohrbach, A., Schuth, S., Ballhaus, C., Munker, C., Matveev, S., & Qopoto, C. (2005). Petrological constraints on the origin of arc picrites, New Georgia Group, Solomon Islands. *Contributions to Mineralogy and Petrology* **149**, 685-698

Sack, R.O, & Ghiorso, M.S. (1991). Chromite as a petrogenetic indicator. Mineralogical Society of America - *Reviews in Mineralogy* **25**, 323-354

Scowen, P.A.H., Roeder, P.L., & Helz, R.T. (1991). Reequilibration of chromite within Kilauea Iki lava lake, Hawaii. *Contributions to Mineralogy and Petrology* **107**, 8-20

Takashi, A., & Adachi, M. (1995). Ilvaite from a serpentinized peridotite in the Asama igneous complex, Mikabu greenstone belt, Sambagawa metamorphic terrain, central Japan. *Mineralogical Magazine* **59**, 489-496

Zakrzewski, M.A. (1989). Chromian spinels from Kusa, Bergslagen, Sweden. *American Mineralogist* **74**, 448-455

CHAPTER 4

PETROLOGY AND METALLOGENY OF THE TURNAGAIN ALASKAN-TYPE INTRUSION AND ASSOCIATED NI-SULPHIDE MINERALIZATION

4.1 INTRODUCTION

Alaskan-type intrusions are synonymous with Uralian-Alaskan-type and zoned ultramafic intrusions. The term "Uralian-Alaskan-type" originates from the two largest concentrations of these intrusions, in the Ural Mountains (n>15) of Russia (Taylor, 1967) and in southeastern Alaska (n=39) (Himmelberg & Loney, 1995). These intrusions are primarily composed of olivine- and clinopyroxene-rich cumulate rocks and may contain appreciable hornblende- and/or feldspar-bearing lithologies. Many of these intrusions are associated with island arcs and they are only rarely observed in other tectonic environments (e.g. Konder, Inagli, Chad, and Sibakh complexes; Johan, 2002). Alaskan-type intrusions in the Ural Mountains (Garuti *et al.*, 2003), in Columbia and Ecuador (Tistl, 1994), British Columbia (Findlay, 1969), Alaska (Himmelberg and Loney, 1995), and Australia (Barron *et al.*, 1991) have been associated with past and present placer platinum-group metal (PGM) mining operations. Only a few Alaskan-type intrusions contain appreciable sulphide mineralization, including Salt Chuck, Alaska (Loney *et al.*, 1987; Loney & Himmelberg, 1992), Duke Island, Alaska (Thakurta *et al.*, 2004), and Turnagain, British Columbia (Clark, 1975; Nixon, 1998).

The Turnagain Alaskan-type intrusion is a fault-bounded ultramafic intrusion (3.5 x 8 km) composed predominantly of dunite and wehrlite with minor amphibole-bearing phases, which are cross-cut by intermediate to felsic intrusions and dikes. There are two distinct styles of mineralization in the Turnagain intrusion: (1) Ni-(Cu)-sulphide mineralization that occurs in the most magnesian rock types (dunite and wehrlite) with minor local platinum-group element (PGE) enrichment, and (2) microscopic crystals of sperrylite ($PtAs_2$) and stibiopalladinite (Pd_5Sb_2) of probable hydrothermal origin, which was discovered in 2004 within hornblende-clinopyroxene lithologies. Ni-sulphide was first discovered in 1956 along the Turnagain River and the property was staked by Falconbridge (Clark, 1975). In the 1990s, the property was acquired by Bren-Mar Resources (now Hard Creek Nickel Corporation) and is actively being explored today. The historic Ni-rich sulphide showing, the Horsetrail Zone, has been extensively drilled with over 100 diamond drill holes. Other showings and prospects in the intrusion have been explored as well and the current Ni resource (measured and indicated) is 428 Mt grading 0.17% Ni (http://www.hardcreeknickel.com), which represents an increase of 200% from the 2005 estimate.

This study focuses on the petrology and geochemistry of the Turnagain intrusion to better constrain the emplacement and crystallization of magmas that formed the intrusion, and

to assess the origin of Ni-sulphide mineralization in this Alaskan-type intrusion. As part of recent mineral exploration by Hard Creek Nickel Corp., the entire intrusion has been systematically remapped and resampled. New field and petrographic observations, mineral and whole-rock chemistry (including platinum-group elements), and S and Pb isotopes in sulphide separates are presented in an effort to determine the processes responsible the genesis of the Turnagain intrusion and its localized Ni-sulphide mineralization.

4.2 GEOLOGY OF THE TURNAGAIN INTRUSION

4.2.1 Regional Geology

The 28 km^2 Turnagain intrusion is located approximately 70 km east of Dease Lake, British Columbia, in the Omineca Belt (Figure 4.1). This belt is composed of accreted terranes, including Quesnellia, Cache Creek, Slide Mountain, and Yukon-Tanana. The Turnagain intrusion is situated on the eastern edge of Quesnellia and structurally overlies lithologies currently assigned to Ancestral North America, which are Cambrian to Mississippian in age and consist of steeply-dipping graphitic, variably pyritic slates and phyllites of the Road River Group (Gabrielse, 1998) that contain interbeds of marble and tuff. Phyllites flank the eastern, northern, and western edges of the Turnagain intrusion, which is entirely fault-bounded. There is no observed hornfelsing of the surrounding phyllite. The contact between ultramafic rocks and phyllite was observed in numerous drillholes (e.g. DDH03-07, DDH06-158) and, although it is intensely talc-carbonate altered, original fabrics may be locally preserved. Post-intrusive deformation, exhibited by faulting and shearing, in both the Turnagain intrusion and the surrounding phyllites, grades from minor to intense generally in a WNW direction. The steeply-dipping phyllites were likely faulted along pre-existing cleavage, although local quartz-cemented phyllite breccia has been observed at the ultramafic-country rock contact in recent drill holes. A weakly metamorphosed volcanic wacke has been observed in both outcrop and drillcore to the south of the Turnagain intrusion. This unit, considered to correlate with the hornfels unit in the northwestern part of the intrusion (Figure 4.1), has also been correlated to a similar unit to the southeast of the Turnagain intrusion (Erdmer *et al.*, 2005).

Surface exposure of the Turnagain intrusion is generally poor (~20% of the total surface area is exposed) and much of the outcrop occurs in the northern third of the intrusion above treeline in the alpine region (Figure 4.2). The Horsetrail Zone contains scattered outcrops exposing most of the major lithologies, and other rare outcrops are found along the

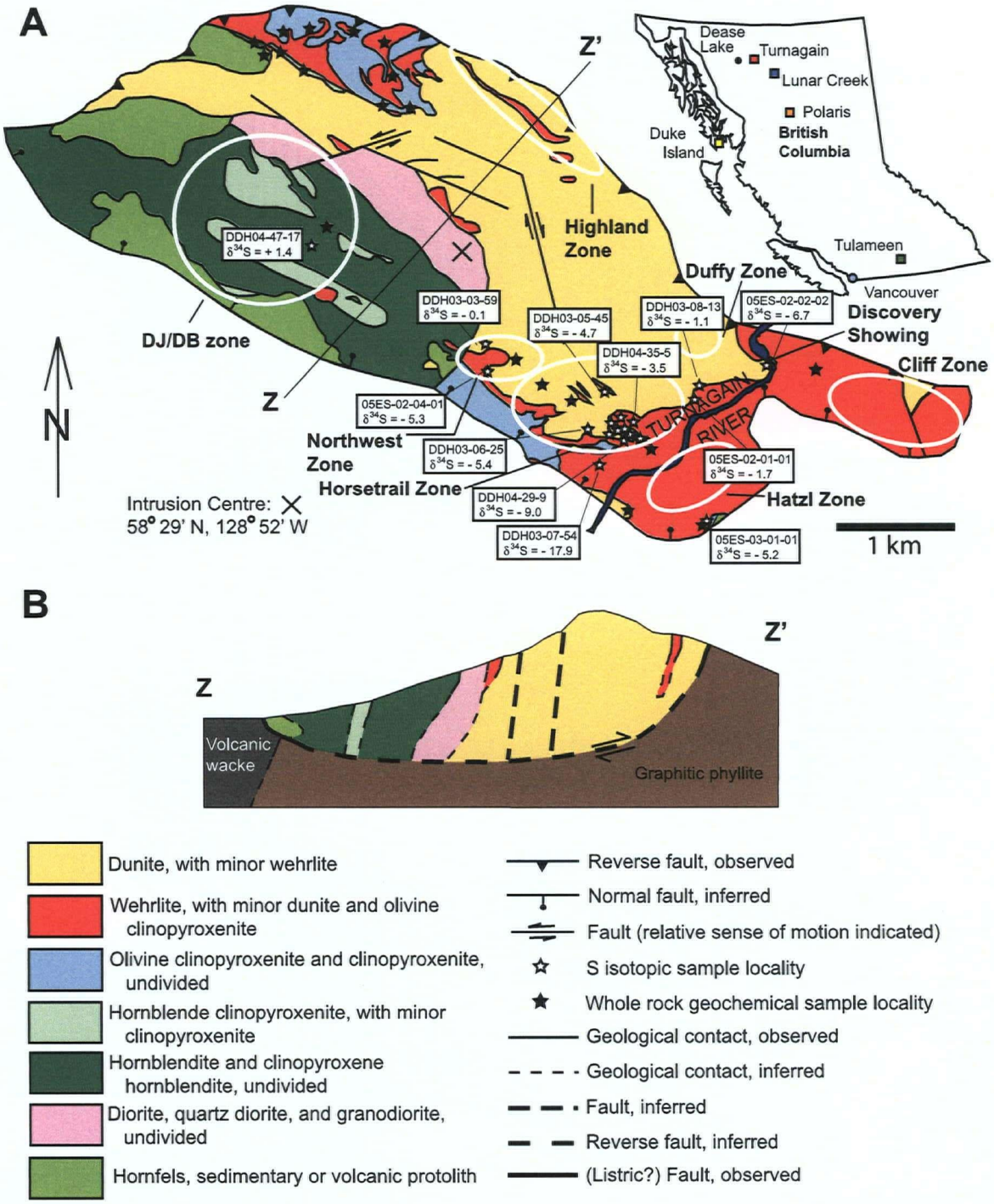

Figure 4.1: A) Simplified geological map of the Turnagain Alaskan-type intrusion showing major lithologies, structures, and sample locations for whole rock geochemistry and sulphide sulphur and lead isotopic compositions. Note that some lithologies are composites (e.g. olivine clinopyroxenite). Also shown are the main mineralized zones (from W to E): Northwest Zone, greater Horsetrail Zone (including Silesia to the south, and Fishing Rock to the east), Hatzl Zone, Cliff Zone, Duffy Zone, and Highland Zone. The inset in the upper right corner shows a map of British Columbia with the location of the Turnagain intrusion, and other major Alaskan-type intrusions in B.C. and Alaska. B) Interpreted cross-section (Z-Z') through the Turnagain intrusion, with all major lithologies, structures and contacts indicated.

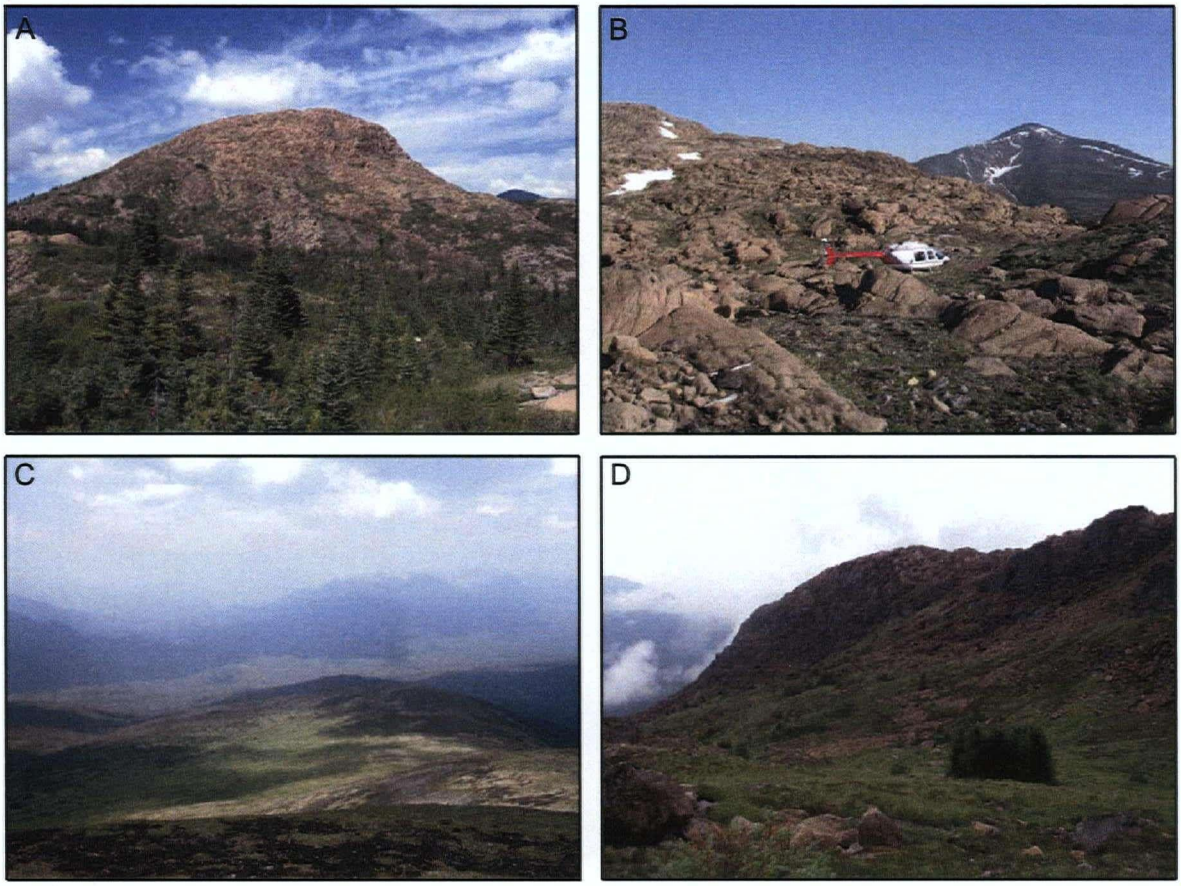

Figure 4.2: Photographs of dunite exposures in the Turnagain intrusion. A) Photograph of the resistant dunite core in the alpine region (view to the northwest). B) Photograph showing the extensive exposures of dunite in the highest elevations of the alpine region (view to the northwest). C) Photograph of a ridge of dunite, looking to the southwest from the top of the hornfels (volcanic wacke) knob in the northwest corner of the intrusion. The lack of outcrop beyond this ridge coincides with a magnetic-low anomaly. D) Photograph of the dunite core from within a long valley in the northern part of the intrusion, looking southeast. The small ridge (just visible in the lower left-hand corner) is primarily composed of wehrlite. The valley is filled with talus and runs parallel to the northern-bounding fault of the intrusion.

Turnagain River. The southern and western areas of the Turnagain intrusion are completely covered by 5-15 m of till, wheras east of the Turnagain River much of the intrusion is covered with up to 50 m of glaciofluvial gravels. Contacts between lithologies in the northern region of the Turnagain intrusion are generally observed, whereas most contacts in and around the Horsetrail Zone are inferred from drill core. Contacts in the western and southern areas are inferred from airborne and ground geophysics as well as recent drill core.

The current geological map for the Turnagain intrusion, which is continuously updated based on results from new drilling in relatively unknown areas, is largely based on the efforts of Clark (1975) and Nixon (1998). The original mapping and petrographic investigations of Clark (1975; 1978; 1980) lead to a wealth of fundamental information about the Turnagain intrusion. Subsequent investigations by Nixon *et al.* (1989) and Nixon (1998) focused on the origin of the Turnagain intrusion with respect to regional geological interpretations, as well as the origin of associated Ni-(Cu)-sulphide and platinum-group element (PGE) mineralization.

4.2.2 Ultramafic Rocks

4.2.2.1 Dunite and Chromitite

With the exception of hornblendite and diorite, the majority of the rocks exposed in the Turnagain intrusion are dominated by cumulus olivine and/or clinopyroxene. Dunite is volumetrically the most important lithology in the Turnagain intrusion and occurs in outcrop throughout the alpine regions of the intrusion, but is also observed in all major outcroppings in the Horsetrail Zone and the Cliff Zone (northeastern corner of the intrusion, Figure 4.1). Dunite weathers to a buff colour that is especially apparent in the alpine exposures (Figure 4.2B, Figure 4.3.1A). Most dunite is composed of large amounts of olivine (>90 vol.%) with small amounts of interstitial clinopyroxene, disseminated chromite, and locally interstitial phlogopite. Olivine grain size in dunite is commonly ~1 mm (Figure 4.4.1A), however olivine as large as 2 cm across or larger has been observed. Uncommonly large olivine occurs in association with much smaller olivine (<1 mm) in a porphyroclastic texture, which is interpreted to represent the product of high strain at high temperature. Olivine (~1 cm) with irregular grain boundaries, as well as parting, has also been observed in samples from the alpine area or in associated dunite below treeline (Figure 4.4.1B). Disseminated chromite is commonly 200-300 μm in diameter, exhibits euhedral to subhedral habits, and may have magnetite or ferritchromit overgrowths (Chapter 3). Chromite can also contain polyphase

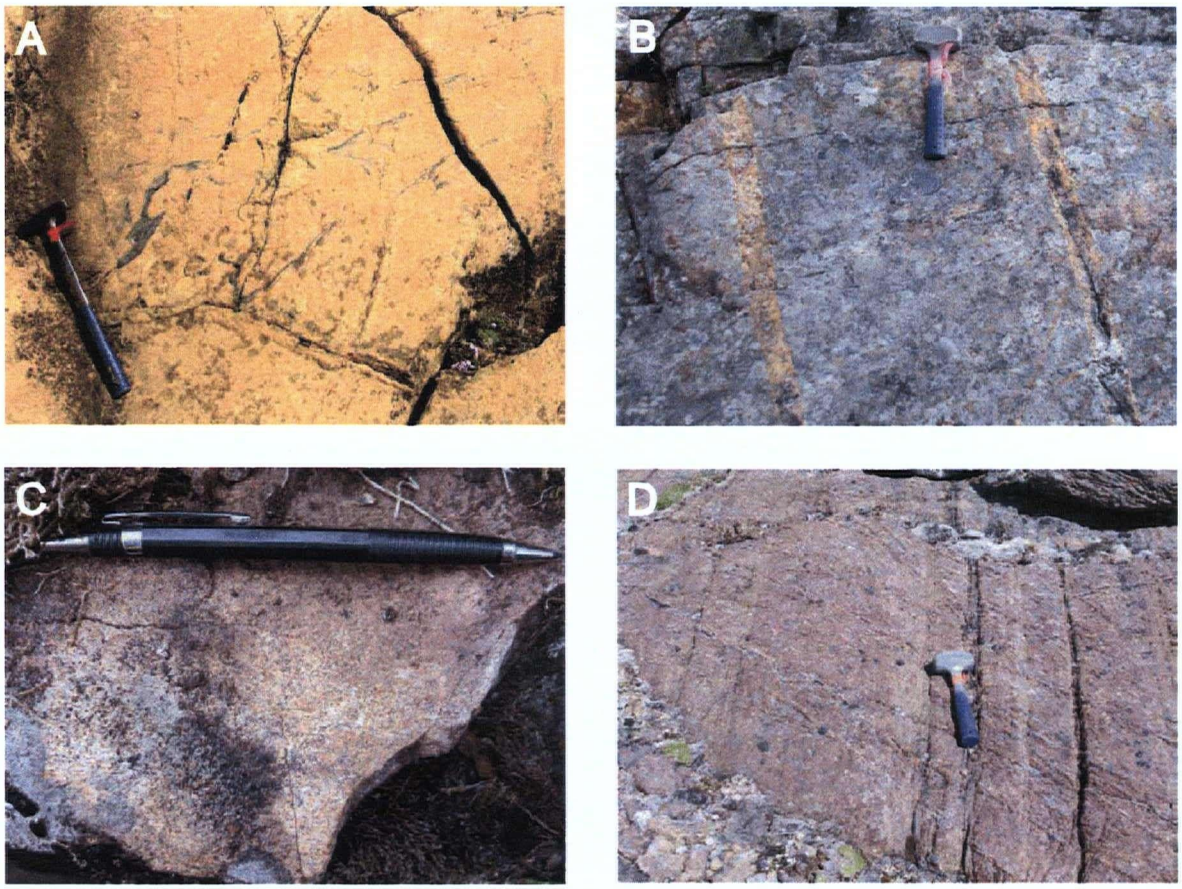

Figure 4.3.1: Photographs of outcrop-scale features in the Turnagain intrusion. A) Disrupted chromitite schleiren in alpine dunite. Hammer is 50 cm long. B) Olivine clinopyroxenite in alpine area with two cross-cutting dunite "dikes". Hammer is 30 cm long. C) Wehrlite showing atypical differential weathering of olivine (buff) and interstitial clinopyroxene (grey). Pencil is 12 cm long. D) Modal banding in wehrlite in the northwestern alpine region. Hammer is 30 cm long.

Figure 4.3.2: Photographs of outcrop-scale features in the Turnagain intrusion (continued). E) Modal banding in wehrlite, represented by alternating modal abundances of clinopyroxene (grey) and olivine (buff). Pencil is 12 cm long. F) Thick band (~1 m) of olivine clinopyroxenite (grey) within wehrlite (brown). Hammer is 30 cm long. G) Two olivine clinopyroxenite dikes (grey) cutting dunite (brown) parallel to the eastern dunite-olivine clinopyroxenite contact in the northwest. The photograph was taken 2 m east of the contact. H) Olivine clinopyroxenite dike swarm, cutting dunite, at the termination of exposure. This dike swarm originates from the easternmost dunite-olivine clinopyroxenite contact and is continuous for over 100 m. Hammer is 30 cm long.

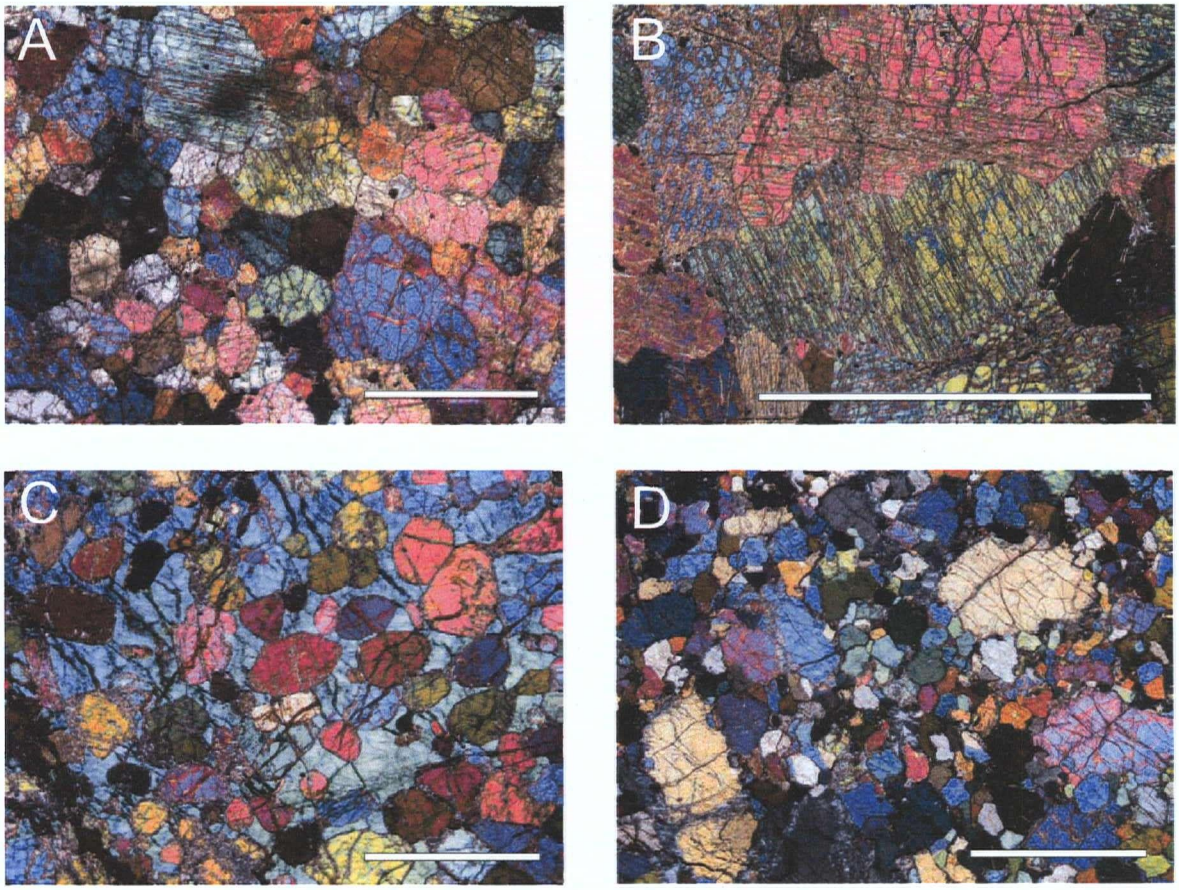

Figure 4.4.1: Photomicrographs (transmitted light, crossed-polarizers) of silicate mineral textures in the Turnagain intrusion. Scale bars (solid white bars) on all photos are 1 mm in length. A) Dunite (04ES-19-01-03) showing typical annealed texture (120° grain boundary intersections). Small black dots are disseminated chromian spinel. Note the large difference in size between individual olivine grains. B) Dunite (04ES-06-01-01) showing strong parting in olivine and irregular grain boundaries. C) Oikocrystic clinopyroxene in wehrlite (04ES-15-05-04). Note the well-preserved euhedral crystal faces of some olivine grains. D) Wehrlite (05ES-05-05-01) exhibiting large (1 mm) and small (<200 μm) olivine grains, as well as small to medium (300 μm) cumulus clinopyroxene grains.

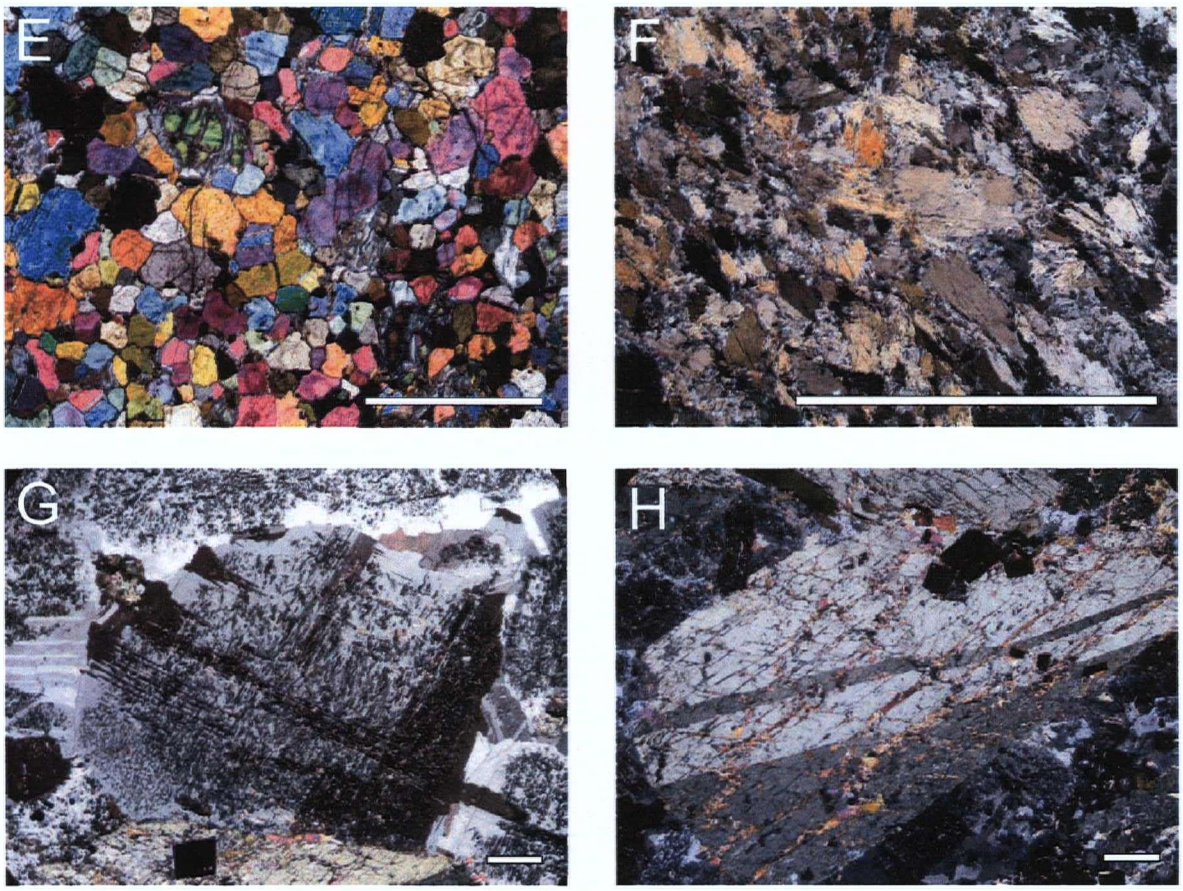

Figure 4.4.2: Photomicrographs (transmitted light, crossed- polarizers) of silicate mineral textures in the Turnagain intrusion (continued). Scale bars (solid white bars) on all photos are 1 mm in length. E) Olivine clinopyroxenite (04ES-10-02-03) with abundant cumulus clinopyroxene and rarely-preserved olivine (mostly serpentinized). Note the core of an olivine in the upper-middle-left of the photograph with a serpentine margin. F) Fine-grained hornblendite dike (04ES-20-11-01) with randomly-oriented amphibole grains. Not visible at this scale are small crystals of titanite along amphibole grain boundaries. G) Diorite (DDH04-57-12.89.2) with large (cumulus) plagioclase grain. H) Diorite (DDH04-57-12-89.2) with large twinned, euhedral (cumulus), amphibole grain.

silicate inclusions or sulphide inclusions. Chromitite, observed in dunite from the alpine region of the intrusion (Figure 4.3.1A), is sparsely distributed and occurs as wisps, bands, rare layers, pods, and schleiren. It commonly contains coarser chromite than dunite, up to 1 mm in some cases, and is almost completely unimodal (99% chromite). The irregular distribution and habit of chromite in the chromitites suggests that these rocks were disrupted or deformed at high temperatures following crystallization.

Dunite has been observed to cross-cut other ultramafic lithologies or the Turnagain intrusion, especially rocks that are spatially close to the alpine dunite. Dunite and olivine clinopyroxenite are locally juxtaposed together in the northwestern part of the intrusion (Figure 4.1), with no fault or obvious intrusive relationship, which may indicate the presence of primary igneous layering. However, in the above example, ~3 cm-wide dunite dikes were observed cutting the olivine clinopyroxenite (Figure 4.3.1B). Continuous dikes (over 100 m) of olivine clinopyroxenite (up to 10 cm wide) have also been observed cutting dunite (Figure 4.3.2G, H). Clark (1975) noted deformation of igneous layering at the contact with dunite in the northwestern part of the Turnagain intrusion.

Serpentinized dunite is common near major faults, although dunite typically contains only minor amounts (~10 vol.%) of serpentine minerals. Alpine dunite commonly contains small fractures filled with green, slickensided serpentine, and dunite from other parts of the intrusion is black due to an abundance of secondary magnetite. Black serpentine also contains traces of elemental carbon, graphite, and locally sulphide. Lizardite (green, well-foliated) is the most common serpentine mineral. Crysotile (fibrous and white) is only rarely found associated with serpentine veins/slips, and antigorite (massive meshes of interlocking needles) is generally only found in the Horsetrail Zone.

4.2.2.2 Wehrlite

Most exposures of wehrlite occur in the northwestern alpine region of the Turnagain intrusion (Figure 4.1), around/within the Horsetrail Zone, and in the Cliff Zone. Phlogopite from a wehrlite in the Hatzl zone (far southeastern edge of the intrusion) was dated at 189±1.3 Ma by Ar-Ar geochronology (see Chapter 2 for details). Two types of wehrlite occur in the Turnagain intrusion. The most common type is composed of cumulus olivine (1-5 mm) and interstitial clinopyroxene (Figure 4.3.1C). It typically weathers to a light brown colour and is easily distinguished from dunite in alpine exposures. Locally, clinopyroxene forms oikocrysts

up to 2 cm wide (Figure 4.4.1C). Wehrlite also contains disseminated chromite (50-150 μm) and rare interstitial phlogopite. The other type of wehrlite contains what is interpreted to represent cumulus clinopyroxene (Figure 4.3.1D, 4.3.2E) and occurs in exposures in the northwestern part of the intrusion as well as in exposures east of the Turnagain River (Cliff Zone) (Figure 4.1). This cumulus clinopyroxene has an elongate, prismatic habit and is typically finer-grained than coexisting olivine, about 200 μm in diameter (Figure 4.4.1D), although locally clinopyroxene up to 3 mm in length can occur. Wehrlite dikes have been observed to cross-cut dunite. Both types of wehrlite commonly contain abundant serpentine (up to 85 vol.%) replacing olivine.

4.2.2.3 Olivine Clinopyroxenite and Clinopyroxenite

Olivine clinopyroxenite and commonly pegmatitic clinopyroxenite are exposed in the northwestern part of the Turnagain intrusion (Figure 4.1) (clinopyroxenite is rarely exposed elsewhere and is generally only observed in drillcore). Interlayered olivine clinopyroxenite and wehrlite/dunite have been observed in recent drillcore from east of the Turnagain River, however layering is typically absent from outcrop exposures. Pegmatitic clinopyroxenite is observed as dikes that cross-cut dunite and wehrlite, and has also been observed in the northwest as segregations, presumably representing trapped volatile-rich residual melt, within olivine clinopyroxenite. Most olivine clinopyroxenite in the Turnagain intrusion is composed of cumulus olivine and clinopyroxene (both ~2 mm in diameter) with minor amounts of fine-grained interstitial clinopyroxene. Olivine clinopyroxenite weathers grey in colour with small olivine grains weathering to a buff colour. Locally, modal banding has been observed (Figure 4.3.2F). A few examples of olivine clinopyroxenite occur without cumulus clinopyroxene (e.g. sample 05ES-02-01-01) and instead contain cumulus olivine within oikocrytic clinopyroxene (Figure 4.4.1C). Chromite is rare in olivine clinopyroxenite (see Chapter 2). Where present, chromite is fine-grained (<150 μm) and is commonly encased in cumulus clinopyroxene. Chromite in olivine clinopyroxenite also does not exhibit significant secondary magnetite growth on the rims of grains, as observed in dunites and wehrlites. Dikes of olivine clinopyroxenite and clinopyroxenite have been observed cross-cutting both wehrlite and dunite, and locally biotite occurs along the contacts. These dikes are commonly pegmatitic, and one such example contains clinopyroxene crystals up to 20 cm in length. Olivine is

typically completely serpentinized in olivine clinopyroxenite (Figure 4.4.2E), although unaltered cores may be preserved.

Magnetite clinopyroxenite, an intermediate rock type between olivine clinopyroxenite and hornblende clinopyroxenite, has only been observed in drillcore from the east-central portion of the intrusion (Figure 1). Magnetite clinopyroxenite exhibits two types of magnetite: (1) cumulus (primary) magnetite crystals up to 5 mm in diameter coexisting with coarse (1-3 cm in length) clinopyroxene, and (2) round blebs of intergrown serpentine and secondary magnetite (up to 3 cm) in a matrix of small diopside crystals (~1 mm). Cumulus magnetite may exhibit modal banding and is interpreted to be comagmatic with its hosting clinopyroxene. The magnetite-serpentine blebs from the second type of magnetite clinopyroxenite are interpreted to represent clasts of dunite that were brecciated during the intrusion of their host clinopyroxenite.

4.2.2.4 Hornblende Clinopyroxenite

Although outcrops of hornblende clinopyroxenite are scarce, it comprises a major portion (~10% of the surface area) of the Turnagain intrusion. Much of the hornblende clinopyroxenite in the intrusion occurs in the west-central portion of the intrusion in an area called the DJ-DB Zone, which is a zone that is prospective for PGE mineralization (Figure 4.1). However a prominent dike-like body (1.2 km long x 15 m wide), exposed at the southern margin of the interbanded wehrlite and olivine clinopyroxenite in the northwest, provides the best exposure (Figure 4.1). Unweathered hornblende clinopyroxenite is generally porphyritic in texture and contains bright grey-green, equant clinopyroxene (1-4 cm long) and interstitial black amphibole (up to 2 cm long). Some samples contain abundant interstitial biotite, up to 35 vol.%. Magnetite crystals, typically 7 mm up to 1 cm in diameter, occurs in about 20% of all hornblende clinopyroxenite. Locally, magnetite in hornblende clinopyroxenite represents 5 vol.% of the rock. Examples of this rock type in the DJ-DB Zone are commonly pegmatitic, consisting of large (up to 10 cm wide) equant clinopyroxene and abundant interstitial amphibole. Although typically unaltered, large amounts (up to 85 vol.%) of secondary brown amphibole were noted in hornblende clinopyroxenite adjacent to the large block of hornfels in the southern DJ zone (DDH05-84).

4.2.2.5 Hornblendite

Hornblendite in the Turnagain in trusion is poorly exposed but makes up about 20 vol.% of the ultramafic lithologies. Hornblendite may contain coarse, equant clinopyroxene or interstitial plagioclase, and rarely biotite. There are three types of hornblendite present in the Turnagain intrusion. The first type is megacrystic to pegmatitic (with crystals up to 5 cm in length) and found in the DJ-DB Zone in the west-central portion of the intrusion. The other two types contain abundant (50-60 vol.%) cumulus amphibole, up to 1 cm in width, and 10-20 vol.% cumulus amphibole, respectively, with fine-grained interstitial hornblende matrices (<50 μm). Hornblendite commonly grades into hornblende clinopyroxenite or feldspathic hornblendite, which contains sub-rounded plagioclase grains 3-10 mm in length, rarely with irregular grain boundaries, within a matrix of hornblende crystals up to 2 cm long. Examples of hornblendite containing minor amounts of clinopyroxene are observed to have either porphyritic clinopyroxene surrounded by coarse-grained hornblende (1-2 cm in length) or oikocrystic hornblende encasing fine (2 mm) clinopyroxene. Exposures of hornblendite are rare, and the most accessible outcrop of hornblendite is found as a splay of unknown length off the above mentioned hornblende-rich 'dike' (Figure 4.1). This 30 cm-wide splay is characterized by fine-grained anhedral amphibole (Figure 4.4.2F) and intrudes the metasedimentary block in the northwest. Sample 04ES-00-07-04 from this dike was dated using both Ar-Ar (amphibole) and U-Pb (titanite) methods, and the obtained ages from this sample are 189±1.4 Ma and 190.3±4.6 Ma, respectively (see Chapter 2). Alteration in amphibole-bearing lithologies is distinct from that observed in olivine-bearing rocks in the Turnagain intrusion. Although minor, alteration minerals in hornblendite include chlorite and epidote after amphibole, chlorite after clinopyroxene and plagioclase, and sericite after plagioclase.

4.2.3 Other Rocks

4.2.3.1 Diorite

Diorite covers 10% of the exposed surface area in the Turnagain intrusion and occurs mainly in the central part of the intrusion (Figure 4.1). Although this unit is referred to as diorite, the central occurrence is actually a mixture of diorite, quartz diorite, and minor granodiorite, and contains an outer margin (~10 m thick) with significant amphibole (up to 95 vol.%). This margin may be easily confused for hornblendite (Clark, 1975). However, the presence of cumulus/porphyritic plagioclase helps to distinguish diorite from feldspathic hornblendite. It is

common for diorite to contain brecciated clasts of dunite, wehrlite, and olivine clinopyroxenite. In general, diorite contains 75 vol.% amphibole, 20 vol.% plagioclase, and minor amounts of quartz, biotite, apatite, and zircon. An outcrop of diorite from the northern margin of the central body (sample 04ES-00-07-01), near the contact with dunite, yielded a U-Pb (zircon) minimum age of 189.2±0.6 Ma (see Chapter 2). Diorite also occurs as thin (5-20 cm in width) dikes that are observed to intrude the more magnesian lithologies of the Turnagain intrusion. These dikes are typically felsic, with 5 vol.% amphibole, and also contain abundant quartz. One very coarse-grained leucocratic diorite (sample DDH04-57-12-89.2), with large cumulus crystals of amphibole and plagioclase (Figure 4.4.2G, H), yielded a U-Pb (zircon) age of 185.2±0.35 Ma (Chapter 2).

4.2.3.2 Hornfels

The hornfels unit (Figure 4.1) refers specifically to a greenish-gray, banded, volcanosedimentary rock (volcanic wacke) found either as large blocks in the northwest (Figure 4.2C) and southwest parts of the intrusion, or as xenoliths observed in drillcore. The hornfels unit is equigranular, with grain sizes typically between 0.5-1 mm, and is composed of approximately 45 vol.% epidote, 35 vol.% plagioclase, 10 vol.% amphibole, 5 vol.% quartz, and 5 vol.% biotite. The large block of hornfels in the northwest part of the intrusion contains pods and seams of two-mica granite not observed elsewhere that are interpreted to represent partial melts of country rock. Detrital zircons (subrounded to angular) are common in this lithology and one sample from the northwestern portion of the intrusion (sample 04ES-00-07-02) yielded a minimum U-Pb (zircon) depositional age of 301 Ma (latest Pennsylvanian-earliest Permian) with Precambrian inheritance (see Chapter 2). This unit commonly contains alternating 1-10 mm-wide bands of quartz- and chlorite-rich horizons, which may represent original bedding planes. Based on the above evidence, this unit is interpreted to be a volcanic wacke that was intruded by, and incorporated into, the Turnagain intrusion.

4.2.4 Sulphide

Sulphide occurs in nearly all rocks in the Turnagain intrusion. However it is observed predominantly in dunite and wehrlite. "Barren" olivine-dominated cumulate rocks (dunite and wehrlite) in the Turnagain intrusion typically contain 0.5-1 vol.% disseminated sulphide. Sulphide abundances in the mineralized zones (Horsetrail Zone and associated satellite zones;

Figure 4.1) range from 2 vol.% up to 20 vol.% or more. These zones contain disseminated, blebby, minor net-textured and rarely semi-massive sulphide. The Northwest, Silesia, and Fishing Rock Zones (to the west, south, and east of the Horsetrail, respectively, Figure 4.1) are relatively small compared to the Horsetrail Zone, which is unconstrained at depth (T. Hitchins, pers. comm., 2004). The mineralization to the east of the Turnagain River, in an area called the Hatzl Zone, is currently unconstrained with respect to grade, tonnage, or spatial distribution. All of the zones were originally interpreted to be separate areas of sulphide mineralization, but new and proposed drilling results indicate that many of them are connected at depth. The typical sulphide assemblage within the mineralized zones consists of pyrrhotite (~90 vol.% of total sulphide) and pentlandite with trace amounts of chalcopyrite. Pentlandite is distinguished from pyrrhotite in hand sample and drillcore by its lighter colour and reflection of light from cleavage planes. Visual estimates of the nickel grade are inaccurate because the Ni content in pentlandite ranges from 10 to 45 wt.% (Hard Creek Nickel Corp. internal reports). Sulphide in clinopyroxene- and amphibole-rich lithologies, rocks that are not prospective for Ni, typically consists of varying proportions of pyrrhotite, pyrite, and chalcopyrite. Clark (1975) and H. Kucha (Hard Creek Nickel Corp. internal reports) studied the sulphide mineralogy in detail and also observed minor amounts of violarite, bornite, millerite, molybdenite, vallerite, mackinawite, and oxysulphides.

Disseminated sulphides are typically fine-grained (0.1-0.5 mm) and occur throughout most of the olivine-rich lithologies of the Turnagain intrusion. Disseminated ore in the Horsetrail Zone is common near the margins of the zone, however it is low grade (<0.17% sulphide nickel) and represents the limit of currently economic sulphide mineralization. Serpentinized dunite and wehrlite proximal to the northern bounding fault, in the Highland Zone (Figure 4.1), contain ~0.5 vol.% disseminated pentlandite, similar in texture to sulphide shown in Figure 4.5C. These fine-grained pentlandite occurrences are interpreted to have formed by Ni-enrichment of primary sulphide during serpentinization.

Blebby sulphide is common in the mineralized zones (e.g. Northwest Zone) and is observed as small (2-3 mm) to large (~1.5 cm), sub-rounded (Figure 4.5A) to elongate (Figure 4.5D-F), sulphide aggregations. The aggregations are typically surrounded by olivine grains and some sulphide is commonly present between olivine grains adjacent to the sulphide bleb. These blebs are interpreted to represent isolated droplets of sulphide liquid that crystallized *in situ*. Note that the bleb shown in Figure 4.5A is completely surrounded by magnetite, which is

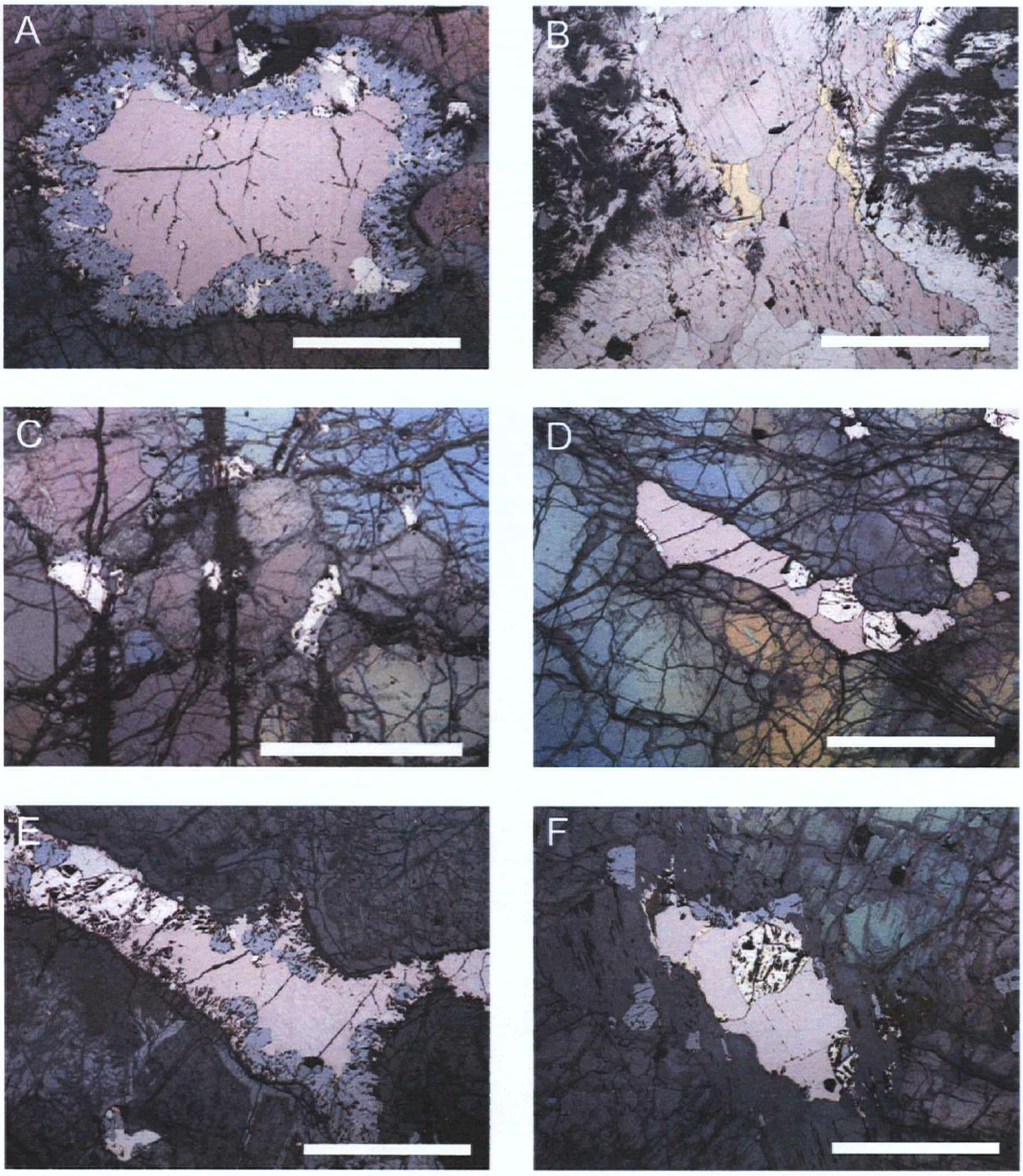

Figure 4.5: Photomicrographs (reflected light, crossed polars) of sulphide textures in the Turnagain intrusion. Scale bars on all photos are 200 μm in length. Colours in silicate minerals represent minor surficial and internal reflections. A) Dunite (DDH03-12-4) showing a fringe of secondary magnetite surrounding a single sulphide bleb containing pyrrhotite (brown) and pentlandite (light yellow). B) Dunite (05ES-02-02-02) containing intergrown semi-massive pyrrhotite and chalcopyrite. Note the small needles of serpentine (black) around the edges of the massive sulphide, as well as the sulphide outside the main sulphide mass. C) Dunite (DDH04-36-16) with small blebs of pentlandite and two thin serpentine veins. D) Wehrlite (DDH04-36-5) showing an elongate bleb of pyrrhotite with smaller crystals of pentlandite. E) Wehrlite (DDH04-28-6) showing an elongate bleb of pyrrhotite with magnetite and pentandite crystals. Note the tweed-like texture in the bottom portion of the bleb. F) Wehrlite (DDH03-08-13) showing a pyrrhotite bleb with minor chalcopyrite and two large pentlandite grains. The grey grains are chromian spinel.

a common feature of sulphide in partially serpentinized rocks in the Turnagain intrusion. Occurrences of angular sulphide blebs (some up to 3 cm in width) have been noted in drillcore from all of the major mineralized zones. These blebs typically contain the same proportion of pyrrhotite and pentlandite as the more rounded blebs, however angular blebs are also observed in olivine clinopyroxenite, not just dunite and wehrlite. Olivine clinopyroxenite in the Turnagain intrusion does not contain contemporaneous Ni-rich sulphide mineralization, most likely because it formed from a less magnesian, sulphur- and nickel-depleted magma compared to the magma(s) that formed dunite and wehrlite, and as such the rare angular blebs could not have precipitated *in situ*. The angular are interpreted to represent clasts of sulphide, originally in a massive horizon, that were brecciated during a magma influx or turbidity current and subsequently redistributed (W. Peredery, pers. comm., 2006).

Net-textured sulphide is not common in the Horsetrail, Northwest, Silesia, and Fishing Rock Zones or the Discovery showing (Figure 4.1), but is noted in local accumulations and horizons. This sulphide texture typically contains olivine grains of varying sizes within a sulphide matrix. Due to the amount of pentlandite present in such horizons (up to 10 vol.%), net-textured sulphides represent a high-grade target for exploration. However their apparent thickness is commonly only a few centimetres and rarely exceeds 20 cm.

Semi-massive and massive sulphide (Figure 4.5B) occurs in all economic zones within the Turnagain intrusion. The difference between the two types of sulphide lies in their gangue-mineral content: semi-massive sulphide contains abundant silicate and other minerals (e.g. graphite), whereas massive sulphide does not. Both of these sulphide textural types typically have sharp contacts with surrounding rocks indicating that they may represent sulphide that was remobilized. Such horizons of massive and semi-massive sulphide are typically only 5 cm or less in width and are dominantly composed of pyrrhotite and minor chalcopyrite with trace amounts of pentlandite. Semi-massive and massive sulphides in the Turnagain intrusion therefore are rarely prospective for nickel.

4.2.5 Inclusions

Xenoliths of country rock within the Turnagain intrusion are restricted to the mineralized zones, and these have only been observed in drillcore. No inclusions have been observed in areas of abundant outcrop (e.g. alpine dunite, Figure 4.2) or nearly continuous exposure. The inclusions within the Turnagain intrusion are, without exception, hornfelsed equivalents of

wallrocks. Figure 4.6 displays inclusions from six different drill holes within mineralized zones. The two most commonly encountered inclusions are metavolcanic wacke (MVwk) and metaphyllite (MPhy). The third type of inclusion, calc-silicate (CS), occurs as isolated inclusions (Figure 4.6E, F) or as interbeds within the other types of inclusions (Figure 4.6A). The metavolcanic wacke, described as the hornfels unit above (section 4.2.3.2), also occurs as smaller blocks within drillcore (Figure 4.6A-C). The inclusions of metavolcanic wacke are typically identical in mineralogy and texture to the larger blocks of hornfels. Rarely, the metavolcanic wacke inclusions are slightly coarser grained and contain small seams of two-mica granite (partial melt) that may cross-cut banding. It is uncommon, but noted, to observe interbeds of metavolcanic wacke and metaphyllite in the same inclusion (Figure 4.6B, C).

Metaphyllite inclusions (MPhy) are texturally and mineralogically different from their "Road River" phyllite predecessors. Metaphyllite commonly contains brown-coloured areas that are mineralogically dominated by graphite and pyrrhotite with interlayered quartz (Figure 4.6B-D). Graphite and pyrrhotite wisps and seams (typically semi-massive sulphide), interpreted to represent partially digested inclusions of phyllite, were also previously observed by Clark (1975) within ultramafic lithologies. The lack of pyrite (FeS_2) and the abundance of pyrrhotite ($Fe_{1-X}S$) indicate that sulphur was released into the host magma during contact metamorphism of the phyllite inclusions.

Calc-silicate inclusions (CS) are typically white in colour and relatively small (as small as 2-3 cm in width). However, as noted above, they may occur as interbeds within either metavolcanic wacke or metaphyllite. Calc-silicate inclusions are fine-grained (<1 mm) and typically consist of a mixture of carbonate (calcite, magnesite), wollastonite, diopside, quartz, and locally grossular. Note that in Figure 4.6E and F the calc-silicate inclusions have a slight reddish colour indicating their high garnet content. Calc-silicate xenoliths typically do not display extensive digestion, incorporation into their host rocks, or redox halos.

4.3 ANALYTICAL TECHNIQUES

4.3.1 Mineral Chemistry

The olivine, clinopyroxene, amphibole, and biotite contents of each sample, textural relationships with other phases, and relative degree of alteration were carefully documented using both transmitted and reflected light microscopy prior to analysis. Samples were selected to represent the various rock types found in the Turnagain intrusion. For each sample, typically

AltDn
MVwk
CS
MVwk
AltDn
AltDn
MVwk
MVwk
A

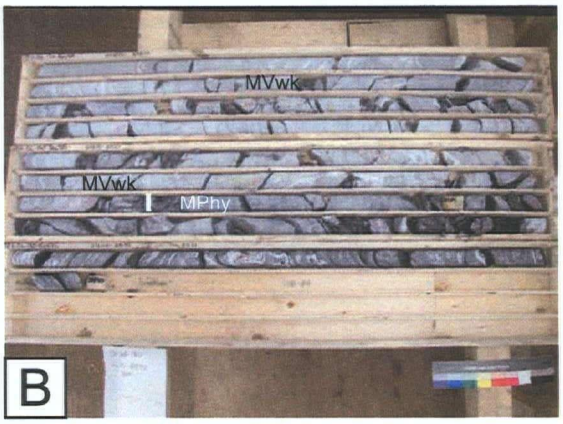
MVwk
MVwk
MPhy
B

MPhy
MVwk
MVwk
MPhy
C

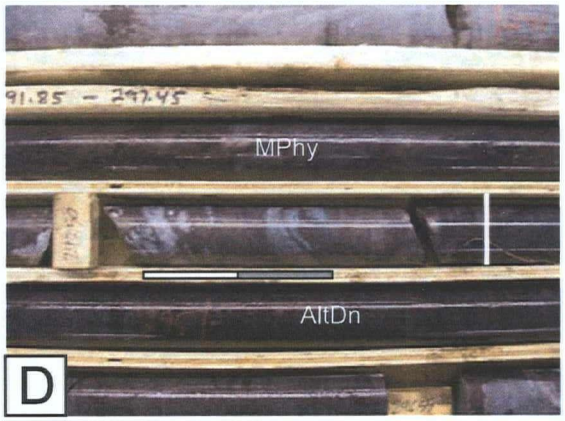
91.85 - 297.45
MPhy
AltDn
D

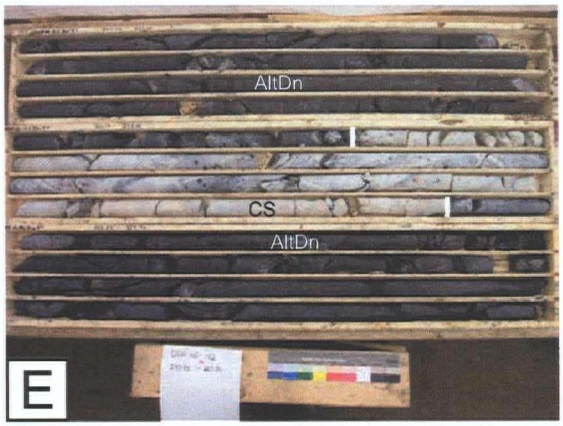
AltDn
CS
AltDn
E

AltDn
CS
AltDn
F

Figure 4.6: Photographs of sedimentary xenoliths in NQ size drillcore (2006) from the Turnagain intrusion. Core boxes are 1.5 m long, white lines indicate interlithological contacts, and labels indicate lithology. A) DDH06-123, 201-218 m. Inclusion of interbedded metavolcanic wacke (MVwk) and calc-silicate (CS) within altered dunite (AltDn) changing down-hole to a larger MVwk inclusion. B) DDH06-130, 202-219 m. Large inclusion of coarsely interbedded MVwk and metaphyllite (MPhy). C) DDH06-143, 71-88 m. Large inclusion of gradationally bedded MVwk and MPhy. Note the very small (5-20 cm) beds of MVwk in the transition zone between the two lithologies. D) DDH06-163, 294.5 m. Strongly hornfelsed metaphyllite. The only minerals present are quartz (white-blue) and a fine-grained mixture of graphite and pyrrhotite (brown). Scale-bar is 10 cm long. E) DDH06-152, 247-263 m. Inclusion of CS within AltDn. Note the slight reddish colour associated with grossular. The grey zones within the inclusion are interpreted to be highly-altered dunite. F) DDH06-153, 174-190 m. Small inclusion of CS in AltDn. This inclusion also contains grossular, but unlike the inclusion documented above, contains no intermixed dunite.

three different grains were analyzed with three spot analyses per grain (core, intermediate position, and rim). Representative analyses for olivine and clinopyroxene, and complete analyses for amphibole and biotite are found in Tables 4.1 to 4.4, respectively. Complete analytical results for olivine and clinopyroxene are listed in Appendices II and III. Garnet analyses are listed in Appendix IV.

A total of 25 samples were selected for microprobe analysis, carbon-coated, and documented using the Philips XL-30 scanning electron microscope at the University of British Columbia, Vancouver, B.C. Quantitative analyses were carried out in wavelength-dispersion mode using the Cameca SX-50 electron microprobe with a beam diameter of 10 μm, an accelerating voltage of 15 keV, and a beam current of 20 nA with 20 s peak count-time and 10 s background count-time. A list of X-ray lines and elements considered, as well as their standards, can be found in Appendix V. Data reduction of all analytical results was undertaken using the "PAP" $\phi(\rho Z)$ procedure of Pouchou & Pichoir (1985). A total of 354 points were analyzed (207 olivine, 91 clinopyroxene, 48 amphibole, 8 biotite, 9 garnet). Olivine and clinopyroxene were assumed to be stoichiometric. Ferric iron in olivine was assumed to be zero, and ferric iron in clinopyroxene was calculated using the stoichiometric technique of Lindsley (1983). In amphibole, ferric iron and other cation ratios were calculated using the method of Holland & Blundy (1994) and mineral names were assigned using the nomenclature of Leake *et al.* (1997). Chemical compositions of amphibole were calculated on the basis of 23 oxygens (16 cations ideal, with vacancy in A site). Biotite stoichiometry was calculated using standard techniques (22 oxygens, 16 cations, 2 OH ± Cl ± F ideal). The term 'biotite' refers to the biotite solid solution containing phlogopite (Mg# = 0.85-1.00) and annite (Mg# = 0.00-0.15) end-members. Garnet cation distributions were also calculated using standard stoichiometric techniques.

4.3.2 Major and Trace Elements

For whole rock analyses, only the freshest portions of individual samples were taken in the field and any remaining weathered surfaces were systematically removed during sample processing. All samples were crushed using a hydraulic piston crusher between WC plates. A 100 gram aliquot of each crushed sample was powdered using the Fritsch Pulverisette planetary mono- and-multi mills in agate jars.

Table 4.1a: Representative olivine compositions from olivine-bearing ultramafic lithologies of the Turnagain intrusion

Rock type:	Chromitite			Chromitite			Dunite			Dunite			Dunite			Wehrlite		
Sample:	05ES-01-01-01			05ES-01-04-01			04ES-10-05-01			04ES-08-01-01			04ES-19-01-02			04ES-10-06-01		
Cluster:	1			2			1			2			2			5		
Style:	porph.	porph.	porph.	mgb.	mgb.	mgb.	cumu.	cumu.	cumu.	cumu.	cumu.	cumu.	cumu.	cumu.	cumu.	porph.	porph.	porph.
Zone:	rim	mid	core	rim	mid	core	rim	mid	core	rim	mid	core	rim	mid	core	rim	mid	core
Oxides (wt. %)																		
SiO_2	41.58	41.11	41.10	41.71	41.71	41.90	42.17	41.26	40.86	40.86	40.66	40.85	41.48	41.45	41.22	40.91	40.70	40.47
Cr_2O_3	0.02	0.02	0.03	0.21	0.01	0.02	0.00	0.01	0.00	0.00	0.02	0.06	0.04	0.03	0.03	0.00	0.00	0.06
FeO	7.31	8.73	8.81	3.93	4.74	4.79	3.44	8.91	9.17	9.08	9.70	10.31	7.85	7.44	7.36	8.87	9.66	10.46
MnO	0.15	0.15	0.19	0.10	0.09	0.09	0.43	0.15	0.17	0.18	0.16	0.17	0.12	0.19	0.16	0.33	0.21	0.21
MgO	50.49	49.82	49.81	54.01	52.79	53.01	54.63	49.59	49.61	49.53	48.77	48.67	50.39	51.18	51.00	49.57	48.68	47.94
NiO	0.25	0.33	0.23	0.36	0.47	0.51	0.00	0.35	0.30	0.10	0.07	0.12	0.22	0.13	0.25	0.25	0.31	0.39
CaO	0.05	0.07	0.06	0.07	0.10	0.13	0.02	0.07	0.13	0.10	0.18	0.15	0.34	0.08	0.04	0.03	0.04	0.02
Total	99.85	100.23	100.23	100.39	99.92	100.45	100.69	100.33	100.24	99.85	99.57	100.35	100.43	100.48	100.06	99.95	99.61	99.56
Cations (p.f.u.)																		
Si	1.008	1.001	1.000	0.992	1.001	1.001	0.998	1.004	0.997	1.000	1.000	1.000	1.003	1.000	0.999	1.000	1.002	1.000
Cr	0.000	0.000	0.001	0.004	0.000	0.000	0.000	0.000	0.000	0.000	0.000	0.001	0.001	0.000	0.001	0.000	0.000	0.001
Fe	0.148	0.178	0.179	0.078	0.095	0.096	0.068	0.181	0.187	0.186	0.200	0.211	0.159	0.150	0.149	0.181	0.199	0.216
Mn	0.003	0.003	0.004	0.002	0.002	0.002	0.009	0.003	0.004	0.004	0.003	0.004	0.002	0.004	0.003	0.007	0.004	0.004
Mg	1.825	1.808	1.808	1.915	1.889	1.887	1.927	1.799	1.805	1.807	1.789	1.776	1.817	1.840	1.842	1.806	1.786	1.767
Ni	0.005	0.006	0.005	0.007	0.009	0.010	0.000	0.007	0.006	0.002	0.001	0.002	0.004	0.002	0.005	0.005	0.006	0.008
Ca	0.001	0.002	0.002	0.002	0.002	0.003	0.000	0.002	0.003	0.003	0.005	0.004	0.009	0.002	0.001	0.001	0.001	0.001
Total	2.991	2.999	2.998	3.000	2.999	2.999	3.002	2.996	3.003	3.000	2.999	2.998	2.995	2.999	3.000	3.000	2.998	2.997
End Members (%)																		
Fo	92.5	91.1	91.0	96.1	95.2	95.2	96.6	90.8	90.6	90.7	90.0	89.4	92.0	92.5	92.5	90.9	90.0	89.1
Fa	7.5	8.9	9.0	3.9	4.8	4.8	3.4	9.2	9.4	9.3	10.0	10.6	8.0	7.5	7.5	9.1	10.0	10.9

Crystal textural style is abbreviated: porph. (porphyroclast), cumu. (cumulus), def. (deformed), mgb. (modified grain boundaries)
Note: Other phases (cpx, chr) were also analyzed on certain sections, such that "Cluster" refers to a specific location on each section

Table 4.1b: Representative olivine compositions from olivine-bearing ultramafic lithologies of the Turnagain intrusion

Rock type:	Wehrlite			Wehrlite			Wehrlite			Olivine Cpxite			Olivine Clinopyroxenite			Olivine Clinopyroxenite		
Sample:	04ES-09-01-01			04ES-09-01-01			04ES-15-01-05			04ES-06-06-01			05ES-05-01-01			04ES-01-04-01		
Cluster:	1			4			1			1			4			1		
Style:	porph.	porph.	porph.	porph.	porph.	porph.	def.	def.	def.	cumu.	cumu.	cumu.	cumu.	cumu.	cumu.	cumu.	cumu.	cumu.
Zone:	rim	mid	core	mid	mid	core	rim	mid	core	rim	mid	core	rim	mid	core	rim	mid	core
Oxides (wt. %)																		
SiO_2	40.06	39.91	40.23	39.83	39.78	39.92	40.53	40.69	40.49	39.92	40.09	40.32	39.22	39.43	39.17	40.44	40.18	40.31
Cr_2O_3	0.00	0.00	0.00	0.00	0.00	0.00	0.02	0.02	0.00	0.04	0.02	0.02	0.00	0.01	0.02	0.01	0.01	0.02
FeO	12.69	13.18	12.98	12.78	12.40	13.07	10.79	11.50	11.17	12.96	12.87	13.14	14.95	15.63	15.61	12.27	12.73	12.75
MnO	0.28	0.18	0.19	0.21	0.24	0.19	0.22	0.18	0.24	0.25	0.23	0.21	0.23	0.26	0.22	0.16	0.22	0.21
MgO	45.82	45.41	45.67	45.66	45.72	45.64	47.80	47.44	47.53	46.30	46.01	46.53	44.46	44.21	44.25	46.38	46.67	46.55
NiO	0.20	0.25	0.22	0.18	0.25	0.19	0.27	0.29	0.38	0.10	0.04	0.05	0.08	0.08	0.14	0.09	0.11	0.05
CaO	0.05	0.05	0.01	0.00	0.02	0.02	0.02	0.08	0.06	0.03	0.04	0.05	0.03	0.01	0.02	0.00	0.03	0.05
Total	99.09	98.98	99.31	98.67	98.41	99.04	99.65	100.22	99.88	99.61	99.31	100.33	98.98	99.62	99.44	99.35	99.95	99.95
Cations (p.f.u.)																		
Si	1.005	1.004	1.007	1.004	1.004	1.003	1.002	1.003	1.001	0.997	1.003	1.000	0.996	0.997	0.993	1.008	0.999	1.001
Cr	0.000	0.000	0.000	0.000	0.000	0.000	0.000	0.000	0.000	0.001	0.000	0.000	0.000	0.000	0.000	0.000	0.000	0.000
Fe	0.266	0.277	0.272	0.269	0.262	0.275	0.223	0.237	0.231	0.271	0.269	0.272	0.318	0.331	0.331	0.256	0.265	0.265
Mn	0.006	0.004	0.004	0.005	0.005	0.004	0.005	0.004	0.005	0.005	0.005	0.005	0.005	0.006	0.005	0.003	0.005	0.004
Mg	1.713	1.704	1.705	1.715	1.720	1.710	1.762	1.744	1.752	1.724	1.716	1.720	1.683	1.667	1.673	1.723	1.729	1.724
Ni	0.004	0.005	0.004	0.004	0.005	0.004	0.005	0.006	0.007	0.002	0.001	0.001	0.002	0.002	0.003	0.002	0.002	0.001
Ca	0.001	0.001	0.000	0.000	0.001	0.001	0.001	0.002	0.002	0.001	0.001	0.001	0.001	0.000	0.001	0.000	0.001	0.001
Total	2.995	2.996	2.993	2.996	2.996	2.997	2.997	2.996	2.999	3.001	2.996	2.999	3.004	3.003	3.006	2.992	3.001	2.998
End Members (%)																		
Fo	86.6	86.0	86.2	86.4	86.8	86.2	88.8	88.0	88.4	86.4	86.4	86.3	84.1	83.4	83.5	87.1	86.7	86.7
Fa	13.4	14.0	13.8	13.6	13.2	13.8	11.2	12.0	11.6	13.6	13.6	13.7	15.9	16.6	16.5	12.9	13.3	13.3

Crystal textural style is abbreviated: porph. (porphyroclast), cumu. (cumulus), def. (deformed), mgb. (modified grain boundaries)
Note: Other phases (cpx, chr) were also analyzed on certain sections, such that "Cluster" refers to a specific location on each section

Table 4.2a: Representative clinopyroxene compositions from clinopyroxene-bearing ultramafic lithologies of the Turnagain intrusion

Rock Type:	Wehrlite			Wehrlite			Wehrlite			Olivine Clinopyroxenite			Olivine Clinopyroxenite			Olivine Clinopyroxenite		
Sample:	04ES-10-06-01			04ES-11-03-03			04ES-09-01-01			04ES-06-06-01			05ES-05-01-01			04ES-01-04-01		
Cluster:	1			6			5			5			6			2		
Style:	cumu.	cumu.	cumu.	inter.	inter.	inter.	inter.	inter.	inter.	cumu.	cumu.	cumu.	cumu.	cumu.	cumu.	inter.	inter.	inter.
Zone:	rim	mid	core	rim	mid	core	rim	mid	core	rim	mid	core	rim	mid	core	rim	mid	core
Oxides (wt. %)																		
SiO_2	54.02	53.50	54.01	54.20	54.41	54.03	54.78	54.27	54.42	54.19	53.96	54.14	53.91	53.61	53.29	53.84	54.76	54.56
TiO_2	0.17	0.16	0.19	0.14	0.17	0.19	0.08	0.12	0.06	0.16	0.11	0.14	0.22	0.25	0.18	0.12	0.11	0.12
Al_2O_3	1.17	1.11	1.10	0.78	0.95	0.93	0.25	0.36	0.41	0.74	0.88	1.08	1.12	1.20	1.23	0.81	0.80	0.71
Cr_2O_3	0.58	0.73	0.68	0.42	0.57	0.53	0.13	0.16	0.20	0.48	0.50	0.61	0.42	0.54	0.42	0.61	0.71	0.59
FeO*	3.03	2.70	2.73	3.02	3.52	3.54	2.06	2.83	3.02	2.86	3.19	3.39	3.98	4.43	4.31	3.09	3.51	3.29
MnO	0.07	0.10	0.13	0.12	0.12	0.17	0.10	0.09	0.08	0.13	0.12	0.14	0.12	0.09	0.15	0.11	0.13	0.06
MgO	17.66	17.53	17.60	17.61	17.55	17.64	17.46	17.66	17.40	17.54	17.24	17.47	17.09	17.48	17.45	17.70	17.95	18.15
CaO	23.24	23.69	23.25	23.61	22.61	22.67	25.03	24.11	24.18	23.43	23.47	22.83	23.38	22.35	22.32	22.66	22.77	22.67
Na_2O	0.25	0.29	0.28	0.27	0.29	0.29	0.05	0.12	0.13	0.20	0.18	0.19	0.29	0.29	0.24	0.22	0.22	0.21
Total	100.20	99.81	99.98	100.17	100.19	100.00	99.94	99.71	99.89	99.74	99.66	99.99	100.52	100.24	99.59	99.15	100.95	100.37
Cations (p.f.u.)																		
Si	1.962	1.967	1.968	1.960	1.961	1.953	1.958	1.958	1.974	1.958	1.982	1.976	1.981	1.973	1.978	1.971	1.961	1.972
Ti	0.004	0.005	0.004	0.007	0.006	0.007	0.007	0.005	0.004	0.007	0.002	0.003	0.003	0.004	0.005	0.005	0.007	0.007
$Al^{(IV)}$	0.038	0.033	0.032	0.040	0.039	0.047	0.042	0.042	0.026	0.042	0.018	0.024	0.019	0.027	0.022	0.029	0.039	0.028
$Al^{(VI)}$	0.008	0.014	0.018	0.009	0.004	0.006	0.010	0.011	0.004	0.009	0.021	0.010	0.014	0.007	0.019	0.011	0.011	0.009
Cr	0.021	0.019	0.019	0.015	0.010	0.017	0.016	0.012	0.014	0.022	0.013	0.020	0.014	0.012	0.016	0.015	0.018	0.013
Fe^{3+}	0.009	0.000	0.000	0.012	0.021	0.019	0.013	0.017	0.009	0.007	0.000	0.000	0.000	0.009	0.000	0.002	0.006	0.000
Fe^{2+}	0.073	0.083	0.088	0.120	0.095	0.107	0.122	0.115	0.080	0.105	0.072	0.106	0.099	0.083	0.107	0.106	0.092	0.101
Mn	0.002	0.004	0.003	0.004	0.003	0.004	0.003	0.005	0.003	0.003	0.002	0.004	0.003	0.004	0.004	0.005	0.004	0.004
Mg	0.940	0.956	0.953	0.946	0.934	0.936	0.951	0.956	0.966	0.939	0.918	0.966	0.957	0.956	0.952	0.959	0.939	0.930
Ca	0.938	0.907	0.905	0.885	0.927	0.903	0.875	0.879	0.917	0.904	0.955	0.881	0.896	0.921	0.881	0.886	0.917	0.928
Na	0.009	0.010	0.009	0.009	0.009	0.010	0.010	0.008	0.008	0.009	0.013	0.008	0.010	0.009	0.010	0.010	0.009	0.008
Total	4.004	3.999	3.998	4.006	4.011	4.009	4.007	4.009	4.004	4.004	3.997	3.998	3.997	4.005	3.994	4.001	4.003	4.000
End Members (%)																		
Wo	46.4	47.7	46.6	47.0	45.4	45.4	49.1	47.6	47.8	46.8	47.0	45.9	46.8	44.9	45.1	45.6	45.1	44.9
En	49.1	49.1	49.1	48.8	49.1	49.2	47.7	48.5	47.8	48.7	48.0	48.8	47.6	48.8	49.0	49.6	49.5	50.0
Fs	4.5	3.2	4.3	4.2	5.5	5.4	3.2	3.9	4.4	4.5	5.0	5.3	5.7	6.3	5.9	4.8	5.4	5.1
Mg#	0.920	0.898	0.919	0.903	0.888	0.910	0.886	0.893	0.922	0.899	0.929	0.900	0.918	0.899	0.900	0.969	0.913	0.907

Crystal textural style is abbreviated: cumu. (cumulus), inter. (intercumulus)
Note: Other phases (ol, chr, mt) were also analyzed on certain sections, such that "Cluster" refers to a specific location on each thin section

Table 4.2b: Representative clinopyroxene compositions from clinopyroxene-bearing ultramafic lithologies of the Turnagain intrusion

Rock Type:	Hornblende Clinopyroxenite			Hornblende Clinopyroxenite			Hornblende Clinopyroxenite		
Sample:	DDH04-47-7-49			04ES-09-02-02			DDH05-84-19-104		
Cluster:	5			3			5		
Style:	cumu.	cumu.	cumu.	cumu.	cumu.	cumu.	cumu.	cumu.	cumu.
Zone:	rim	mid	core	rim	mid	core	rim	mid	core
Oxides (wt. %)									
SiO_2	49.54	49.73	49.90	53.33	52.74	53.79	50.74	51.37	50.77
TiO_2	0.65	0.53	0.62	0.17	0.17	0.04	0.44	0.35	0.40
Al_2O_3	4.79	4.52	4.48	0.68	0.90	0.30	3.83	2.94	3.60
Cr_2O_3	0.00	0.01	0.03	0.04	0.07	0.02	0.03	0.01	0.00
FeO*	7.73	7.41	7.06	6.42	6.90	6.54	7.56	7.45	7.48
MnO	0.16	0.20	0.15	0.22	0.22	0.24	0.13	0.18	0.16
MgO	13.43	13.41	13.92	15.67	15.55	15.32	13.78	13.93	13.87
CaO	23.37	23.19	23.09	23.05	22.30	24.16	23.15	23.31	23.26
Na_2O	0.24	0.28	0.28	0.13	0.13	0.06	0.26	0.19	0.27
Total	99.91	99.28	99.54	99.70	98.97	100.47	99.92	99.73	99.79
Cations (p.f.u.)									
Si	1.918	1.897	1.913	1.854	1.870	1.867	1.977	1.972	1.985
Ti	0.010	0.011	0.010	0.018	0.015	0.018	0.005	0.005	0.001
$Al^{(IV)}$	0.082	0.103	0.087	0.146	0.130	0.133	0.023	0.028	0.015
$Al^{(VI)}$	0.047	0.055	0.043	0.066	0.070	0.065	0.007	0.011	0.000
Cr	0.000	0.000	0.000	0.000	0.000	0.001	0.001	0.002	0.001
Fe^{3+}	0.021	0.036	0.031	0.052	0.041	0.042	0.010	0.010	0.015
Fe^{2+}	0.211	0.198	0.175	0.190	0.192	0.179	0.189	0.206	0.187
Mn	0.006	0.005	0.004	0.005	0.006	0.005	0.007	0.007	0.008
Mg	0.775	0.772	0.813	0.750	0.752	0.776	0.866	0.867	0.843
Ca	0.932	0.931	0.933	0.937	0.934	0.926	0.916	0.893	0.955
Na	0.007	0.010	0.007	0.009	0.010	0.010	0.005	0.005	0.002
Total	4.011	4.018	4.015	4.026	4.020	4.021	4.005	4.005	4.011
End Members (%)									
Wo	49.9	49.7	49.2	46.5	45.4	48.1	48.8	48.6	49.0
En	39.9	40.0	41.3	43.9	44.1	42.4	40.4	40.4	40.6
Fs	10.1	10.2	9.5	9.6	10.5	9.4	10.8	11.0	10.4
Mg#	0.780	0.791	0.816	0.818	0.829	0.828	0.802	0.790	0.805

Crystal textural style is abbreviated: cumu. (cumulus), inter. (intercumulus)
Note: Other phases (ol, chr, mt) were also analyzed on certain sections, such that "Cluster" refers to a specific location on each thin section

Table 4.3a: Amphibole compositions from ultramafic rocks of the Turnagain intrusion

Rock Type:	Hornblende Clinopyroxenite								Hornblende Clinopyroxenite								Hornblende Clinopyroxenite							
Sample	DDH04-47-7-49								DDH05-84-19-104								04ES-09-02-02							
Cluster	1			6		9			3			4		7			2				4			
Description	inter.	inter.	inter.	inter.	inter.	inter.	inter.	inter.	inter.	inter.	inter.	inter.	inter.	inter.	inter.	inter.	cumu.	cumu.	cumu.	cumu.	cumu.	cumu.	cumu.	cumu.
Location	rim	mid	core	rim	core	rim	mid	core	rim	mid	core	Rim	Mid	rim	mid	core	rim	mid	mid	core	rim	mid	mid	core
Oxides (wt. %)																								
SiO_2	39.25	39.39	39.17	39.35	39.38	39.82	39.47	39.59	40.14	40.23	39.88	39.85	40.08	40.81	40.31	40.66	48.15	48.71	48.75	49.25	49.09	47.23	46.00	48.10
TiO_2	1.65	1.54	1.53	1.62	1.56	1.49	1.56	1.55	1.36	1.40	1.48	1.31	1.42	1.17	1.41	1.36	0.81	1.26	1.23	0.89	1.22	1.46	1.87	1.25
Al_2O_3	13.92	14.07	14.04	13.71	13.99	14.20	13.89	13.98	13.39	13.34	13.25	13.05	13.28	12.77	12.80	12.71	7.49	7.78	7.36	7.18	7.21	8.27	9.71	7.59
Cr_2O_3	0.00	0.06	0.00	0.02	0.07	0.00	0.00	0.00	0.03	0.03	0.04	0.03	0.00	0.05	0.05	0.00	0.23	0.17	0.13	0.15	0.22	0.21	0.15	0.16
Fe_2O_3*	7.28	7.32	7.68	7.05	7.80	6.93	7.08	7.16	7.00	6.54	6.95	5.78	6.26	6.74	6.05	6.61	3.98	3.82	3.64	3.70	3.61	4.25	4.17	3.59
FeO*	5.70	5.54	5.19	5.78	5.48	4.73	5.80	5.60	5.50	5.76	5.55	7.37	5.94	5.62	6.46	5.39	6.11	5.41	5.58	5.75	5.16	6.60	5.33	6.69
MnO	0.14	0.17	0.13	0.15	0.12	0.10	0.13	0.12	0.09	0.15	0.12	0.09	0.12	0.13	0.09	0.12	0.16	0.17	0.15	0.13	0.15	0.15	0.12	0.14
MgO	13.10	13.14	13.19	13.05	13.18	13.79	13.06	13.21	13.68	13.62	13.58	13.03	13.55	13.85	13.56	14.07	16.18	17.10	17.08	16.56	17.21	15.53	15.96	15.86
CaO	12.23	12.24	12.18	12.32	12.31	12.35	12.15	12.18	12.13	12.15	12.20	12.15	12.14	12.22	12.16	12.15	12.32	11.72	11.65	11.84	11.95	11.40	11.55	12.09
Na_2O	1.65	1.64	1.58	1.67	1.72	1.66	1.67	1.68	1.61	1.58	1.51	1.84	1.54	1.69	1.75	1.72	1.16	0.84	0.75	1.19	0.86	1.17	0.98	1.07
K_2O	1.61	1.60	1.62	1.39	1.50	1.50	1.50	1.50	1.81	1.87	1.90	1.93	1.96	1.56	1.78	1.63	0.54	0.68	0.59	0.48	0.56	0.73	0.91	0.55
Cl	0.08	0.05	0.08	0.07	0.06	0.06	0.07	0.07	0.05	0.03	0.04	0.14	0.08	0.16	0.06	0.06	0.09	0.06	0.10	0.07	0.09	0.18	0.18	0.11
F	0.00	0.00	0.00	0.00	0.00	0.00	0.00	0.00	0.00	0.00	0.00	0.00	0.00	0.00	0.00	0.00	0.10	0.16	0.09	0.10	0.09	0.07	0.16	0.17
H_2O*	1.95	1.96	1.95	1.95	1.97	1.97	1.95	1.96	1.97	1.98	1.96	1.93	1.95	1.94	1.96	1.97	1.99	1.99	2.01	2.01	2.02	1.97	1.93	1.95
Total	98.57	98.73	98.34	98.13	99.14	98.62	98.35	98.59	98.76	98.70	98.46	98.50	98.32	98.71	98.46	98.44	99.31	99.86	99.11	99.32	99.43	99.23	99.01	99.31
Cations (p.f.u.)																								
Si	5.864	5.868	5.855	5.897	5.849	5.901	5.899	5.897	5.967	5.986	5.955	5.991	5.992	6.064	6.027	6.049	6.941	6.936	6.988	7.051	7.005	6.834	6.650	6.939
$Al_{(IV)}$	2.136	2.132	2.145	2.103	2.151	2.099	2.101	2.103	2.033	2.014	2.045	2.009	2.008	1.936	1.973	1.951	1.059	1.064	1.012	0.949	0.995	1.166	1.350	1.061
$Al_{(VI)}$	0.315	0.339	0.329	0.318	0.297	0.381	0.347	0.351	0.313	0.326	0.287	0.303	0.332	0.300	0.283	0.278	0.213	0.241	0.231	0.262	0.218	0.244	0.304	0.230
Ti	0.185	0.172	0.172	0.183	0.174	0.166	0.175	0.173	0.152	0.157	0.166	0.148	0.160	0.130	0.159	0.152	0.087	0.135	0.133	0.096	0.130	0.159	0.203	0.135
Cr	0.000	0.007	0.000	0.002	0.009	0.000	0.000	0.000	0.003	0.004	0.004	0.003	0.000	0.006	0.006	0.000	0.026	0.019	0.014	0.017	0.025	0.024	0.017	0.018
Fe^{3+}*	0.818	0.821	0.864	0.795	0.872	0.772	0.796	0.803	0.784	0.733	0.781	0.653	0.704	0.753	0.681	0.741	0.432	0.409	0.393	0.399	0.388	0.463	0.453	0.389
Mg	2.918	2.918	2.939	2.915	2.919	3.046	2.911	2.933	3.032	3.020	3.022	2.921	3.019	3.067	3.022	3.119	3.477	3.630	3.650	3.535	3.661	3.351	3.440	3.411
Mn	0.018	0.021	0.017	0.019	0.016	0.013	0.017	0.015	0.011	0.019	0.015	0.012	0.015	0.017	0.012	0.015	0.020	0.020	0.018	0.016	0.018	0.018	0.015	0.017
$Fe^{2+}_{(M)}$	0.713	0.691	0.649	0.725	0.680	0.587	0.725	0.698	0.684	0.717	0.693	0.927	0.743	0.698	0.808	0.671	0.737	0.546	0.561	0.675	0.559	0.740	0.568	0.799
$Ca_{(M)}$	0.034	0.032	0.030	0.043	0.034	0.036	0.028	0.027	0.022	0.024	0.031	0.033	0.027	0.028	0.029	0.024	0.008	0.000	0.000	0.000	0.000	0.000	0.000	0.000
$Fe^{2+}_{(B)}$	0.000	0.000	0.000	0.000	0.000	0.000	0.000	0.000	0.000	0.000	0.000	0.000	0.000	0.000	0.000	0.000	0.000	0.098	0.107	0.014	0.056	0.059	0.075	0.008
$Ca_{(B)}$	1.924	1.921	1.920	1.935	1.924	1.926	1.918	1.917	1.910	1.913	1.921	1.923	1.916	1.917	1.919	1.913	1.895	1.788	1.790	1.816	1.827	1.767	1.788	1.869
$Na_{(B)}$	0.076	0.079	0.080	0.065	0.076	0.074	0.082	0.083	0.090	0.087	0.079	0.077	0.084	0.083	0.081	0.087	0.105	0.115	0.103	0.170	0.117	0.174	0.136	0.123
$Na_{(A)}$	0.402	0.395	0.378	0.421	0.418	0.404	0.403	0.401	0.375	0.370	0.357	0.460	0.362	0.404	0.427	0.408	0.220	0.117	0.105	0.161	0.119	0.154	0.139	0.175
K	0.307	0.305	0.309	0.267	0.284	0.284	0.286	0.286	0.344	0.355	0.362	0.371	0.374	0.295	0.340	0.309	0.099	0.124	0.107	0.088	0.102	0.135	0.167	0.100
Total	15.710	15.700	15.687	15.687	15.702	15.688	15.689	15.687	15.719	15.725	15.720	15.831	15.736	15.699	15.767	15.717	15.319	15.241	15.212	15.249	15.221	15.289	15.306	15.276
OH	1.980	1.987	1.980	1.983	1.984	1.985	1.983	1.983	1.988	1.992	1.989	1.963	1.978	1.959	1.985	1.985	1.931	1.911	1.934	1.937	1.937	1.924	1.883	1.895
Cl	0.020	0.013	0.020	0.017	0.016	0.015	0.017	0.017	0.012	0.008	0.011	0.037	0.022	0.041	0.015	0.015	0.023	0.016	0.025	0.017	0.023	0.045	0.045	0.028
F	0.000	0.000	0.000	0.000	0.000	0.000	0.000	0.000	0.000	0.000	0.000	0.000	0.000	0.000	0.000	0.000	0.046	0.073	0.041	0.046	0.041	0.031	0.072	0.077
Mg#	0.656	0.659	0.660	0.657	0.653	0.691	0.657	0.662	0.674	0.676	0.672	0.649	0.676	0.679	0.670	0.688	0.749	0.775	0.775	0.765	0.785	0.726	0.758	0.740

Crystal textural style is abbreviated: cumu. (cumulus), inter. (interstitial), porph. (porphyritic)
Note: Other phases (cpx, mt, phlog) were also analyzed on certain sections, such that "Cluster" refers to a specific location on each thin section
* Calculated

Table 4.3b: Amphibole compositions from ultramafic rocks of the Turnagain intrusion

Rock Type:	Hornblendite															Hornblendite								
Sample	05ES-05-06-02															04ES-00-07-04								
Cluster	2			4			5				6					1			2			3		
Description	porph.	porph.	porph.	porph.	porph.	porph.	porph.	porph.	porph.	porph.	porph.	cumu.	cumu.	cumu.	cumu.	porph.	porph.	porph.	porph.	porph.	porph.	porph.	porph.	porph.
Location	mid	mid	core	rim	mid	mid	core	rim	mid	mid	core	rim	mid	mid	core	rim	mid	core	rim	mid	core	rim	mid	core
Oxides (wt. %)																								
SiO_2	40.82	40.98	41.28	41.44	40.71	41.01	40.78	40.90	40.69	40.70	40.73	46.98	45.39	44.75	45.00	43.13	45.79	42.72	41.28	42.00	41.64	42.41	42.16	42.26
TiO_2	2.03	2.11	1.97	1.98	2.12	2.07	1.97	1.99	2.13	2.08	2.03	1.58	1.93	1.77	1.39	1.56	1.34	2.23	2.39	2.24	2.26	2.09	1.96	2.10
Al_2O_3	12.88	12.73	12.80	12.51	12.92	13.16	13.30	12.50	13.05	13.29	12.93	9.44	11.12	11.10	10.97	11.80	10.57	11.30	12.49	11.87	12.18	11.54	11.62	11.42
Cr_2O_3	0.01	0.02	0.00	0.02	0.04	0.03	0.02	0.00	0.01	0.00	0.05	0.17	0.11	0.07	0.05	0.06	0.01	0.06	0.04	0.09	0.11	0.01	0.02	0.03
Fe_2O_3*	5.61	5.30	5.33	5.16	5.40	4.58	5.92	5.85	5.22	4.71	5.01	4.05	4.11	4.66	4.58	4.60	1.30	4.59	4.52	4.26	4.55	5.02	5.40	5.38
FeO*	8.11	8.27	8.10	8.91	8.58	8.00	6.94	8.34	8.35	8.71	8.09	4.26	4.71	4.23	4.21	9.38	12.37	9.24	11.28	11.14	10.86	9.48	9.52	9.26
MnO	0.16	0.16	0.15	0.20	0.19	0.18	0.10	0.23	0.19	0.14	0.14	0.11	0.16	0.17	0.11	0.34	0.45	0.37	0.31	0.34	0.33	0.22	0.26	0.27
MgO	12.51	12.57	12.67	12.36	12.20	12.75	13.26	12.26	12.32	12.29	12.59	16.96	16.18	16.16	16.41	12.40	10.97	12.47	10.86	10.98	11.08	12.29	12.16	12.28
CaO	11.63	11.61	11.44	11.68	11.53	11.73	10.81	11.35	11.50	11.71	11.68	11.97	11.72	11.78	11.67	11.65	10.89	11.44	11.48	11.21	11.48	11.57	11.68	11.56
Na_2O	1.88	1.95	1.87	1.86	1.90	1.85	1.80	1.82	1.87	1.93	1.88	0.95	1.11	1.08	1.16	1.78	1.01	1.73	1.73	1.61	1.69	1.71	1.75	1.72
K_2O	1.07	0.98	1.07	1.07	1.02	1.12	1.76	1.04	1.07	1.11	1.10	0.83	1.00	0.94	0.85	0.75	1.25	0.72	0.97	0.82	0.81	0.86	0.90	0.81
Cl	0.14	0.11	0.07	0.09	0.14	0.06	0.10	0.11	0.12	0.08	0.08	0.08	0.13	0.15	0.09	0.17	0.32	0.21	0.11	0.10	0.14	0.11	0.21	0.15
F	0.00	0.00	0.00	0.00	0.00	0.00	0.00	0.00	0.00	0.00	0.00	0.17	0.17	0.15	0.15	0.00	0.00	0.01	0.00	0.00	0.02	0.00	0.00	0.00
H_2O*	1.95	1.96	1.97	1.97	1.94	1.98	1.97	1.95	1.95	1.97	1.96	1.98	1.96	1.94	1.95	1.97	1.92	1.94	1.96	1.95	1.94	1.97	1.94	1.95
Total	98.81	98.74	98.71	99.26	98.68	98.53	98.72	98.32	98.46	98.73	98.27	99.54	99.81	98.95	98.60	99.60	98.19	99.01	99.42	98.60	99.09	99.26	99.57	99.21
Cations (p.f.u.)																								
Si	6.082	6.105	6.137	6.154	6.082	6.104	6.057	6.128	6.082	6.071	6.092	6.711	6.501	6.466	6.511	6.358	6.827	6.338	6.171	6.300	6.226	6.291	6.256	6.278
$Al_{(IV)}$	1.918	1.895	1.863	1.846	1.918	1.896	1.943	1.872	1.918	1.929	1.908	1.289	1.499	1.534	1.489	1.642	1.173	1.662	1.829	1.700	1.774	1.709	1.744	1.722
$Al_{(VI)}$	0.344	0.341	0.381	0.343	0.357	0.412	0.385	0.335	0.381	0.407	0.371	0.299	0.379	0.357	0.381	0.407	0.683	0.315	0.372	0.398	0.374	0.307	0.287	0.277
Ti	0.228	0.236	0.220	0.222	0.238	0.232	0.221	0.225	0.239	0.233	0.229	0.170	0.207	0.192	0.151	0.173	0.151	0.248	0.268	0.252	0.255	0.233	0.218	0.235
Cr	0.001	0.002	0.000	0.003	0.004	0.003	0.003	0.000	0.001	0.000	0.005	0.019	0.012	0.008	0.006	0.007	0.001	0.007	0.005	0.011	0.013	0.001	0.002	0.004
Fe^{3+}*	0.629	0.594	0.596	0.577	0.607	0.512	0.661	0.659	0.587	0.529	0.563	0.436	0.443	0.506	0.499	0.510	0.146	0.512	0.508	0.481	0.512	0.560	0.603	0.601
Mg	2.779	2.792	2.807	2.736	2.717	2.828	2.936	2.738	2.745	2.733	2.808	3.611	3.456	3.481	3.539	2.724	2.438	2.758	2.419	2.455	2.470	2.717	2.690	2.720
Mn	0.021	0.020	0.018	0.026	0.024	0.023	0.013	0.029	0.023	0.018	0.018	0.014	0.019	0.021	0.014	0.043	0.056	0.046	0.040	0.044	0.041	0.027	0.032	0.034
$Fe^{2+}_{(M)}$	0.997	1.015	0.978	1.094	1.053	0.989	0.782	1.015	1.023	1.080	1.006	0.451	0.483	0.434	0.410	1.135	1.525	1.115	1.388	1.359	1.336	1.154	1.167	1.130
$Ca_{(M)}$	0.000	0.000	0.000	0.000	0.000	0.000	0.000	0.000	0.000	0.000	0.000	0.000	0.000	0.000	0.000	0.000	0.000	0.000	0.000	0.000	0.000	0.000	0.000	0.000
$Fe^{2+}_{(B)}$	0.013	0.015	0.030	0.012	0.019	0.007	0.080	0.030	0.021	0.007	0.007	0.058	0.081	0.077	0.100	0.021	0.017	0.032	0.022	0.038	0.022	0.022	0.014	0.021
$Ca_{(B)}$	1.857	1.853	1.822	1.859	1.845	1.871	1.720	1.822	1.841	1.872	1.871	1.832	1.799	1.825	1.810	1.841	1.740	1.818	1.839	1.802	1.839	1.839	1.857	1.840
$Na_{(B)}$	0.129	0.132	0.148	0.129	0.136	0.122	0.200	0.148	0.138	0.122	0.122	0.109	0.120	0.098	0.091	0.138	0.243	0.150	0.139	0.160	0.139	0.139	0.130	0.138
$Na_{(A)}$	0.413	0.431	0.391	0.406	0.415	0.413	0.319	0.379	0.404	0.437	0.423	0.154	0.187	0.203	0.235	0.369	0.048	0.346	0.362	0.308	0.351	0.352	0.373	0.356
K	0.203	0.187	0.204	0.203	0.195	0.214	0.334	0.198	0.205	0.212	0.210	0.151	0.182	0.173	0.157	0.141	0.237	0.135	0.185	0.158	0.154	0.162	0.171	0.154
Total	15.616	15.617	15.594	15.609	15.610	15.626	15.652	15.577	15.608	15.649	15.633	15.305	15.369	15.377	15.391	15.510	15.285	15.482	15.547	15.465	15.505	15.514	15.545	15.510
OH	1.964	1.971	1.983	1.977	1.964	1.986	1.976	1.973	1.970	1.979	1.981	1.900	1.888	1.894	1.907	1.956	1.919	1.942	1.973	1.975	1.955	1.971	1.944	1.962
Cl	0.036	0.029	0.017	0.023	0.036	0.014	0.024	0.027	0.030	0.021	0.019	0.020	0.033	0.037	0.023	0.044	0.081	0.054	0.027	0.025	0.036	0.028	0.055	0.038
F	0.000	0.000	0.000	0.000	0.000	0.000	0.000	0.000	0.000	0.000	0.000	0.079	0.079	0.069	0.071	0.000	0.000	0.005	0.000	0.000	0.009	0.001	0.002	0.000
Mg#	0.629	0.632	0.636	0.619	0.618	0.652	0.658	0.616	0.627	0.629	0.641	0.793	0.774	0.774	0.778	0.620	0.591	0.624	0.558	0.566	0.569	0.610	0.601	0.608

Crystal textural style is abbreviated: cumu. (cumulus), inter. (interstitial), porph. (porphyritic)
Note: Other phases (cpx, mt, phlog) were also analyzed on certain sections, such that "Cluster" refers to a specific location on each thin section
* Calculated

Table 4.4: Biotite compositions from biotite-bearing ultramafic rocks of the Turnagain intrusion

Rock Type:	Hornblende Clinopyroxenite				Wehrlite	
Sample:	DDH05-84-19-104				05ES-03-01-01	
Cluster:	6		11		2	
Description:	inter.	inter.	inter.	inter.	inter.	inter.
Location:	mid	core	mid	core	rim	core
Oxides (wt. %)						
SiO_2	36.47	36.55	36.84	36.33	39.16	39.06
TiO_2	1.31	1.54	1.56	1.53	1.10	1.15
Al_2O_3	14.89	15.27	15.12	15.14	13.85	14.30
Cr_2O_3	0.03	0.00	0.01	0.00	1.16	1.22
FeO	17.70	15.98	17.75	17.39	4.61	5.19
MnO	0.02	0.02	0.00	0.00	0.06	0.07
MgO	14.64	16.16	15.01	14.68	24.95	23.75
BaO	0.61	0.49	0.65	0.53	0.44	0.51
CaO	0.15	0.09	0.09	0.14	0.08	0.06
Na_2O	0.24	0.24	0.21	0.18	0.06	0.06
K_2O	9.44	9.31	9.87	9.73	8.73	9.30
Cl	0.04	0.09	0.03	0.04	0.00	0.04
F	0.00	0.00	0.00	0.00	0.10	0.08
H_2O*	1.96	1.97	1.99	1.96	2.08	2.06
Total	97.51	97.72	99.13	97.66	96.36	96.85
Cations (p.f.u.)						
Si	5.550	5.494	5.520	5.516	5.639	5.630
$Al^{(IV)}$	2.450	2.506	2.480	2.484	2.350	2.370
$Al^{(VI)}$	0.220	0.200	0.190	0.226	0.000	0.059
Ti	0.150	0.174	0.176	0.174	0.119	0.124
Cr	0.003	0.000	0.001	0.000	0.132	0.139
Fe	2.253	2.008	2.224	2.208	0.555	0.626
Mn	0.003	0.003	0.000	0.000	0.007	0.009
Mg	3.321	3.622	3.351	3.323	5.354	5.103
Ba	0.037	0.029	0.038	0.032	0.025	0.029
Ca	0.024	0.015	0.014	0.022	0.012	0.009
Na	0.072	0.070	0.062	0.054	0.016	0.017
K	1.833	1.786	1.887	1.884	1.604	1.710
Total	15.916	15.906	15.944	15.923	15.812	15.824
Cl	0.011	0.023	0.007	0.011	0.000	0.011
F	0.000	0.000	0.000	0.000	0.006	0.004
OH	1.989	1.977	1.993	1.989	1.994	1.985
Mg#	0.60	0.64	0.60	0.60	0.91	0.89

Crystal textural style is abbreviated: inter. (interstitial)

Note: Other phases (ol, cpx, chr, mt) were also analyzed on certain sections, such that "Cluster" refers to a specific location on each thin section

* Calculated

Major and trace element concentrations (Table 4.5) of 23 whole rock powders, 3 blind duplicates, and one procedural duplicate (Appendix VI) were analyzed at Activation Laboratories Ltd. (Actlabs) in Ancaster, Ontario. For the major elements, a 0.2 g sample was fused in a graphite crucible after it was mixed with a combination of lithium metaborate/lithium tetraborate. The mixture, once molten, was poured into 5% HNO_3 and shaken for 30 minutes until dissolved. The samples then were analyzed for selected trace elements and major oxides using a simultaneous/sequential Thermo Jarrell-Ash Enviro II inductively coupled plasma optical emission spectrometer (ICP-EOS). Additional trace elements were analyzed by both the INAA (instrumental neutron activation analysis) and ICP-MS (inductively couple plasma mass spectrometry) methods. Internal calibration was achieved using a variety of international reference materials and independent control samples. For the INAA analyses, 1.5-2.5 g of sample was weighed into small polyethylene vials and irradiated with control international reference material CANMET WMS-1 and NiCr flux wires at a thermal neutron flux of 7×10^{12} $ncm^{-2}s^{-2}$ in the McMaster Nuclear Reactor. The samples were measured on an Ortec high-purity Ge detector linked to a Canberra Series 95 multichannel following a 7-day decay. Activities for each element were compared to a detector calibration developed from multiple international certified reference materials and decay- and weight-corrected. For the ICP-MS analyses, 0.25 g of sample was digested in HF, followed by a mixture of HNO_3 and $HClO_4$, heated and taken to dryness. The samples were brought back into solution with HCl. Samples were analyzed using a Perkin Elmer Optima 3000 ICP. In-lab standards or certified reference materials were used for quality control. The normalizing values for the REE (chondrite) and extended trace elements (primitive mantle) are from McDonough & Sun (1995).

4.3.3 Platinum Group Elements

The PGE concentrations of 21 whole rock samples, 3 blind duplicates, and 1 procedural duplicate were determined by the NiS fire-assay technique at Geoscience Laboratories (Sudbury, Ontario) following the procedures outlined in Jackson *et al.* (1990) and Richardson & Burnham (2003). Nickel, sulphur, sodium carbonate and sodium tetraborate are added to a 15 g aliquot of sample powder. This mixture is then fused for 1.5 hrs in a fire-clay crucible at 1050°C, after which the crucible is broken to recover the nickel sulphide button after cooling. The button, in order to remove the NiS matrix, is then dissolved using hydrochloric acid in a

Table 4.5a: Major (wt. % oxide)and trace element abundances (ppm) in mafic/ultramafic rocks of the Turnagain intrusion

Rock Type:	Dunite	Dunite	Dunite	Dunite	Dunite	Dunite	Wehrlite	Wehrlite	Wehrlite	Wehrlite	Wehrlite
Sample Prefix:	04ES	04ES	04ES	04ES	05ES	05ES	04ES	04ES	05ES	05ES	05ES
Sample #:	03-01-02	06-01-01	03-02-01	07-02-01	04-06-01	04-05-01	03-04-01	07-02-04	05-06-01	05-02-01	05-03-01
Oxides (wt. %)											
SiO_2	38.17	38.08	37.04	35.64	36.47	35.80	37.86	38.14	39.04	39.19	38.49
TiO_2	0.04	0.01	0.01	0.01	0.03	0.04	0.03	0.02	0.09	0.03	0.05
Al_2O_3	0.32	0.05	0.03	0.07	0.22	0.61	0.17	0.15	0.37	0.18	0.33
Fe_2O_3*	7.15	9.26	12.02	7.72	14.22	9.78	14.93	13.69	12.12	13.53	11.32
MgO	48.54	48.00	46.86	45.13	41.56	41.26	41.18	42.40	43.10	42.73	43.02
MnO	0.10	0.14	0.13	0.10	0.23	0.13	0.19	0.21	0.20	0.21	0.18
CaO	0.29	0.01	0.13		0.06	0.05	1.43	1.06	2.94	2.08	2.07
Na_2O	0.02	0.03	0.01		0.04	0.04	0.02	0.03	0.05	0.03	0.06
K_2O	0.20	0.03	0.04	0.08	0.11	0.09	0.03	0.12	0.08		0.10
P_2O_5											
LOI	5.06	3.72	3.37	11.29	7.00	11.44	4.06	3.96	0.92	1.79	4.18
Total	99.93	99.36	99.65	100.10	99.95	99.23	99.91	99.77	99.41	99.77	99.79
S	0.09	0.07	0.39	0.11	0.08	0.18	1.39	0.18	0.03	0.18	0.06
Mg #:	0.931	0.911	0.885	0.921	0.853	0.893	0.845	0.860	0.876	0.862	0.883
Trace Elements (ppm)											
Co	141	160	209	126	163	125	206	167	163	175	136
Cr	2580	2850	2000	3360	1600	4350	3640	2660	3740	4240	5390
Cu	9	18	492	5	34		261	126	72	471	17
Ni	3310	2185	1760	1790	1190	2360	1740	988	1080	1590	1940
Sc	3.2	3.2	3.6	2.8	5.7	3.8	10.9	8.7	15.0	9.7	11.7
V						14	114	12	31.5	7	27
Zn	42	46	34	35	55	61	102	58	56.5	62	69
Rb	2										
Ba	16				2	8					
Th						0.13					
U			0.31			0.10		0.44			
Ta											
Nb	0.2						0.2				
La						0.41					
Ce						0.6					
Pb											
Pr					0.02	0.08			0.03		
Sr	2				2	3	4	3	7	7	7
Nd	0.15				0.14	0.40	0.15	0.09	0.22	0.14	0.15
Zr						2					
Hf											
Sm	0.07		0.02	0.01	0.05	0.12	0.07	0.04	0.10	0.07	0.07
Eu						0.021	0.013		0.039	0.016	0.022
Gd	0.08				0.02	0.13	0.07	0.06	0.13	0.07	0.09
Tb	0.01					0.02	0.01		0.02		0.01
Dy	0.07				0.03	0.16	0.08	0.04	0.16	0.06	0.09
Ho	0.01					0.04	0.02		0.03	0.01	0.02
Er	0.05				0.01	0.12	0.05	0.02	0.10	0.04	0.06
Tm	0.01					0.02	0.01		0.01	0.01	0.01
Yb	0.06		0.02		0.02	0.12	0.05	0.04	0.09	0.04	0.06
Lu	0.008					0.017	0.006	0.004	0.015	0.006	0.008
Y					4	4	2		0		1

Note: Blank entries represent values that were below detection limits.
Abbreviated rock types: cpxite (clinopyroxenite), hblite (hornblendite)
Abbreviated minerals: ol (olivine), hbl (hornblende)
Mg# = Mg/(Mg+Fe) assuming all iron as Fe^{2+}
* Total

Table 4.5b: Major (wt. % oxide)and trace element abundances (ppm) in mafic/ultramafic rocks of the Turnagain intrusion

Rock Type:	Wehrlite	Wehrlite	Wehrlite	Ol Cpxite	Ol Cpxite	Cpxite	Cpxite	Hbl Cpxite	Hblite	Hblite	Diorite	Wacke
Sample Prefix:	05ES	05ES	05ES	04ES	05ES	05ES	05ES	04ES	05ES	04ES	DDH04	04ES
Sample #:	05-01-02	03-01-01	05-05-01	10-02-04	05-01-01	05-04-01	03-01-02	09-02-02	05-06-02	00-07-04	57-12-89.2	00-07-02
Oxides (wt. %)												
SiO_2	38.20	37.07	42.85	50.62	51.23	48.99	49.04	47.14	38.53	41.93	53.56	49.67
TiO_2	0.04	0.07	0.11	0.19	0.20	0.38	0.29	0.75	2.32	2.16	0.29	0.80
Al_2O_3	0.21	0.50	0.42	1.00	1.05	2.21	2.07	4.20	12.06	12.21	20.82	16.19
Fe_2O_3*	18.60	15.13	10.71	8.07	7.45	7.65	8.55	11.64	15.51	14.30	4.14	10.01
MgO	37.72	34.25	35.67	21.74	22.45	18.65	20.30	16.46	12.99	11.95	3.60	4.86
MnO	0.25	0.16	0.17	0.15	0.13	0.15	0.19	0.16	0.21	0.26	0.09	0.20
CaO	2.28	1.56	7.40	17.76	17.26	19.12	15.25	16.04	13.85	11.62	7.68	9.82
Na_2O	0.06	0.02	0.03	0.17	0.17	0.20	0.17	0.63	0.67	0.78	6.02	3.57
K_2O	0.01	0.08	0.05	0.12	0.10	0.08	0.11	0.40	0.32	0.89	1.17	1.86
P_2O_5							0.03	0.14	0.01	0.31	0.19	0.37
LOI	2.45	11.07	2.38			2.20	3.37	2.35	3.31	2.80	2.12	1.88
Total	99.83	99.92	99.78	99.08	99.34	99.65	99.36	99.92	99.78	99.20	99.68	99.23
S	0.66	1.65	0.23	0.78	0.42	0.04	0.33	1.08	0.14	0.35	0.10	0.31
Mg #:	0.801	0.818	0.868	0.842	0.857	0.829	0.825	0.737	0.624	0.624	0.633	0.491
Trace Elements (ppm)												
Co	192	181	163	110	98	59	56	151	85	66	15	30
Cr	683	1910	1380	2610	3200	1480	2690	1320	38	404	11	79
Cu	475	233	248	381	292	292	47	249	133	84	12	101
Ni	858	956	777	335	511	173	56	130	132	136	9	20
Sc	11.1	14.5	28.8	58.8	55.4	68.1	41.8	68.8	69.3	73.7	12.9	36.1
V	23	54	49	101	81	147	265	343	645	492	110	291
Zn	88	34	41	22	18	20	57	49	69	99	29	74
Rb								3		12.0	11	28
Ba		6			1	12	36	35	69	422	1980	700
Th		0.06					0.29	0.17	0.10	0.36	0.07	1.54
U							0.16	0.08	0.06	0.12	0.09	0.21
Ta								0.1		0.2	0.1	0.3
Nb	0.5		0.5			0.3	0.5	1.8	1.6	3.9	2.3	4.1
La	0.07	0.19	0.09	0.17	0.19	0.52	1.56	4.47	2.11	6.61	1.50	10.50
Ce	0.2	0.5	0.3	0.8	0.8	2.0	3.8	14.5	7.0	20.5	3.4	21.6
Pb						5		13	34	36	5	12
Pr	0.03	0.09	0.07	0.18	0.18	0.41	0.64	2.57	1.40	3.35	0.52	2.65
Sr	7	4	14	32	35	71	60	62	336	284	2808	949
Nd	0.23	0.59	0.53	1.33	1.33	2.64	3.60	12.60	8.64	18.25	2.62	11.60
Zr					2	7	12	14	30	49	17	38
Hf						0.3	0.4	0.7	1.3	2.1	0.7	1.4
Sm	0.11	0.24	0.24	0.61	0.60	1.04	1.16	3.69	3.26	5.95	0.80	2.99
Eu	0.032	0.051	0.077	0.200	0.204	0.318	0.277	0.928	1.310	1.845	0.386	1.020
Gd	0.13	0.28	0.30	0.84	0.80	1.31	1.36	3.62	4.10	7.18	0.86	3.21
Tb	0.02	0.05	0.06	0.16	0.15	0.25	0.25	0.63	0.76	1.33	0.15	0.56
Dy	0.13	0.32	0.35	0.95	0.92	1.57	1.56	3.49	4.74	7.91	0.95	3.42
Ho	0.03	0.06	0.07	0.18	0.18	0.31	0.31	0.65	0.97	1.62	0.19	0.70
Er	0.08	0.17	0.19	0.52	0.49	0.86	0.90	1.84	2.79	4.54	0.57	2.13
Tm	0.01	0.02	0.03	0.07	0.07	0.12	0.13	0.26	0.39	0.65	0.09	0.31
Yb	0.08	0.14	0.16	0.42	0.44	0.74	0.81	1.49	2.25	3.82	0.53	1.82
Lu	0.011	0.022	0.022	0.055	0.053	0.100	0.108	0.193	0.310	0.530	0.073	0.287
Y	2			2	5	10	8	19	28	42	4	19

Note: Blank entries represent values that were below detection limits.
Abbreviated rock types: cpxite (clinopyroxenite), hblite (hornblendite)
Abbreviated minerals: ol (olivine), hbl (hornblende)
Mg# = Mg/(Mg+Fe) assuming all iron as Fe^{2+}
* Total

closed Teflon vessel. Any Au or PGE that may have been dissolved during button dissolution are recovered by co-precipitation with tellurium. This produces a concentrate that contains Au and all PGE. The concentrate is vacuum-filtered and re-dissolved in aqua regia prior to analysis by ICP-MS. Osmium is not reported because, at the aqua regia re-dissolution stage, it may be lost as a volatile oxide. PGE concentrations in the samples, detection limits, duplicate results, and reference material values are reported in Table 4.6. The normalizing values for PGE (primitive mantle) are from Maier & Barnes (1999).

4.3.4 Sulphur Isotopes - Sulphide

A total of 27 samples from sulphide-rich lithologies including 3 blind duplicates, sampled from drillcore and outcrop, were analyzed for their sulphur isotopic composition. Samples of massive sulphide were sampled using a scriber with a tungsten-carbide tip and all other samples were crushed using a steel hammer and base. Sulphide was then hand-picked using a binocular microscope to assure the lack of any attached silicate, oxide, or other phases. $\delta^{34}S$ was determined on separates that yielded appreciable sulphide. Most ultramafic samples contained pyrrhotite±pentlandite with trace amounts of pyrite, although some also contained chalcopyrite. Hornblende-rich samples typically contained pyrite and/or chalcopyrite (see Table 4.7). Sulphur was extracted online with continuous-flow technology, using a Finnigan MAT 252 isotope-ratio mass spectrometer, at the Queen's Facility for Isotope Research, Queen's University, Kingston, Ontario. All values are reported in units of per mil (‰), and were corrected using the NIST standard 8556. Sulphur is reported relative to Cañon Diablo Troilite (CDT). Analytical precision for $\delta^{34}S$ is 0.3 ‰.

4.3.5 Lead Isotopes - Sulphide

A total of 16 sulphide samples from sulphide-rich lithologies, 2 duplicates, sampled from drillcore and outcrop, and the standard reference material NBS-981 were analyzed for their lead isotopic composition and the results are presented in Table 4.8. All samples were subject to the separation procedure described above for sulphur isotopes. Sulphide separates chosen for analysis were then leached in dilute hydrochloric acid to remove surface contamination before dissolution in nitric acid. Ion exchange columns were employed for the separation and purification of Pb. The samples were converted to bromide form, and the solution was passed through ion exchange columns in hydrobromic acid, and the lead eluted in 6N hydrochloric acid. Approximately 25-50 ng of the

Table 4.6: PGE concentrations of representative ultramafic rocks from the Turnagain intrusion

Rock Type:	Sample: prefix	number	MgO (wt. %)	S (wt. %)	Ni (ppm)	Ir (ppb)	Ru (ppb)	Rh (ppb)	Pd (ppb)	Pt (ppb)	Au (ppb)	Cu (ppm)	Pd/Pt	Cu/Pd
dunite	04ES	03-01-02	51.2	0.09	3310	13.6	9.44	6.27	36.44	44.47	1.97	9	0.82	247
dunite	04ES	06-01-01*	50.2	0.07	2185	1.63	4.67	0.515	0.96	0.975		18	0.98	18750
dunite	04ES	03-02-01	48.7	0.39	1760	1.76	2.73	1.81	23.35	24.13	1.85	492	0.97	21071
dunite	04ES	07-02-01	50.8	0.11	1790	2.77	3.34	0.98	4.18	3.51		5	1.19	1196
dunite	05ES	04-06-01	44.7	0.08	1190	1.17	0.87	1.62	10.85	10.26		34	1.06	3134
dunite	05ES	04-05-01	47.0	0.18	2360	1.3	3.09	0.55	5.58	8.57			0.65	
wehrlite	04ES	03-04-01	43.0	1.4	1740	1.46	3.04	1.41	11.54	9.53	2.37	261	1.21	22617
wehrlite	04ES	07-02-04	44.3	0.18	988	3.36	2.62	8.1	102.58	82.62	2.90	126	1.24	1228
wehrlite	05ES	05-06-01*	43.8	0.03	1080	1.2	0.24	1.88	45.08	35.33	5.89	72	1.28	1597
wehrlite	05ES	05-02-01	43.6	0.18	1590	2.94	2.25	3.29	52.61	52.33	17.65	471	1.01	8953
wehrlite	05ES	05-03-01	45.0	0.06	1940	4.21	4.25	4.68	54.6	85.42	1.72	17	0.64	311
wehrlite	05ES	05-01-02	38.7	0.66	858	1.17	2.36	0.75	7.02	6.72		475	1.04	67664
wehrlite	05ES	03-01-01	38.5	1.7	956	0.07	0.16	0.1	4.54	1.77	0.89	233	2.56	51322
wehrlite	05ES	05-05-01	36.6	0.23	777	1.05	2.25	0.88	7.23	8.49		248	0.85	34302
ol cpxite	04ES	10-02-04	21.9	0.78	335	0.48	0.15	0.28	5.75	6.4	1.12	381	0.90	66261
ol cpxite	05ES	05-01-01	22.6	0.42	511	1.86	0.5	1.53	23.15	33.32	1.12	292	0.69	12613
cpxite	05ES	05-04-01	19.1	0.04	173	0.23		0.29	1.77	4		292	0.44	164972
cpxite	05ES	03-01-02	21.1	0.33	56	0.06		0.17	4.11	4.22	0.77	47	0.97	11436
hbl cpxite	04ES	09-02-02	16.9	1.1	130				2.15	0.86	8.02	249	2.50	115814
hblite	05ES	05-06-02	13.5	0.14	132				0.41			133		324390
hblite	04ES	00-07-04*	12.4	0.35	136	0.06	0	0.17	4.11	4.35	0.76	84	0.94	20463
Detection Limit:						0.04	0.13	0.08	0.11	0.14	0.71			
Intl_STD	TDB	1-0506				0.08	0.27	0.48	4.91	22.87	6.45			
Intl_STD	TDB	1-0507				0.07	0.26	0.46	4.70	22.71	6.05			
Accepted Value:						n/a	n/a	n/a	5.8	22.4	6.3			
original	04ES	06-01-01				1.77	5.18	0.53	1.18	1.2				
duplicate	05ES	05-07-01				1.49	4.16	0.5	0.74	0.75				
original	05ES	05-06-01				1.2	0.22	1.67	45.29	35.08	5.24			
duplicate	04ES	00-07-01				1.2	0.26	2.09	44.87	35.58	6.53			
original	04ES	00-07-04				0.06		0.17	4.10	4.48	0.75			
duplicate	05ES	03-02-01				0.06		0.17	4.11	4.22	0.77			

Some rock types have been abbreviated: cpxite (clinopyroxenite), hblite (hornblendite)
The last part of the table contains 2 internal standard analyses and 3 sample sets (sample followed by its respective blind duplicate)
Samples with an asterisk represent the average between the specific analysis and its blind duplicate
Blank entries represent analyses that were below detection

Table 4.7: Sulphur isotopic data from the Turnagain intrusion and surrounding lithologies

Sample	Rock Type	Depth (m)	Mineralogy	Texture	S content (%)	$\delta^{34}S$ (CDT)
DDH03-12-4	dunite	31.9	po+pn	diss. to crs. bleb., mt rim	37.6	-9.7
DDH04-29-9	dunite	63.8	po+pn	fine bleb.	14.6	-9.0
DDH03-16-24	dunite	166	po+pn	msv. remob.	42.7	-6.9
05ES-02-02-02	dunite	N/A	po+pn+cpy+py	crs. bleb., mt rim	32.0	-6.7
05ES-02-02-02A	dunite	N/A	po+pn	net tex., mt frac.	40.2	-6.4
DDH03-18-13	dunite	84.8	po+pn	diss. to crs. bleb.+ inter.	41.0	-5.4
05ES-02-04-01	dunite	N/A	po+pn	diss. to inter.	37.7	-5.3
DDH04-37-6	dunite	39.7	po+/-pn+/-cpy	fine bleb. + minor remob.	33.3	-5.1
DDH04-24-31	dunite	220.4	po+cpy+/-pn	fine to med. bleb.	38.4	-4.1
DDH04-36-16	dunite	108.1	po+pn	diss. to fine bleb.	29.6	-3.4
DDH04-36-5	wehrlite	39.7	po+pn	diss. to med. bleb.	40.9	-8.4
DDH04-33-5	wehrlite	37.9	po+pn	crs. bleb.	33.8	-8.2
DDH04-23-11	wehrlite	76.2	po+pn	net tex., mt rim + frac.	36.8	-8.0
DDH03-06-25	wehrlite	181.5	po+pn	msv. remob.	32.3	-5.4
05ES-03-01-01	wehrlite	N/A	po+pn	crs. bleb.	37.4	-5.2
DDH04-28-6	wehrlite	44.8	po+pn+/-cpy	fine bleb. to net tex.	37.0	-4.8
DDH03-05-45	wehrlite	325	po	med. bleb. to inter.	42.9	-4.7
DDH03-07-25	wehrlite	183	po+pn+cpy	fine bleb., mt rim + frac.	35.4	-3.9
DDH04-35-5	wehrlite	40.1	po+pn	diss. to med. bleb.	32.2	-3.5
05ES-02-01-01	wehrlite	N/A	po+pn+cpy	net tex., heavy alt.	30.2	-1.7
DDH03-08-13	wehrlite	100.7	po+/-pn	diss. to fine bleb.	35.2	-1.1
DDH03-05-8	clinopyroxenite	89.7	po	remob.	38.6	-1.3
DDH03-09-18	clinopyroxenite	134.3	po	med. bleb.	41.3	-0.6
DDH04-47-17	hbl clinopyroxenite	126.5	py	crs. bleb.	58.4	1.4
DDH03-03-59	hornblendite	426	py	med. bleb.	43.2	-0.1
04ES-13-01-02	felsic tuff(?)	N/A	py	porph.	45.5	-1.7
DDH03-07-54	graphitic phyllite	389	py	porph.	55.8	-17.9

Textures are abbreviated as follows: med. (medium), crs. (coarse), diss. (disseminated), bleb. (blebby), msv. (massive), net tex. (net textured), porph. (porphyroblastic), remob. (remobilized), inter. (interstitial), mt rim (magnetite rim), frac. (fracture)
Minerals are abbreviated as follows: po (pyrrhotite), pn (pentlandite), cpy (chalcopyrite), py (pyrite)
N/A in "Depth" column indicates that the sample is from a surface exposure

Table 4.8: Pb isotopic compositions of selected sulphide fractions from the Turnagain intrusion and surrounding lithologies

Sample Number	Rock Type	Depth	Mineral	206Pb/ 204Pb	2σ	207Pb/ 204Pb	2σ	208Pb/ 204Pb	2σ	207Pb/ 206Pb	2σ	208Pb/ 206Pb	2σ
DDH03-16-24	dunite	166	po±pn	18.794	0.015	15.679	0.012	38.36	0.03	0.8343	0.0006	2.027	0.001
05ES-02-02-02	dunite	N/A	po+pn+cpy±py	18.845	0.027	15.644	0.025	38.62	0.07	0.8302	0.0005	2.042	0.002
05ES-02-02-02A	dunite	N/A	po+pn	18.826	0.022	15.632	0.026	38.50	0.08	0.8303	0.0004	2.045	0.002
DDH04-37-6	dunite	39.7	po±pn±cpy	18.944	0.030	15.681	0.031	38.46	0.09	0.8278	0.0004	2.030	0.002
DDH03-06-25	wehrlite	181.5	po+pn	19.003	0.023	15.675	0.017	38.72	0.05	0.8249	0.0007	2.023	0.002
DDH04-28-6	wehrlite	44.8	po+pn±cpy	19.078	0.025	15.724	0.022	38.62	0.06	0.8242	0.0002	2.024	0.001
DDH03-05-45	wehrlite	325	po	18.561	0.021	15.527	0.017	38.40	0.04	0.8366	0.0006	2.054	0.001
DDH03-07-25	wehrlite	183	po+pn+cpy	18.882	0.035	15.648	0.034	37.91	0.10	0.8287	0.0004	2.008	0.002
DDH03-08-13	wehrlite	100.7	po±pn	18.726	0.020	15.584	0.016	38.50	0.04	0.8322	0.0007	2.041	0.001
DDH03-05-08	clinopyroxenite	89.7	po±pn	18.106	0.015	15.636	0.012	38.12	0.03	0.8636	0.0007	2.091	0.002
DDH04-47-17	hbl clinopyroxenite	126.5	py±po	18.732	0.015	15.605	0.013	38.45	0.03	0.8331	0.0006	2.038	0.001
DDH03-03-59	hornblendite	426	po+pn	18.855	0.024	15.634	0.016	38.71	0.05	0.8292	0.0009	2.039	0.002
04ES-13-01-02	felsic tuff	N/A	py	19.155	0.033	15.649	0.033	38.57	0.10	0.8170	0.0004	2.013	0.002
DDH03-07-54	graphitic phyllite	389	py	18.920	0.020	15.629	0.024	38.47	0.08	0.8260	0.0004	2.033	0.002

Minerals are abbreviated as follows: po (pyrrhotite), pn (pentlandite), cpy (chalcopyrite), py (pyrite)
Note: All errors are 2σ absolute
N/A in "Depth" column indicates that the sample is from a surface exposure

lead in chloride form was loaded on a rhenium filament using a phosphoric acid-silica gel emitter, and isotopic compositions were determined in peak-switching mode using a modified VG54R thermal ionization mass spectrometer at the Pacific Centre for Isotopic and Geochemical Research, University of British Columbia. The measured ratios were corrected for instrumental mass fractionation of 0.10%/amu (Faraday collector) per mass unit based on repeated measurements of the N.B.S. SRM 981 Standard Isotopic Reference Material and the values recommended by Thirlwall (2000). Errors were numerically propagated including all mass fractionation and analytical errors, using the technique of Roddick (1987). All errors are quoted at the 2σ level.

4.4 RESULTS

4.4.1 Olivine Mineral Chemistry

Olivine core compositions from olivine-bearing ultramafic rocks of the Turnagain intrusion become progressively less magnesian from chromitites (Fo_{91-96}) through dunites ($Fo_{89-92.5}$) and wehrlites (Fo_{85-90}) to olivine clinopyroxenites (~Fo_{83-87}) (Figure 4.7A, Table 4.1). The most Mg-rich olivine in dunite not associated with chromitite is $Fo_{92.5}$, which is consistent with crystallization from a primitive parent magma in equilibrium with olivine in mantle peridotite, as originally proposed by Nixon (1998). Olivine grains from chromitites extend to more Mg-rich compositions (up to Fo_{96}), however these are likely due to Fe-Mg exchange between olivine and neighbouring chromite during sub-solidus re-equilibration (Clark, 1978). The progressive decrease in the forsterite content of olivine with decreasing olivine abundance in the Turnagain cumulate rocks is consistent with progressive decrease in the Mg/Fe of the parent magma(s) due to continued olivine precipitation.

There is a general positive correlation between the forsterite and Ni contents in olivine for all olivine-bearing lithologies in the Turnagain intrusion (Figure 4.7B). Three distinct groups can be identified within this trend. The first group contains the majority of the olivine core analyses, ranging from Fo_{91} and Ni = 3150 ppm down to $Fo_{83.5}$ and Ni = 1000 ppm, and reflects progressive Mg and Ni depletion due to olivine crystallization. The second group consists of olivine grains enclosed within or adjacent to chromitite. These compositions extend to higher Mg (Fo_{96}) and Ni (2750-4715 ppm) contents, and appear to reflect sub-solidus exchange between olivine and chromite as noted above. The third group consists of olivine core compositions that are distinctly depleted in Ni at a given Fo content, relative to the olivine

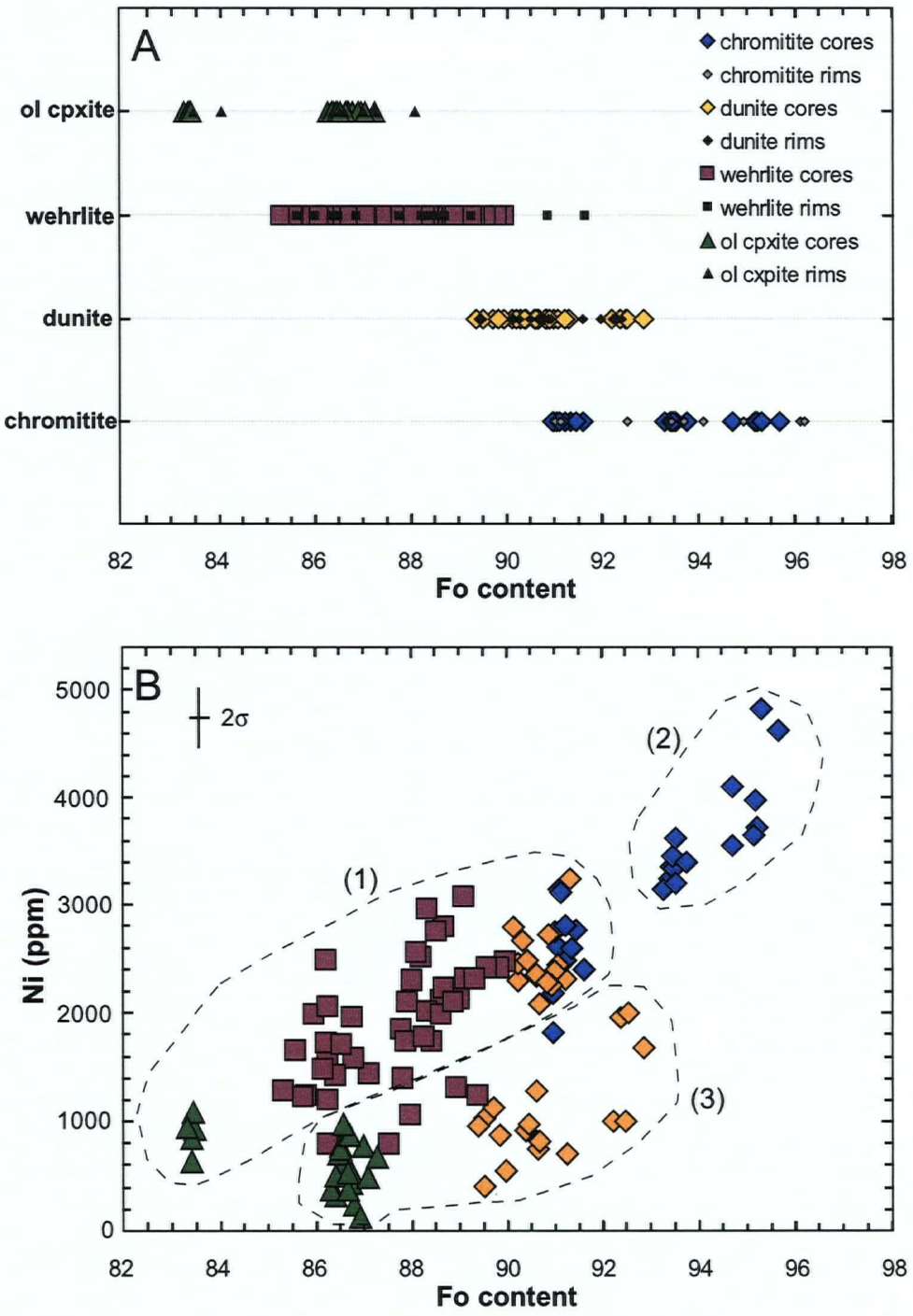

Figure 4.7: Olivine chemistry from the Turnagain intrusion. A) Forsterite content vs. rock type showing the intra- and interlithological olivine compositional variation (cores and rims). Note the systematic progressive decrease in Fo content of olivine from dunite through wehrlite to olivine clinopyroxenite. Olivine in chromitite has Mg-rich olivine extending up to Fo_{96} due to subsolidus re-equilibration with chromite B) Forsterite content vs. Ni (ppm) showing three distinct populations: olivine from dunite, wehrlite, and olivine clinopyroxenite with "normal" Ni concentrations (1); olivine from chromitite (2) with high Mg/Fe and Ni; and dunite, wehrlite, and olivine clinopyroxenite showing relative Ni depletion (3) compared to the first population.

compositions in the first group (Figure 4.7B). This Ni depletion is consistent with the effect of sulphide liquid saturation and segregation in the parent magma(s) to these specific dunite, wehrlite, and olivine clinopyroxenite samples, with Ni being strongly partitioned into the sulphide liquid relative to coexisting olivine (e.g. sulphide/silicate liquid partition coefficient for Ni in basaltic melts is ~800 (Peach *et al.*, 1990)).

4.4.2 Clinopyroxene Mineral Chemistry

Clinopyroxene (diopside) compositions in the Turnagain intrusion range from Mg# = 0.77 to 0.97 (Figure 4.8A, Table 4.2), where Mg# = $Mg/(Mg+Fe^{2+})$. There are no systematic compositional differences between interstitial and cumulus clinopyroxene. There is also relatively little variation in clinopyroxene Mg# in wehrlite and olivine clinopyroxenite, and significant variation between olivine clinopyroxenite and hornblende clinopyroxenite (Figure 4.8A). The lower Mg# (0.84) of clinopyroxene from hornblende clinopyroxenite is consistent with its crystallization from more evolved magmas depleted in Mg due to abundant early olivine (and clinopyroxene) crystallization. The Al and Ti contents of clinopyroxene are also distinctive between the different lithologies of the Turnagain intrusion. The magnesian diopside grains in wehrlite and olivine clinopyroxenite are Al-poor (Al_2O_3 = 0.25-1.54 wt.%) (Figure 4.8B), whereas the lower Mg# of clinopyroxene grains from hornblende clinopyroxenites extend to higher Al_2O_3 (0.30-5.27 wt.%) and TiO_2 (0.04-0.72 wt.%) contents.

4.4.3 Amphibole and Biotite Chemistry

Primary cumulus amphibole in the Turnagain intrusion occurs in hornblende clinopyroxenite, hornblendite, and hornblende diorite. Due to the significant size difference between cumulus amphibole (~200-1000 μm) and interstitial amphibole (<75 μm) in hornblendites (Figure 4.4.2F), only cumulus amphibole was analyzed (Table 4.3). Amphibole is generally halogen-poor (Cl+F = 1-5% of OH site), contains a moderate amount of alkalis (Na+K = 0.315-0.908 c.p.f.u.), Ti (0.096-0.239 c.p.f.u.), and Al (1.213-2.480 c.p.f.u.), and has a compositional range between magnesiohastingsite and hornblende (based on the classification scheme of Leake *et al.*, 1997) (Table 4.3). Small amounts of biotite (1-3 vol.%) are commonly observed in dunite and wehrlite, whereas hornblende clinopyroxenite may contain 10 vol.% biotite. Rare, but locally significant pegmatoidal biotite clinopyroxenite, observed both at surface and in drill core from the DJ Zone (Figure 4.1), may contain 50-60 vol.% biotite. The biotite occurrence in

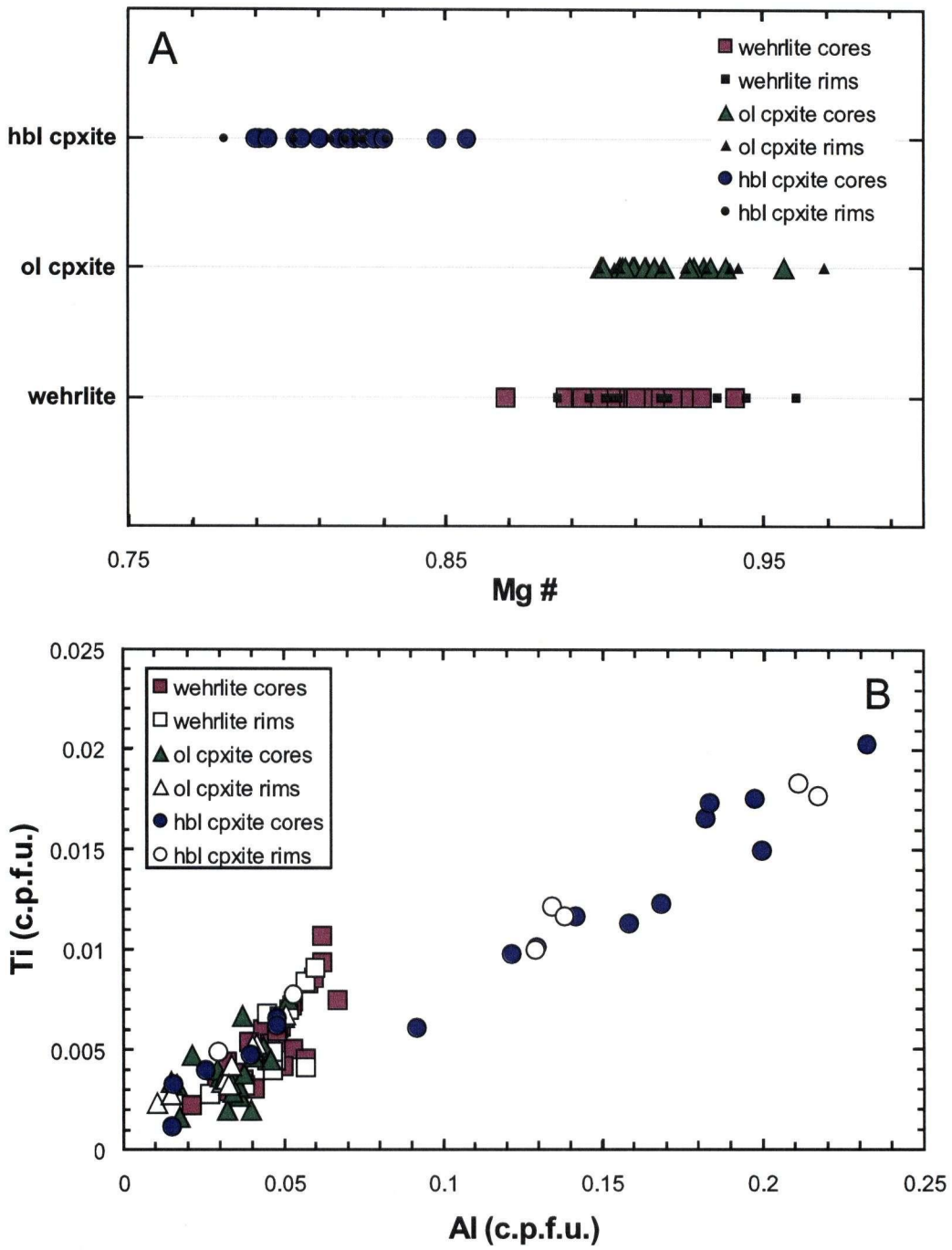

Figure 4.8: Clinopyroxene chemistry from the Turnagain intrusion. A) Mg# vs. rock type. Note that clinopyoxene from olivine clinopyroxenite and wehrlite have similar Mg#. B) Al vs. Ti. Note the small range in both Al and Ti in the Mg-rich lithologies, but the wide range (and linear correlation) of Al and Ti contents in hornblende clinopyroxenite.

these rocks suggests that it crystallized in place of hornblende. Biotite analyses in wehrlite are typically more magnesian (phlogopite, Mg# = 0.90) than analyses in hornblende clinopyroxenite (biotite, Mg# = 0.60) (Table 4.4).

4.4.4 Major and Trace Element Geochemistry

Whole rock samples from the Turnagain intrusion display a large distribution in major element oxide contents (Figure 4.9) and trace element concentrations, which are largely controlled by the abundance and type of cumulus minerals, and the relative proportions of cumulus to intercumulus phases. There are four main lithological groupings: (1) high-Mg rocks (dunite and wehrlite), (2) intermediate-Mg rocks (olivine clinopyroxenite and hornblende clinopyroxenite), (3) hornblendites, and (4) dioritic rocks, represented by one sample (DDH04-57-12-89) in this study.

4.4.4.1 Group 1: High-Mg Olivine-rich Rocks

These rocks are dominated by cumulus olivine and chromite with interstitial, and rarely cumulus, clinopyroxene. Their whole rock MgO contents range from 35 to 51 wt.% and they have a restricted range in Mg# (0.80-0.95), consistent with the presence of abundant cumulus olivine (>Fo_{90}) and minor amounts of clinopyroxene. With respect to elements compatible in olivine or chromite, the high-Mg rocks contain significant Cr (500-5500 ppm) and Ni (800-3400 ppm) (Figure 4.10). The high-Mg rocks are also extremely poor in all elements not incorporated into olivine or chromite (e.g. Ca, Al, Ti, REE) to the extent that incompatible trace element abundances are generally at or below detection limits for nearly all of the dunites analyzed. Wehrlites exhibit slightly concave-down chrondrite-normalized rare earth element patterns (Figure 4.11A) ranging from 0.3-0.8 x chondrite (La) with a $(La/Yb)_{cn}$ of 0.4-0.9. Wehrlites generally exhibit similar extended trace element patterns (Figure 4.11B). The single dunite sample (05ES-04-05-01) with trace element concentrations significantly above detection limits has distinctive LREE-enrichment relative to all other ultramafic samples from the Turnagain intrusion (Figure 4.11A). This sample contains abundant 1-2 mm serpentine veinlets with minor rutile and chlorite, thus the distinctive chemistry is likely due to post-crystallization modification during fluid-rock interaction and serpentinization, which may have implications for minor LREE mobility in rocks of the Turnagain intrusion during serpentinization.

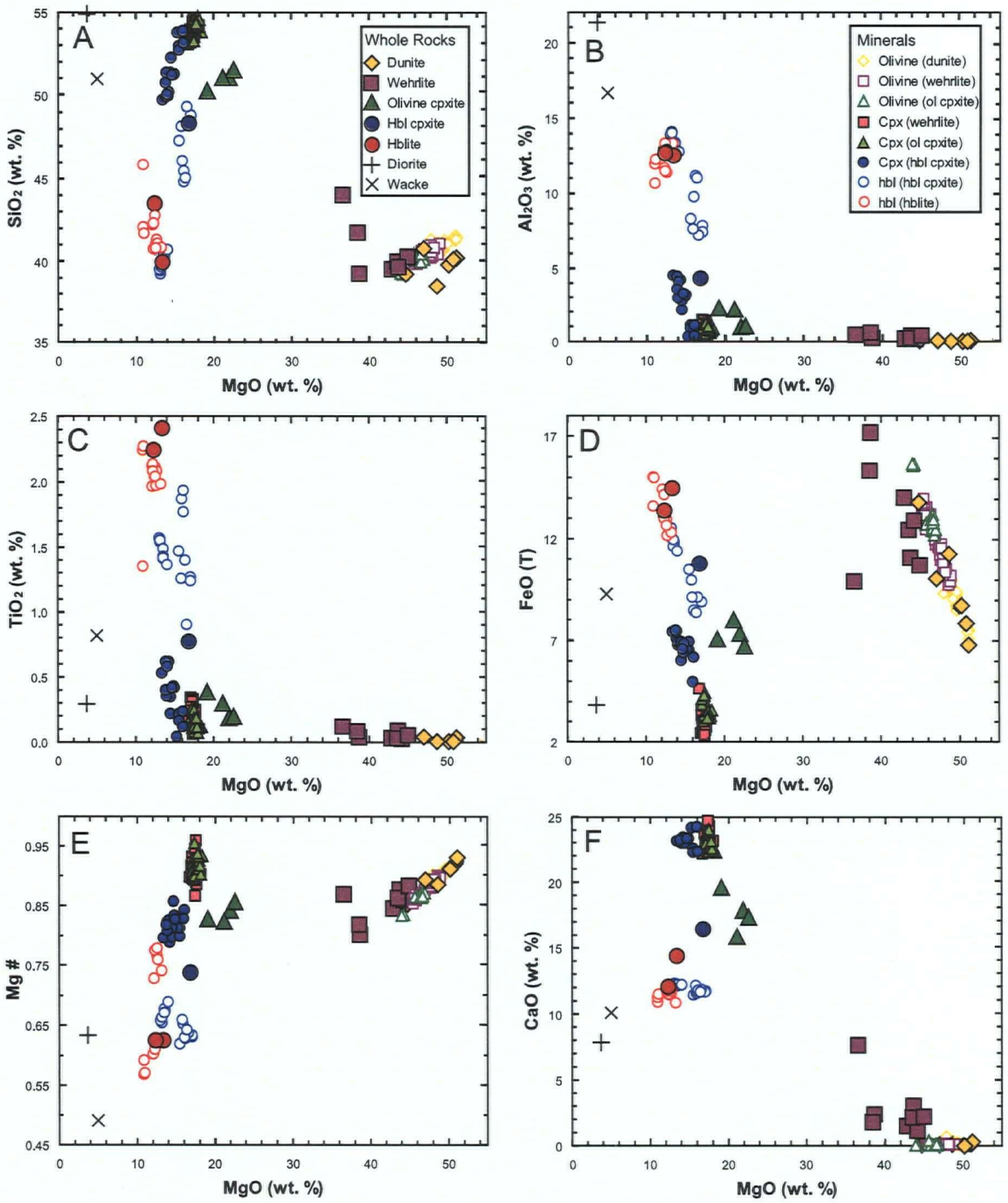

Figure 4.9: Select major element oxides and Mg# vs. MgO for whole rock samples from the Turnagain intrusion. Individual whole rock analyses are plotted as large symbols shaded in grey, with the exception of hornblendite (open circles). Mineral analyses from specific lithologies have the same symbol as the whole rock sample, however they are smaller and variably shaded i.e. olivine from dunite is diamond-shaped, but smaller and open. Whole rock Mg# = Mg/(Mg+Fe). Note the large compositional gap between dunite/wehrlite and olivine clinopyroxenite/hornblende clinopyroxenite. All ultramafic rock types have high Mg# (~0.80) reflecting accumulation of olivine and/or clinopyroxene, whereas the hornblendites have relatively low Mg# (0.63). Abbreviations are: cpx (clinopyroxene), cpxite (clinopyroxenite), hbl (hornblende), hblite (hornblendite).

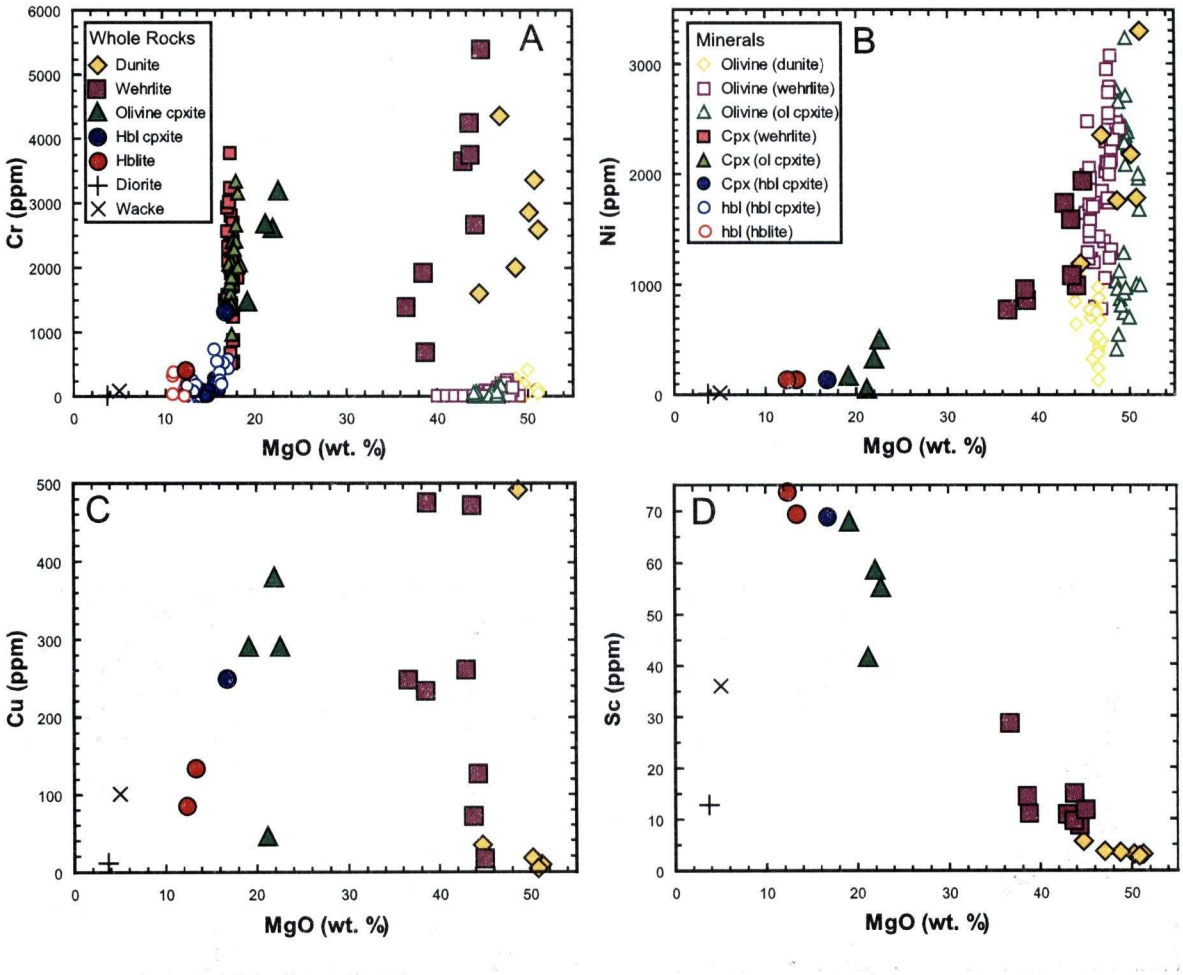

Figure 4.10: Select trace element concentrations vs. MgO for whole rock samples from the Turnagain intrusion. The same symbol style as Figure 9 is applied here. The large compositional gap present in Figure 9, between olivine cumulate rocks and clinopyroxene-hornblende cumulate rocks, is also apparent with respect to trace elements.

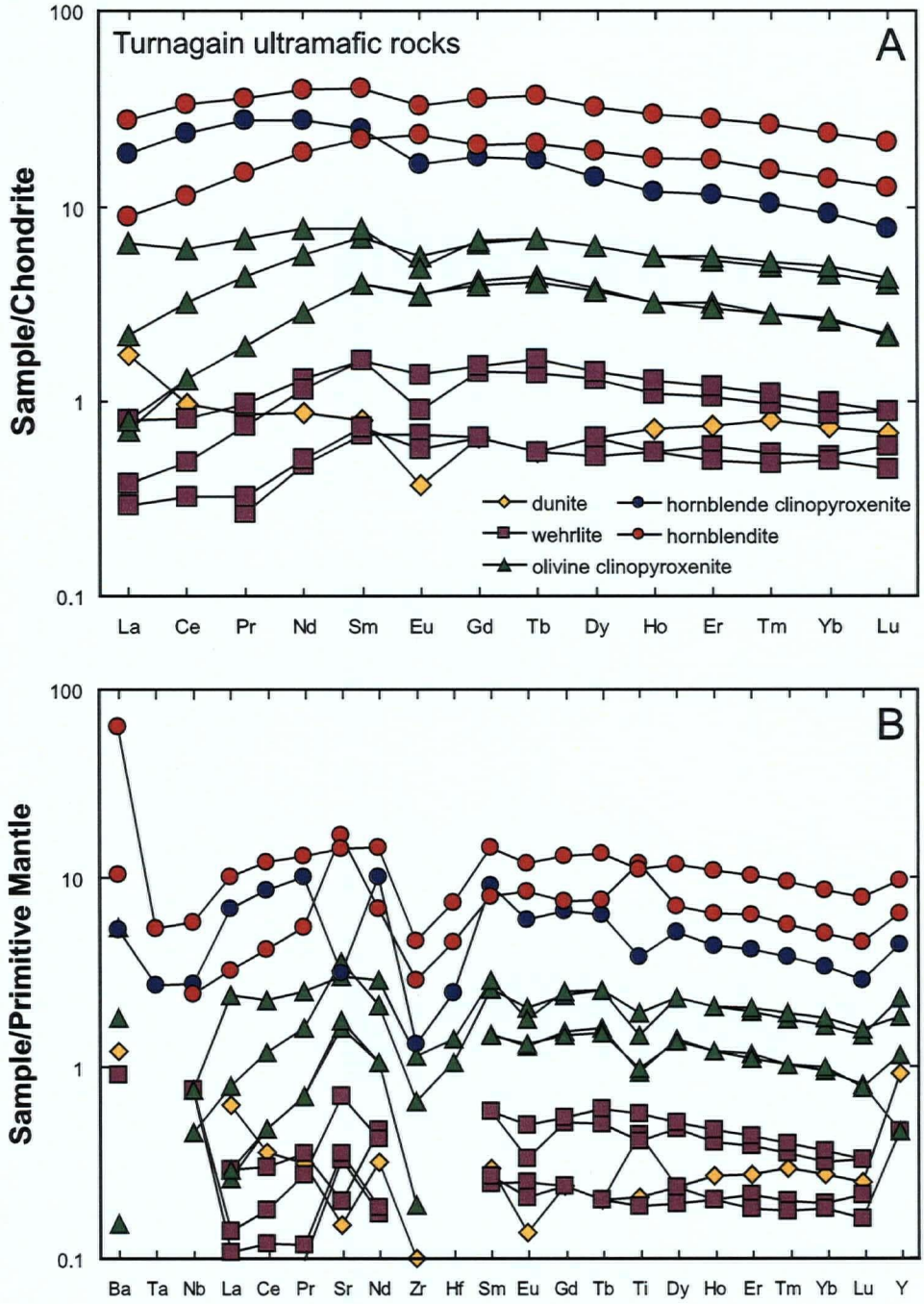

Figure 4.11: Chondrite-normalized rare earth element and primitive mantle-normalized trace element diagrams for whole rocks from the Turnagain intrusion (normalizing values from McDonough and Sun, 1998). A) Ultramafic rocks from the Turnagain intrusion, showing a progressive overall enrichment in REE and in LREE from wehrlite to olivine clinopyroxenite to hornblendite. Note that, with the exception of one sample, REE concentrations in the dunite samples were near or below detection limits and have not been plotted. B) Note the very low abundances of trace elements in the most magnesian rock types, consistent with their status as cumulate rocks, and the prominent negative Zr-Hf and Ta-Nb anomalies in all rock types where concentrations are above detection limits.

4.4.4.2 Group 2: Intermediate-Mg Clinopyroxene-Rich Rocks

Olivine clinopyroxenite and hornblende clinopyroxenite, like the high-Mg olivine-rich rocks, exhibit major element oxide contents that correlate with their clinopyroxene-dominant mineralogy. They have a relatively restricted MgO range (16-22 wt.%) and Mg# (0.75-0.85), both of which are lower than in the olivine-rich rocks, which is consistent with the presence of abundant cumulus clinopyroxene. Clinopyroxene-rich lithologies have relatively high whole rock Al_2O_3 (1-2 wt.%) and CaO (16-20 wt.%) contents (Figure 4.9) and exhibit moderate Cr enrichment (1200-3200 ppm) (Figure 4.10A). Note that, with respect to major elements, the whole rock hornblende clinopyroxenite sample (05ES-05-06-02) plots between its respective amphibole and clinopyroxene mineral compositions in Figure 4.9. Chondrite-normalized REE patterns show a concave-down shape similar to the high-Mg group ($(La/Yb)_{cn}$ = 0.3-2.0), but with higher REE contents (0.8-9 x chondrite La) (Figure 4.11A). The clinopyroxene-rich rocks also have similar primitive mantle-normalized trace element patterns to high-Mg rocks, but again with higher overall abundances. Negative Ta-Nb and Zr-Hf anomalies are present where the abundances of these elements are above detection limits (Figure 4.11B).

4.4.4.3 Group 3: Hornblendites

The whole rock hornblendite samples are characterized by moderate MgO contents (12-13 wt.%) with a relatively low Mg# (0.64) (Figure 4.9) and have significantly higher CaO (~13 wt.%), Al_2O_3 (~13 wt.%), and TiO_2 (~2.4 wt.%) contents compared with high-Mg rocks. Incompatible trace elements are also enriched in hornblendites (10-30 x chondrite La) (Figure 4.11A) compared with clinopyroxene-rich lithologies. The hornblendites, similar to the intermediate-Mg and high-Mg rocks, display concave-down REE patterns with $(La/Yb)_{cn}$ from 0.6-1.2. Note that the two analyzed hornblendite samples have sub-parallel REE patterns but distinctly different concentrations. The most REE-rich hornblendite (04ES-00-07-04) is an extremely fine-grained rock (grain size <1 mm) and thus has a composition closest to the original silicate magma (where the interstitial amphibole and other accessory phases represent the chilled melt). The other hornblendite (05ES-05-06-02) is coarse-grained and contains substantial large cumulus amphibole crystals resulting in dilution to lower incompatible element concentrations. The primitive mantle-normalized trace element patterns of the hornblendites are sub-parallel to the clinopyroxene-rich lithologies and olivine-rich lithologies,

albeit at higher concentrations (Figure 4.11B), and exhibit prominent negative Ta-Nb and Zr-Hf anomalies.

4.4.4.4 Group 4: Dioritic Rocks

The dioritic rocks are represented by a single whole rock sample in this study (DDH04-57-12). This sample is a cumulate-textured hornblende diorite composed of coarse amphibole (15 vol.%) and plagioclase (80 vol.%) and contains moderate silica (55 wt.%) and high alumina (21 wt.%) contents and has a comparable Mg# (0.64) to the hornblendites (Figure 4.9). These characteristics are consistent with the high modal plagioclase and moderate amphibole contents of this sample. The hornblende diorite contains low abundances of all incompatible trace elements, comparable to dunite (Table 4.5), reflecting its cumulate nature. This sample displays a significant positive Eu anomaly (Eu/Eu* = 1.418) and, with respect to primitive mantle-normalized trace elements, displays high positive Sr and Ba anomalies (2800 ppm and 1980 ppm, respectively), which is consistent with the high modal abundance of cumulus plagioclase.

4.4.5 Platinum-Group Elements

Concentrations of Pt and Pd in whole rock samples from the Turnagain intrusion range from <0.14-85 ppb Pt and 0.4-102 ppb Pd, respectively (Figure 4.12A, Table 4.6). Pt/Pd ratios vary between 0.4-2.5 with an average value of 0.9 and a median value of ~1 (Figure 4.12A). The absolute abundances of the PGE vary systematically between rock types (Figures 4.12, 4.13). Most olivine clinopyroxenite and all hornblende-bearing lithologies have low to negligible PGE contents, dunite is characterized by low to moderate PGE concentrations, and wehrlite contains the highest PGE concentrations of all ultramafic lithologies in the Turnagain intrusion. There is no correlation between whole rock PGE content and sulphur (Figure 4.12B), which suggests that the PGE reside as discrete PGM alloy phases (e.g. Pt_3Fe, or isoferroplatinum) in wehrlite. Primitive mantle-normalized PGE patterns show an overall increase from Ir to Pt with a Pt/Ir ratio varying from 0.6-72 (mean value of 19.1), with some samples exhibiting a negative Ru anomaly (Figure 4.13); a common trait of PGM alloys in chromitites from other Alaskan-type intrusions (G. Nixon, pers. comm., 2007).

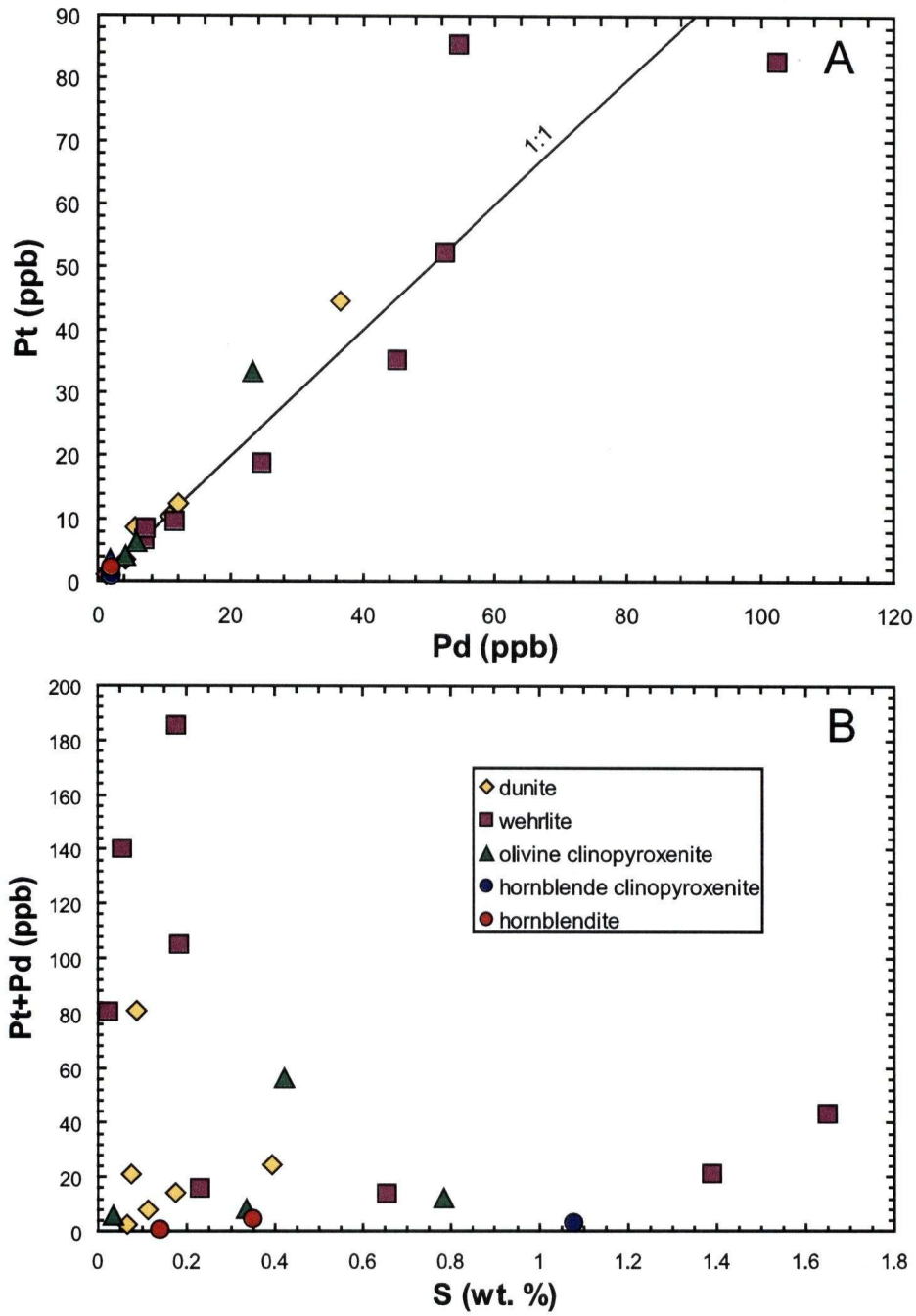

Figure 4.12: Platinum-group element compositional variations for whole rocks from the Turnagain intrusion. A) Pd vs. Pt. B) S vs. Pt+Pd. Note that wehrlite samples contain the highest Pt and Pd abundances. The absence of a positive correlation between sulphur and metal contents indicates that the PGE are likely contained in discrete platinum group minerals or alloys and not in sulphides.

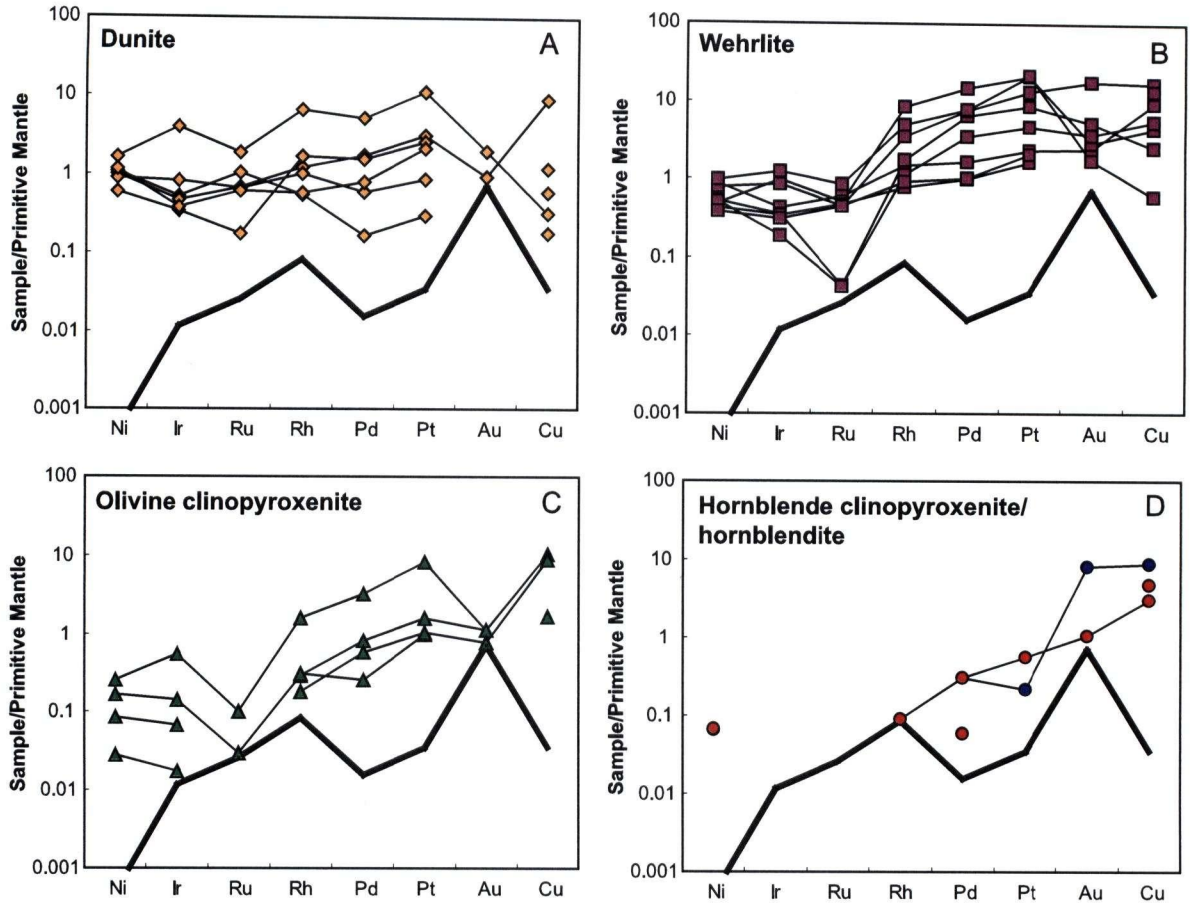

Figure 4.13: Primitive-mantle normalized platinum group element diagrams for whole rocks from the Turnagain intrusion (normalizing values from Maier and Barnes (1999)). The thick black line in all graphs represents the detection limits. Wehrlites have the highest overall abundances of PGE and distinct positive slopes from Ru to Pt.

4.4.6 Sulphur Isotopic Compositions

The range of sulphur isotopic compositions of sulphide separates from lithologies in the Turnagain intrusion and proximal host rocks is presented in Figure 4.14. Pyrite from the Road River phyllite has the most negative $\delta^{34}S$ value at -17.8 ‰ (Table 4.7). Sulphides from dunite and wehrlite (mostly pyrrhotite and pentlandite) show large ranges in their sulphur isotopic compositions ($\delta^{34}S$ = -10 ‰ to -1 ‰), with dunite sulphide shifted to more negative values ($\delta^{34}S$ = -9.7 ‰ to -3.4 ‰) relative to wehrlite sulphide ($\delta^{34}S$ = -8.4 ‰ to -1.1 ‰). Sulphide separates from olivine clinopyroxenite and hornblende-bearing lithologies in the Turnagain intrusion have sulphur isotopic compositions close to mantle values (0 ± 3 ‰, Schneider, 1970; Sakai *et al.*, 1984; Ripley, 1999). There is no direct correlation between the presence of alteration associated with sulphide in dunite and wehrlite (see Figure 4.6) and its sulphur isotopic composition.

4.4.7 Lead Isotopic Compositions

The range of lead isotopic compositions of sulphide separates from various lithologies within, and proximal to, the Turnagain intrusion is: $^{206}Pb/^{204}Pb$ = 18.11-19.16 , $^{207}Pb/^{204}Pb$ = 15.53-15.72, $^{208}Pb/^{204}Pb$ = 37.91-38.72 (Table 4.8). There is no apparent correlation between the lead isotopic composition of a sulphide separate and its host lithology. The sulphide analyses form a broadly linear array between the mantle Pb growth curve and the upper continental crust (Zartman & Zoe, 1981) and/or average Cordilleran shale curve (Godwin & Sinclair, 1982), which is interpreted as a mixing line (Figure 4.15A). The Pb isotopic composition of most of the sulphide separates is shifted towards more radiogenic values relative to mantle values, indicating a greater contribution of Pb from crustal sources.

4.5 DISCUSSION

4.5.1 Parent Magma Characteristics

The petrology and geochemistry of rocks from the Turnagain Alaskan-type intrusion indicate that it was formed by the emplacement and crystallization of Mg-rich, primitive, hydrous magmas in an arc setting. The primitive nature of the parent magmas is constrained by the Mg-rich olivine compositions (up to $Fo_{92.5}$) in dunite that has not re-equilibrated with chromite. The hydrous nature of the parent magma is supported by 1) primary interstitial phlogopite in the olivine-clinopyroxene cumulates, 2) late interstitial to cumulus hornblende in rocks from

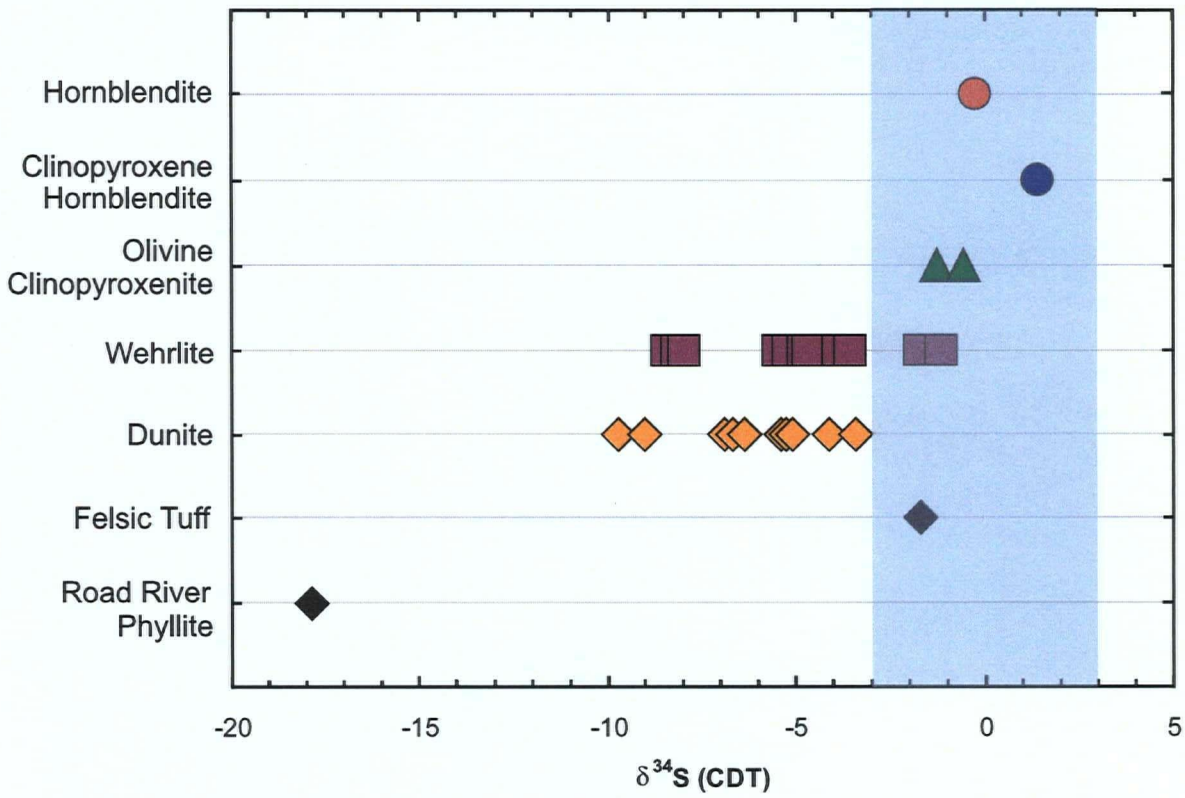

Figure 4.14: Sulphur isotopic composition of sulphide vs. lithology in the Turnagain intrusion. Note the wide variation in $\delta^{34}S$ in both dunite and wehrlite, extending towards the highly negative value of pyrite from the Road River phyllite ($\delta^{34}S$ = -17.9 ‰). The blue region represents the mantle range of $\delta^{34}S$.

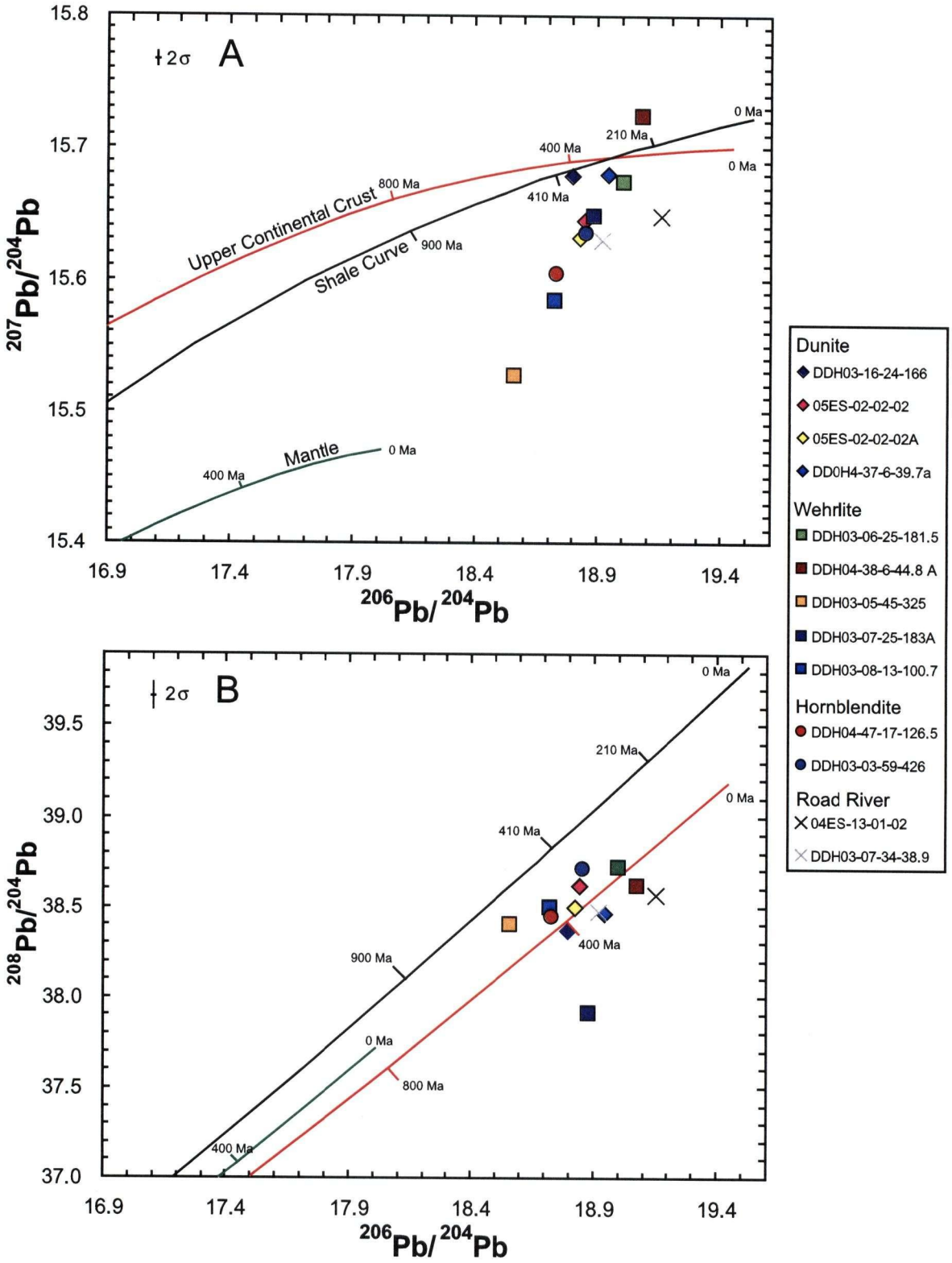

Figure 4.15: Lead isotopic compositions (A: $^{206}Pb/^{204}Pb$ vs. $^{207}Pb/^{204}Pb$, B: $^{206}Pb/^{204}Pb$ vs. $^{208}Pb/^{204}Pb$) of sulphide from the Turnagain intrusion with upper continental crust and mantle growth curves from Zartman & Doe (1981) and the shale curve from Godwin and Sinclair (1982).

the central part of the intrusion, 3) the late appearance of plagioclase as a cumulus phase relative to clinopyroxene and hornblende (e.g. Gaetani *et al.*, 1993), and 4) the presence of a fine- grained hornblendite dike (sample 04ES-00-07-04) that intruded wallrocks of the Turnagain intrusion. Sub-parallel trace element patterns, especially the rare earth elements (REE), indicate a genetic association between the different ultramafic rock types of the Turnagain intrusion. The range in concentrations reflects the relative abundances of cumulus olivine (and spinel), which both contain extremely low abundances of incompatible trace elements, cumulus and interstitial clinopyroxene, hornblende, and accessory minerals that crystallized from an evolved interstitial melt. The arc geochemical signature for the Turnagain parent magmas is based on combined trace element and Nd isotopic (see Chapter 2) characteristics of the analyzed samples. The prominent negative high field strength element (HFSE) anomalies (Figure 4.11B), specifically Nb and Ta, is typical of arc-derived magmas, reflecting (for example) the retention of the HFSE in refactory minerals such as rutile during subduction and magma genesis (e.g. Ryerson & Watson, 1987). Additionally, the most radiogenic Nd compositions of samples from the Turnagain intrusion (Chapter 2) fall within the general range of Paleozoic arc-derived mafic volcanic rocks from the northern Canadian Cordillera (ε_{Nd} = +4 to +7; Piercey *et al.*, 2006).

4.5.2 Sequence of Crystallization

The relative order of crystallization and emplacement in the Turnagain intrusion is dunite → wehrlite → olivine clinopyroxenite → hornblende clinopyroxenite → hornblendite → diorite. The entire sequence of rocks crystallized and cooled down to ~350°C at 190±1 Ma, based on the combined results from U-Pb and Ar-Ar geochronometry (Chapter 2). Cross-cutting relations and ferromagnesian silicate $Mg/(Mg+Fe^{2+})$ (e.g. $Fo_{olivine}$, $Mg\#_{cpx}$, $Mg\#_{hbl}$) are consistent with the sequential crystallization and emplacement of ultramafic and mafic lithologies in the Turnagain intrusion. Dunite (~Fo_{91}) cumulates are cross-cut by wehrlite dikes, wehrlite (~Fo_{87}) is cross-cut by olivine clinopyroxenite dikes, olivine clinopyroxenite (~Fo_{85}, $Mg\#_{cpx}$ = 0.92) is cross-cut by hornblende clinopyroxenite dikes, hornblende clinopyroxenite ($Mg\#_{cpx}$ = 0.81, $Mg\#_{hbl}$ = 0.65) is cross-cut by hornblendite dikes, and hornblendite ($Mg\#_{hbl}$ = 0.60) is cross-cut by diorite. Later lithologies typically cross-cut all earlier lithologies (e.g. diorite dikes are observed to intrude dunite at the southeastern contact between these two lithologies (Figure 4.1)), however some contacts between lithologies (e.g.

dunite-wehrlite) may be gradational. There are local examples of dunite dikes cutting olivine clinopyroxenite (Figure 4.3.1B), near the contact between these two lithologies in the northwestern part of the intrusion (Figure 4.1). These "dikes" are interpreted to represent fractures within the olivine clinopyroxenite through which primitive melts were injected. The primitive melts dissolved clinopyroxene and precipitated olivine, similar to dunite dikes observed in ophiolites (Kelemen & Dick, 1995; Braun & Kelemen, 2002). Alternatively, the dikes could represent injected dunite cumulates. The dunite dikes in the Turnagain intrusion do not appear to present replacive dunites as observed in other Alaskan-type intrusions (e.g. Duke Island, Alaska; Irvine, 1974). Combined with trace-element and PGE results, the chemical and lithological constraints on the evolution of the Turnagain intrusion imply that all lithologies are genetically related and that they crystallized from an evolving magma in an open system.

4.5.3 Implications for associated volcanic rocks

Based on petrologic and geochemical relations, the Turnagain intrusion can be interpreted as part of a magmatic feeder system to an arc volcano. The relationship between Alaskan-type intrusions and basaltic volcanic rocks has been discussed since some of the earliest studies of these intrusions (e.g. Findlay, 1969; Irvine, 1974; Clark, 1975). This association has typically been spatial, as belts of basaltic volcanic rocks have been observed to be broadly sub-parallel to belts of Alaskan-type intrusions. A temporal association between volcanic rocks and Alaskan-type intrusions has been established in B.C. (Late Triassic Takla/Nicola/Stuhini Groups; Nixon *et al.*, 1997), Columbia (Tistl *et al.*, 1994), and Kamchatka (Batanova *et al.*, 2005), and a genetic relationship between ankaramitic dikes and Alaskan-type intrusions was proposed by Mossman *et al.* (2000). Arc ankaramite and picritic ankaramite have been observed as volcanic rocks near, or intruded by, Alaskan-type intrusions in southern Alaska (Irvine, 1974) and the Kamchatka Peninsula, Russia (Batanova *et al.*, 2005), and as dikes cross-cutting Alaskan-type intrusions in New Zealand (Mossman *et al.*, 2000; Spandler *et al.*, 2003) and central Mexico (Hernandez, 2000). Arc ankaramite dikes, with a whole rock $CaO/Al_2O_3>1$, share three key characteristics with Alaskan-type intrusions: mineralogy, crystallization sequence, and zonation. Ankaramite dikes are typically composed of olivine and clinopyroxene phenocrysts set in a groundmass containing hornblende and minor plagioclase. The crystallization sequence in the ankaramite dikes is olivine → clinopyroxene → hornblende → plagioclase, similar to that in many Alaskan-type intrusions. Finally, the

zonation in these dikes is delimited by olivine and clinopyroxene phenocrysts at the centre, which reduce in size outwards and grade into fine-grained hornblende that may contain interstitial plagioclase adjacent to the margin. Extrusive equivalents of the Turnagain and other Alaskan-type intrusions should occur as olivine+clinopyroxene-phyric basalts in the field, characterized by primitive mineral compositions, and as such may potentially be found in any arc mafic volcanic formations of Early Jurassic age in B.C. (e.g. Rossland Group, southern B.C.).

4.5.4 Origin of sulphide mineralization in the Turnagain intrusion

The presence of abundant sulphide, predominantly pyrrhotite and pentlandite, in the Turnagain intrusion is unusual for Alaskan-type intrusions. Basalts generated in subduction zone settings (arc basalts) typically contain 900-2500 ppm sulphur, higher than mid-ocean ridge basalts at comparable FeO (Wallace, 2005). The speciation of dissolved S in arc magmas is important in the genesis of magmatic sulphide in the Turnagain intrusion. Sulphur may exist in multiple valence states (S^{2-}, S^{0}, S^{4+}, S^{6+}) depending on the relative oxygen fugacity (fO_2) of its hosting magma. The relative oxygen fugacity and sulphur content of basaltic melts, illustrated in Figure 4.16, are critical factors in assessing the development of sulphide saturation (e.g. Jugo *et al.*, 2004; 2005). At fO_2 values at or below the reference oxygen buffer fayalite + O_2 $\leftrightarrow$ magnetite + quartz (FMQ), the dominant sulphur species in basaltic liquids is sulphide (S^{2-}) (Figure 4.16A), where ΔFMQ is the fO_2 relative to FMQ. Magmas with a relatively high fO_2 (greater than ΔFMQ = 0 to +1) will have S dominantly speciated as sulphate (SO_4^{2-}), and as such need significantly more S (approximately an order of magnitude more) to become sulphate-saturated (Figure 4.16B). This is consistent with the observations that most arc magmas are relatively oxidized (e.g. Ballhaus *et al.*, 1991; Carmichael, 1991; Parkinson & Arculus, 1999; Rohrbach *et al.*, 2005), and the general absence of magmatic sulphide deposits associated with most arc plutonic and volcanic rocks. As documented in this study, the Turnagain intrusion contains abundant localized sulphide mineralization (pyrrhotite+pentlandite), thus requiring that the fO_2 of the parent magmas was relatively low, especially compared with other typical arc magmas (Figure 4.16). This reduced nature of the parent magmas is consistent with the extremely low ferric iron content and $Fe^{3+}/\Sigma Fe$ (e.g. Parkinson & Arculus, 1999) of chromite from chromitite in the intrusion (Figure 3.10; Chapter 3). In addition, relatively early sulphide saturation in the crystallization sequence of the

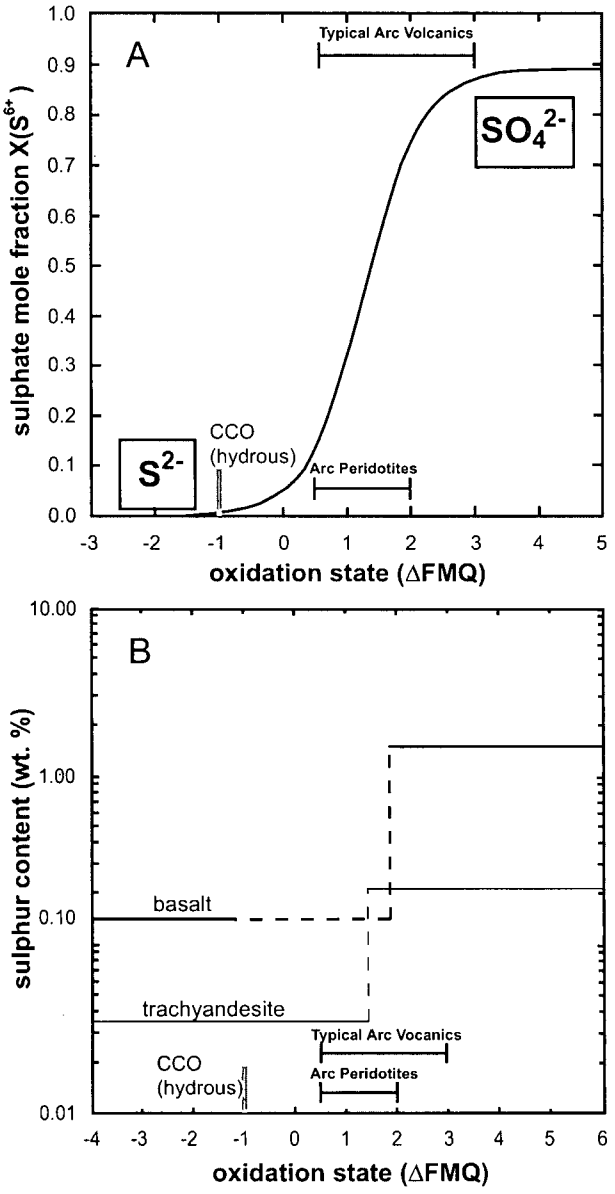

Figure 4.16: Diagrams showing the effects of oxygen fugacity on sulphur speciation and saturation in silicate magmas. The ranges in fO_2 for arc magmas (Carmichael, 1991; Rohrbach *et al.*, 2005) and arc peridotites (Parkinson & Arculus, 1999) are plotted as closed lines. A) Oxidation state (log ΔFMQ) vs. sulphate mole fraction, modified from Jugo *et al.* (2004). Note the transition between sulphide (S^{2-}) and sulphate (SO_4^{2-}) between ΔFMQ = 0 to +2.5. B) Oxidation state (log ΔFMQ) vs. sulphur content required to induce saturation, modified from Jugo *et al.* (2005). An order of magnitude more sulphur is needed to saturate a silicate magma in sulphate than sulphide.

Turnagain intrusion is demonstrated by the local presence of crystallized *mss* inclusions in chromite grains (Figure 3.3D, Chapter 3) and Ni-depletion of olivine in some dunite and wehrlite samples (Figure 4.7B).

Sulphide separates from the Turnagain intrusion display $\delta^{34}S$ values from +1 ‰ (mantle-like; e.g. Ripley, 1999) down to -9.7 ‰ (Figure 4.14), shifted in the direction of pyrite from the enclosing graphitic phyllite (-17.9 ‰). Many of the analyzed sulphide separates exhibit highly radiogenic Pb isotopic compositions (Figure 4.15), consistent with the incorporation of crustal Pb, and some whole rock ultramafic samples exhibit low ε_{Nd} values (Figure 2.10B; Chapter 2) outside the range for typical mafic volcanics. Combined, these results indicate that crustal material was added to the Turnagain parent magmas, especially S, which may have aided in achieving sulphide saturation. Inclusions of graphitic, pyritic phyllite are observed in drillcore from areas proximal to or within the sulphide-mineralized zones of the Turnagain intrusion (Figure 4.6). The pyrite in these inclusions has been completely converted to pyrrhotite, which is indicative of the prograde reaction $2\ FeS_2 \leftrightarrow 2\ FeS + S_2$. The phyllite inclusions released sulphur and carbon into the surrounding mafic liquid during heating and partial assimilation, with the graphite acting as a reducing agent, possibly following reactions such as $CO_3^{2-}{}_{(melt)} \leftrightarrow CO_{2(g)} + O^{2-}{}_{(melt)}$ (Nixon, 1998) or $C_{(s)} + O_{(melt)} \leftrightarrow CO_{(g)}$. The fact that partially digested phyllite with remnant graphite is still present in many ultramafic rocks from the mineralized zones indicates that the magmas proximal to these inclusions may have had a fO_2 near the CCO buffer (carbon-carbon monoxide) (ΔFMQ = -1 at upper crustal pressures and hydrous conditions; Parkinson & Arculus, 1999). Therefore the phyllite inclusions acted as both a sulphur source and a reducing agent, thus allowing the Turnagain intrusion to achieve early sulphide saturation.

4.5.5. Petrogenesis of the Turnagain intrusion and associated Ni-sulphide mineralization

The Turnagain Alaskan-type intrusion was formed in a subduction zone and the parent magma were likely generated from the fluid-fluxed partial melting of a peridotitic mantle wedge (e.g. Spandler *et al.*, 2003; Green *et al.*, 2004; Batanova *et al.*, 2005). The parental magma generated in this setting was hydrous, likely volatile-rich (S, Cl), and primitive, as defined by the high forsterite content of olivine ($Fo_{92.5}$). This magma ascended through the mantle lithosphere and overlying crust with relatively minor interaction, based on the highly magnesian olivine compositions, the mineral assemblage of the hornfelsed volcanic wacke

(epidote + plagioclase ± amphibole ± biotite), and the whole rock Nd isotopic compositions of the various lithologies (Chapter 2), until it reached the upper crust. The intrusion was emplaced and crystallized within a tectonically active environment, perhaps explaining the presence of erratic chromitite schieren in dunite and rare modal layering in other lithologies (interpreted to have formed by magmatic turbidity currents), as evidenced by the presence of Alaskan-type intrusions along major structures (Nixon *et al.*, 1997; Krause *et al.*, 2006). The magmas differentiated and cooled in a relatively short interval of time at 190 Ma, producing the entire range of lithologies present in the Turnagain intrusion, with periodic injections of primitive melt, as evidenced from the near-constant Pt/Pd ratio and possibly the dunite dikes. Stoping of roof- and wall-rocks, as observed by hornfelsed inclusions of phyllite and volcanic wacke, introduced significant amounts of local crustal material that were partially incorporated into the magma. Metasedimentary inclusions are only observed within or near areas containing abundant sulphide. The pyrite-rich graphitic phyllite, the dominant host rock enclosing the intrusion, released S and C into the surrounding magma during heating. Many Alaskan-type intrusions are typically hosted in intrusive rocks, volcanic sequences, and juvenile clastic sedimentary rocks, and as such do not appear to be prospective for magmatic sulphide mineralization. The composition of the host rocks of the Turnagain intrusion is distinct from those that host other Alaskan-type intrusions, and thus the key factor that promoted locally abundant sulphide mineralization in Turnagain intrusion was this distinctive package of pyritic and graphitic phyllites.

4.6 CONCLUSION

The origin, emplacement, and crystallization of the Turnagain Alaskan-type intrusion in north-central British Columbia are constrained by 1) the high forsterite content ($Fo_{92.5}$) of olivine from the central dunite, 2) the progressively decreasing Fo content of olivine, Mg# of clinopyroxene and hornblende, and decreasing whole rock Mg# from ultramafic lithologies in the intrusion, 3) cross-cutting relationships between lithologies, 4) sub-parallel rare earth element (REE) patterns between ultramafic lithologies, 5) the presence of phlogopite in early olivine cumulates (dunite, wehrlite), the presence of late, primary hornblende in clinopyroxene-hornblende cumulates, and the absence of early plagioclase, and 6) high field strength element (HFSE) depletions, especially Ta and Nd, in all ultramafic rocks. These results indicate that the Turnagain parent magmas were primitive melts generated in the mantle, within a subduction zone setting, and that each lithology

in the crystallization sequence formed from progressively fractionated magmas. Disseminated to semi-massive Ni-sulphide mineralization, which occurs in a number of zones within the Turnagain intrusion, is variable in tenor and texture. A number of features constrain the origin of the sulphide-rich zones: 1) olivine from select dunite and wehrlite samples exhibits Ni-depletion, 2) the $\delta^{34}S$ values of sulphide separates span a wide range, from mantle-like values (0±1.1 ‰) down to light values (-9.7 ‰), with the most magnesian rocks (dunites) systematically shifted to lighter $\delta^{34}S$ values, 3) the Pb isotopic compositions of the sulphide separates indicate the presence of a significant component of radiogenic Pb derived from upper crustal rocks, and 4) partially digested inclusions of graphitic phyllite found in the mineralized zones contain pyrrhotite instead of pyrite. These results indicate that the sulphide mineralization in the Turnagain intrusion occurred as a result of assimilation of local upper crustal material, specifically the hosting Road River phyllite, which contains significant graphite and pyrite ($\delta^{34}S$ = -17.9‰). The graphite acted as a reducing agent such that sulphur in the parent magmas was dominantly speciated as sulphide (S^{2-}) rather than sulphate (SO_4^{2-}), which is typical of most arc-derived magmas. The reduced nature and the addition of crustal sulphur allowed for sulphide saturation to occur in the regions of the Turnagain intrusion where the majority of graphitic phyllite inclusions occur, and where the addition of crustal S was needed to saturate in earlier lithologies. The composition of the country rocks was critical in allowing the Turnagain Alaskan-type intrusion to host magmatic Ni-sulphide mineralization.

4.7 ACKNOWLEDGEMENTS

I am grateful to Hard Creek Nickel Corp. for continued field support for this project and to Jim Reed of Pacific Western Helicopters for his exemplary logistical support in the field. Special thanks to Tony Hitchins, Bruce Northcote, Chris Baldys, and Mark Jarvis (President) of Hard Creek Nickel Corp. for their generous support and interactions throughout the period of my M.Sc. thesis at UBC. Thanks to Mati Raudsepp at the University of British Columbia for guidance in the use of the electron microprobe and support during the research phase of this manuscript, Janet Gabites at the Pacific Centre for Isotopic and Geochemical Research (UBC) for processing the sulphide Pb isotopic analyses, and Andrew Greene for input into this manuscript. Thanks also to Reza Tafti of the Mineral Deposits Research Unit (UBC) for support during the research phase of this manuscript as well as Dr. Akira Isiwatari for mailing his published works on the Alaskan-type intrusions in Kamchatka, China, and Japan. Funding for this project was provided by a research grant from Hard Creek Nickel Corp. (formerly Canadian Metals Exploration Ltd.).

4.8 REFERENCES

Ballhaus, C., Berry, R.F., & Green, D.H. (1991). High pressure experimental calibration of the olivine-orthopyroxene-spinel oxygen geobarometer: implications for the oxidation state of the upper mantle. *Contributions to Mineralogy and Petrology* **107** (1), 27-40

Barron, L.M., Suppel, D.W., Slansky, E., Johan, Z., Ohnenstetter, M., & Spencer, R. (1991). The Fifield platinum province (FPP). *Geological Society of Australia Abstracts* **29**, 3

Batanova, V.G., Pertsev, A.N., Kamenetsky, V.S., Ariskin, A.A., Mochalov, A.G., & Sobolev, A.V. (2005). Crustal evolution of island-arc ultramafic magma: Galmoenan pyroxenite-dunite plutonic complex, Koryak Highland (Far East Russia). *Journal of Petrology* **46**, 1345-1366

Braun, M.G., & Kelemen, P.B. (2002). Dunite distribution in the Oman ophiolite: Implications for melt flux through porous dunite conduits. *Geochemistry Geophysics Geosystems* **3**, 8603, doi:10.1029/2001GC000289, 21p

Carmichael, I.S.E. (1991). The redox states of basic and silicic magmas: a reflection of their source regions? *Contributions to Mineralogy and Petrology* **106**, 129-141

Clark, T. (1975). Geology of an ultramafic complex on the Turnagain River, northwestern B.C.; unpublished PhD dissertaion, *Queen's University*, 454p.

Clark, T. (1978). Oxide minerals in the Turnagain ultramafic complex, northwestern British Columbia. *Canadian Journal of Earth Sciences* **15**, 1893-1903

Clark, T. (1980). Petrology of the Turnagain ultramafic complex, northwestern British Columbia. *Canadian Journal of Earth Sciences* **17**, 744-757

Erdmer, P., Mihalynuk, M.G., Gabrielse, H., Heaman, L.M., & Creaser, R.A. (2005). Mississippian volcanic assemblage conformably overlying Cordilleran miogeoclinal strata, Turnagain River area, northern British Columbia, is not part of an accreted terrane. *Canadian Journal of Earth Sciences* **42**, 1449-1465

Findlay, D.C. (1969). Origin of the Tulameen ultramafic-gabbro complex, southern British Columbia. *Canadian Journal of Earth Sciences* **6**, 399-425

Gabrielse, H. (1998). Geology of Cry Lake and Dease Lake map areas, north-central British Columbia. *Geological Survey of Canada* Bulletin **504**, 147p

Gaetani, G.A., Grove, T.L., & Bryan, W.B. (1993). The influence of water on the petrogenesis of subduction-related igneous rocks. *Nature* **365**, 332-334

Garuti, G., Pushkarev, E.V., & Zaccarini, F. (2003). Composition and paragenesis of Pt alloys from chromitites of the Uralian-Alaskan-type Kytlym and Uktus complexes, northern and central Urals, Russia. *Canadian Mineralogist* **40**, 1127-1146

Godwin, C.J., & Sinclair, A.J. (1982). Average lead isotope growth curves for shale-hosted zinc-lead deposits, Canadian Cordillera. *Economic Geology* **7**, 675-690

Green, D.H., Schmidt, M.W., & Hibberson, W.O. (2004). Island-arc ankaramites: Primitive melts from fluxed refractory lherzolitic mantle. *Journal of Petrology* **45**, 391-403

Hernandez, L.E.O. (2000). An arc ankaramite occurrence in central Mexico. *Revista Mexicana de Ciencias Geológicas* **17**, 34-44

Himmelberg, G.R., & Loney, R.A. (1995). Characteristics and petrogenesis of Alaskan-type ultramafic-mafic intrusions, southeastern Alaska. *United States Geological Survey Professional Paper* Report **P 1564**, 47p

Holland, T., & Blundy, J. (1994). Non-ideal interactions in calcic amphiboles and their bearing on amphibole-plagioclase thermometry. *Contributions to Mineralogy and Petrology* **116**, 433-47

Irvine, T.N. (1974). Petrology of the Duke Island ultramafic complex, southeastern Alaska. *Geological Society of America – Memoir* **138**, 240p

Jackson, S.E., Fryer, B.J., Gosse, W., Healey, D.C., Longerich, H.P., & Strong, D.F. (1990). Determination of the precious metals in geological materials by inductively coupled plasma-mass spectrometry (ICP-MS) with nickel sulfide fire-assay collection and tellurium coprecipitation. *Chemical Geology* **83**, 119-132.

Johan, Z. (2002). Alaskan-types complexes and their platinum-group element mineralization. *In*: Cabri, L.J. (ed.) The Geology, Geochemistry, Mineralogy and Mineral Beneficiation of Platinum-Group Elements. *Canadian Institute of Mining, Metallurgy and Petroleum* Special Volume **54**, 669-719

Jugo, P.J., Luth, R.W., & Richards, J.P. (2004). Experimental data on the speciation of sulfur as a function of oxygen fugacity in basaltic melts. *Geochimica et Cosmochimia Acta* **69**, 497-503

Jugo, P.J., Luth, R.W., & Richards, J.P. (2005). An experimental study of the sulfur content in basaltic melts saturated with immiscible sulfide or sulfate liquids at 1300°C and 1.0 GPa. *Journal of Petrology* **46**, 783-798

Kelemen, P.B. & Dick, H.J.B. (1995). Focused melt flow and localized deformation in the upper mantle: Juxtaposition of replacive dunite and ductile shear zones in the Josephine peridotites, SW Oregon. *Journal of Geophysical Research* **100**, 423-438

Krause, J., Brügmann, G.E., Pushkarev, E.V. (2007). Accessory and rock forming minerals monitoring the evolution of zoned mafic-ultramafic complexes in the Central Ural Mountains. *Lithos* **95**, 19-42

Leake, B.E., Woolley, A.R., Arps, C.E.S., Birch, W.D., Gilbert, M.C., Grice, J.D., Hawthorne, F.C., Kato, A., Kisch, H.J., Krivovichev, V.G., Linthout, K., Laird, J., Mandarin, J.A., Maresch, W., Nickel, E.H., Rock, N.M.S., Schumacher, J.C., Smith, D.C., Stephenson, N.C.N., Ungaretti, L., Whittaker, E.J.W., & Youzhi, G. (1997). Nomenclature of amphiboles: Report of the subcommittee on amphiboles of the International Mineralogical Association, Commission on New Minerals and Mineral Names. *Canadian Mineralogist* **35**, 219-246

Lindsley, D.H. (1983). Pyroxene thermometry. *American Mineralogist* **68**, 477-493

Loney, R.A., Himmelberg, G.R., & Shaw, N.B. (1987). Salt Chuck palladium-bearing ultramafic body, Prince of Wales Island. *U.S. Geological Survey* Circular Report **C 0998**, 126-127

Loney, R.A., & Himmelberg, G.R. (1992). Petrogenesis of the Pd-rich intrusion at Salt Chuck, Prince of Wales Island: An Early Paleozoic Alaskan-type ultramafic body. *Canadian Mineralogist* **30**, 1005-1022

Maier, W.D., & Barnes, S.-J. (1999): Platinum-group elements in silicate rocks of the Lower, Critical and Main Zones at Union section, western Bushveld Complex. *Journal of Petrology* **40**, 1647-1671

McDonough, W.F., & Sun, S.S. (1995). The composition of the Earth. *Chemical Geology* **120**, 223-253

Mossman, D.J., Coombs, D.S., Kawachi, Y., & Reay, A. (2000). High-Mg arc ankaramitic dikes, Greenhills Complex, Southland, New Zealand. *Canadian Mineralogist* **38**, 191-216

Nixon, G.T., Ash, C.H., Connelly, J.N., & Case, G. (1989). Geology and noble metal geochemistry of the Turnagain ultramafic complex, northern British Columbia. *B.C. Ministry of Energy, Mines, and Petroleum Resources*, Open File **1989-18**

Nixon, G.T., Hammack, J.L., Ash, C.H., Cabri, L.J., Case, G., Connelly, J.N., Heaman, L.M., Laflamme, J.H.G., Nuttall, C., Paterson, W.P.E., & Wong, R.H. (1997). Geology and platinum-group-element mineralization of Alaskan-type ultramafic-mafic complexes in British Columbia. *B.C. Geological Survey* Bulletin **93**, 141p

Nixon, G.T. (1998). Ni-Cu sulphide mineralization in the Turnagain Alaskan-type complex: A unique magmatic environment. *Geological Fieldwork 1997, B.C. Ministry of Energy, Mines, and Petroleum Resources* Paper **1998-1**, 18-1 - 18-11

Parkinson, I.J., & Arculus, R.J. (1999). The redox state of subduction zones: insights from arc-peridotites. *Chemical Geology* **160**, 409-423

Peach, C.L., Mathez, E.A., & Keays, R.R. (1990). Sulfide melt-silicate melt distribution coefficients for noble metals and other chalcophile elements as deduced from MORB: Implications for partial melting. *Geochimica et Cosmochimica Acta* **54**, 3379-3389

Piercey, S.J., Nelson, J.-A.L., Dusel-Bacon, C., Simard, R.-L., & Roots, C.F. (2006). Paleozoic magmatism and crustal recycling along the ancient Pacific margin of North America, northern Cordillera. *In*: Colpron, M., and Nelson, J.L. (ed.) Paleozoic Evolution and Metallogeny of Pericratonic Terranes at the Ancient Pacific Margin of North America. *Geological Association of Canada* Special Paper **45**, 281-322

Pouchou, J.L., & Pichoir, F. (1985). PAP $\phi(\rho Z)$ procedure for improved quantitative microanalysis. *Microbeam Analysis* **1985**, 104-106.

Richardson, T., & Burnham, O.M. (2003). NiS fire-assay at the Geoscience Laboratories (Geo Labs): determination of the Pt-group elements and Au in geological materials at low levels using nickel sulphide fire-assay with ICP-MS finish. 34th Annual Canadian Mineral Analysts (CMA) Conference and Exhibit, September 15-18, 2003, Ottawa, ON, Canada, 8p

Ripley, E.M. (1999). Systematics of sulphur and oxygen isotopes in mafic igneous rocks and related Cu-Ni-PGE mineralization. *In*: Keays, R.R., Lesher C.M., Lightfoot, P.C., & Farrow, C.E.G. (ed.) Dynamic Processes in Magmatic Ore Deposits and Their Application to Mineral Exploration. *Geological Association of Canada*, Short Course Notes **13**, 133-158

Roddick, J.C. (1987). Generalized numerical error analysis with application to geochronology and thermodynamics. *Geochimica et Cosmochimica Acta* **51**, 2129-2135.

Rohrbach, A., Schuth, S., Ballhaus, C., Munker, C., Matveev, S., & Qopoto, C. (2005). Petrological constraints on the origin of arc picrites, New Georgia Group, Solomon Islands. *Contributions to Mineralogy and Petrology* **149**, 685-698

Ryerson, F.J., & Watson, E.B. (1987). Rutile saturation in magmas: implications for Ti-Nb-Ta depletion in island-arc basalts. *Earth and Planetary Science Letters* **86**, 225-239

Sakai, H., DeMarais, D., Veda, A., & Moore, J.G. (1984). Concentrations and isotope ratios of carbon, nitrogen, and sulfur in ocean-floor basalts. *Geochimica et Cosmochimica Acta* **48**, 2433-2441

Schneider, A. (1970). The sulfur isotopic composition of basaltic rocks. *Contributions to Mineralogy and Petrology* **25**, 95-124

Spandler, C.J., Arculus, R.J., Eggins, S.M., Mavrogenes, J.A., Price, R.C., & Reay, A.J. (2003). Petrogenesis of the Greenhills Complex, Southland, New Zealand: Magmatic differentiation and cumulate formation at the roots of a Permian island-arc volcano. *Contributions to Mineralogy and Petrology* **144**, 703-721

Taylor, H.P.Jr., (1967). The zoned ultramafic complexes of southeastern Alaska. *In*: Wyllie, P.J. (ed.) Ultramafic and Related Rocks, *John Wiley and Sons*, New York, 97-121

Thakurta, J., Ripley, E.M., & Li, C. (2004). Mineralogic and sulfur isotopic studies of Cu-Ni mineralization in the Duke Island Complex, Alaska. *Abstracts with Programs - Geological Society of America* **36**, 515-516

Thirlwall, M.F. (2000). Inter-laboratory and other errors in Pb-isotope analyses investigated using a ^{207}Pb-^{204}Pb double spike. *Chemical Geology* **163**, 299-322.

Tistl, M. (1994). Geochemistry of platinum-group elements of the zoned ultramafic Alto Condoto Complex, Northwest Colombia. *Economic Geology* **89**, 158-167

Tistl, M., Burgath, K.P., Hoehndorf, A., Kreuzer, H., Munox, R., & Salinas, R. (1994). Origin and emplacement of Tertiary ultramafic complexes in northwest Columbia: Evidence from geochemistry and K-Ar, Sm-Nd, and Rb-Sr isotopes. *Earth and Planetary Science Letters* **126**, 41-59

Wallace, P.J. (2005). Volatiles in subduction zone magmas: concentrations and fluxes based on melt inclusion and volcanic gas data. *Journal of Volcanology and Geothermal Research* **140**, 217-240

Zartman, R.E., & Doe, B.R. (1981). Lead-isotope evolution. *U. S. Geological Survey* Professional Paper **P 1275**, 169-170

CHAPTER 5

SUMMARY AND CONCLUSIONS

5.1 SUMMARY AND CONCLUSIONS

This comprehensive study of the Turnagain Alaskan-type intrusion in north-central British Columbia, Canada, is based on the combined results of field relations, petrography, mineral (spinel, olivine, clinopyroxene, and amphibole) chemistry, whole rock major and trace element geochemistry, neodymium isotopic geochemistry, sulphide sulphur and lead isotopic geochemistry, and Ar-Ar and U-Pb geochronology. The major goals of this study included 1) constraining the age and source of the parent magmas to the Turnagain intrusion, 2) evaluating the origin and petrogenesis of the intrusion, and 3) identifying the mechanism(s) responsible for the genesis of anomalous nickeliferrous sulphide mineralization in an Alaskan-type intrusion.

The magmas parental to the Turnagain intrusion were hydrous and primitive, and were derived in a subduction zone. The intrusion consists of cumulate dunite ($\sim Fo_{olivine} = 91$), wehrlite ($\sim Fo_{olivine} = 87$), olivine clinopyroxenite ($\sim Fo_{olivine} = 85$, $Mg\#_{cpx} = 0.92$), hornblende clinopyroxenite ($Mg\#_{cpx} = 0.81$, $Mg\#_{hbl} = 0.65$), hornblendite ($Mg\#_{hbl} = 0.60$), and diorite. This intrusive sequence and their relative order of emplacement is constrained by cross-cutting relationships. Olivine, clinopyroxene, and amphibole chemistry suggest that all lithologies crystallized from a progressively fractionating parent magma. Trace element geochemistry, especially the rare earth elements, of whole rock ultramafic samples indicates a genetic relationship between all lithologies, and corroborates their relationship by crystallization from a progressively evolving liquid. All lithologies in the Turnagain intrusion, based on the similarity of Ar-Ar (phlogopite, hornblende) and U-Pb (zircon, titanite) geochronological results, were emplaced and crystallized in a short time interval at 190±1 Ma. The presence of irregularly distributed chromitite schleiren in the central dunite, which may have formed by gravity flows in a upper crustal magma chamber, is consistent with the emplacement of the Turnagain intrusion in an active tectonic setting. The hydrous nature of the Turnagain intrusion, based on the presence of early interstitial and late cumulus hydrous phases and late plagioclase, indicate that the parent magmas were generated in a subduction zone setting and the high forsterite content of olivine in dunite (maximum of $Fo_{92.5}$ in olivine that did not re-equilibrate with chromite) requires that the parent magmas were in equilibrium with the peridotitic mantle from which they were generated.

Chromite in the Turnagain intrusion exhibits chemical trends that can be related to specific magmatic and post-magmatic processes. All disseminated chromite, due to its

relatively small volume proportion in dunite, wehrlite, and olivine clinopyroxenite has been compositionally modified by olivine and clinopyroxene fractionation, oxidation, re-equilibration with silicate phases, and equilibration with interstitial liquid. Each of these processes is clearly delineated on chromite compositional plots that establish post-crystallization processes based on inter- and intra-sample trends. Primitive chromite compositions ($Cr/(Fe^{3+}+Cr+Al) = 0.90$, $Fe^{2+}/(Fe^{2+}+Mg) = 0.3$, $Fe^{3+}/(Fe^{3+}+Cr+Al) = 0.75$) in the Turnagain intrusion occur in chromitite and are the most primitive spinel compositions observed in Alaskan-type intrusions to date. The ferric iron content of chromite from chromitite, and the $Fe^{3+}/\Sigma Fe$, in the Turnagain intrusion is extremely low and reflects the relatively low oxygen fugacity (f_{O2}) of the parent magmas. The relatively reduced nature of the Turnagain intrusion may have been an intrinsic property of its parent magmas, however the majority of arc-derived plutonic rocks are relatively oxidized ($\Delta FMQ = +1$ to $+3.5$, e.g. Carmichael, 1991). Therefore a reducing agent added to the magmas was required to lower the fO_2 enough to allow the parent magmas to saturate in sulphide (e.g. Jugo *et al.*, 2004; 2005). Thus the ferric iron content and $Fe^{3+}/\Sigma Fe$ of chromite from chromitite in Alaskan-type intrusions could be considered as a possible exploration tool for evaluating the sulphide mineralization potential of Alaskan-type intrusions.

Sulphide in the Turnagain intrusion occurs in localized areas of dunite and wehrlite as disseminated to semi-massive pyrrhotite and pentlandite with other minor phases (e.g. violarite, molybdenite). Hornfelsed inclusions of wallrocks have been intersected in drillcore within the sulphide-mineralized zones. The inclusions are dominantly volcanic wacke, graphitic phyllite, and lesser quartzite and marble. The inclusions of graphitic phyllite are the most important in the context of sulphide mineralization in the Turnagain intrusion because they contain sulphide and graphite. The graphitic phyllite proximal to the Turnagain intrusion is pyrite-rich (FeS_2), whereas the inclusions contain pyrrhotite ($Fe_{1-X}S$). The prograde reaction between these two minerals released sulphur into the Turnagain magmas, and the graphite in the inclusions acted as a reducing agent. The localized Ni-sulphide mineralization in the Turnagain intrusion is therefore the result of the interaction between sulphur- and graphite-rich fluids released from the graphitic phyllite inclusions and the primitive, hydrous parent magmas. Assimilation of crustal material is also demonstrated by systematic variations in sulphide sulphur and lead, and whole-rock neodymium isotopic compositions. Sulphur isotopic analyses of sulphide separates ($\delta^{34}S = +1.2$ to -9.7 ‰) indicate that crustal sulphur

was added to the Turnagain intrusion, especially the more magnesian lithologies. The lead isotopic results ($^{206}Pb/^{204}Pb$ = 18.11-19.15, $^{207}Pb/^{204}Pb$ = 15.53-15.72, $^{208}Pb/^{204}Pb$ = 37.91-38.72) indicate that much of the lead in sulphide originated from an upper crustal source. Finally, the neodymium isotopic results from ultramafic rocks in the Turnagain intrusion indicate that the mantle-derived parent magmas (ε_{Nd} = +5 to +6) were heterogeneously contaminated by crustal material such that some results are shifted towards more crustal values ($\varepsilon_{Nd(190)}$ = +2 to -3).

Finally, the Turnagain intrusion, which ascended through and stalled in graphitic phyllite and volcanic wacke, was dated by Ar-Ar and U-Pb geochronology at 190±1Ma, which has implications for the tectonic history of this part of northern British Columbia. The wallrocks were previously assigned to the paleo-passive margin of Ancestral North America by Gabrielse (1998) as the undifferentiated Road River and Earn Groups, with an overlying volcanic/sedimentary package of "unknown affinity". The graphitic phyllites are, however, conformably overlain by a volcanic wacke, as observed in outcrop by Erdmer *et al.* (2005) and in drillcore (this study). A minimum depositional age of 301 Ma for the volcanic wacke was determined by U-Pb dating of detrital zircon. The volcanic wacke also contains zircon grains with numerous Precambrian inherited cores. The lithological characteristics, age, and REE chemistry of the volcanic wacke are similar to the Lay Range Assemblage/Harper Ranch Subterrane of Quesnellia and the Klinkit Group of Yukon-Tanana. Inclusions of "Road River" phyllite and volcanic wacke in two Early Jurassic arc-derived intrusions (the Turnagain intrusion and Ring Complex to the southeast) requires that the wallrocks were situated in crust above a subduction zone, and the only known subduction zones of Early Jurassic age were located beneath the Stikine, Quesnel, and Yukon-Tanana terranes. Therefore the volcanic wacke and graphitic phyllites, along with the Turnagain Alaskan-type intrusion, belong to either the Quesnel terrane or the Yukon-Tanana terrane. However, these two terranes (along with the Stikine terrane) may have been part of a super-terrane after ~360 Ma (e.g. Simard *et al.*, 2003; Nelson & Friedman, 2004; Nelson *et al.*, 2006). Alaskan-type intrusions are well-documented in Quesnellia (e.g. Nixon *et al.*, 1997), but none have been described to date in Yukon-Tanana. If Alaskan-type intrusions were to be found hosted in the Klinkit Group, the proposed genetic association between Quesnellia and Yukon-Tanana would be further supported.

5.2 REFERENCES

Carmichael, I.S.E. (1991). The redox states of basic and silicic magmas: a reflection of their source regions? *Contributions to Mineralogy and Petrology* **106**, 129-141

Erdmer, P., Mihalynuk, M.G., Gabrielse, H., Heaman, L.M., & Creaser, R.A. (2005). Mississippian volcanic assemblage conformably overlying Cordilleran miogeoclinal strata, Turnagain River area, northern British Columbia, is not part of an accreted terrane. *Canadian Journal of Earth Sciences* **42**, 1449-1465

Gabrielse, H. (1998). Geology of Cry Lake and Dease Lake map areas, north-central British Columbia; *Geological Survey of Canada*, Bulletin **504**, 147p

Jugo, P.J., Luth, R.W., & Richards, J.P. (2004). Experimental data on the speciation of sulfur as a function of oxygen fugacity in basaltic melts. *Geochimica et Cosmochimia Acta* **69** (2), 497-503

Jugo, P.J., Luth, R.W., & Richards, J.P. (2005). An experimental study of the sulfur content in basaltic melts saturated with immiscible sulfide or sulfate liquids at 1300°C and 1.0 GPa. *Journal of Petrology* **46** (4), 783-798

Nelson, J.L., & Friedman, R. (2004). Superimposed Quesnel (late Paleozoic-Jurassic) and Yukon-Tanana (Devonian –Mississippian) arc assemblages, Cassiar Mountains, northern British Columbia: field, U-Pb, and igneous petrochemical evidence. *Canadian Journal of Earth Sciences* **41**, 1201-1235

Nelson, J.L., Colpron, M., Piercey, S.J., Dusel-Bacon, C., Murphy, D.C., & Roots, C.F. (2006). Paleozoic tectonic and metallogenetic evolution of pericratonic terranes in Yukon, northern British Columbia and eastern Alaska. *In*: Colpron, M., and Nelson, J.L. (ed.) Paleozoic Evolution and Metallogeny of Pericratonic Terranes at the Ancient Pacific Margin of North America. *Geological Association of Canada*, Special Paper **45**, 323-260

Nixon, G.T., Hammack, J.L., Ash, C.H., Cabri, L.J., Case, G., Connelly, J.N., Heaman, L.M., Laflamme, J.H.G., Nuttall, C., Paterson, W.P.E., & Wong, R.H. (1997). Geology and platinum-group-element mineralization of Alaskan-type ultramafic-mafic complexes in British Columbia. *Geological Survey of British Columbia* Bulletin **93**, 141p

Piercey, S.J., Nelson, J.-A.L., Dusel-Bacon, C., Simard, R.-L., Roots, C.F. (2006). Paleozoic magmatism and crustal recycling along the Ancient Pacific Margin of North America, Northern Cordillera. *In*: Colpron, M., and Nelson, J.L. (ed.) Paleozoic Evolution and Metallogeny of Pericratonic Terranes at the Ancient Pacific Margin of North America. *Geological Association of Canada*, Special Paper **45**, 281-322

Simard, R-L., Dostal, J., & Roots, C.F. (2003). Development of late Paleozoic volcanic arcs in the Canadian Cordillera: an example from the Klinkit Group, northern British Columbia and southern Yukon. *Canadian Journal of Earth Sciences* **40**, 907-924

APPENDICES

Appendix I: Spinel compositions from spinel-bearing ultramafic rocks of the Turnagain intrusion

Rock:	Chromitite															Chromitite		
Sample:	05ES-01-01-01															05ES-01-04-01		
Cluster:	7			6			5			4			3			7		
Grain Number:	1			1			1			1			1			1		
Style:	m. anh.			m. sub.			m. sub.			m. eu.			m. anh.			l. anh.		
Zone:	Rim	Mid	Core	Rim	Mid	Core	Rim	Mid	Core	Rim	Mid	Core	Rim	Mid	Core	Rim	Mid	Mid
Oxides (wt. %)																		
SiO_2	0.02	0.02	0.03	0.01	0.02	0.02	0.00	0.00	0.16	0.01	0.02	0.00	0.00	0.00	0.03	0.00	0.00	0.08
TiO_2	0.63	0.61	0.66	0.55	0.60	0.61	0.59	0.51	0.54	0.61	0.59	0.56	0.65	0.55	0.54	0.22	0.21	0.24
Al_2O_3	7.02	6.82	6.70	6.53	6.61	6.63	6.77	6.25	6.16	6.77	6.64	6.46	7.14	6.61	6.53	4.60	5.84	5.83
Cr_2O_3	58.93	59.39	59.52	60.32	59.60	59.77	59.17	59.90	60.97	59.12	59.05	59.34	59.03	59.86	60.40	66.65	63.40	62.91
V_2O_3	0.34	0.30	0.32	0.28	0.34	0.26	0.33	0.27	0.23	0.33	0.31	0.29	0.31	0.31	0.34	0.00	0.03	0.01
Fe_2O_3	5.01	4.47	4.57	4.35	4.78	4.57	5.06	4.59	4.24	5.09	5.12	5.01	4.76	4.85	4.83	3.98	5.62	6.05
FeO	19.21	18.64	18.70	18.17	18.23	18.14	18.41	18.08	18.37	18.08	17.86	17.89	18.19	18.01	17.99	11.55	11.32	11.14
MnO	0.10	0.15	0.19	0.10	0.13	0.16	0.14	0.14	0.16	0.19	0.14	0.14	0.14	0.17	0.09	0.00	0.00	0.00
MgO	9.74	9.88	9.89	10.19	10.19	10.18	10.09	10.02	10.00	10.24	10.30	10.22	10.29	10.30	10.48	14.23	14.42	14.51
NiO	0.10	0.06	0.08	0.05	0.06	0.07	0.05	0.06	0.05	0.06	0.06	0.06	0.09	0.08	0.07	0.16	0.20	0.20
CaO	0.00	0.00	0.00	0.00	0.00	0.00	0.00	0.00	0.01	0.02	0.01	0.01	0.00	0.00	0.00	0.01	0.00	0.02
Total	101.11	100.34	100.64	100.56	100.57	100.40	100.61	99.82	100.89	100.51	100.08	99.97	100.58	100.74	101.30	101.40	101.05	100.99
Cations (p.f.u.)																		
Ti	0.016	0.015	0.016	0.014	0.015	0.015	0.015	0.013	0.014	0.015	0.015	0.014	0.016	0.014	0.014	0.005	0.005	0.006
Cr	1.550	1.572	1.572	1.592	1.572	1.580	1.561	1.596	1.608	1.559	1.564	1.575	1.553	1.576	1.580	1.714	1.625	1.612
Al	0.275	0.269	0.264	0.257	0.260	0.261	0.266	0.248	0.242	0.266	0.262	0.256	0.280	0.259	0.255	0.176	0.223	0.223
V	0.008	0.007	0.007	0.006	0.008	0.006	0.007	0.006	0.005	0.007	0.007	0.006	0.007	0.007	0.007	0.000	0.001	0.000
Fe^{3+}*	0.125	0.112	0.115	0.109	0.120	0.115	0.127	0.116	0.106	0.128	0.129	0.127	0.119	0.121	0.120	0.097	0.137	0.148
Fe^{2+}*	0.534	0.522	0.522	0.507	0.509	0.507	0.514	0.510	0.512	0.504	0.500	0.502	0.506	0.501	0.498	0.314	0.307	0.302
Mn	0.003	0.004	0.005	0.003	0.004	0.004	0.004	0.004	0.005	0.005	0.004	0.004	0.004	0.005	0.002	0.000	0.000	0.000
Mg	0.483	0.493	0.493	0.507	0.507	0.507	0.502	0.503	0.497	0.509	0.514	0.512	0.510	0.512	0.517	0.690	0.697	0.701
Ni	0.003	0.002	0.002	0.001	0.002	0.002	0.001	0.002	0.001	0.002	0.002	0.002	0.002	0.002	0.002	0.004	0.005	0.005
Ca	0.000	0.000	0.000	0.000	0.000	0.000	0.000	0.000	0.000	0.001	0.000	0.000	0.000	0.000	0.000	0.000	0.000	0.001
Total	2.997	2.996	2.996	2.997	2.996	2.997	2.997	2.998	2.990	2.997	2.996	2.998	2.998	2.998	2.996	3.001	3.001	2.997
Trivalent End Members																		
Cr/Σ3+	0.795	0.805	0.806	0.813	0.805	0.808	0.799	0.814	0.822	0.798	0.800	0.805	0.796	0.805	0.808	0.862	0.819	0.813
Al/Σ3+	0.141	0.138	0.135	0.131	0.133	0.133	0.136	0.127	0.124	0.136	0.134	0.131	0.143	0.133	0.130	0.089	0.112	0.112
Fe/Σ3+	0.064	0.058	0.059	0.056	0.061	0.059	0.065	0.059	0.054	0.065	0.066	0.065	0.061	0.062	0.062	0.049	0.069	0.074

Crystal textural style is abbreviated: euh. (euhedral), sub. (subhedral), anh. (anhedral), interg. (intergrown), irreg. (irregular); l. (large), m. (medium), s. (small)
Grain number refers to a particular grain within a cluster: most clusters have multiple grain
Note: Other phases (ol, cpx, hbl) were also analyzed on certain sections, such that Cluster refers to a specific location on each section

Appendix I(continued): Spinel compositions from spinel-bearing ultramafic rocks of the Turnagain intrusion

Rock:	Chromitite													Chromitite				
Sample:	05ES-01-04-01													05ES-01-03-01				
Cluster:	7	6			5				4					1				2
Grain Number:	1	1			1				1					1				1
Style:		l. anh.				l. anh.				l. anh.					l. eu.			l. eu.
Zone:	Core	Rim	Mid	Mid	Core	Rim	Mid	Mid	Core	Rim	Mid	Mid	Core	Rim	Mid	Mid	Core	Rim
Oxides (wt. %)																		
SiO_2	0.09	0.00	0.00	0.00	0.00	0.00	0.00	0.00	0.05	0.00	0.03	0.10	0.00	0.00	0.00	0.04	0.00	0.00
TiO_2	0.24	0.22	0.27	0.30	0.22	0.30	0.27	0.29	0.28	0.23	0.25	0.23	0.27	0.21	0.22	0.22	0.23	0.23
Al_2O_3	5.80	5.07	5.80	5.82	5.94	5.26	5.88	5.92	5.99	4.77	5.77	5.82	5.96	4.88	5.18	5.46	5.54	5.48
Cr_2O_3	63.75	65.24	62.85	63.17	62.86	64.23	62.47	62.92	63.28	64.51	62.62	62.89	63.00	62.90	61.92	61.88	61.03	62.10
V_2O_3	0.03	0.02	0.02	0.00	0.05	0.04	0.01	0.02	0.00	0.00	0.03	0.05	0.07	0.01	0.00	0.03	0.00	0.02
Fe_2O_3	5.44	3.82	5.43	5.97	5.82	4.35	5.52	5.36	5.20	4.30	5.37	5.51	5.54	6.45	6.51	6.63	6.85	6.12
FeO	11.68	11.22	11.59	11.68	11.78	12.69	12.03	12.15	12.28	12.48	11.62	11.86	12.04	14.58	14.26	13.93	13.67	13.39
MnO	0.00	0.04	0.02	0.07	0.00	0.03	0.00	0.00	0.00	0.04	0.05	0.03	0.01	0.05	0.08	0.09	0.07	0.09
MgO	14.26	14.19	14.09	14.26	14.14	13.40	13.80	13.86	13.85	13.29	13.96	13.92	14.01	12.23	12.29	12.63	12.62	12.87
NiO	0.18	0.13	0.16	0.18	0.17	0.12	0.14	0.17	0.15	0.13	0.15	0.16	0.15	0.10	0.09	0.12	0.12	0.14
CaO	0.05	0.00	0.01	0.00	0.01	0.00	0.01	0.02	0.01	0.00	0.01	0.06	0.02	0.03	0.00	0.00	0.01	0.00
Total	101.53	99.96	100.26	101.44	100.99	100.43	100.14	100.70	101.09	99.75	99.87	100.61	101.07	101.42	100.56	101.02	100.13	100.44
Cations (p.f.u.)																		
Ti	0.006	0.006	0.007	0.007	0.005	0.007	0.007	0.007	0.007	0.006	0.006	0.006	0.007	0.005	0.006	0.005	0.006	0.006
Cr	1.628	1.695	1.626	1.616	1.615	1.670	1.621	1.623	1.626	1.693	1.627	1.622	1.618	1.639	1.623	1.609	1.600	1.621
Al	0.221	0.196	0.224	0.222	0.228	0.204	0.227	0.228	0.229	0.187	0.223	0.224	0.228	0.189	0.202	0.212	0.217	0.213
V	0.001	0.000	0.001	0.000	0.001	0.001	0.000	0.000	0.000	0.000	0.001	0.001	0.001	0.000	0.000	0.001	0.000	0.000
Fe^{3+}*	0.132	0.094	0.134	0.145	0.142	0.108	0.136	0.132	0.127	0.107	0.133	0.135	0.136	0.160	0.162	0.164	0.171	0.152
Fe^{2+}*	0.315	0.308	0.317	0.316	0.320	0.349	0.330	0.331	0.334	0.346	0.319	0.324	0.327	0.402	0.395	0.383	0.379	0.370
Mn	0.000	0.001	0.001	0.002	0.000	0.001	0.000	0.000	0.000	0.001	0.001	0.001	0.000	0.001	0.002	0.002	0.002	0.002
Mg	0.687	0.695	0.688	0.688	0.685	0.657	0.675	0.674	0.671	0.657	0.684	0.677	0.679	0.601	0.607	0.619	0.624	0.633
Ni	0.005	0.004	0.004	0.005	0.004	0.003	0.004	0.004	0.004	0.004	0.004	0.004	0.004	-	-	-	-	-
Ca	0.002	0.000	0.000	0.000	0.000	0.000	0.000	0.001	0.000	0.000	0.000	0.002	0.001	0.001	0.000	0.000	0.000	0.000
Total	2.997	3.001	3.001	3.001	3.001	3.000	3.001	3.001	2.998	3.001	2.999	2.996	3.000	2.998	2.998	2.996	2.998	2.997
Trivalent End Members																		
Cr/Σ3+	0.822	0.854	0.820	0.815	0.814	0.843	0.817	0.819	0.820	0.852	0.820	0.819	0.817	0.824	0.817	0.811	0.805	0.816
Al/Σ3+	0.111	0.099	0.113	0.112	0.115	0.103	0.115	0.115	0.116	0.094	0.113	0.113	0.115	0.095	0.102	0.107	0.109	0.107
Fe/Σ3+	0.067	0.048	0.067	0.073	0.072	0.054	0.069	0.066	0.064	0.054	0.067	0.068	0.068	0.080	0.082	0.083	0.086	0.077

Crystal textural style is abbreviated: euh. (euhedral), sub. (subhedral), anh. (anhedral), interg. (intergrown), irreg. (irregular); l. (large), m. (medium), s. (small)
Grain number refers to a particular grain within a cluster: most clusters have multiple grain
Note: Other phases (ol, cpx, hbl) were also analyzed on certain sections, such that Cluster refers to a specific location on each section

Appendix I(continued): Spinel compositions from spinel-bearing ultramafic rocks of the Turnagain intrusion

Rock:	Chromitite											Dunite						
Sample:	05ES-01-03-01											04ES-19-01-02						
Cluster:	2			3				4				1						
Grain Number:	1							1				1						
Style:				m. anh.				m. eu.				l. sub.						
Zone:	Mid	Mid	Core	Rim	Mid	Mid	Core	Rim	Mid	Mid	Core	Mid	Mid	Mid	Mid	Mid	Mid	Core
Oxides (wt. %)																		
SiO_2	0.02	0.01	0.02	0.01	0.02	0.02	0.02	0.00	0.00	0.02	0.00	0.04	0.02	0.03	0.08	0.06	0.00	0.01
TiO_2	0.25	0.22	0.24	0.24	0.23	0.24	0.28	0.21	0.21	0.25	0.22	0.77	0.81	0.82	0.73	0.80	0.89	0.71
Al_2O_3	5.45	5.56	5.53	5.26	5.55	5.52	5.66	4.93	5.47	5.59	5.47	8.74	8.87	8.86	8.81	8.81	8.75	8.37
Cr_2O_3	61.93	61.29	61.44	62.68	62.32	61.23	61.91	62.33	61.24	62.19	62.63	53.75	55.41	55.43	55.51	55.75	54.45	54.04
V_2O_3	0.02	0.03	0.03	0.02	0.01	0.02	0.03	0.00	0.04	0.02	0.00	0.18	0.15	0.15	0.15	0.15	0.15	0.12
Fe_2O_3	6.37	6.72	6.73	6.61	6.53	6.88	6.28	6.50	6.56	6.33	6.54	6.37	4.31	4.34	4.32	4.66	4.65	5.70
FeO	13.57	13.41	13.50	14.52	14.24	13.79	14.01	13.75	13.61	13.86	13.71	23.15	22.63	22.21	21.78	22.23	22.26	23.16
MnO	0.02	0.02	0.06	0.07	0.16	0.09	0.00	0.01	0.06	0.05	0.08	0.34	0.30	0.24	0.35	0.29	0.31	0.39
MgO	12.82	12.85	12.83	12.42	12.52	12.61	12.68	12.59	12.61	12.76	12.91	7.05	7.35	7.64	7.72	7.73	7.41	6.68
NiO	0.13	0.14	0.12	0.13	0.12	0.13	0.13	0.11	0.13	0.13	0.14	-	-	-	-	-	-	-
CaO	0.00	0.01	0.00	0.02	0.01	0.01	0.01	0.01	0.02	0.01	0.01	0.00	0.00	0.00	0.01	0.00	0.01	0.00
Total	100.57	100.25	100.50	101.98	101.70	100.53	100.99	100.45	99.94	101.22	101.70	100.40	99.83	99.73	99.47	100.48	98.88	99.18
Cations (p.f.u.)																		
Ti	0.006	0.006	0.006	0.006	0.006	0.006	0.007	0.005	0.005	0.006	0.005	0.020	0.021	0.021	0.019	0.020	0.023	0.018
Cr	1.615	1.602	1.603	1.620	1.612	1.599	1.608	1.633	1.608	1.612	1.616	1.439	1.487	1.485	1.490	1.483	1.474	1.470
Al	0.212	0.216	0.215	0.203	0.214	0.215	0.219	0.193	0.214	0.216	0.210	0.349	0.355	0.354	0.352	0.349	0.353	0.339
V	0.000	0.001	0.001	0.001	0.000	0.000	0.001	0.000	0.001	0.000	0.000	0.004	0.003	0.003	0.003	0.003	0.003	0.003
Fe^{3+}*	0.158	0.167	0.167	0.163	0.161	0.171	0.155	0.162	0.164	0.156	0.161	0.162	0.110	0.111	0.110	0.118	0.120	0.147
Fe^{2+}*	0.374	0.371	0.373	0.397	0.390	0.381	0.385	0.381	0.378	0.380	0.374	0.656	0.642	0.630	0.618	0.626	0.637	0.667
Mn	0.001	0.001	0.002	0.002	0.004	0.002	0.000	0.000	0.002	0.001	0.002	0.010	0.009	0.007	0.010	0.008	0.009	0.011
Mg	0.630	0.633	0.631	0.605	0.610	0.621	0.621	0.622	0.624	0.624	0.628	0.356	0.372	0.386	0.391	0.388	0.378	0.342
Ni	-	-	-	-	-	-	-	-	-	-	-	-	-	-	-	-	-	-
Ca	0.000	0.001	0.000	0.001	0.000	0.000	0.000	0.000	0.001	0.000	0.000	0.000	0.000	0.000	0.001	0.000	0.000	0.000
Total	2.996	2.997	2.996	2.997	2.997	2.997	2.997	2.998	2.997	2.996	2.997	2.996	2.998	2.997	2.995	2.995	2.999	2.998
Trivalent End Members																		
Cr/Σ3+	0.814	0.807	0.808	0.816	0.811	0.806	0.811	0.822	0.810	0.812	0.813	0.738	0.762	0.762	0.763	0.760	0.757	0.751
Al/Σ3+	0.107	0.109	0.108	0.102	0.108	0.108	0.111	0.097	0.108	0.109	0.106	0.179	0.182	0.182	0.180	0.179	0.181	0.173
Fe/Σ3+	0.080	0.084	0.084	0.082	0.081	0.086	0.078	0.081	0.083	0.079	0.081	0.083	0.056	0.057	0.057	0.061	0.062	0.075

Crystal textural style is abbreviated: euh. (euhedral), sub. (subhedral), anh. (anhedral), interg. (intergrown), irreg. (irregular); l. (large), m. (medium), s. (small)
Grain number refers to a particular grain within a cluster: most clusters have multiple grain
Note: Other phases (ol, cpx, hbl) were also analyzed on certain sections, such that Cluster refers to a specific location on each section

Appendix I(continued): Spinel compositions from spinel-bearing ultramafic rocks of the Turnagain intrusion

Rock:	Dunite																	
Sample:	04ES-19-01-02																	
Cluster:	2														3			
Grain Number:	1			2											1			2
Style:	s. anh.			l. anh.											s. sub.			m. sub.
Zone:	Rim	Mid	Core	Rim	Mid	Mid	Mid	Mid	Mid	Mid	Mid	Mid	Mid	Core	Rim	Mid	Core	Rim
Oxides (wt. %)																		
SiO_2	0.03	0.06	0.02	0.25	0.01	0.00	0.07	0.17	0.02	0.00	0.01	0.05	0.05	0.06	0.05	0.01	0.03	0.03
TiO_2	0.76	0.94	0.79	0.05	0.55	0.72	0.73	0.74	0.88	0.77	0.89	0.81	0.76	0.39	0.78	0.81	0.83	0.42
Al_2O_3	8.73	8.99	8.98	0.04	2.71	8.87	8.95	8.85	8.92	8.88	9.04	9.05	8.94	2.15	8.78	9.01	9.00	7.37
Cr_2O_3	54.61	54.66	54.58	3.34	48.55	54.85	54.41	55.04	54.73	55.44	55.68	54.92	54.68	32.04	55.15	54.72	55.01	52.94
V_2O_3	0.18	0.14	0.10	0.03	0.19	0.13	0.14	0.15	0.15	0.11	0.14	0.15	0.18	0.12	0.16	0.16	0.13	0.20
Fe_2O_3	5.15	4.31	4.71	67.65	18.21	4.84	4.61	4.84	4.76	4.58	4.05	4.79	4.79	35.06	4.49	4.09	4.16	8.83
FeO	23.24	22.84	22.75	28.29	22.00	22.73	22.38	22.29	21.67	21.76	21.90	21.75	22.76	22.88	23.26	22.83	22.92	21.74
MnO	0.42	0.32	0.34	0.09	1.07	0.33	0.37	0.35	0.35	0.31	0.33	0.27	0.32	0.73	0.31	0.40	0.28	0.69
MgO	6.86	7.17	7.12	2.12	6.29	7.16	7.20	7.47	7.86	7.84	7.89	7.91	7.20	5.43	6.91	7.01	7.11	7.17
NiO	-	-	-	-	-	-	-	-	-	-	-	-	-	-	-	-	-	-
CaO	0.00	0.03	0.01	0.01	0.01	0.01	0.02	0.01	0.04	0.02	0.00	0.03	0.00	0.00	0.02	0.00	0.00	0.00
Total	99.99	99.46	99.42	101.86	99.58	99.63	98.88	99.91	99.39	99.72	99.92	99.73	99.68	98.86	99.90	99.03	99.46	99.39
Cations (p.f.u.)																		
Ti	0.019	0.024	0.020	0.001	0.015	0.018	0.019	0.019	0.023	0.020	0.022	0.021	0.019	0.011	0.020	0.021	0.021	0.011
Cr	1.469	1.472	1.472	0.098	1.362	1.477	1.473	1.473	1.469	1.484	1.486	1.468	1.470	0.920	1.483	1.482	1.483	1.440
Al	0.350	0.361	0.361	0.002	0.113	0.356	0.361	0.353	0.357	0.354	0.360	0.360	0.358	0.092	0.352	0.364	0.361	0.299
V	0.004	0.003	0.002	0.001	0.004	0.003	0.003	0.003	0.003	0.002	0.003	0.003	0.004	0.003	0.004	0.004	0.003	0.004
Fe^{3+*}	0.132	0.110	0.121	1.887	0.486	0.124	0.119	0.123	0.121	0.117	0.103	0.122	0.123	0.958	0.115	0.105	0.107	0.229
Fe^{2+*}	0.661	0.651	0.649	0.877	0.652	0.647	0.641	0.631	0.615	0.616	0.618	0.615	0.647	0.695	0.662	0.654	0.653	0.625
Mn	0.012	0.009	0.010	0.003	0.032	0.009	0.011	0.010	0.010	0.009	0.010	0.008	0.009	0.022	0.009	0.012	0.008	0.020
Mg	0.348	0.364	0.362	0.117	0.333	0.364	0.368	0.377	0.398	0.396	0.397	0.399	0.365	0.294	0.351	0.358	0.361	0.368
Ni	-	-	-	-	-	-	-	-	-	-	-	-	-	-	-	-	-	-
Ca	0.000	0.001	0.000	0.000	0.000	0.000	0.001	0.000	0.002	0.001	0.000	0.001	0.000	0.000	0.001	0.000	0.000	0.000
Total	2.997	2.995	2.998	2.986	2.998	2.999	2.995	2.990	2.997	2.999	2.998	2.996	2.996	2.995	2.996	2.998	2.997	2.997
Trivalent End Members																		
Cr/Σ3+	0.753	0.757	0.753	0.049	0.694	0.755	0.754	0.756	0.754	0.759	0.763	0.753	0.754	0.467	0.761	0.760	0.760	0.732
Al/Σ3+	0.179	0.186	0.185	0.001	0.058	0.182	0.185	0.181	0.183	0.181	0.185	0.185	0.184	0.047	0.180	0.186	0.185	0.152
Fe/Σ3+	0.068	0.057	0.062	0.950	0.248	0.063	0.061	0.063	0.062	0.060	0.053	0.063	0.063	0.486	0.059	0.054	0.055	0.116

Crystal textural style is abbreviated: euh. (euhedral), sub. (subhedral), anh. (anhedral), interg. (intergrown), irreg. (irregular); l. (large), m. (medium), s. (small)
Grain number refers to a particular grain within a cluster: most clusters have multiple grain
Note: Other phases (ol, cpx, hbl) were also analyzed on certain sections, such that Cluster refers to a specific location on each section

Appendix I(continued): Spinel compositions from spinel-bearing ultramafic rocks of the Turnagain intrusion

Rock:	Dunite						Dunite											
Sample:	04ES-19-01-02						04ES-03-02-01											
Cluster:	3						2										4	
Grain Number:	2						1				2						1	
Style:					m. sub.						l. sub.						m. sub.	
Zone:	Mid	Mid	Mid	Core	Rim	Mid	Mid	Mid	Mid	Core	Mid	Mid	Mid	Mid	Mid	Core	Mid	Mid
Oxides (wt. %)																		
SiO_2	0.02	0.02	0.01	0.05	0.07	0.04	0.05	0.00	0.01	0.03	0.03	0.01	0.01	0.03	0.02	0.00	0.07	0.00
TiO_2	0.80	0.81	0.83	0.79	0.02	0.50	0.48	0.43	0.47	0.43	0.44	0.44	0.41	0.48	0.41	0.45	0.41	0.43
Al_2O_3	9.21	9.04	9.01	9.12	0.03	0.54	7.16	7.11	6.97	7.08	7.02	6.85	6.81	6.76	6.81	6.66	1.18	7.04
Cr_2O_3	54.64	55.28	55.27	55.68	5.58	34.24	45.71	47.15	47.76	48.05	44.92	46.79	46.99	47.96	48.41	47.32	29.87	45.24
V_2O_3	0.22	0.14	0.14	0.17	0.04	0.08	0.08	0.07	0.04	0.06	0.10	0.08	0.08	0.09	0.11	0.09	0.06	0.08
Fe_2O_3	4.32	4.25	3.85	3.57	65.02	33.26	15.95	15.11	14.53	14.21	16.12	15.74	15.19	14.78	14.62	15.06	36.60	16.39
FeO	22.95	22.73	22.66	22.80	29.52	25.69	25.01	23.93	23.54	23.16	24.75	24.34	23.70	23.37	23.11	22.71	25.32	24.53
MnO	0.47	0.40	0.27	0.29	0.08	1.17	0.24	0.30	0.29	0.25	0.32	0.35	0.25	0.29	0.27	0.23	1.13	0.31
MgO	7.05	7.24	7.27	7.24	1.34	3.16	5.37	6.02	6.23	6.47	5.22	5.74	6.01	6.39	6.58	6.61	3.24	5.48
NiO	-	-	-	-	-	-	-	-	-	-	-	-	-	-	-	-	-	-
CaO	0.01	0.02	0.00	0.00	0.02	0.03	0.00	0.00	0.00	0.00	0.00	0.00	0.01	0.01	0.02	0.02	0.01	0.00
Total	99.68	99.94	99.31	99.72	101.71	98.72	100.05	100.13	99.84	99.74	98.93	100.34	99.45	100.16	100.36	99.15	97.89	99.51
Cations (p.f.u.)																		
Ti	0.020	0.021	0.021	0.020	0.001	0.014	0.013	0.011	0.012	0.011	0.012	0.011	0.011	0.012	0.011	0.012	0.012	0.011
Cr	1.469	1.482	1.490	1.494	0.165	1.009	1.258	1.290	1.309	1.315	1.251	1.282	1.296	1.310	1.318	1.304	0.886	1.251
Al	0.369	0.361	0.362	0.365	0.001	0.024	0.294	0.290	0.285	0.289	0.292	0.280	0.280	0.275	0.276	0.273	0.052	0.290
V	0.005	0.003	0.003	0.004	0.001	0.002	0.002	0.002	0.001	0.001	0.002	0.002	0.002	0.002	0.002	0.002	0.002	0.002
Fe^{3+}*	0.111	0.108	0.099	0.091	1.828	0.933	0.418	0.393	0.379	0.370	0.427	0.411	0.399	0.384	0.379	0.395	1.033	0.431
Fe^{2+}*	0.652	0.644	0.646	0.647	0.922	0.801	0.728	0.693	0.683	0.670	0.729	0.706	0.691	0.675	0.665	0.662	0.794	0.718
Mn	0.013	0.011	0.008	0.008	0.002	0.037	0.007	0.009	0.008	0.007	0.010	0.010	0.007	0.009	0.008	0.007	0.036	0.009
Mg	0.357	0.366	0.370	0.366	0.075	0.175	0.278	0.311	0.322	0.334	0.274	0.296	0.313	0.329	0.338	0.343	0.181	0.286
Ni	-	-	-	-	-	-	-	-	-	-	-	-	-	-	-	-	-	-
Ca	0.000	0.001	0.000	0.000	0.001	0.001	0.000	0.000	0.000	0.000	0.000	0.000	0.000	0.000	0.001	0.001	0.000	0.000
Total	2.997	2.998	2.998	2.996	2.995	2.997	2.997	2.999	2.999	2.998	2.997	2.999	2.999	2.998	2.998	2.999	2.996	2.999
Trivalent End Members																		
Cr/Σ3+	0.754	0.759	0.764	0.766	0.083	0.513	0.639	0.654	0.664	0.666	0.635	0.650	0.656	0.665	0.668	0.661	0.449	0.634
Al/Σ3+	0.189	0.185	0.186	0.187	0.001	0.012	0.149	0.147	0.144	0.146	0.148	0.142	0.142	0.140	0.140	0.139	0.026	0.147
Fe/Σ3+	0.057	0.055	0.051	0.047	0.917	0.475	0.212	0.199	0.192	0.188	0.217	0.208	0.202	0.195	0.192	0.200	0.524	0.219

Crystal textural style is abbreviated: euh. (euhedral), sub. (subhedral), anh. (anhedral), interg. (intergrown), irreg. (irregular); l. (large), m. (medium), s. (small)
Grain number refers to a particular grain within a cluster: most clusters have multiple grain
Note: Other phases (ol, cpx, hbl) were also analyzed on certain sections, such that Cluster refers to a specific location on each section

Appendix I(continued): Spinel compositions from spinel-bearing ultramafic rocks of the Turnagain intrusion

Rock:	Dunite																	
Sample:	04ES-03-02-01																	
Cluster:	4											5						
Grain Number:	1			2								1						
Style:				l. sub.								l. sub.						
Zone:	Mid	Mid	Core	Mid	Mid	Mid	Mid	Mid	Mid	Mid	Core	Rim	Mid	Mid	Mid	Mid	Mid	Mid
Oxides (wt. %)																		
SiO_2	0.03	0.02	0.01	0.02	0.05	0.00	0.03	0.00	0.00	0.03	0.03	0.08	0.03	0.00	0.03	0.00	0.00	0.00
TiO_2	0.43	0.43	0.42	0.46	0.47	0.46	0.47	0.41	0.45	0.42	0.39	0.02	0.74	0.58	0.45	0.44	0.42	0.41
Al_2O_3	6.95	6.98	6.88	6.06	6.81	6.98	7.06	6.88	6.94	6.92	6.71	0.02	0.60	6.36	6.85	6.81	6.80	6.88
Cr_2O_3	47.56	47.49	48.44	42.83	43.67	44.09	44.96	45.19	46.01	46.56	46.01	0.57	27.18	38.63	44.90	47.74	49.07	49.83
V_2O_3	0.09	0.06	0.08	0.06	0.09	0.13	0.08	0.11	0.10	0.07	0.09	0.02	0.01	0.07	0.10	0.12	0.10	0.11
Fe_2O_3	15.27	14.69	14.44	19.59	17.60	17.30	16.78	16.37	16.32	15.30	15.80	68.76	40.45	23.24	17.07	14.79	14.31	13.51
FeO	23.93	23.01	22.81	25.90	25.67	25.52	25.01	24.44	24.59	24.24	23.65	29.45	26.57	26.02	24.94	23.00	21.18	21.31
MnO	0.27	0.27	0.22	0.39	0.37	0.27	0.35	0.31	0.30	0.20	0.36	0.14	1.09	0.62	0.38	0.29	0.25	0.28
MgO	6.11	6.47	6.78	4.45	4.64	4.91	5.25	5.45	5.63	5.71	5.83	0.93	2.88	4.31	5.23	6.55	7.78	7.73
NiO	-	-	-	-	-	-	-	-	-	-	-	-	-	-	-	-	-	-
CaO	0.02	0.01	0.00	0.01	0.01	0.00	0.00	0.01	0.00	0.00	0.00	0.01	0.00	0.00	0.02	0.00	0.01	0.00
Total	100.67	99.42	100.07	99.77	99.39	99.68	99.97	99.18	100.35	99.46	98.86	99.99	99.54	99.84	99.95	99.75	99.92	100.06
Cations (p.f.u.)																		
Ti	0.011	0.011	0.011	0.012	0.013	0.012	0.012	0.011	0.012	0.011	0.010	0.000	0.021	0.015	0.012	0.011	0.011	0.011
Cr	1.295	1.304	1.320	1.198	1.218	1.223	1.240	1.255	1.262	1.286	1.278	0.017	0.799	1.081	1.240	1.308	1.330	1.348
Al	0.282	0.286	0.280	0.253	0.283	0.289	0.290	0.285	0.284	0.285	0.278	0.001	0.026	0.265	0.282	0.278	0.275	0.278
V	0.002	0.001	0.002	0.001	0.002	0.003	0.002	0.003	0.002	0.002	0.002	0.000	0.000	0.002	0.002	0.003	0.002	0.002
Fe^{3+}*	0.396	0.384	0.375	0.521	0.467	0.457	0.441	0.433	0.426	0.402	0.418	1.977	1.132	0.619	0.449	0.386	0.369	0.348
Fe^{2+}*	0.689	0.669	0.657	0.766	0.758	0.749	0.730	0.718	0.713	0.708	0.695	0.941	0.826	0.770	0.729	0.666	0.607	0.610
Mn	0.008	0.008	0.006	0.012	0.011	0.008	0.010	0.009	0.009	0.006	0.011	0.005	0.034	0.019	0.011	0.008	0.007	0.008
Mg	0.314	0.335	0.348	0.235	0.244	0.257	0.273	0.285	0.291	0.298	0.306	0.053	0.160	0.228	0.272	0.338	0.398	0.394
Ni	-	-	-	-	-	-	-	-	-	-	-	-	-	-	-	-	-	-
Ca	0.001	0.000	0.000	0.000	0.000	0.000	0.000	0.000	0.000	0.000	0.000	0.000	0.000	0.000	0.001	0.000	0.000	0.000
Total	2.997	2.999	2.999	2.998	2.996	2.999	2.998	2.999	2.999	2.998	2.998	2.995	2.998	2.999	2.997	2.999	2.999	2.999
Trivalent End Members																		
Cr/Σ3+	0.656	0.661	0.669	0.607	0.619	0.621	0.629	0.636	0.640	0.652	0.648	0.009	0.408	0.550	0.629	0.663	0.674	0.683
Al/Σ3+	0.143	0.145	0.142	0.128	0.144	0.147	0.147	0.144	0.144	0.144	0.141	0.000	0.013	0.135	0.143	0.141	0.139	0.141
Fe/Σ3+	0.201	0.194	0.190	0.264	0.237	0.232	0.224	0.219	0.216	0.204	0.212	0.991	0.578	0.315	0.228	0.196	0.187	0.176

Crystal textural style is abbreviated: euh. (euhedral), sub. (subhedral), anh. (anhedral), interg. (intergrown), irreg. (irregular); l. (large), m. (medium), s. (small)
Grain number refers to a particular grain within a cluster: most clusters have multiple grain
Note: Other phases (ol, cpx, hbl) were also analyzed on certain sections, such that Cluster refers to a specific location on each section

Appendix I(continued): Spinel compositions from spinel-bearing ultramafic rocks of the Turnagain intrusion

Rock:	Dunite				Dunite													
Sample:	04ES-03-02-01				04ES-08-01-01													
Cluster:	5				1									2				
Grain Number:	1	2			1			2						1			2	
Style:		s. eu.			s. eu.			m. sub.						s. eu.			l. sub.	
Zone:	Core	Rim	Mid	Core	Rim	Mid	Core	Mid	Mid	Mid	Mid	Mid	Core	Rim	Mid	Core	Rim	Mid
Oxides (wt. %)																		
SiO_2	0.02	0.01	0.02	0.00	0.12	0.05	0.01	0.01	0.00	0.00	0.05	0.02	0.02	0.05	0.03	0.03	0.05	0.00
TiO_2	0.47	0.48	0.46	0.48	0.39	0.49	0.48	0.70	0.55	0.49	0.48	0.49	0.48	0.53	0.54	0.52	0.02	1.01
Al_2O_3	6.72	7.70	6.96	7.04	5.94	6.87	6.94	4.78	7.07	7.08	6.99	6.99	6.96	7.47	7.28	7.35	0.00	2.91
Cr_2O_3	50.24	44.00	47.32	47.22	38.98	44.74	45.08	34.02	39.23	41.17	42.61	43.95	43.80	44.81	46.40	46.49	2.06	30.59
V_2O_3	0.07	0.06	0.08	0.11	0.06	0.05	0.08	0.07	0.08	0.07	0.07	0.06	0.09	0.06	0.09	0.07	0.01	0.04
Fe_2O_3	13.72	17.56	15.39	15.57	22.67	16.87	16.76	27.82	22.78	20.39	19.73	18.83	18.57	16.75	15.98	15.97	67.87	33.99
FeO	21.46	22.87	22.41	22.57	24.38	24.82	25.03	24.47	24.32	23.33	23.39	22.99	22.82	22.94	22.81	22.94	29.51	26.50
MnO	0.25	0.29	0.17	0.26	0.52	0.21	0.25	1.32	0.49	0.23	0.14	0.24	0.17	0.24	0.22	0.22	0.08	1.27
MgO	7.79	6.68	7.05	7.00	4.87	5.33	5.28	4.22	5.63	6.20	6.37	6.67	6.71	6.64	6.90	6.84	1.09	3.30
NiO	-	-	-	-	-	-	-	-	-	-	-	-	-	-	-	-	-	-
CaO	0.01	0.00	0.00	0.00	0.01	0.00	0.02	0.00	0.00	0.00	0.00	0.01	0.00	0.00	0.01	0.02	0.00	0.00
Total	100.74	99.64	99.87	100.25	97.94	99.43	99.90	97.42	100.15	98.96	99.83	100.25	99.63	99.48	100.26	100.46	100.69	99.62
Cations (p.f.u.)																		
Ti	0.012	0.012	0.012	0.012	0.011	0.013	0.013	0.019	0.014	0.013	0.012	0.013	0.013	0.014	0.014	0.013	0.000	0.028
Cr	1.351	1.202	1.289	1.282	1.107	1.241	1.245	0.985	1.080	1.140	1.169	1.198	1.201	1.227	1.259	1.260	0.062	0.883
Al	0.270	0.314	0.283	0.285	0.252	0.284	0.286	0.206	0.290	0.292	0.286	0.284	0.285	0.305	0.295	0.297	0.000	0.125
V	0.002	0.001	0.002	0.003	0.001	0.001	0.002	0.002	0.002	0.002	0.002	0.001	0.002	0.001	0.002	0.002	0.000	0.001
Fe^{3+*}	0.351	0.456	0.399	0.402	0.613	0.445	0.440	0.766	0.597	0.538	0.515	0.489	0.485	0.436	0.413	0.412	1.935	0.934
Fe^{2+*}	0.610	0.661	0.646	0.648	0.732	0.728	0.731	0.749	0.708	0.683	0.679	0.663	0.662	0.664	0.655	0.657	0.935	0.809
Mn	0.007	0.009	0.005	0.008	0.016	0.006	0.007	0.041	0.015	0.007	0.004	0.007	0.005	0.007	0.006	0.006	0.003	0.039
Mg	0.395	0.344	0.362	0.358	0.261	0.278	0.275	0.231	0.292	0.324	0.330	0.343	0.347	0.343	0.353	0.349	0.062	0.180
Ni	-	-	-	-	-	-	-	-	-	-	-	-	-	-	-	-	-	-
Ca	0.000	0.000	0.000	0.000	0.000	0.000	0.001	0.000	0.000	0.000	0.000	0.000	0.000	0.000	0.000	0.001	0.000	0.000
Total	2.998	2.999	2.998	2.999	2.993	2.997	2.999	2.999	2.999	2.999	2.997	2.998	2.998	2.997	2.998	2.998	2.997	2.999
Trivalent End Members																		
Cr/Σ3+	0.685	0.610	0.654	0.651	0.562	0.630	0.632	0.503	0.549	0.579	0.593	0.608	0.610	0.623	0.640	0.640	0.031	0.455
Al/Σ3+	0.137	0.159	0.143	0.145	0.128	0.144	0.145	0.105	0.147	0.148	0.145	0.144	0.144	0.155	0.150	0.151	0.000	0.064
Fe/Σ3+	0.178	0.231	0.202	0.204	0.311	0.226	0.223	0.392	0.304	0.273	0.262	0.248	0.246	0.222	0.210	0.209	0.969	0.481

Crystal textural style is abbreviated: euh. (euhedral), sub. (subhedral), anh. (anhedral), interg. (intergrown), irreg. (irregular); l. (large), m. (medium), s. (small)
Grain number refers to a particular grain within a cluster: most clusters have multiple grain
Note: Other phases (ol, cpx, hbl) were also analyzed on certain sections, such that Cluster refers to a specific location on each section

Appendix I(continued): Spinel compositions from spinel-bearing ultramafic rocks of the Turnagain intrusion

Rock:	Dunite																	
Sample:	04ES-08-01-01																	
Cluster:	2								3									
Grain Number:	2								1			2						
Style:									s. sub.			l. sub.						
Zone:	Mid	Mid	Mid	Mid	Mid	Mid	Mid	Core	Rim	Mid	Core	Rim	Mid	Mid	Mid	Mid	Mid	Mid
Oxides (wt. %)																		
SiO_2	0.00	0.01	0.00	0.03	0.01	0.00	0.03	0.01	0.03	0.01	0.01	0.13	0.02	0.03	0.01	0.00	0.01	0.02
TiO_2	0.45	0.46	0.50	0.43	0.47	0.47	0.47	0.47	0.54	0.54	0.58	0.01	0.55	0.53	0.52	0.49	0.48	0.47
Al_2O_3	5.89	6.98	7.10	7.24	7.10	7.17	7.22	7.10	7.32	7.32	7.27	0.01	7.49	7.40	7.28	7.25	7.26	7.06
Cr_2O_3	44.28	45.96	46.79	47.40	47.52	47.83	47.95	47.69	45.01	45.87	45.92	1.07	44.08	44.28	44.61	45.44	46.12	45.96
V_2O_3	0.08	0.09	0.05	0.05	0.06	0.06	0.10	0.05	0.06	0.07	0.04	0.02	0.08	0.09	0.06	0.10	0.11	0.05
Fe_2O_3	18.94	16.84	15.79	15.14	15.28	15.04	14.76	15.44	16.15	15.47	15.48	68.97	18.05	17.02	17.77	16.94	16.57	16.19
FeO	24.13	22.95	21.96	21.97	21.73	22.05	22.24	22.00	23.86	24.10	23.98	28.99	23.45	22.97	23.05	22.84	22.81	22.49
MnO	0.24	0.17	0.19	0.19	0.22	0.20	0.15	0.22	0.28	0.25	0.26	0.10	0.19	0.23	0.26	0.19	0.28	0.23
MgO	5.69	6.77	7.31	7.29	7.47	7.33	7.28	7.39	5.95	5.90	5.95	1.38	6.55	6.55	6.68	6.84	6.90	6.83
NiO	-	-	-	-	-	-	-	-	-	-	-	-	-	-	-	-	-	-
CaO	0.00	0.00	0.02	0.00	0.00	0.01	0.01	0.00	0.00	0.02	0.02	0.02	0.00	0.00	0.00	0.00	0.00	0.00
Total	99.70	100.23	99.71	99.73	99.86	100.15	100.20	100.37	99.19	99.54	99.53	100.69	100.46	99.11	100.25	100.09	100.53	99.31
Cations (p.f.u.)																		
Ti	0.012	0.012	0.013	0.011	0.012	0.012	0.012	0.012	0.014	0.014	0.015	0.000	0.014	0.014	0.013	0.013	0.012	0.012
Cr	1.229	1.251	1.274	1.289	1.290	1.296	1.298	1.290	1.243	1.262	1.264	0.032	1.197	1.218	1.214	1.237	1.250	1.261
Al	0.243	0.283	0.288	0.293	0.288	0.289	0.291	0.286	0.301	0.300	0.298	0.000	0.303	0.304	0.295	0.294	0.293	0.289
V	0.002	0.002	0.001	0.001	0.001	0.001	0.002	0.001	0.001	0.002	0.001	0.000	0.002	0.002	0.001	0.002	0.002	0.001
Fe^{3+}*	0.500	0.437	0.409	0.392	0.395	0.388	0.380	0.397	0.424	0.405	0.406	1.962	0.467	0.445	0.460	0.439	0.427	0.423
Fe^{2+}*	0.708	0.661	0.633	0.632	0.624	0.632	0.637	0.629	0.697	0.701	0.698	0.916	0.674	0.668	0.664	0.658	0.653	0.653
Mn	0.007	0.005	0.005	0.006	0.006	0.006	0.004	0.006	0.008	0.007	0.008	0.003	0.006	0.007	0.008	0.006	0.008	0.007
Mg	0.298	0.348	0.375	0.374	0.382	0.374	0.371	0.377	0.310	0.306	0.309	0.078	0.336	0.340	0.343	0.351	0.352	0.353
Ni	-	-	-	-	-	-	-	-	-	-	-	-	-	-	-	-	-	-
Ca	0.000	0.000	0.001	0.000	0.000	0.001	0.000	0.000	0.000	0.001	0.001	0.001	0.000	0.000	0.000	0.000	0.000	0.000
Total	2.999	2.999	3.000	2.998	2.999	2.999	2.998	2.999	2.998	2.999	2.999	2.992	2.998	2.997	2.999	2.999	2.999	2.998
Trivalent End Members																		
Cr/Σ3+	0.623	0.635	0.646	0.653	0.654	0.657	0.659	0.654	0.631	0.642	0.642	0.016	0.609	0.619	0.616	0.628	0.634	0.639
Al/Σ3+	0.123	0.144	0.146	0.149	0.146	0.147	0.148	0.145	0.153	0.153	0.152	0.000	0.154	0.154	0.150	0.149	0.149	0.146
Fe/Σ3+	0.254	0.221	0.208	0.198	0.200	0.197	0.193	0.201	0.216	0.206	0.206	0.984	0.237	0.226	0.234	0.223	0.217	0.214

Crystal textural style is abbreviated: euh. (euhedral), sub. (subhedral), anh. (anhedral), interg. (intergrown), irreg. (irregular); l. (large), m. (medium), s. (small)
Grain number refers to a particular grain within a cluster: most clusters have multiple grain
Note: Other phases (ol, cpx, hbl) were also analyzed on certain sections, such that Cluster refers to a specific location on each section

Appendix I(continued): Spinel compositions from spinel-bearing ultramafic rocks of the Turnagain intrusion

Rock:	Dunite																	Wehrlite
Sample:	04ES-10-05-01																	04ES-11-03-03
Cluster:	3	6			2		5			2			4		2			4
Grain Number:	2	1					1						1					1
Style:		m. eu.			s. eu.		s. eu.			m. eu.			s. eu.		s. eu.		m. sub.	
Zone:	Core	Rim	Mid	Core	Mid	Core	Rim	Mid	Core	Rim	Mid	Core	Mid	Core	Rim	Mid	Rim	Mid
Oxides (wt. %)																		
SiO_2	0.00	0.00	0.05	0.10	0.05	0.00	0.04	0.03	0.00	0.02	0.00	0.02	0.00	0.02	0.01	0.01	0.06	0.03
TiO_2	0.54	0.58	0.79	0.70	0.80	0.78	0.52	0.75	0.73	0.70	0.75	0.76	0.64	0.64	0.61	0.66	0.67	1.51
Al_2O_3	7.08	4.89	7.54	7.48	7.64	7.59	0.65	7.57	7.66	7.68	7.78	7.75	6.90	6.87	5.86	7.00	2.73	9.00
Cr_2O_3	46.35	46.77	50.65	51.00	49.33	50.39	33.65	51.05	50.85	48.88	51.15	50.78	53.29	53.68	49.81	52.52	15.26	41.57
V_2O_3	0.04	0.19	0.26	0.22	0.26	0.26	0.09	0.21	0.24	0.25	0.24	0.24	0.21	0.24	0.27	0.23	0.10	0.32
Fe_2O_3	16.45	17.12	9.43	9.50	10.62	9.73	34.34	9.37	9.47	10.56	9.15	9.56	8.66	8.52	12.95	8.45	49.60	14.16
FeO	22.73	20.27	25.39	24.33	25.08	25.15	20.38	25.36	25.10	24.83	25.16	24.90	23.09	23.05	20.56	23.46	27.85	26.50
MnO	0.23	2.90	0.34	0.39	0.54	0.38	3.07	0.38	0.38	0.96	0.29	0.40	0.30	0.33	2.39	0.31	1.03	0.38
MgO	6.93	6.36	5.35	5.88	5.42	5.47	5.26	5.37	5.53	5.07	5.61	5.70	6.72	6.81	6.72	6.34	2.18	4.83
NiO	-	-	-	-	-	-	-	-	-	-	-	-	-	-	-	-	-	-
CaO	0.01	0.02	0.00	0.01	0.00	0.02	0.01	0.00	0.00	0.02	0.00	0.00	0.02	0.00	0.00	0.00	0.01	0.01
Total	100.36	99.11	99.82	99.59	99.73	99.76	98.01	100.09	99.96	98.97	100.14	100.11	99.83	100.16	99.19	98.98	99.50	98.31
Cations (p.f.u.)																		
Ti	0.014	0.015	0.021	0.018	0.021	0.020	0.014	0.020	0.019	0.018	0.019	0.020	0.017	0.016	0.016	0.017	0.019	0.040
Cr	1.259	1.303	1.390	1.397	1.354	1.382	0.982	1.397	1.391	1.354	1.395	1.385	1.452	1.457	1.374	1.445	0.448	1.156
Al	0.287	0.203	0.308	0.305	0.312	0.310	0.028	0.309	0.312	0.317	0.316	0.315	0.280	0.278	0.241	0.287	0.120	0.373
V	0.001	0.004	0.006	0.005	0.006	0.006	0.002	0.005	0.005	0.006	0.006	0.006	0.005	0.005	0.006	0.005	0.002	0.007
Fe^{3+}*	0.425	0.454	0.246	0.248	0.277	0.254	0.954	0.244	0.247	0.278	0.238	0.248	0.225	0.220	0.340	0.221	1.387	0.375
Fe^{2+}*	0.653	0.597	0.737	0.705	0.728	0.730	0.630	0.734	0.726	0.728	0.726	0.718	0.665	0.662	0.600	0.683	0.866	0.779
Mn	0.007	0.086	0.010	0.011	0.016	0.011	0.096	0.011	0.011	0.029	0.008	0.012	0.009	0.010	0.071	0.009	0.032	0.011
Mg	0.355	0.334	0.277	0.303	0.280	0.283	0.289	0.277	0.285	0.265	0.289	0.293	0.345	0.348	0.350	0.329	0.121	0.253
Ni	-	-	-	-	-	-	-	-	-	-	-	-	-	-	-	-	-	-
Ca	0.000	0.001	0.000	0.000	0.000	0.001	0.000	0.000	0.000	0.001	0.000	0.000	0.001	0.000	0.000	0.000	0.000	0.000
Total	3.000	2.998	2.995	2.993	2.995	2.997	2.997	2.997	2.998	2.997	2.998	2.997	2.998	2.996	2.997	2.997	2.996	2.995
Trivalent End Members																		
Cr/Σ3+	0.639	0.665	0.715	0.716	0.697	0.710	0.500	0.716	0.713	0.694	0.716	0.711	0.742	0.745	0.703	0.740	0.229	0.607
Al/Σ3+	0.146	0.104	0.159	0.157	0.161	0.159	0.014	0.158	0.160	0.163	0.162	0.162	0.143	0.142	0.123	0.147	0.061	0.196
Fe/Σ3+	0.216	0.232	0.127	0.127	0.143	0.130	0.486	0.125	0.126	0.143	0.122	0.127	0.115	0.113	0.174	0.113	0.709	0.197

Crystal textural style is abbreviated: euh. (euhedral), sub. (subhedral), anh. (anhedral), interg. (intergrown), irreg. (irregular); l. (large), m. (medium), s. (small)
Grain number refers to a particular grain within a cluster: most clusters have multiple grain
Note: Other phases (ol, cpx, hbl) were also analyzed on certain sections, such that Cluster refers to a specific location on each section

Appendix I(continued): Spinel compositions from spinel-bearing ultramafic rocks of the Turnagain intrusion

Rock:	Wehrlite																
Sample:	04ES-11-03-03																
Cluster:	4							2									
Grain Number:	1			2				1								2	
Style:				m. sub.				l. irreg.								m. anh.	
Zone:	Mid	Mid	Core	Rim	Mid	Mid	Core	Rim	Mid	Mid	Mid	Mid	Mid	Mid	Core	Mid	Core
Oxides (wt. %)																	
SiO_2	0.01	0.00	0.00	0.01	0.00	0.00	0.00	0.02	0.01	0.03	0.06	0.01	0.05	0.03	0.03	0.04	0.04
TiO_2	1.45	1.44	1.48	1.26	1.28	1.29	1.35	1.36	1.66	1.55	1.49	1.37	1.26	1.19	1.19	1.59	1.56
Al_2O_3	9.54	9.62	9.61	10.47	10.27	10.24	10.23	9.23	9.25	8.82	8.69	8.37	8.03	7.80	7.57	9.36	9.48
Cr_2O_3	42.62	42.70	42.64	43.31	43.96	44.58	44.37	45.81	45.10	46.26	46.57	47.81	48.57	49.40	49.08	44.73	44.05
V_2O_3	0.28	0.27	0.35	0.30	0.29	0.30	0.32	0.26	0.21	0.20	0.20	0.18	0.21	0.19	0.21	0.29	0.28
Fe_2O_3	13.46	13.67	13.71	13.03	12.24	11.66	11.65	11.17	11.77	11.24	11.28	10.32	10.72	10.09	10.01	11.36	12.09
FeO	26.44	26.53	26.57	26.18	26.04	26.05	26.10	24.88	25.27	25.14	25.05	24.78	24.92	24.75	24.43	26.32	26.27
MnO	0.39	0.38	0.36	0.40	0.34	0.34	0.31	0.40	0.27	0.27	0.31	0.26	0.31	0.38	0.37	0.35	0.81
MgO	5.08	5.14	5.21	5.50	5.52	5.54	5.54	5.96	6.08	6.04	6.05	6.04	6.03	5.97	5.97	5.27	5.07
NiO	-	-	-	-	-	-	-	-	-	-	-	-	-	-	-	-	-
CaO	0.01	0.01	0.00	0.01	0.00	0.00	0.01	0.07	0.02	0.02	0.02	0.02	0.02	0.01	0.01	0.02	0.00
Total	99.28	99.76	99.92	100.45	99.95	100.00	99.87	99.17	99.65	99.57	99.70	99.16	100.12	99.81	98.88	99.33	99.65
Cations (p.f.u.)																	
Ti	0.038	0.037	0.038	0.032	0.033	0.033	0.035	0.035	0.043	0.040	0.039	0.036	0.033	0.031	0.031	0.041	0.040
Cr	1.169	1.166	1.161	1.167	1.190	1.206	1.202	1.250	1.225	1.260	1.267	1.309	1.320	1.348	1.353	1.224	1.204
Al	0.390	0.391	0.390	0.420	0.414	0.413	0.413	0.376	0.375	0.358	0.352	0.342	0.325	0.318	0.311	0.382	0.386
V	0.006	0.006	0.008	0.007	0.007	0.007	0.007	0.006	0.005	0.004	0.005	0.004	0.005	0.004	0.005	0.007	0.006
Fe^{3+}*	0.351	0.355	0.355	0.334	0.315	0.300	0.300	0.290	0.304	0.291	0.292	0.269	0.277	0.262	0.263	0.296	0.315
Fe^{2+}*	0.767	0.766	0.765	0.746	0.746	0.745	0.748	0.718	0.726	0.724	0.721	0.718	0.717	0.715	0.712	0.762	0.759
Mn	0.012	0.011	0.011	0.012	0.010	0.010	0.009	0.012	0.008	0.008	0.009	0.008	0.009	0.011	0.011	0.010	0.024
Mg	0.263	0.264	0.268	0.279	0.282	0.282	0.283	0.307	0.311	0.310	0.310	0.312	0.309	0.307	0.310	0.272	0.261
Ni	-	-	-	-	-	-	-	-	-	-	-	-	-	-	-	-	-
Ca	0.000	0.001	0.000	0.000	0.000	0.000	0.000	0.003	0.001	0.001	0.001	0.001	0.001	0.000	0.000	0.001	0.000
Total	2.997	2.997	2.997	2.997	2.997	2.997	2.997	2.996	2.997	2.997	2.995	2.998	2.996	2.997	2.996	2.995	2.995
Trivalent End Members																	
Cr/Σ3+	0.612	0.610	0.609	0.607	0.620	0.628	0.628	0.653	0.643	0.660	0.663	0.682	0.687	0.699	0.702	0.644	0.632
Al/Σ3+	0.204	0.205	0.205	0.219	0.216	0.215	0.216	0.196	0.197	0.188	0.184	0.178	0.169	0.165	0.161	0.201	0.203
Fe/Σ3+	0.184	0.186	0.186	0.174	0.164	0.156	0.157	0.151	0.160	0.153	0.153	0.140	0.144	0.136	0.136	0.156	0.165

Crystal textural style is abbreviated: euh. (euhedral), sub. (subhedral), anh. (anhedral), interg. (intergrown), irreg. (irregular); l. (large), m. (medium), s. (small)
Grain number refers to a particular grain within a cluster: most clusters have multiple grain
Note: Other phases (ol, cpx, hbl) were also analyzed on certain sections, such that Cluster refers to a specific location on each section

Appendix I(continued): Spinel compositions from spinel-bearing ultramafic rocks of the Turnagain intrusion

Rock:	Wehrlite											Wehrlite						
Sample:	04ES-11-03-03									04ES-15-01-05								
Cluster:	1									7						6		
Grain Number:	1			2						1		2				1		
Style:	s. eu.			m. sub.						s. eu.		m. sub.				m. sub.		
Zone:	Rim	Mid	Core	Rim	Mid	Mid	Mid	Mid	Core	Mid	Core	Mid	Mid	Mid	Core	Mid	Mid	Core
Oxides (wt. %)																		
SiO_2	0.02	0.00	0.06	0.03	0.03	0.02	0.02	0.00	0.01	0.03	0.04	0.03	0.02	0.03	0.03	0.04	0.05	0.00
TiO_2	1.75	1.72	1.69	1.81	1.58	1.52	1.59	1.56	1.64	1.17	1.48	1.41	1.67	1.37	1.46	1.38	1.51	1.34
Al_2O_3	10.07	9.82	9.87	10.18	9.69	9.87	9.98	9.83	10.07	14.94	15.41	14.31	14.38	14.27	14.27	14.45	14.52	14.10
Cr_2O_3	41.38	42.63	42.79	39.97	43.41	44.05	43.83	44.25	43.39	48.11	48.54	50.35	51.19	50.31	50.07	49.22	49.73	50.37
V_2O_3	0.28	0.27	0.28	0.25	0.29	0.32	0.29	0.33	0.28	0.35	0.31	0.20	0.17	0.22	0.23	0.18	0.14	0.21
Fe_2O_3	13.34	12.79	12.67	14.07	12.19	12.13	12.26	12.25	12.43	3.71	2.21	2.35	1.51	2.47	2.40	2.68	2.35	2.40
FeO	27.12	27.14	27.31	26.22	26.33	26.35	26.64	26.52	26.34	23.66	23.62	22.71	23.39	22.94	22.70	23.49	23.44	23.13
MnO	0.55	0.36	0.37	1.00	0.38	0.37	0.33	0.34	0.31	0.34	0.20	0.48	0.28	0.27	0.30	0.27	0.30	0.18
MgO	4.75	4.92	4.84	4.91	5.25	5.42	5.37	5.46	5.53	7.57	7.89	8.14	8.16	8.12	8.25	7.64	7.83	7.96
NiO	-	-	-	-	-	-	-	-	-	-	-	-	-	-	-	-	-	-
CaO	0.02	0.00	0.00	0.00	0.00	0.01	0.00	0.00	0.02	0.02	0.00	0.04	0.02	0.02	0.02	0.00	0.00	0.02
Total	99.27	99.64	99.89	98.44	99.16	100.05	100.30	100.55	100.02	99.90	99.69	100.03	100.79	100.03	99.74	99.36	99.87	99.70
Cations (p.f.u.)																		
Ti	0.046	0.045	0.044	0.047	0.041	0.039	0.041	0.040	0.042	0.029	0.037	0.035	0.041	0.034	0.036	0.034	0.037	0.033
Cr	1.135	1.165	1.167	1.103	1.189	1.194	1.186	1.194	1.175	1.253	1.260	1.308	1.320	1.307	1.303	1.290	1.295	1.315
Al	0.412	0.400	0.401	0.419	0.396	0.399	0.403	0.395	0.407	0.580	0.597	0.554	0.553	0.553	0.554	0.565	0.564	0.549
V	0.006	0.006	0.006	0.006	0.007	0.007	0.006	0.007	0.006	0.008	0.007	0.004	0.004	0.005	0.005	0.004	0.003	0.005
Fe^{3+}*	0.348	0.333	0.329	0.370	0.318	0.313	0.316	0.315	0.320	0.092	0.055	0.058	0.037	0.061	0.059	0.067	0.058	0.060
Fe^{2+}*	0.787	0.785	0.788	0.766	0.763	0.756	0.762	0.757	0.754	0.652	0.649	0.624	0.638	0.630	0.625	0.651	0.646	0.639
Mn	0.016	0.011	0.011	0.029	0.011	0.011	0.009	0.010	0.009	0.010	0.005	0.013	0.008	0.008	0.008	0.008	0.008	0.005
Mg	0.246	0.254	0.249	0.256	0.271	0.277	0.274	0.278	0.282	0.372	0.386	0.399	0.397	0.398	0.405	0.378	0.385	0.392
Ni	-	-	-	-	-	-	-	-	-	-	-	-	-	-	-	-	-	-
Ca	0.001	0.000	0.000	0.000	0.000	0.001	0.000	0.000	0.001	0.001	0.000	0.001	0.001	0.001	0.001	0.000	0.000	0.001
Total	2.996	2.997	2.994	2.996	2.995	2.996	2.996	2.997	2.997	2.995	2.995	2.996	2.998	2.996	2.996	2.996	2.996	2.998
Trivalent End Members																		
Cr/Σ3+	0.599	0.614	0.615	0.583	0.625	0.627	0.623	0.627	0.618	0.651	0.659	0.681	0.691	0.680	0.680	0.671	0.676	0.684
Al/Σ3+	0.217	0.211	0.212	0.221	0.208	0.209	0.211	0.208	0.214	0.301	0.312	0.289	0.289	0.288	0.289	0.294	0.294	0.285
Fe/Σ3+	0.184	0.175	0.173	0.195	0.167	0.164	0.166	0.165	0.168	0.048	0.029	0.030	0.019	0.032	0.031	0.035	0.030	0.031

Crystal textural style is abbreviated: euh. (euhedral), sub. (subhedral), anh. (anhedral), interg. (intergrown), irreg. (irregular); l. (large), m. (medium), s. (small)
Grain number refers to a particular grain within a cluster: most clusters have multiple grain
Note: Other phases (ol, cpx, hbl) were also analyzed on certain sections, such that Cluster refers to a specific location on each section

Appendix I(continued): Spinel compositions from spinel-bearing ultramafic rocks of the Turnagain intrusion

Rock:	Wehrlite															Wehrlite		
Sample:	04ES-15-01-05															04ES-16-08-01		
Cluster:	6			5						2						6		
Grain Number:	2			1												1		
Style:	s. sub.			m. eu.						m. sub.						s. eu.		
Zone:	Rim	Mid	Core	Mid	Mid	Mid	Mid	Mid	Core	Mid	Mid	Mid	Mid	Mid	Core	Rim	Mid	Core
Oxides (wt. %)																		
SiO_2	0.07	0.03	0.03	0.06	0.04	0.03	0.02	0.01	0.02	0.07	0.04	0.03	0.02	0.07	0.02	0.04	0.02	0.03
TiO_2	1.09	1.21	1.23	1.30	1.58	1.22	1.26	1.14	1.83	1.23	1.96	1.35	1.20	2.54	1.86	1.24	0.99	0.90
Al_2O_3	12.65	12.69	12.46	14.98	14.72	14.67	14.53	14.57	14.50	15.92	15.54	15.49	15.44	14.86	15.01	8.00	8.92	8.90
Cr_2O_3	50.37	51.63	52.16	49.44	49.38	50.01	50.30	50.56	50.62	47.60	48.93	49.09	48.44	48.75	49.11	37.46	43.84	43.86
V_2O_3	0.20	0.14	0.17	0.24	0.21	0.24	0.22	0.24	0.16	0.41	0.32	0.29	0.38	0.20	0.30	0.09	0.09	0.12
Fe_2O_3	3.64	2.67	2.85	2.80	2.27	2.57	2.38	2.39	0.94	3.27	1.40	2.80	2.87	0.99	1.70	18.91	14.09	14.28
FeO	23.72	23.65	23.75	23.18	23.26	22.97	23.03	23.03	23.50	23.37	23.79	22.90	22.64	23.84	23.50	25.66	25.82	25.40
MnO	0.34	0.28	0.28	0.29	0.21	0.25	0.23	0.23	0.22	0.32	0.29	0.30	0.26	0.26	0.26	1.55	0.33	0.35
MgO	6.97	7.26	7.35	8.01	8.03	8.08	8.05	8.06	8.04	8.00	8.18	8.42	8.33	8.24	8.15	3.89	5.09	5.28
NiO	-	-	-	-	-	-	-	-	-	-	-	-	-	-	-	-	-	-
CaO	0.08	0.03	0.02	0.07	0.06	0.03	0.02	0.00	0.01	0.00	0.00	0.00	0.00	0.01	0.02	0.03	0.02	0.03
Total	99.15	99.59	100.30	100.38	99.77	100.08	100.03	100.24	99.85	100.20	100.43	100.66	99.58	99.75	99.91	96.85	99.21	99.15
Cations (p.f.u.)																		
Ti	0.028	0.030	0.031	0.032	0.039	0.030	0.031	0.028	0.045	0.030	0.048	0.033	0.030	0.063	0.046	0.034	0.026	0.024
Cr	1.339	1.365	1.371	1.278	1.284	1.297	1.306	1.310	1.316	1.227	1.259	1.259	1.255	1.265	1.273	1.071	1.207	1.207
Al	0.501	0.500	0.488	0.577	0.571	0.567	0.562	0.563	0.562	0.612	0.596	0.592	0.596	0.575	0.580	0.341	0.366	0.365
V	0.005	0.003	0.004	0.005	0.004	0.005	0.005	0.005	0.004	0.009	0.007	0.006	0.008	0.004	0.006	0.002	0.002	0.003
Fe^{3+}*	0.092	0.067	0.071	0.069	0.056	0.063	0.059	0.059	0.023	0.080	0.034	0.068	0.071	0.024	0.042	0.515	0.369	0.374
Fe^{2+}*	0.667	0.661	0.660	0.634	0.640	0.630	0.632	0.631	0.646	0.637	0.647	0.621	0.621	0.654	0.644	0.776	0.752	0.739
Mn	0.010	0.008	0.008	0.008	0.006	0.007	0.006	0.006	0.006	0.009	0.008	0.008	0.007	0.007	0.007	0.047	0.010	0.010
Mg	0.350	0.362	0.364	0.390	0.394	0.395	0.394	0.394	0.394	0.389	0.397	0.407	0.407	0.403	0.398	0.210	0.264	0.274
Ni	-	-	-	-	-	-	-	-	-	-	-	-	-	-	-	-	-	-
Ca	0.003	0.001	0.001	0.003	0.002	0.001	0.001	0.000	0.000	0.000	0.000	0.000	0.000	0.000	0.001	0.001	0.001	0.001
Total	2.994	2.997	2.997	2.995	2.996	2.996	2.997	2.997	2.998	2.993	2.995	2.996	2.995	2.995	2.996	2.997	2.998	2.997
Trivalent End Members																		
Cr/Σ3+	0.693	0.706	0.710	0.664	0.672	0.673	0.678	0.678	0.692	0.639	0.666	0.656	0.653	0.679	0.672	0.556	0.621	0.620
Al/Σ3+	0.259	0.259	0.253	0.300	0.299	0.294	0.292	0.291	0.296	0.319	0.315	0.309	0.310	0.308	0.306	0.177	0.188	0.188
Fe/Σ3+	0.048	0.035	0.037	0.036	0.029	0.033	0.031	0.031	0.012	0.042	0.018	0.036	0.037	0.013	0.022	0.267	0.190	0.192

Crystal textural style is abbreviated: euh. (euhedral), sub. (subhedral), anh. (anhedral), interg. (intergrown), irreg. (irregular); l. (large), m. (medium), s. (small)
Grain number refers to a particular grain within a cluster: most clusters have multiple grain
Note: Other phases (ol, cpx, hbl) were also analyzed on certain sections, such that Cluster refers to a specific location on each section

Appendix I(continued): Spinel compositions from spinel-bearing ultramafic rocks of the Turnagain intrusion

Rock:	Wehrlite																	
Sample:	04ES-16-08-01																	
Cluster:	6							4										
Grain Number:	2			3				1				2						
Style:	s. eu.			s. eu.				s. sub.				m. sub.						
Zone:	Rim	Mid	Core	Rim	Mid	Mid	Core	Rim	Mid	Mid	Core	Rim	Mid	Mid	Mid	Mid	Mid	Mid
Oxides (wt. %)																		
SiO_2	0.11	0.00	0.06	0.01	0.04	0.03	0.03	0.06	0.03	0.01	0.02	0.05	0.04	0.04	0.03	0.05	0.01	0.04
TiO_2	0.79	1.06	1.01	1.03	1.01	1.05	1.03	1.69	0.92	0.74	0.71	0.87	1.25	1.15	0.96	0.97	1.00	1.10
Al_2O_3	6.60	8.08	7.92	7.99	8.01	7.85	7.99	9.82	10.40	9.40	9.18	4.87	9.15	8.87	8.35	8.28	8.38	8.28
Cr_2O_3	46.05	47.84	48.90	49.53	49.73	50.34	50.02	38.04	42.19	46.21	48.86	38.97	44.45	45.29	47.93	48.31	48.39	48.70
V_2O_3	0.09	0.04	0.06	0.08	0.08	0.08	0.09	0.11	0.06	0.06	0.10	0.10	0.11	0.09	0.09	0.08	0.07	0.09
Fe_2O_3	13.28	11.86	11.94	11.56	11.60	11.46	10.92	16.52	14.19	11.45	10.38	22.43	13.40	13.21	11.69	11.69	11.41	11.38
FeO	24.05	24.86	21.20	20.19	19.79	19.79	20.46	25.57	25.68	24.50	24.52	24.77	26.01	25.11	24.14	23.69	23.76	23.88
MnO	2.19	0.23	0.27	0.18	0.26	0.25	0.20	1.61	0.45	0.33	0.34	2.04	0.36	0.28	0.33	0.30	0.34	0.37
MgO	4.31	5.89	8.12	8.88	9.11	9.22	8.70	4.64	5.18	5.72	6.05	3.75	5.29	5.81	6.27	6.62	6.56	6.63
NiO	-	-	-	-	-	-	-	-	-	-	-	-	-	-	-	-	-	-
CaO	0.00	0.02	0.02	0.00	0.00	0.01	0.00	0.04	0.00	0.00	0.00	0.09	0.05	0.03	0.00	0.01	0.02	0.01
Total	97.46	99.87	99.51	99.45	99.64	100.09	99.43	98.09	99.10	98.42	100.17	97.94	100.11	99.89	99.80	100.00	99.94	100.47
Cations (p.f.u.)																		
Ti	0.021	0.027	0.026	0.026	0.026	0.027	0.026	0.045	0.024	0.019	0.018	0.024	0.032	0.030	0.025	0.025	0.026	0.028
Cr	1.310	1.306	1.318	1.329	1.329	1.340	1.343	1.058	1.155	1.272	1.321	1.122	1.210	1.233	1.304	1.309	1.312	1.313
Al	0.280	0.329	0.318	0.320	0.319	0.311	0.320	0.407	0.424	0.386	0.370	0.209	0.371	0.360	0.339	0.334	0.339	0.333
V	0.002	0.001	0.001	0.002	0.002	0.002	0.002	0.003	0.001	0.001	0.002	0.002	0.002	0.002	0.002	0.002	0.002	0.002
Fe^{3+}*	0.359	0.308	0.306	0.295	0.295	0.290	0.279	0.438	0.370	0.300	0.267	0.615	0.347	0.342	0.303	0.301	0.294	0.292
Fe^{2+}*	0.723	0.718	0.604	0.573	0.560	0.557	0.581	0.753	0.743	0.713	0.701	0.754	0.749	0.723	0.695	0.679	0.681	0.681
Mn	0.067	0.007	0.008	0.005	0.007	0.007	0.006	0.048	0.013	0.010	0.010	0.063	0.011	0.008	0.009	0.009	0.010	0.011
Mg	0.231	0.303	0.413	0.449	0.459	0.463	0.440	0.244	0.267	0.297	0.308	0.204	0.272	0.298	0.322	0.338	0.335	0.337
Ni	-	-	-	-	-	-	-	-	-	-	-	-	-	-	-	-	-	-
Ca	0.000	0.001	0.001	0.000	0.000	0.000	0.000	0.001	0.000	0.000	0.000	0.004	0.002	0.001	0.000	0.000	0.001	0.000
Total	2.993	3.000	2.996	2.999	2.997	2.998	2.998	2.996	2.998	2.999	2.998	2.996	2.997	2.997	2.997	2.997	2.999	2.997
Trivalent End Members																		
Cr/Σ3+	0.672	0.672	0.678	0.684	0.684	0.690	0.692	0.556	0.593	0.650	0.675	0.577	0.627	0.637	0.670	0.673	0.675	0.678
Al/Σ3+	0.144	0.169	0.164	0.164	0.164	0.160	0.165	0.214	0.218	0.197	0.189	0.107	0.193	0.186	0.174	0.172	0.174	0.172
Fe/Σ3+	0.184	0.159	0.158	0.152	0.152	0.150	0.144	0.230	0.190	0.153	0.136	0.316	0.180	0.177	0.156	0.155	0.151	0.151

Crystal textural style is abbreviated: euh. (euhedral), sub. (subhedral), anh. (anhedral), interg. (intergrown), irreg. (irregular); l. (large), m. (medium), s. (small)
Grain number refers to a particular grain within a cluster: most clusters have multiple grain
Note: Other phases (ol, cpx, hbl) were also analyzed on certain sections, such that Cluster refers to a specific location on each section

Appendix I(continued): Spinel compositions from spinel-bearing ultramafic rocks of the Turnagain intrusion

Rock:	Wehrlite											Wehrlite					
Sample:	04ES-16-08-01											04ES-10-06-01					
Cluster:	4		5									6					
Grain Number:	2		1						2			1			2		
Style:			m. sub.						s. eu.			m. sub.			m. sub.		
Zone:	Mid	Core	Mid	Mid	Mid	Mid	Mid	Core	Rim	Mid	Core	Rim	Mid	Core	Rim	Mid	Core
Oxides (wt. %)																	
SiO_2	0.01	0.02	0.04	0.03	0.05	0.08	0.04	0.01	0.04	0.05	0.02	0.04	0.01	0.03	0.69	0.04	0.04
TiO_2	1.01	1.09	0.99	0.90	0.80	0.81	0.79	0.80	1.04	0.92	0.88	1.24	1.00	1.11	0.28	1.07	1.07
Al_2O_3	8.39	8.31	11.74	10.90	10.46	9.94	10.15	10.24	8.06	7.69	7.48	10.25	10.62	10.37	1.29	10.31	10.50
Cr_2O_3	47.81	47.74	42.95	45.30	46.69	46.20	47.18	46.85	45.50	48.74	49.40	34.72	40.68	40.35	10.29	40.46	41.22
V_2O_3	0.07	0.08	0.09	0.11	0.08	0.07	0.12	0.07	0.10	0.03	0.13	0.19	0.23	0.19	0.02	0.16	0.19
Fe_2O_3	12.07	11.54	12.65	11.62	11.14	11.15	10.97	10.84	13.27	11.87	11.68	20.34	15.91	16.44	58.44	16.56	15.88
FeO	23.59	23.55	24.23	24.18	24.23	23.12	24.50	24.29	25.62	24.97	25.01	24.12	25.51	25.77	26.10	25.66	25.90
MnO	0.30	0.31	0.32	0.31	0.39	0.35	0.33	0.32	0.51	0.28	0.31	2.71	0.35	0.39	0.90	0.45	0.31
MgO	6.72	6.61	6.51	6.50	6.38	6.71	6.25	6.27	4.93	5.68	5.75	4.72	5.66	5.54	3.06	5.52	5.59
NiO	-	-	-	-	-	-	-	-	-	-	-	-	-	-	-	-	-
CaO	0.00	0.02	0.00	0.01	0.01	0.00	0.00	0.00	0.19	0.10	0.05	0.00	0.02	0.00	0.10	0.02	0.03
Total	99.97	99.28	99.53	99.86	100.23	98.44	100.35	99.70	99.25	100.32	100.71	98.34	99.99	100.16	101.16	100.27	100.73
Cations (p.f.u.)																	
Ti	0.026	0.028	0.025	0.023	0.020	0.021	0.020	0.021	0.027	0.024	0.023	0.033	0.026	0.028	0.008	0.028	0.027
Cr	1.294	1.302	1.152	1.215	1.252	1.259	1.266	1.264	1.258	1.329	1.343	0.963	1.100	1.092	0.297	1.094	1.108
Al	0.339	0.338	0.469	0.436	0.418	0.404	0.406	0.412	0.332	0.312	0.303	0.424	0.428	0.418	0.056	0.416	0.421
V	0.002	0.002	0.002	0.002	0.002	0.002	0.003	0.002	0.002	0.001	0.003	0.004	0.005	0.004	0.000	0.004	0.004
Fe^{3+*}	0.311	0.299	0.323	0.297	0.284	0.289	0.280	0.279	0.349	0.308	0.302	0.537	0.409	0.423	1.606	0.426	0.406
Fe^{2+*}	0.675	0.679	0.687	0.686	0.687	0.666	0.695	0.693	0.749	0.720	0.719	0.708	0.730	0.737	0.797	0.734	0.736
Mn	0.009	0.009	0.009	0.009	0.011	0.010	0.009	0.009	0.015	0.008	0.009	0.081	0.010	0.011	0.028	0.013	0.009
Mg	0.343	0.340	0.329	0.329	0.323	0.344	0.316	0.319	0.257	0.292	0.294	0.247	0.289	0.282	0.167	0.282	0.283
Ni	-	-	-	-	-	-	-	-	-	-	-	-	-	-	-	-	-
Ca	0.000	0.001	0.000	0.000	0.000	0.000	0.000	0.000	0.007	0.004	0.002	0.000	0.001	0.000	0.004	0.001	0.001
Total	2.999	2.998	2.997	2.997	2.997	2.995	2.997	2.999	2.997	2.997	2.998	2.996	2.997	2.997	2.962	2.996	2.996
Trivalent End Members																	
Cr/Σ3+	0.666	0.671	0.593	0.624	0.641	0.645	0.649	0.647	0.649	0.682	0.689	0.501	0.568	0.565	0.152	0.565	0.573
Al/Σ3+	0.174	0.174	0.241	0.224	0.214	0.207	0.208	0.211	0.171	0.160	0.156	0.220	0.221	0.216	0.028	0.215	0.217
Fe/Σ3+	0.160	0.154	0.166	0.152	0.145	0.148	0.144	0.142	0.180	0.158	0.155	0.279	0.211	0.219	0.820	0.220	0.210

Crystal textural style is abbreviated: euh. (euhedral), sub. (subhedral), anh. (anhedral), interg. (intergrown), irreg. (irregular); l. (large), m. (medium), s. (small)
Grain number refers to a particular grain within a cluster: most clusters have multiple grain
Note: Other phases (ol, cpx, hbl) were also analyzed on certain sections, such that Cluster refers to a specific location on each section

Appendix I(continued): Spinel compositions from spinel-bearing ultramafic rocks of the Turnagain intrusion

Rock:	Wehrlite						Olivine Clinopyroxenite											
Sample:	04ES-10-06-01						04ES-06-06-01											
Cluster:	2			1						8						7		
Grain Number:	1			1			2			1				2		1		
Style:	m. sub.			m. anh.			m. anh.			m. sub.				s. anh.		m. anh.		
Zone:	Rim	Mid	Core	Rim	Mid	Core	Rim	Mid	Core	Mid	Mid	Mid	Core	Mid	Core	Rim	Mid	Mid
Oxides (wt. %)																		
SiO_2	0.00	0.02	0.05	0.01	0.00	0.03	0.03	0.03	0.00	0.00	0.02	0.02	0.00	0.00	0.06	0.02	0.03	0.06
TiO_2	0.91	0.96	0.89	0.79	0.94	0.94	0.11	0.94	0.89	1.13	1.09	1.06	1.08	0.90	1.03	1.11	1.28	1.10
Al_2O_3	12.76	11.86	11.74	12.14	11.14	11.50	0.03	12.00	11.86	9.09	9.18	9.16	9.10	8.81	9.40	7.13	7.68	7.49
Cr_2O_3	40.57	43.47	43.64	43.35	43.98	43.81	4.83	42.33	42.92	46.48	47.13	47.69	48.02	44.03	44.41	42.33	45.25	45.57
V_2O_3	0.20	0.14	0.16	0.13	0.16	0.16	0.00	0.20	0.16	0.32	0.36	0.28	0.34	0.34	0.39	0.43	0.36	0.33
Fe_2O_3	13.53	12.68	12.20	12.38	12.95	12.66	64.67	13.34	13.33	10.52	10.00	9.96	9.68	13.94	12.61	16.23	12.52	13.12
FeO	22.71	24.23	23.94	23.02	23.86	23.74	28.70	24.16	24.21	25.65	25.37	25.83	25.76	26.25	26.54	25.42	26.42	25.72
MnO	2.03	0.60	0.27	0.31	0.30	0.28	0.35	0.37	0.30	0.48	0.73	0.39	0.41	0.93	0.31	1.56	0.65	1.09
MgO	6.39	6.56	6.72	7.17	6.84	6.96	1.43	6.68	6.70	5.30	5.38	5.34	5.43	4.59	4.94	4.42	4.56	4.66
NiO	-	-	-	-	-	-	-	-	-	-	-	-	-	-	-	-	-	-
CaO	0.01	0.00	0.01	0.09	0.01	0.00	0.00	0.00	0.01	0.00	0.00	0.02	0.03	0.00	0.03	0.03	0.03	0.01
Total	99.12	100.51	99.62	99.38	100.17	100.08	100.17	100.05	100.39	98.97	99.26	99.76	99.84	99.80	99.72	98.69	98.77	99.16
Cations (p.f.u.)																		
Ti	0.023	0.024	0.023	0.020	0.024	0.024	0.003	0.024	0.023	0.030	0.028	0.027	0.028	0.024	0.027	0.030	0.034	0.029
Cr	1.088	1.154	1.167	1.156	1.173	1.167	0.145	1.127	1.140	1.278	1.290	1.300	1.307	1.210	1.214	1.187	1.262	1.266
Al	0.510	0.469	0.468	0.483	0.443	0.456	0.002	0.476	0.470	0.372	0.375	0.372	0.369	0.361	0.383	0.298	0.319	0.310
V	0.005	0.003	0.004	0.003	0.003	0.003	0.000	0.005	0.004	0.007	0.008	0.006	0.008	0.008	0.009	0.010	0.008	0.008
Fe^{3+}*	0.345	0.321	0.311	0.314	0.329	0.321	1.846	0.338	0.337	0.275	0.260	0.258	0.251	0.365	0.328	0.433	0.332	0.347
Fe^{2+}*	0.644	0.680	0.677	0.650	0.673	0.669	0.910	0.681	0.680	0.746	0.735	0.745	0.742	0.763	0.767	0.754	0.779	0.756
Mn	0.058	0.017	0.008	0.009	0.009	0.008	0.011	0.011	0.009	0.014	0.022	0.012	0.012	0.027	0.009	0.047	0.019	0.032
Mg	0.323	0.329	0.339	0.361	0.344	0.349	0.081	0.335	0.336	0.275	0.277	0.274	0.279	0.238	0.255	0.234	0.240	0.244
Ni	-	-	-	-	-	-	-	-	-	-	-	-	-	-	-	-	-	-
Ca	0.000	0.000	0.000	0.003	0.000	0.000	0.000	0.000	0.000	0.000	0.000	0.001	0.001	0.000	0.001	0.001	0.001	0.001
Total	2.998	2.998	2.996	2.998	2.998	2.997	2.998	2.997	2.998	2.997	2.995	2.996	2.997	2.996	2.993	2.994	2.995	2.994
Trivalent End Members																		
Cr/Σ3+	0.560	0.594	0.600	0.592	0.603	0.600	0.073	0.581	0.586	0.664	0.670	0.673	0.678	0.625	0.631	0.619	0.659	0.658
Al/Σ3+	0.263	0.241	0.241	0.247	0.228	0.235	0.001	0.245	0.241	0.193	0.195	0.193	0.192	0.186	0.199	0.155	0.167	0.161
Fe/Σ3+	0.178	0.165	0.160	0.161	0.169	0.165	0.926	0.174	0.173	0.143	0.135	0.134	0.130	0.188	0.170	0.226	0.174	0.180

Crystal textural style is abbreviated: euh. (euhedral), sub. (subhedral), anh. (anhedral), interg. (intergrown), irreg. (irregular); l. (large), m. (medium), s. (small)
Grain number refers to a particular grain within a cluster: most clusters have multiple grain
Note: Other phases (ol, cpx, hbl) were also analyzed on certain sections, such that Cluster refers to a specific location on each section

Appendix I(continued): Spinel compositions from spinel-bearing ultramafic rocks of the Turnagain intrusion

Rock:	Olivine Clinopyroxenite											Olivine Clinopyroxenite					
Sample:	04ES-06-06-01											04ES-01-04-01					
Cluster:	7				4.5				2			5					
Grain Number:	1	2			1							1				2	
Style:		m. anh.			l. anh.				m. anh.			m. irreg.				s. eu.	
Zone:	Core	Rim	Mid	Core	Mid	Mid	Mid	Core	Mid	Mid	Core	Rim	Mid	Mid	Core	Mid	Core
Oxides (wt. %)																	
SiO_2	0.02	0.03	0.03	0.05	0.04	0.05	0.05	0.02	0.01	0.00	0.02	0.05	0.02	0.05	0.01	0.04	0.03
TiO_2	1.11	1.22	1.44	2.11	1.05	1.05	1.04	1.07	0.84	0.98	1.02	0.85	0.86	0.87	0.79	0.90	0.86
Al_2O_3	7.67	5.68	6.23	0.34	8.74	8.60	8.49	8.53	8.25	8.61	8.35	8.52	8.29	8.17	8.10	8.99	8.86
Cr_2O_3	45.38	42.41	42.90	21.09	46.87	47.79	48.06	48.20	46.95	48.60	48.48	53.59	55.09	55.38	55.37	53.34	52.62
V_2O_3	0.37	0.39	0.54	0.24	0.27	0.24	0.25	0.22	0.25	0.24	0.22	0.30	0.25	0.23	0.26	0.26	0.27
Fe_2O_3	13.08	17.21	15.80	42.67	10.27	10.02	9.72	9.56	11.33	9.68	10.11	5.58	4.93	4.71	4.83	4.88	5.27
FeO	26.25	25.92	26.93	27.42	26.42	26.05	25.90	26.19	25.75	26.26	26.30	24.73	24.78	24.67	24.30	23.73	23.35
MnO	0.76	1.50	0.93	2.22	0.35	0.47	0.49	0.42	0.78	0.35	0.41	0.29	0.29	0.24	0.32	0.37	0.26
MgO	4.61	3.91	4.02	2.15	4.73	4.96	4.99	4.88	4.70	4.96	4.92	5.87	6.09	6.17	6.29	6.46	6.57
NiO	-	-	-	-	-	-	-	-	-	-	-	-	-	-	-	-	-
CaO	0.00	0.09	0.06	0.02	0.00	0.02	0.00	0.00	0.03	0.01	0.01	0.25	0.05	0.02	0.00	0.08	0.07
Total	99.25	98.36	98.88	98.31	98.74	99.24	99.00	99.10	98.90	99.69	99.85	100.03	100.67	100.50	100.27	99.05	98.17
Cations (p.f.u.)																	
Ti	0.029	0.033	0.038	0.060	0.028	0.028	0.027	0.028	0.022	0.026	0.027	0.022	0.022	0.022	0.020	0.023	0.023
Cr	1.260	1.206	1.209	0.632	1.298	1.316	1.326	1.330	1.303	1.333	1.330	1.452	1.484	1.494	1.496	1.449	1.442
Al	0.317	0.241	0.262	0.015	0.361	0.353	0.349	0.351	0.341	0.352	0.342	0.344	0.333	0.328	0.326	0.364	0.362
V	0.009	0.009	0.013	0.006	0.006	0.006	0.006	0.005	0.006	0.005	0.005	0.007	0.006	0.005	0.006	0.006	0.006
Fe^{3+}*	0.346	0.466	0.424	1.218	0.271	0.262	0.255	0.251	0.299	0.253	0.264	0.144	0.126	0.121	0.124	0.126	0.137
Fe^{2+}*	0.771	0.780	0.803	0.870	0.774	0.759	0.756	0.765	0.756	0.762	0.763	0.709	0.706	0.704	0.694	0.682	0.677
Mn	0.023	0.046	0.028	0.071	0.010	0.014	0.014	0.012	0.023	0.010	0.012	0.008	0.008	0.007	0.009	0.011	0.008
Mg	0.241	0.210	0.213	0.121	0.247	0.258	0.260	0.254	0.246	0.257	0.255	0.300	0.309	0.314	0.320	0.331	0.339
Ni	-	-	-	-	-	-	-	-	-	-	-	-	-	-	-	-	-
Ca	0.000	0.004	0.002	0.001	0.000	0.001	0.000	0.000	0.001	0.000	0.000	0.009	0.002	0.001	0.000	0.003	0.003
Total	2.995	2.994	2.993	2.995	2.995	2.995	2.995	2.997	2.997	2.998	2.997	2.994	2.996	2.995	2.997	2.996	2.996
Trivalent End Members																	
Cr/Σ3+	0.655	0.630	0.638	0.339	0.673	0.681	0.687	0.688	0.670	0.688	0.687	0.748	0.764	0.769	0.769	0.747	0.743
Al/Σ3+	0.165	0.126	0.138	0.008	0.187	0.183	0.181	0.182	0.176	0.182	0.176	0.177	0.171	0.169	0.168	0.188	0.186
Fe/Σ3+	0.180	0.244	0.224	0.653	0.140	0.136	0.132	0.130	0.154	0.130	0.136	0.074	0.065	0.062	0.064	0.065	0.071

Crystal textural style is abbreviated: euh. (euhedral), sub. (subhedral), anh. (anhedral), interg. (intergrown), irreg. (irregular); l. (large), m. (medium), s. (small)
Grain number refers to a particular grain within a cluster: most clusters have multiple grain
Note: Other phases (ol, cpx, hbl) were also analyzed on certain sections, such that Cluster refers to a specific location on each section

Appendix I(continued): Spinel compositions from spinel-bearing ultramafic rocks of the Turnagain intrusion

Rock:	Olivine Clinopyroxenite							Olivine Clinopyroxenite							Hornblende Clinopyroxenite			
Sample:	04ES-01-04-01							05ES-05-01-01							DDH04-47-7-49			
Cluster:	6				2			8			9				3			
Grain Number:	1							1			1				1			
Style:	m. sub.				m. anh.			s. eu.							l. anh.			
Zone:	Rim	Mid	Mid	Core	Rim	Mid	Mid	Core	Rim	Mid	Core	Rim	Mid	Core	Mid	Mid	Mid	Mid
Oxides (wt. %)																		
SiO_2	0.02	0.03	0.33	0.32	0.24	0.03	0.04	0.01	0.03	0.00	0.03	0.01	0.02	0.02	0.03	0.02	0.05	0.05
TiO_2	0.84	0.81	0.76	0.72	0.84	0.83	0.85	0.86	2.42	2.48	2.51	3.08	3.13	3.13	0.15	2.83	3.62	3.73
Al_2O_3	8.77	7.99	7.80	7.70	7.00	8.95	8.83	8.73	4.18	4.44	4.64	6.63	6.48	6.50	0.12	0.69	2.71	1.22
Cr_2O_3	54.05	55.06	55.11	55.11	39.85	52.54	53.14	53.67	26.90	27.45	28.34	29.49	30.10	30.21	0.12	0.15	0.18	0.18
V_2O_3	0.23	0.19	0.19	0.22	0.24	0.32	0.28	0.27	0.07	0.08	0.11	0.19	0.15	0.20	0.69	0.48	0.43	0.38
Fe_2O_3	4.91	4.96	5.48	5.59	19.25	5.46	5.54	4.95	32.01	31.67	30.20	26.23	26.42	26.69	67.96	61.90	58.63	60.00
FeO	23.53	23.61	23.28	23.11	25.89	25.73	25.95	25.62	25.19	25.31	25.09	26.10	27.29	27.49	31.70	33.48	34.32	34.40
MnO	0.23	0.28	0.34	0.27	1.13	0.36	0.30	0.35	3.87	3.92	4.07	3.54	2.02	1.96	0.08	0.20	0.26	0.21
MgO	6.62	6.55	6.72	6.79	3.95	5.25	5.32	5.43	2.79	2.98	3.08	3.59	4.01	4.07	0.09	0.23	0.51	0.31
NiO	-	-	-	-	-	-	-	-	-	-	-	-	-	-	-	-	-	-
CaO	0.16	0.02	0.04	0.08	0.15	0.06	0.02	0.02	0.34	0.26	0.17	0.10	0.03	0.04	0.00	0.04	0.00	0.00
Total	99.35	99.51	100.04	99.90	98.51	99.52	100.27	99.90	97.80	98.60	98.24	98.96	99.67	100.31	100.95	100.01	100.71	100.48
Cations (p.f.u.)																		
Ti	0.022	0.021	0.020	0.018	0.022	0.021	0.022	0.022	0.067	0.068	0.069	0.083	0.084	0.083	0.004	0.081	0.102	0.106
Cr	1.464	1.496	1.487	1.488	1.124	1.434	1.441	1.460	0.787	0.795	0.821	0.836	0.846	0.843	0.004	0.005	0.005	0.005
Al	0.354	0.324	0.314	0.310	0.294	0.364	0.357	0.354	0.182	0.192	0.200	0.280	0.272	0.271	0.005	0.031	0.119	0.054
V	0.005	0.004	0.004	0.005	0.006	0.007	0.006	0.006	0.002	0.002	0.003	0.004	0.004	0.005	0.017	0.012	0.011	0.009
Fe^{3+}*	0.127	0.128	0.141	0.144	0.517	0.142	0.143	0.128	0.891	0.873	0.833	0.708	0.707	0.709	1.944	1.776	1.648	1.706
Fe^{2+}*	0.674	0.679	0.664	0.660	0.772	0.743	0.744	0.737	0.779	0.775	0.769	0.783	0.811	0.812	1.008	1.068	1.072	1.087
Mn	0.007	0.008	0.010	0.008	0.034	0.010	0.009	0.010	0.121	0.122	0.126	0.108	0.061	0.059	0.003	0.006	0.008	0.007
Mg	0.338	0.336	0.342	0.346	0.210	0.270	0.272	0.278	0.154	0.163	0.168	0.192	0.212	0.214	0.005	0.013	0.028	0.017
Ni	-	-	-	-	-	-	-	-	-	-	-	-	-	-	-	-	-	-
Ca	0.006	0.001	0.001	0.003	0.006	0.002	0.001	0.001	0.014	0.010	0.007	0.004	0.001	0.002	0.000	0.002	0.000	0.000
Total	2.997	2.997	2.981	2.981	2.985	2.995	2.995	2.997	2.998	2.999	2.997	2.998	2.997	2.997	2.991	2.994	2.993	2.993
Trivalent End Members																		
Cr/Σ3+	0.753	0.768	0.766	0.766	0.581	0.739	0.742	0.752	0.423	0.428	0.443	0.458	0.464	0.463	0.002	0.002	0.003	0.003
Al/Σ3+	0.182	0.166	0.162	0.160	0.152	0.188	0.184	0.182	0.098	0.103	0.108	0.154	0.149	0.148	0.003	0.017	0.067	0.031
Fe/Σ3+	0.065	0.066	0.072	0.074	0.267	0.073	0.074	0.066	0.479	0.469	0.449	0.388	0.387	0.389	0.995	0.980	0.930	0.966

Crystal textural style is abbreviated: euh. (euhedral), sub. (subhedral), anh. (anhedral), interg. (intergrown), irreg. (irregular); l. (large), m. (medium), s. (small)
Grain number refers to a particular grain within a cluster: most clusters have multiple grain
Note: Other phases (ol, cpx, hbl) were also analyzed on certain sections, such that Cluster refers to a specific location on each section

Appendix I(continued): Spinel compositions from spinel-bearing ultramafic rocks of the Turnagain intrusion

Rock:	Hornblende Clinopyroxenite									Hornblende Clinopyroxenite							
Sample:	DDH04-47-7-49									DDH05-84-19-104							
Cluster:	3	4			5				9				8				
Grain Number:	1	1			1				1				1				
Style:		l. anh.				l. anh.				l. interg.				l. anh.			
Zone:	Core	Rim	Mid	Mid	Core	Rim	Mid	Mid	Core	Rim	Mid	Mid	Core	Rim	Mid	Mid	Core
Oxides (wt. %)																	
SiO_2	0.01	0.03	0.05	0.02	0.04	0.03	0.03	0.03	0.03	0.02	0.00	0.04	0.03	0.01	0.04	0.03	0.03
TiO_2	3.55	4.00	2.33	2.03	2.56	0.35	3.04	3.19	3.27	0.15	0.09	0.08	0.01	0.21	0.07	0.08	0.08
Al_2O_3	3.45	0.16	3.77	1.30	1.43	0.16	0.78	1.12	2.27	0.03	0.06	0.07	0.04	0.04	0.13	0.18	0.18
Cr_2O_3	0.15	0.09	0.17	0.13	0.11	0.13	0.12	0.15	0.13	0.49	0.45	0.47	0.46	0.60	0.48	0.37	0.38
V_2O_3	0.42	0.22	0.52	0.59	0.49	0.73	0.45	0.45	0.46	0.94	0.94	0.87	0.92	0.85	0.97	0.95	0.95
Fe_2O_3	57.77	61.29	60.21	63.38	62.12	67.39	61.56	60.85	59.94	67.70	67.60	68.25	67.51	67.23	67.13	67.77	67.50
FeO	34.13	34.56	33.29	33.29	33.50	31.82	33.76	33.83	34.04	32.00	31.87	32.00	31.60	31.70	31.62	32.03	31.76
MnO	0.30	0.26	0.23	0.17	0.17	0.02	0.25	0.22	0.26	0.02	0.06	0.08	0.06	0.08	0.06	0.06	0.08
MgO	0.58	0.22	0.67	0.27	0.33	0.15	0.19	0.29	0.46	0.12	0.10	0.11	0.14	0.12	0.16	0.09	0.14
NiO	-	-	-	-	-	-	-	-	-	-	-	-	-	-	-	-	-
CaO	0.00	0.00	0.00	0.01	0.02	0.01	0.04	0.00	0.03	0.04	0.03	0.04	0.00	0.09	0.01	0.00	0.03
Total	100.37	100.83	101.25	101.19	100.76	100.78	100.21	100.12	100.90	101.50	101.19	102.02	100.77	100.93	100.67	101.56	101.13
Cations (p.f.u.)																	
Ti	0.100	0.114	0.065	0.057	0.072	0.010	0.087	0.091	0.092	0.004	0.003	0.002	0.000	0.006	0.002	0.002	0.002
Cr	0.004	0.003	0.005	0.004	0.003	0.004	0.004	0.004	0.004	0.015	0.013	0.014	0.014	0.018	0.014	0.011	0.011
Al	0.152	0.007	0.164	0.058	0.063	0.007	0.035	0.050	0.100	0.002	0.003	0.003	0.002	0.002	0.006	0.008	0.008
V	0.010	0.006	0.013	0.015	0.012	0.018	0.011	0.011	0.011	0.023	0.024	0.022	0.023	0.021	0.024	0.024	0.024
Fe^{3+}*	1.622	1.749	1.673	1.792	1.761	1.929	1.762	1.739	1.687	1.925	1.929	1.931	1.934	1.922	1.923	1.925	1.925
Fe^{2+}*	1.065	1.096	1.028	1.046	1.056	1.012	1.074	1.074	1.064	1.011	1.010	1.006	1.006	1.007	1.006	1.011	1.006
Mn	0.010	0.008	0.007	0.005	0.005	0.001	0.008	0.007	0.008	0.001	0.002	0.003	0.002	0.002	0.002	0.002	0.002
Mg	0.032	0.013	0.037	0.015	0.018	0.008	0.011	0.017	0.026	0.007	0.005	0.006	0.008	0.007	0.009	0.005	0.008
Ni	-	-	-	-	-	-	-	-	-	-	-	-	-	-	-	-	-
Ca	0.000	0.000	0.000	0.000	0.001	0.001	0.001	0.000	0.001	0.001	0.001	0.001	0.000	0.004	0.001	0.000	0.001
Total	2.995	2.996	2.991	2.993	2.993	2.990	2.994	2.994	2.993	2.989	2.990	2.988	2.988	2.990	2.987	2.988	2.988
Trivalent End Members																	
Cr/Σ3+	0.002	0.002	0.003	0.002	0.002	0.002	0.002	0.002	0.002	0.008	0.007	0.007	0.007	0.009	0.007	0.006	0.006
Al/Σ3+	0.085	0.004	0.089	0.031	0.035	0.004	0.019	0.028	0.056	0.001	0.001	0.002	0.001	0.001	0.003	0.004	0.004
Fe/Σ3+	0.912	0.994	0.908	0.967	0.964	0.994	0.978	0.970	0.942	0.992	0.992	0.991	0.992	0.990	0.990	0.990	0.990

Crystal textural style is abbreviated: euh. (euhedral), sub. (subhedral), anh. (anhedral), interg. (intergrown), irreg. (irregular); l. (large), m. (medium), s. (small)
Grain number refers to a particular grain within a cluster: most clusters have multiple grain
Note: Other phases (ol, cpx, hbl) were also analyzed on certain sections, such that Cluster refers to a specific location on each section

Appendix I(continued): Spinel compositions from spinel-bearing ultramafic rocks of the Turnagain intrusion

Rock:	Hornblende Clinopyroxenite			
Sample:	DDH05-84-19-104			
Cluster:	1			
Grain Number:	1			
Style:	l. anh.			
Zone:	Rim	Mid	Mid	Core
Oxides (wt. %)				
SiO_2	0.01	0.02	0.05	0.01
TiO_2	0.04	0.05	0.08	0.14
Al_2O_3	0.04	0.06	0.18	0.15
Cr_2O_3	0.37	0.42	0.37	0.38
V_2O_3	0.89	0.86	0.91	0.93
Fe_2O_3	67.86	68.12	67.80	67.77
FeO	31.85	31.98	31.85	32.10
MnO	0.00	0.01	0.02	0.00
MgO	0.11	0.09	0.17	0.11
NiO	-	-	-	-
CaO	0.00	0.01	0.02	0.00
Total	101.16	101.61	101.46	101.59
Cations (p.f.u.)				
Ti	0.001	0.001	0.002	0.004
Cr	0.011	0.012	0.011	0.011
Al	0.002	0.003	0.008	0.006
V	0.022	0.022	0.023	0.023
Fe^{3+*}	1.937	1.936	1.926	1.925
Fe^{2+*}	1.010	1.010	1.006	1.013
Mn	0.000	0.000	0.001	0.000
Mg	0.006	0.005	0.010	0.006
Ni	-	-	-	-
Ca	0.000	0.000	0.001	0.000
Total	2.990	2.990	2.987	2.989
Trivalent End Members				
Cr/Σ3+	0.006	0.006	0.006	0.006
Al/Σ3+	0.001	0.001	0.004	0.003
Fe/Σ3+	0.993	0.992	0.990	0.991

Crystal textural style is abbreviated: euh. (euhedral), sub. (subhedral), anh. (anhedral), interg. (intergrown), irreg. (irregular); l. (large), m. (medium), s. (small)
Grain number refers to a particular grain within a cluster: most clusters have multiple grain
Note: Other phases (ol, cpx, hbl) were also analyzed on certain sections, such that Cluster refers to a specific location on each section

Appendix II: Olivine compositions from olivine-bearing ultramafic lithologies of the Turnagain intrusion

Rock type:	Chromitite													Chromitite				
Sample:	05ES-01-01-01													05ES-01-04-01				
Cluster:	1				3				8					1				2
Style:	porph.	porph.	porph.	porph.	porph.	cumu.	cumu.	cumu.	cumu.	cumu.	cumu.	cumu.	cumu.	cumu.	cumu.	cumu.	cumu.	mgb.
Zone:	rim	mid	mid	mid	core	rim	mid	mid	core	rim	mid	mid	mid	core	rim	mid	core	rim
Oxides (wt. %)																		
SiO_2	41.58	41.11	40.91	40.81	41.10	40.76	40.93	40.86	41.02	40.99	40.91	40.95	41.12	41.11	41.87	41.51	41.82	41.71
Cr_2O_3	0.02	0.02	0.00	0.00	0.03	0.00	0.00	0.01	0.00	0.01	0.00	0.01	0.01	0.01	0.00	0.03	0.02	0.21
FeO	7.31	8.73	8.81	8.57	8.81	8.72	8.43	8.81	8.33	8.64	8.57	8.68	8.16	8.65	5.04	5.27	5.26	3.93
MnO	0.15	0.15	0.17	0.14	0.19	0.15	0.17	0.17	0.19	0.17	0.11	0.12	0.19	0.15	0.07	0.09	0.06	0.10
MgO	50.49	49.82	49.71	49.93	49.81	49.61	49.86	49.79	49.95	49.85	49.95	49.77	49.95	49.79	52.73	52.69	52.61	54.01
NiO	0.25	0.33	0.28	0.32	0.23	0.32	0.33	0.35	0.35	0.27	0.36	0.40	0.31	0.40	0.42	0.52	0.45	0.36
CaO	0.05	0.07	0.09	0.05	0.06	0.04	0.09	0.06	0.08	0.03	0.06	0.07	0.07	0.07	0.11	0.12	0.13	0.07
Total	99.85	100.23	99.96	99.81	100.23	99.58	99.80	100.05	99.92	99.96	99.97	99.99	99.82	100.18	100.24	100.23	100.35	100.39
Cations (p.f.u.)																		
Si	1.008	1.001	0.999	0.998	1.000	0.999	1.000	0.998	1.000	1.000	0.998	1.000	1.003	1.001	1.002	0.996	1.001	0.992
Cr	0.000	0.000	0.000	0.000	0.001	0.000	0.000	0.000	0.000	0.000	0.000	0.000	0.000	0.000	0.000	0.001	0.000	0.004
Fe	0.148	0.178	0.180	0.175	0.179	0.179	0.172	0.180	0.170	0.176	0.175	0.177	0.166	0.176	0.101	0.106	0.105	0.078
Mn	0.003	0.003	0.004	0.003	0.004	0.003	0.003	0.004	0.004	0.003	0.002	0.002	0.004	0.003	0.001	0.002	0.001	0.002
Mg	1.825	1.808	1.810	1.820	1.808	1.813	1.816	1.812	1.816	1.813	1.817	1.811	1.816	1.808	1.882	1.885	1.878	1.915
Ni	0.005	0.006	0.005	0.006	0.005	0.006	0.006	0.007	0.007	0.005	0.007	0.008	0.006	0.008	0.008	0.010	0.009	0.007
Ca	0.001	0.002	0.002	0.001	0.002	0.001	0.002	0.002	0.002	0.001	0.002	0.002	0.002	0.002	0.003	0.003	0.003	0.002
Total	2.991	2.999	3.001	3.002	2.998	3.001	3.000	3.002	3.000	2.999	3.002	3.000	2.997	2.998	2.998	3.002	2.998	3.000
End Members (%)																		
Fo	92.5	91.1	91.0	91.2	91.0	91.0	91.3	91.0	91.4	91.1	91.2	91.1	91.6	91.1	94.9	94.7	94.7	96.1
Fa	7.5	8.9	9.0	8.8	9.0	9.0	8.7	9.0	8.6	8.9	8.8	8.9	8.4	8.9	5.1	5.3	5.3	3.9

Crystal textural style is abbreviated: porph. (porphyroclast), cumu. (cumulus), def. (deformed), mgb. (modified grain boundaries)
Note: Other phases (cpx, chr) were also analyzed on certain sections, such that "Cluster" refers to a specific location on each section

Appendix II (continued): Olivine compositions from olivine-bearing ultramafic lithologies of the Turnagain intrusion

Rock type:	Chromitite						Chromitite									
Sample:	05ES-01-04-01						05ES-01-03-01									
Cluster:	2			3			7				6			5		
Style:	mgb.	mgb.	mgb.	cumu.	cumu.	cumu.	porph.	porph.	porph.	porph.	mgb.	mgb.	mgb.	mgb.	mgb.	mgb.	mgb.
Zone:	mid	mid	core	rim	mid	core	rim	mid	mid	core	rim	mid	core	rim	mid	mid	core
Oxides (wt. %)																	
SiO_2	41.71	41.59	41.90	41.14	41.50	41.56	41.78	41.57	41.43	41.41	41.58	41.38	41.32	41.58	41.52	41.50	41.25
Cr_2O_3	0.01	0.01	0.02	0.09	0.00	0.03	0.02	0.00	0.00	0.03	0.00	0.01	0.00	0.03	0.00	0.00	0.04
FeO	4.74	4.82	4.79	3.81	4.33	4.70	6.44	6.52	6.64	6.47	6.24	6.44	6.44	5.83	6.39	6.40	6.20
MnO	0.09	0.07	0.09	0.05	0.08	0.10	0.08	0.13	0.11	0.12	0.10	0.14	0.12	0.14	0.08	0.13	0.09
MgO	52.79	52.88	53.01	53.62	53.35	53.35	51.37	51.70	51.60	51.43	51.76	51.73	51.56	52.04	51.49	51.64	51.96
NiO	0.47	0.47	0.51	0.63	0.59	0.61	0.41	0.41	0.40	0.43	0.42	0.43	0.44	0.40	0.46	0.41	0.43
CaO	0.10	0.10	0.13	0.11	0.08	0.12	0.09	0.12	0.13	0.14	0.13	0.13	0.14	0.08	0.13	0.14	0.12
Total	99.92	99.93	100.45	99.45	99.92	100.47	100.18	100.46	100.31	100.02	100.23	100.25	100.02	100.10	100.08	100.22	100.09
Cations (p.f.u.)																	
Si	1.001	0.999	1.001	0.990	0.995	0.993	1.006	1.000	0.999	1.000	1.001	0.998	0.999	1.001	1.002	1.000	0.995
Cr	0.000	0.000	0.000	0.002	0.000	0.000	0.000	0.000	0.000	0.001	0.000	0.000	0.000	0.001	0.000	0.000	0.001
Fe	0.095	0.097	0.096	0.077	0.087	0.094	0.130	0.131	0.134	0.131	0.126	0.130	0.130	0.117	0.129	0.129	0.125
Mn	0.002	0.001	0.002	0.001	0.002	0.002	0.002	0.003	0.002	0.002	0.002	0.003	0.002	0.003	0.002	0.003	0.002
Mg	1.889	1.892	1.887	1.923	1.908	1.901	1.845	1.854	1.855	1.852	1.858	1.859	1.858	1.867	1.853	1.856	1.869
Ni	0.009	0.009	0.010	0.012	0.011	0.012	0.008	0.008	0.008	0.008	0.008	0.008	0.009	0.008	0.009	0.008	0.008
Ca	0.002	0.003	0.003	0.003	0.002	0.003	0.002	0.003	0.003	0.004	0.003	0.003	0.004	0.002	0.003	0.004	0.003
Total	2.999	3.001	2.999	3.007	3.005	3.006	2.993	3.000	3.001	2.998	2.999	3.002	3.001	2.998	2.998	3.000	3.003
End Members (%)																	
Fo	95.2	95.1	95.2	96.2	95.6	95.3	93.4	93.4	93.3	93.4	93.7	93.5	93.4	94.1	93.5	93.5	93.7
Fa	4.8	4.9	4.8	3.8	4.4	4.7	6.6	6.6	6.7	6.6	6.3	6.5	6.6	5.9	6.5	6.5	6.3

Crystal textural style is abbreviated: porph. (porphyroclast), cumu. (cumulus), def. (deformed), mgb. (modified grain boundaries)
Note: Other phases (cpx, chr) were also analyzed on certain sections, such that "Cluster" refers to a specific location on each section

Appendix II (continued): Olivine compositions from olivine-bearing ultramafic lithologies of the Turnagain intrusion

Rock type:	Dunite								Dunite			Dunite						
Sample:	04ES-10-05-01								04ES-10-05-01			04ES-06-01-01						
Cluster:	3				2				1			1			2			
Style:	mgb.	mgb.	mgb.	mgb.	cumu.	cumu.	cumu.	cumu.	cumu.	cumu.	cumu.	porph.	porph.	porph.	porph.	porph.	porph.	porph.
Zone:	rim	mid	mid	core	rim	mid	mid	core	rim	mid	core	rim	mid	core	rim	mid	mid	core
Oxides (wt. %)																		
SiO_2	41.05	40.72	40.76	41.22	40.43	40.85	41.04	40.90	42.17	41.26	40.86	41.02	41.14	41.06	40.97	40.65	41.29	40.92
Cr_2O_3	0.00	0.00	0.00	0.00	0.01	0.00	0.07	0.00	0.00	0.01	0.00	0.01	0.04	0.12	0.09	0.05	0.00	0.01
FeO	8.91	9.47	9.09	8.66	8.85	8.52	8.77	8.42	3.44	8.91	9.17	8.91	9.33	8.88	9.54	8.92	9.26	9.50
MnO	0.16	0.18	0.18	0.16	0.16	0.16	0.12	0.12	0.43	0.15	0.17	0.18	0.21	0.15	0.17	0.21	0.14	0.14
MgO	49.74	48.52	49.19	49.55	49.78	49.58	49.77	49.59	54.63	49.59	49.61	49.29	48.81	49.83	49.00	49.52	47.90	49.15
NiO	0.29	0.35	0.30	0.31	0.27	0.30	0.30	0.41	0.00	0.35	0.30	0.31	0.34	0.29	0.35	0.29	0.29	0.31
CaO	0.17	0.25	0.06	0.02	0.05	0.05	0.05	0.05	0.02	0.07	0.13	0.06	0.25	0.04	0.30	0.02	0.66	0.05
Total	100.33	99.49	99.59	99.92	99.55	99.45	100.13	99.48	100.69	100.33	100.24	99.79	100.12	100.37	100.41	99.67	99.55	100.08
Cations (p.f.u.)																		
Si	1.000	1.003	1.001	1.006	0.993	1.001	1.000	1.002	0.998	1.004	0.997	1.004	1.005	0.998	1.000	0.997	1.014	1.001
Cr	0.000	0.000	0.000	0.000	0.000	0.000	0.001	0.000	0.000	0.000	0.000	0.000	0.001	0.002	0.002	0.001	0.000	0.000
Fe	0.181	0.195	0.187	0.177	0.182	0.175	0.179	0.172	0.068	0.181	0.187	0.182	0.191	0.181	0.195	0.183	0.190	0.194
Mn	0.003	0.004	0.004	0.003	0.003	0.003	0.002	0.002	0.009	0.003	0.004	0.004	0.004	0.003	0.003	0.004	0.003	0.003
Mg	1.806	1.782	1.800	1.802	1.822	1.812	1.808	1.811	1.927	1.799	1.805	1.798	1.778	1.806	1.783	1.810	1.755	1.792
Ni	0.006	0.007	0.006	0.006	0.005	0.006	0.006	0.008	0.000	0.007	0.006	0.006	0.007	0.006	0.007	0.006	0.006	0.006
Ca	0.004	0.007	0.002	0.000	0.001	0.001	0.001	0.001	0.000	0.002	0.003	0.002	0.007	0.001	0.008	0.001	0.017	0.001
Total	3.000	2.997	2.999	2.994	3.007	2.999	2.997	2.998	3.002	2.996	3.003	2.996	2.993	2.997	2.997	3.001	2.985	2.998
End Members (%)																		
Fo	90.9	90.1	90.6	91.1	90.9	91.2	91.0	91.3	96.6	90.8	90.6	90.8	90.3	90.9	90.2	90.8	90.2	90.2
Fa	9.1	9.9	9.4	8.9	9.1	8.8	9.0	8.7	3.4	9.2	9.4	9.2	9.7	9.1	9.8	9.2	9.8	9.8

Crystal textural style is abbreviated: porph. (porphyroclast), cumu. (cumulus), def. (deformed), mgb. (modified grain boundaries)
Note: Other phases (cpx, chr) were also analyzed on certain sections, such that "Cluster" refers to a specific location on each section

Appendix II (continued): Olivine compositions from olivine-bearing ultramafic lithologies of the Turnagain intrusion

Rock type:	Dunite				Dunite									Dunite				
Sample:	04ES-06-01-01				04ES-08-01-01									04ES-03-02-01				
Cluster:	3				1			2			3			1			2	
Style:	mgb.	mgb.	mgb.	mgb.	cumu.	cumu.	cumu.	cumu.	cumu.	cumu.	cumu.	cumu.	cumu.	cumu.	cumu.	cumu.	cumu.	cumu.
Zone:	rim	mid	mid	core	rim	mid	core	rim	mid	core	rim	mid	core	rim	mid	core	rim	mid
Oxides (wt. %)																		
SiO_2	40.99	41.04	41.02	41.44	40.78	40.87	40.78	40.86	40.66	40.85	40.78	41.02	40.79	41.25	40.85	40.91	40.72	40.84
Cr_2O_3	0.00	0.00	0.00	0.02	0.03	0.03	0.08	0.00	0.02	0.06	0.01	0.00	0.02	0.00	0.02	0.01	0.00	0.00
FeO	8.98	9.10	9.29	7.67	10.23	10.09	10.12	9.08	9.70	10.31	9.46	9.99	9.88	8.20	9.14	9.35	9.28	9.08
MnO	0.20	0.20	0.19	0.17	0.16	0.15	0.17	0.18	0.16	0.17	0.14	0.20	0.12	0.16	0.16	0.14	0.14	0.14
MgO	49.31	49.53	49.16	50.77	48.56	48.45	48.53	49.53	48.77	48.67	49.32	48.88	48.97	50.10	49.39	49.37	49.58	49.40
NiO	0.27	0.27	0.32	0.13	0.14	0.13	0.05	0.10	0.07	0.12	0.03	0.14	0.11	0.06	0.16	0.12	0.16	0.10
CaO	0.15	0.00	0.02	0.00	0.17	0.16	0.15	0.10	0.18	0.15	0.11	0.17	0.18	0.07	0.17	0.16	0.15	0.14
Total	99.91	100.14	100.00	100.20	100.07	99.88	99.89	99.85	99.57	100.35	99.85	100.41	100.06	99.83	99.89	100.06	100.03	99.70
Cations (p.f.u.)																		
Si	1.002	1.002	1.003	1.003	1.001	1.004	1.001	1.000	1.000	1.000	0.999	1.002	0.999	1.004	1.000	1.000	0.996	1.001
Cr	0.000	0.000	0.000	0.000	0.000	0.001	0.002	0.000	0.000	0.001	0.000	0.000	0.000	0.000	0.000	0.000	0.000	0.000
Fe	0.184	0.186	0.190	0.155	0.210	0.207	0.208	0.186	0.200	0.211	0.194	0.204	0.202	0.167	0.187	0.191	0.190	0.186
Mn	0.004	0.004	0.004	0.003	0.003	0.003	0.004	0.004	0.003	0.004	0.003	0.004	0.002	0.003	0.003	0.003	0.003	0.003
Mg	1.798	1.802	1.793	1.832	1.777	1.774	1.776	1.807	1.789	1.776	1.801	1.780	1.789	1.818	1.802	1.799	1.808	1.804
Ni	0.005	0.005	0.006	0.002	0.003	0.003	0.001	0.002	0.001	0.002	0.001	0.003	0.002	0.001	0.003	0.002	0.003	0.002
Ca	0.004	0.000	0.001	0.000	0.004	0.004	0.004	0.003	0.005	0.004	0.003	0.004	0.005	0.002	0.005	0.004	0.004	0.004
Total	2.997	2.998	2.997	2.996	2.998	2.995	2.995	3.000	2.999	2.998	3.001	2.998	3.000	2.996	3.000	3.000	3.004	2.999
End Members (%)																		
Fo	90.7	90.7	90.4	92.2	89.4	89.5	89.5	90.7	90.0	89.4	90.3	89.7	89.8	91.6	90.6	90.4	90.5	90.7
Fa	9.3	9.3	9.6	7.8	10.6	10.5	10.5	9.3	10.0	10.6	9.7	10.3	10.2	8.4	9.4	9.6	9.5	9.3

Crystal textural style is abbreviated: porph. (porphyroclast), cumu. (cumulus), def. (deformed), mgb. (modified grain boundaries)
Note: Other phases (cpx, chr) were also analyzed on certain sections, such that "Cluster" refers to a specific location on each section

Appendix II (continued): Olivine compositions from olivine-bearing ultramafic lithologies of the Turnagain intrusion

Rock type:	Dunite			Dunite								Wehrlite						
Sample:	04ES-03-02-01			04ES-19-01-02								04ES-10-06-01						
Cluster:	2	3		1		2			3			5					4	
Style:	cumu.	cumu.	cumu.	cumu.	cumu.	cumu.	cumu.	cumu.	cumu.	cumu.	cumu.	porph.	porph.	porph.	porph.	porph.	porph.	porph.
Zone:	core	rim	mid	core	rim	core	rim	mid	core	rim	core	rim	mid	mid	mid	core	mid	mid
Oxides (wt. %)																		
SiO_2	40.85	40.74	40.49	41.00	41.67	41.56	41.48	41.45	41.22	41.45	41.31	40.91	40.27	40.70	40.16	40.47	40.16	40.38
Cr_2O_3	0.05	0.01	0.04	0.02	0.00	0.03	0.04	0.03	0.03	0.00	0.01	0.00	0.01	0.00	0.02	0.06	0.00	0.00
FeO	9.35	7.34	9.00	8.57	7.66	7.51	7.85	7.44	7.36	7.56	7.02	8.87	10.58	9.66	10.87	10.46	10.88	9.84
MnO	0.20	0.23	0.15	0.16	0.16	0.21	0.12	0.19	0.16	0.21	0.12	0.33	0.19	0.21	0.22	0.21	0.21	0.32
MgO	49.63	49.99	49.13	49.97	50.88	51.00	50.39	51.18	51.00	50.85	51.08	49.57	48.03	48.68	47.85	47.94	47.60	48.79
NiO	0.12	0.12	0.10	0.09	0.17	0.25	0.22	0.13	0.25	0.27	0.21	0.25	0.27	0.31	0.36	0.39	0.27	0.31
CaO	0.10	0.11	0.18	0.15	0.02	0.03	0.34	0.08	0.04	0.06	0.00	0.03	0.05	0.04	0.04	0.02	0.03	0.03
Total	100.31	98.54	99.09	99.96	100.55	100.58	100.43	100.48	100.06	100.41	99.75	99.95	99.39	99.61	99.52	99.56	99.15	99.67
Cations (p.f.u.)																		
Si	0.996	1.002	0.998	1.000	1.005	1.002	1.003	1.000	0.999	1.002	1.002	1.000	0.998	1.002	0.996	1.000	0.999	0.995
Cr	0.001	0.000	0.001	0.000	0.000	0.001	0.001	0.000	0.001	0.000	0.000	0.000	0.000	0.000	0.000	0.001	0.000	0.000
Fe	0.191	0.151	0.186	0.175	0.155	0.151	0.159	0.150	0.149	0.153	0.142	0.181	0.219	0.199	0.226	0.216	0.226	0.203
Mn	0.004	0.005	0.003	0.003	0.003	0.004	0.002	0.004	0.003	0.004	0.002	0.007	0.004	0.004	0.005	0.004	0.004	0.007
Mg	1.804	1.833	1.806	1.816	1.829	1.833	1.817	1.840	1.842	1.832	1.847	1.806	1.774	1.786	1.769	1.767	1.765	1.793
Ni	0.002	0.002	0.002	0.002	0.003	0.005	0.004	0.002	0.005	0.005	0.004	0.005	0.005	0.006	0.007	0.008	0.005	0.006
Ca	0.003	0.003	0.005	0.004	0.000	0.001	0.009	0.002	0.001	0.002	0.000	0.001	0.001	0.001	0.001	0.001	0.001	0.001
Total	3.002	2.997	3.000	3.000	2.995	2.997	2.995	2.999	3.000	2.998	2.998	3.000	3.002	2.998	3.003	2.997	3.001	3.005
End Members (%)																		
Fo	90.4	92.4	90.7	91.2	92.2	92.4	92.0	92.5	92.5	92.3	92.8	90.9	89.0	90.0	88.7	89.1	88.6	89.8
Fa	9.6	7.6	9.3	8.8	7.8	7.6	8.0	7.5	7.5	7.7	7.2	9.1	11.0	10.0	11.3	10.9	11.4	10.2

Crystal textural style is abbreviated: porph. (porphyroclast), cumu. (cumulus), def. (deformed), mgb. (modified grain boundaries)
Note: Other phases (cpx, chr) were also analyzed on certain sections, such that "Cluster" refers to a specific location on each section

Appendix II (continued): Olivine compositions from olivine-bearing ultramafic lithologies of the Turnagain intrusion

Rock type:	Wehrlite		Wehrlite												Wehrlite			
Sample:	04ES-10-06-01		04ES-16-08-01												04ES-11-03-03			
Cluster:	4	3	2				4			5					2			
Style:	porph.	porph.	porph.	cumu.	cumu.	cumu.	cumu.	cumu.	cumu.	cumu.	cumu.	cumu.	cumu.	cumu.	porph.	porph.	porph.	porph.
Zone:	core	rim	mid	rim	mid	mid	core	rim	mid	core	rim	mid	mid	core	rim	mid	mid	mid
Oxides (wt. %)																		
SiO_2	40.43	40.42	40.55	40.61	40.47	40.38	40.23	40.07	40.51	40.68	40.71	41.00	40.39	40.45	40.37	40.07	40.23	40.38
Cr_2O_3	0.02	0.00	0.00	0.04	0.07	0.02	0.00	0.03	0.01	0.02	0.03	0.01	0.04	0.00	0.02	0.04	0.00	0.02
FeO	11.16	11.13	11.04	11.67	11.52	11.66	11.67	11.11	11.69	11.14	10.95	10.13	11.28	10.65	12.93	13.15	13.51	13.08
MnO	0.21	0.18	0.20	0.21	0.18	0.18	0.22	0.21	0.21	0.21	0.26	0.25	0.25	0.23	0.24	0.27	0.21	0.32
MgO	47.50	47.54	47.79	47.23	47.36	47.06	47.32	46.86	47.62	47.74	47.91	48.98	47.68	48.12	46.06	46.31	45.86	46.15
NiO	0.26	0.35	0.35	0.16	0.13	0.23	0.18	0.16	0.22	0.22	0.09	0.31	0.23	0.17	0.19	0.10	0.16	0.15
CaO	0.02	0.02	0.04	0.05	0.14	0.05	0.08	0.05	0.09	0.06	0.03	0.03	0.06	0.08	0.01	0.01	0.03	0.03
Total	99.60	99.63	99.98	99.96	99.88	99.59	99.69	98.49	100.34	100.07	99.99	100.72	99.91	99.69	99.82	99.96	99.99	100.13
Cations (p.f.u.)																		
Si	1.002	1.001	1.001	1.004	1.001	1.003	0.998	1.004	0.999	1.002	1.003	1.000	0.998	0.999	1.005	0.998	1.003	1.003
Cr	0.000	0.000	0.000	0.001	0.001	0.000	0.000	0.001	0.000	0.000	0.001	0.000	0.001	0.000	0.000	0.001	0.000	0.000
Fe	0.231	0.231	0.228	0.241	0.238	0.242	0.242	0.233	0.241	0.230	0.226	0.207	0.233	0.220	0.269	0.274	0.282	0.272
Mn	0.004	0.004	0.004	0.004	0.004	0.004	0.005	0.004	0.004	0.004	0.006	0.005	0.005	0.005	0.005	0.006	0.004	0.007
Mg	1.754	1.756	1.758	1.740	1.746	1.742	1.751	1.749	1.750	1.754	1.759	1.781	1.757	1.772	1.710	1.720	1.704	1.710
Ni	0.005	0.007	0.007	0.003	0.003	0.005	0.004	0.003	0.004	0.004	0.002	0.006	0.004	0.003	0.004	0.002	0.003	0.003
Ca	0.001	0.001	0.001	0.001	0.004	0.001	0.002	0.001	0.002	0.002	0.001	0.001	0.002	0.002	0.000	0.000	0.001	0.001
Total	2.998	2.999	2.999	2.995	2.996	2.997	3.002	2.995	3.001	2.997	2.996	3.000	3.000	3.001	2.994	3.000	2.997	2.996
End Members (%)																		
Fo	88.4	88.4	88.5	87.8	88.0	87.8	87.8	88.3	87.9	88.4	88.6	89.6	88.3	89.0	86.4	86.3	85.8	86.3
Fa	11.6	11.6	11.5	12.2	12.0	12.2	12.2	11.7	12.1	11.6	11.4	10.4	11.7	11.0	13.6	13.7	14.2	13.7

Crystal textural style is abbreviated: porph. (porphyroclast), cumu. (cumulus), def. (deformed), mgb. (modified grain boundaries)
Note: Other phases (cpx, chr) were also analyzed on certain sections, such that "Cluster" refers to a specific location on each section

Appendix II (continued): Olivine compositions from olivine-bearing ultramafic lithologies of the Turnagain intrusion

Rock type:	Wehrlite								Wehrlite								
Sample:	04ES-11-03-03								04ES-09-01-01								
Cluster:	2	4				5				1				3			4
Style:	porph.	porph.	porph.	porph.	porph.	porph.	porph.	porph.	porph.	porph.	porph.	porph.	porph.	cumu.	cumu.	cumu.	cumu.	porph.
Zone:	core	rim	mid	mid	core	rim	mid	mid	core	rim	mid	mid	core	rim	mid	mid	core	rim
Oxides (wt. %)																		
SiO_2	39.82	40.18	40.68	40.93	40.58	40.17	40.03	40.10	40.17	40.06	39.91	40.02	40.23	40.29	39.86	39.81	39.88	39.98
Cr_2O_3	0.01	0.04	0.00	0.02	0.02	0.00	0.00	0.01	0.00	0.00	0.00	0.02	0.00	0.00	0.06	0.03	0.00	0.00
FeO	12.93	12.45	11.91	10.13	12.28	13.54	13.48	13.55	13.90	12.69	13.18	12.98	12.98	9.51	12.40	12.77	12.97	13.12
MnO	0.55	0.32	0.36	0.34	0.29	0.29	0.26	0.28	0.26	0.28	0.18	0.24	0.19	0.22	0.27	0.24	0.30	0.32
MgO	45.48	46.48	46.95	47.90	46.62	45.53	45.58	45.24	45.47	45.82	45.41	45.79	45.67	44.44	45.76	46.11	45.71	45.50
NiO	0.32	0.15	0.10	0.16	0.18	0.12	0.16	0.21	0.16	0.20	0.25	0.20	0.22	0.19	0.20	0.22	0.26	0.20
CaO	0.04	0.01	0.02	0.04	0.02	0.04	0.04	0.01	0.03	0.05	0.05	0.03	0.01	0.01	0.04	0.01	0.02	0.11
Total	99.14	99.64	100.01	99.51	99.99	99.69	99.54	99.41	100.00	99.09	98.98	99.28	99.31	94.67	98.59	99.18	99.15	99.23
Cations (p.f.u.)																		
Si	1.002	1.001	1.006	1.009	1.006	1.005	1.003	1.006	1.003	1.005	1.004	1.003	1.007	1.039	1.004	0.999	1.002	1.004
Cr	0.000	0.001	0.000	0.000	0.000	0.000	0.000	0.000	0.000	0.000	0.000	0.000	0.000	0.000	0.001	0.001	0.000	0.000
Fe	0.272	0.259	0.246	0.209	0.254	0.283	0.282	0.284	0.290	0.266	0.277	0.272	0.272	0.205	0.261	0.268	0.273	0.275
Mn	0.012	0.007	0.007	0.007	0.006	0.006	0.005	0.006	0.006	0.006	0.004	0.005	0.004	0.005	0.006	0.005	0.006	0.007
Mg	1.705	1.726	1.731	1.760	1.723	1.698	1.702	1.692	1.693	1.713	1.704	1.711	1.705	1.708	1.717	1.724	1.712	1.703
Ni	0.006	0.003	0.002	0.003	0.004	0.003	0.003	0.004	0.003	0.004	0.005	0.004	0.004	0.004	0.004	0.004	0.005	0.004
Ca	0.001	0.000	0.000	0.001	0.000	0.001	0.001	0.000	0.001	0.001	0.001	0.001	0.000	0.000	0.001	0.000	0.001	0.003
Total	2.998	2.997	2.994	2.990	2.993	2.995	2.997	2.994	2.997	2.995	2.996	2.996	2.993	2.961	2.994	3.000	2.998	2.996
End Members (%)																		
Fo	86.2	86.9	87.5	89.4	87.1	85.7	85.8	85.6	85.4	86.6	86.0	86.3	86.2	89.3	86.8	86.6	86.3	86.1
Fa	13.8	13.1	12.5	10.6	12.9	14.3	14.2	14.4	14.6	13.4	14.0	13.7	13.8	10.7	13.2	13.4	13.7	13.9

Crystal textural style is abbreviated: porph. (porphyroclast), cumu. (cumulus), def. (deformed), mgb. (modified grain boundaries)
Note: Other phases (cpx, chr) were also analyzed on certain sections, such that "Cluster" refers to a specific location on each section

Appendix II (continued): Olivine compositions from olivine-bearing ultramafic lithologies of the Turnagain intrusion

Rock type:	Wehrlite			Wehrlite													Olivine Cpxite	
Sample:	04ES-09-01-01			04ES-15-01-05													04ES-06-06-01	
Cluster:	4			1			4					5					1	
Style:	porph.	porph.	porph.	def.	def.	def.	def.	cumu.	cumu.	cumu.	cumu.	cumu.	mgb.	mgb.	mgb.	mgb.	cumu.	cumu.
Zone:	mid	mid	core	rim	mid	mid	core	rim	mid	mid	mid	core	rim	mid	mid	core	rim	mid
Oxides (wt. %)																		
SiO_2	39.83	39.78	39.92	40.53	40.69	40.72	40.49	40.77	40.45	40.33	40.67	40.76	40.97	40.51	40.50	40.79	39.92	40.09
Cr_2O_3	0.00	0.00	0.00	0.02	0.02	0.01	0.00	0.00	0.04	0.00	0.00	0.00	0.04	0.00	0.00	0.00	0.04	0.02
FeO	12.78	12.40	13.07	10.79	11.50	10.48	11.17	11.21	10.92	11.67	11.37	11.50	8.10	10.95	10.68	10.28	12.96	12.87
MnO	0.21	0.24	0.19	0.22	0.18	0.15	0.24	0.22	0.23	0.21	0.22	0.21	0.28	0.24	0.19	0.24	0.25	0.23
MgO	45.66	45.72	45.64	47.80	47.44	48.30	47.53	48.32	48.08	47.69	47.73	47.79	49.85	47.90	47.97	48.27	46.30	46.01
NiO	0.18	0.25	0.19	0.27	0.29	0.29	0.38	0.23	0.28	0.27	0.32	0.32	0.18	0.25	0.27	0.29	0.10	0.04
CaO	0.00	0.02	0.02	0.02	0.08	0.05	0.06	0.04	0.04	0.07	0.07	0.07	0.04	0.04	0.08	0.05	0.03	0.04
Total	98.67	98.41	99.04	99.65	100.22	100.00	99.88	100.79	100.04	100.24	100.39	100.65	99.46	99.89	99.69	99.92	99.61	99.31
Cations (p.f.u.)																		
Si	1.004	1.004	1.003	1.002	1.003	1.001	1.001	0.998	0.997	0.996	1.001	1.001	1.002	1.000	1.001	1.003	0.997	1.003
Cr	0.000	0.000	0.000	0.000	0.000	0.000	0.000	0.000	0.001	0.000	0.000	0.000	0.001	0.000	0.000	0.000	0.001	0.000
Fe	0.269	0.262	0.275	0.223	0.237	0.216	0.231	0.229	0.225	0.241	0.234	0.236	0.166	0.226	0.221	0.211	0.271	0.269
Mn	0.005	0.005	0.004	0.005	0.004	0.003	0.005	0.005	0.005	0.004	0.005	0.004	0.006	0.005	0.004	0.005	0.005	0.005
Mg	1.715	1.720	1.710	1.762	1.744	1.771	1.752	1.764	1.767	1.756	1.751	1.749	1.818	1.763	1.767	1.770	1.724	1.716
Ni	0.004	0.005	0.004	0.005	0.006	0.006	0.007	0.005	0.006	0.005	0.006	0.006	0.004	0.005	0.005	0.006	0.002	0.001
Ca	0.000	0.001	0.001	0.001	0.002	0.001	0.002	0.001	0.001	0.002	0.002	0.002	0.001	0.001	0.002	0.001	0.001	0.001
Total	2.996	2.996	2.997	2.997	2.996	2.998	2.999	3.002	3.001	3.004	2.999	2.999	2.997	3.000	2.999	2.997	3.001	2.996
End Members (%)																		
Fo	86.4	86.8	86.2	88.8	88.0	89.1	88.4	88.5	88.7	87.9	88.2	88.1	91.6	88.6	88.9	89.3	86.4	86.4
Fa	13.6	13.2	13.8	11.2	12.0	10.9	11.6	11.5	11.3	12.1	11.8	11.9	8.4	11.4	11.1	10.7	13.6	13.6

Crystal textural style is abbreviated: porph. (porphyroclast), cumu. (cumulus), def. (deformed), mgb. (modified grain boundaries)
Note: Other phases (cpx, chr) were also analyzed on certain sections, such that "Cluster" refers to a specific location on each section

Appendix II (continued): Olivine compositions from olivine-bearing ultramafic lithologies of the Turnagain intrusion

Rock type:	Olivine Clinopyroxenite											Olivine Clinopyroxenite						
Sample:	04ES-06-06-01											05ES-05-01-01						
Cluster:	1			3				4				3			4			
Style:	cumu.	cumu.	cumu.	cumu.	cumu.	cumu.	cumu.	cumu.	cumu.	cumu.	cumu.	cumu.	cumu.	cumu.	cumu.	cumu.	cumu.	cumu.
Zone:	mid	mid	core	rim	mid	mid	core	rim	mid	mid	mid	core	rim	mid	core	rim	mid	core
Oxides (wt. %)																		
SiO_2	40.38	40.13	40.32	40.36	40.44	40.13	40.28	40.35	40.35	40.24	40.44	40.23	39.14	39.25	39.23	39.22	39.43	39.17
Cr_2O_3	0.02	0.00	0.02	0.02	0.05	0.00	0.02	0.05	0.04	0.00	0.00	0.00	0.00	0.00	0.01	0.00	0.01	0.02
FeO	12.65	12.36	13.14	12.80	12.15	12.72	12.98	12.66	12.60	12.76	12.68	12.89	15.51	15.55	15.59	14.95	15.63	15.61
MnO	0.24	0.22	0.21	0.26	0.33	0.22	0.23	0.21	0.25	0.21	0.22	0.26	0.30	0.26	0.24	0.23	0.26	0.22
MgO	46.43	46.41	46.53	46.25	46.78	46.66	46.34	46.13	46.58	45.79	45.66	46.39	44.13	44.10	44.02	44.46	44.21	44.25
NiO	0.07	0.10	0.05	0.08	0.09	0.06	0.06	0.03	0.03	0.09	0.10	0.10	0.13	0.12	0.11	0.08	0.08	0.14
CaO	0.03	0.03	0.05	0.03	0.02	0.01	0.01	0.03	0.03	0.02	0.35	0.04	0.06	0.02	0.00	0.03	0.01	0.02
Total	99.83	99.24	100.33	99.79	99.86	99.81	99.92	99.46	99.87	99.11	99.44	99.90	99.27	99.29	99.19	98.98	99.62	99.44
Cations (p.f.u.)																		
Si	1.004	1.003	1.000	1.005	1.003	0.999	1.002	1.006	1.002	1.008	1.010	1.001	0.994	0.996	0.997	0.996	0.997	0.993
Cr	0.000	0.000	0.000	0.000	0.001	0.000	0.000	0.001	0.001	0.000	0.000	0.000	0.000	0.000	0.000	0.000	0.000	0.000
Fe	0.263	0.258	0.272	0.266	0.252	0.265	0.270	0.264	0.262	0.267	0.265	0.268	0.329	0.330	0.331	0.318	0.331	0.331
Mn	0.005	0.005	0.005	0.005	0.007	0.005	0.005	0.004	0.005	0.004	0.005	0.005	0.006	0.005	0.005	0.005	0.006	0.005
Mg	1.721	1.729	1.720	1.716	1.730	1.731	1.718	1.715	1.725	1.710	1.700	1.721	1.671	1.669	1.667	1.683	1.667	1.673
Ni	0.001	0.002	0.001	0.002	0.002	0.001	0.001	0.001	0.001	0.002	0.002	0.002	0.003	0.002	0.002	0.002	0.002	0.003
Ca	0.001	0.001	0.001	0.001	0.001	0.000	0.000	0.001	0.001	0.000	0.009	0.001	0.002	0.001	0.000	0.001	0.000	0.001
Total	2.995	2.997	2.999	2.995	2.995	3.001	2.997	2.992	2.996	2.992	2.990	2.999	3.006	3.004	3.003	3.004	3.003	3.006
End Members (%)																		
Fo	86.7	87.0	86.3	86.6	87.3	86.7	86.4	86.7	86.8	86.5	86.5	86.5	83.5	83.5	83.4	84.1	83.4	83.5
Fa	13.3	13.0	13.7	13.4	12.7	13.3	13.6	13.3	13.2	13.5	13.5	13.5	16.5	16.5	16.6	15.9	16.6	16.5

Crystal textural style is abbreviated: porph. (porphyroclast), cumu. (cumulus), def. (deformed), mgb. (modified grain boundaries)
Note: Other phases (cpx, chr) were also analyzed on certain sections, such that "Cluster" refers to a specific location on each section

Appendix II (continued): Olivine compositions from olivine-bearing ultramafic lithologies of the Turnagain intrusion

Rock type:	Olivine Clinopyroxenite							Olivine Clinopyroxenite		
Sample:	04ES-01-04-01							04ES-01-04-01		
Cluster:	5	1			3			4		
Style:	cumu.	cumu.	cumu.	cumu.	cumu.	cumu.	cumu.	cumu.	cumu.	cumu.
Zone:	mid	rim	mid	core	rim	mid	core	rim	mid	core
Oxides (wt. %)										
SiO_2	39.23	40.44	40.18	40.31	40.52	40.36	40.10	40.19	39.94	40.43
Cr_2O_3	0.02	0.01	0.01	0.02	0.00	0.00	0.05	0.00	0.00	0.02
FeO	15.67	12.27	12.73	12.75	11.37	12.47	12.41	12.94	12.76	12.88
MnO	0.24	0.16	0.22	0.21	0.22	0.21	0.19	0.18	0.21	0.21
MgO	43.96	46.38	46.67	46.55	47.29	46.59	46.97	46.30	46.59	46.61
NiO	0.12	0.09	0.11	0.05	0.07	0.02	0.06	0.16	0.07	0.12
CaO	0.03	0.00	0.03	0.05	0.02	0.02	0.05	0.01	0.04	0.03
Total	99.27	99.35	99.95	99.95	99.50	99.68	99.82	99.78	99.61	100.30
Cations (p.f.u.)										
Si	0.996	1.008	0.999	1.001	1.005	1.004	0.996	1.001	0.997	1.001
Cr	0.000	0.000	0.000	0.000	0.000	0.000	0.001	0.000	0.000	0.000
Fe	0.333	0.256	0.265	0.265	0.236	0.259	0.258	0.270	0.266	0.267
Mn	0.005	0.003	0.005	0.004	0.005	0.004	0.004	0.004	0.004	0.004
Mg	1.665	1.723	1.729	1.724	1.748	1.728	1.740	1.720	1.733	1.721
Ni	0.002	0.002	0.002	0.001	0.001	0.000	0.001	0.003	0.001	0.002
Ca	0.001	0.000	0.001	0.001	0.000	0.001	0.001	0.000	0.001	0.001
Total	3.003	2.992	3.001	2.998	2.995	2.996	3.002	2.998	3.003	2.998
End Members (%)										
Fo	83.3	87.1	86.7	86.7	88.1	86.9	87.1	86.4	86.7	86.6
Fa	16.7	12.9	13.3	13.3	11.9	13.1	12.9	13.6	13.3	13.4

Crystal textural style is abbreviated: porph. (porphyroclast), cumu. (cumulus), def. (deformed), mgb. (modified grain boundaries)
Note: Other phases (cpx, chr) were also analyzed on certain sections, such that "Cluster" refers to a specific location on each section

Appendix III: Clinopyroxene compositions from clinopyroxene-bearing ultramafic lithologies of the Turnagain intrusion

Rock Type:	Dunite	Wehrlite										Wehrlite						
Sample:	04ES-08-01-01	04ES-10-06-01										04ES-15-01-05						
Cluster:	n/a	1			2			3				2			3			5
Style:	inter.	inter.	cumu.	cumu.	cumu.	cumu.	cumu.	cumu.	cumu.	cumu.	cumu.	inter.	inter.	inter.	inter.	inter.	inter.	inter.
Zone:	mid	core	rim	mid	core	rim	mid	core	rim	mid	core	rim	mid	core	rim	mid	core	rim
Oxides (wt. %)																		
SiO_2	54.46	52.28	54.02	53.50	54.01	52.14	53.96	53.60	53.69	53.09	53.69	52.48	53.64	53.61	53.16	54.32	53.53	52.76
TiO_2	0.07	0.09	0.17	0.16	0.19	0.14	0.15	0.15	0.15	0.16	0.16	0.27	0.30	0.34	0.39	0.25	0.30	0.26
Al_2O_3	0.92	0.90	1.17	1.11	1.10	1.06	1.17	1.32	1.10	1.03	1.10	1.54	1.33	1.45	1.45	1.05	1.35	1.22
Cr_2O_3	0.47	0.61	0.58	0.73	0.68	0.65	0.65	0.82	0.51	0.43	0.57	0.85	0.88	0.85	0.87	0.70	0.94	0.76
FeO*	2.38	2.79	3.03	2.70	2.73	4.93	2.88	2.89	3.61	4.60	3.19	2.28	2.48	2.43	2.41	2.67	2.85	2.59
MnO	0.06	0.03	0.07	0.10	0.13	0.09	0.11	0.09	0.14	0.10	0.10	0.07	0.11	0.04	0.08	0.09	0.05	0.04
MgO	16.92	16.59	17.66	17.53	17.60	17.39	17.52	17.46	17.42	16.78	17.44	17.90	17.22	17.06	17.00	17.63	17.33	17.45
CaO	24.49	25.03	23.24	23.69	23.25	22.49	23.16	23.12	22.80	22.16	22.94	23.11	23.72	23.80	24.04	23.46	23.40	23.59
Na_2O	0.37	0.41	0.25	0.29	0.28	0.26	0.26	0.31	0.23	0.24	0.26	0.23	0.26	0.28	0.28	0.25	0.29	0.26
Total	100.15	98.73	100.20	99.81	99.98	99.14	99.87	99.75	99.66	98.60	99.46	98.73	99.94	99.87	99.68	100.42	100.05	98.92
Cations (p.f.u.)																		
Si	1.964	1.956	1.962	1.967	1.968	1.959	1.966	1.972	1.968	1.963	1.978	1.963	1.978	1.974	1.975	1.972	1.984	1.972
Ti	0.005	0.004	0.004	0.005	0.004	0.004	0.004	0.004	0.004	0.005	0.003	0.003	0.004	0.004	0.003	0.003	0.002	0.004
$Al^{(IV)}$	0.036	0.044	0.038	0.033	0.032	0.041	0.034	0.028	0.032	0.037	0.022	0.037	0.022	0.026	0.025	0.028	0.016	0.028
$Al^{(VI)}$	0.014	0.004	0.008	0.014	0.018	0.016	0.014	0.017	0.015	0.006	0.011	0.000	0.010	0.010	0.013	0.013	0.005	0.019
Cr	0.017	0.021	0.021	0.019	0.019	0.024	0.015	0.013	0.016	0.016	0.019	0.017	0.014	0.011	0.014	0.017	0.008	0.018
Fe^{3+}	0.004	0.019	0.009	0.000	0.000	0.004	0.005	0.000	0.001	0.012	0.000	0.021	0.000	0.004	0.000	0.000	0.003	0.000
Fe^{2+}	0.088	0.063	0.073	0.083	0.088	0.084	0.106	0.143	0.097	0.111	0.099	0.088	0.087	0.087	0.098	0.098	0.094	0.103
Mn	0.002	0.003	0.002	0.004	0.003	0.003	0.004	0.003	0.003	0.004	0.004	0.004	0.004	0.004	0.004	0.002	0.003	0.004
Mg	0.958	0.956	0.940	0.956	0.953	0.951	0.951	0.929	0.953	0.969	0.954	1.002	0.955	0.940	0.940	0.947	0.947	0.949
Ca	0.905	0.928	0.938	0.907	0.905	0.905	0.895	0.882	0.901	0.874	0.899	0.869	0.916	0.935	0.920	0.912	0.935	0.891
Na	0.009	0.010	0.009	0.010	0.009	0.011	0.008	0.009	0.009	0.008	0.007	0.007	0.007	0.007	0.006	0.008	0.004	0.007
Total	4.002	4.010	4.004	3.999	3.998	4.002	4.002	3.999	4.000	4.006	3.996	4.011	3.998	4.002	3.999	4.000	4.002	3.995
End Members (%)																		
Wo	49.1	50.9	46.4	47.7	46.6	45.5	46.5	46.7	45.8	45.1	46.2	47.1	47.8	48.2	48.7	46.9	47.1	47.9
En	47.2	47.0	49.1	49.1	49.1	49.0	49.0	49.0	48.7	47.5	48.8	50.8	48.3	48.0	47.9	49.0	48.6	49.3
Fs	3.7	2.2	4.5	3.2	4.3	5.5	4.5	4.3	5.4	7.3	5.0	2.1	3.9	3.8	3.5	4.2	4.3	2.8
Mg#	0.936	0.927	0.920	0.898	0.919	0.901	0.870	0.907	0.896	0.910	0.906	0.918	0.915	0.914	0.905	0.907	0.909	0.903

Crystal textural style is abbreviated: cumu. (cumulus), inter. (intercumulus)
Note: Other phases (ol, chr, mt) were also analyzed on certain sections, such that "Cluster" refers to a specific location on each thin section
* Total Fe

Appendix III (continued): Clinopyroxene compositions from clinopyroxene-bearing ultramafic lithologies of the Turnagain intrusion

Rock Type:	Wehrlite		Wehrlite									Wehrlite							
Sample:	04ES-15-01-05		04ES-16-08-01									04ES-11-03-03							
Cluster:	5		1			3			5			1			3		6		
Style:	inter.	inter.	inter.	inter.	inter.	inter.	inter.	inter.	inter.	inter.	inter.	inter.	inter.	inter.	inter.	inter.	inter.	inter.	inter.
Zone:	mid	core	rim	mid	core	rim	mid	core	rim	mid	core	rim	mid	core	mid	core	rim	mid	core
Oxides (wt. %)																			
SiO_2	53.60	53.39	54.36	54.21	53.91	52.85	53.94	53.35	53.43	53.17	53.72	54.14	54.61	54.35	54.16	54.60	54.20	54.41	54.03
TiO_2	0.33	0.31	0.13	0.10	0.19	0.16	0.19	0.18	0.16	0.24	0.27	0.14	0.16	0.13	0.14	0.12	0.14	0.17	0.19
Al_2O_3	1.40	1.38	0.68	0.51	1.07	1.31	0.95	1.01	1.05	1.17	1.20	0.68	0.78	0.71	0.88	0.77	0.78	0.95	0.93
Cr_2O_3	1.10	0.88	0.50	0.54	0.71	0.75	0.79	0.73	0.64	0.75	0.68	0.46	0.42	0.37	0.60	0.50	0.42	0.57	0.53
FeO*	2.54	2.43	2.93	3.22	3.70	2.99	3.12	3.23	2.93	3.63	3.53	3.18	2.86	2.70	3.30	3.28	3.02	3.52	3.54
MnO	0.07	0.05	0.08	0.05	0.10	0.09	0.12	0.11	0.09	0.10	0.13	0.13	0.09	0.15	0.12	0.08	0.12	0.12	0.17
MgO	17.32	17.31	17.84	18.16	17.37	18.33	17.63	17.37	17.95	17.10	17.14	17.35	17.48	17.68	17.60	17.70	17.61	17.55	17.64
CaO	23.68	23.58	23.56	23.17	23.31	22.33	23.64	23.02	22.98	22.90	23.15	24.07	24.04	24.18	23.08	23.05	23.61	22.61	22.67
Na_2O	0.30	0.33	0.24	0.22	0.22	0.24	0.26	0.25	0.23	0.25	0.23	0.20	0.20	0.20	0.30	0.29	0.27	0.29	0.29
Total	100.35	99.66	100.33	100.19	100.57	99.06	100.63	99.26	99.48	99.32	100.05	100.36	100.64	100.47	100.18	100.38	100.17	100.19	100.00
Cations (p.f.u.)																			
Si	1.969	1.967	1.964	1.974	1.936	1.956	1.956	1.947	1.969	1.952	1.947	1.949	1.953	1.961	1.961	1.965	1.960	1.961	1.953
Ti	0.005	0.004	0.005	0.003	0.007	0.008	0.009	0.011	0.007	0.008	0.007	0.009	0.009	0.006	0.006	0.005	0.007	0.006	0.007
$Al^{(IV)}$	0.031	0.033	0.036	0.026	0.064	0.044	0.044	0.053	0.031	0.048	0.053	0.051	0.047	0.039	0.039	0.035	0.040	0.039	0.047
$Al^{(VI)}$	0.011	0.024	0.011	0.012	0.004	0.013	0.018	0.010	0.014	0.010	0.000	0.009	0.013	0.010	0.010	0.005	0.009	0.004	0.006
Cr	0.019	0.020	0.020	0.018	0.025	0.025	0.025	0.025	0.020	0.027	0.022	0.032	0.025	0.015	0.014	0.012	0.015	0.010	0.017
Fe^{3+}	0.000	0.000	0.002	0.000	0.029	0.000	0.000	0.007	0.000	0.004	0.025	0.003	0.003	0.010	0.015	0.016	0.012	0.021	0.019
Fe^{2+}	0.107	0.103	0.106	0.102	0.042	0.076	0.074	0.067	0.081	0.083	0.055	0.074	0.071	0.113	0.108	0.102	0.120	0.095	0.107
Mn	0.004	0.003	0.002	0.003	0.002	0.003	0.001	0.002	0.003	0.002	0.001	0.002	0.002	0.005	0.004	0.005	0.004	0.003	0.004
Mg	0.955	0.956	0.953	0.951	0.984	0.937	0.928	0.928	0.952	0.943	0.960	0.939	0.944	0.928	0.939	0.937	0.946	0.934	0.936
Ca	0.891	0.874	0.895	0.903	0.914	0.927	0.930	0.944	0.911	0.914	0.933	0.923	0.924	0.909	0.901	0.917	0.885	0.927	0.903
Na	0.008	0.009	0.007	0.008	0.008	0.009	0.010	0.010	0.009	0.010	0.009	0.011	0.012	0.009	0.011	0.008	0.009	0.009	0.010
Total	4.000	3.995	4.001	3.999	4.014	3.999	3.996	4.003	3.996	4.002	4.013	4.001	4.002	4.005	4.007	4.008	4.006	4.011	4.009
End Members (%)																			
Wo	47.7	47.7	46.7	45.8	46.5	45.3	47.1	46.5	46.2	46.4	46.5	47.8	47.5	47.9	46.1	45.9	47.0	45.4	45.4
En	48.5	48.7	49.2	49.9	48.2	51.7	48.9	48.8	50.2	48.2	47.9	48.0	48.1	48.7	48.9	49.0	48.8	49.1	49.2
Fs	3.8	3.6	4.1	4.3	5.3	3.0	4.0	4.6	3.6	5.4	5.5	4.2	4.4	3.4	5.0	5.1	4.2	5.5	5.4
Mg #	0.898	0.930	0.903	0.903	0.902	0.960	0.927	0.928	0.936	0.921	0.918	0.945	0.927	0.931	0.894	0.899	0.903	0.888	0.910

Crystal textural style is abbreviated: cumu. (cumulus), inter. (intercumulus)
Note: Other phases (ol, chr, mt) were also analyzed on certain sections, such that "Cluster" refers to a specific location on each thin section
* Total Fe

Appendix III (continued): Clinopyroxene compositions from clinopyroxene-bearing ultramafic lithologies of the Turnagain intrusion

Rock Type:	Wehrlite						Olivine Clinopyroxenite												
Sample:	04ES-09-01-01						04ES-06-06-01												
Cluster:	2		5			6	2				5						6		
Style:	inter.	inter.	inter.	inter.	inter.	inter.	inter.	inter.	cumu.	cumu.	cumu.	cumu.	cumu.	cumu.	cumu.	cumu.	cumu.	cumu.	cumu.
Zone:	mid	core	rim	mid	core	rim	mid	core	rim	mid	core	rim	mid	mid	mid	core	rim	mid	mid
Oxides (wt. %)																			
SiO_2	53.50	53.99	54.78	54.27	54.42	54.33	54.31	54.37	53.76	54.38	53.83	54.19	54.21	53.96	54.64	54.14	54.16	53.96	54.04
TiO_2	0.24	0.24	0.08	0.12	0.06	0.10	0.17	0.12	0.19	0.11	0.12	0.16	0.14	0.11	0.08	0.14	0.20	0.15	0.18
Al_2O_3	1.16	0.86	0.25	0.36	0.41	0.32	0.49	0.34	1.00	0.78	0.85	0.74	0.84	0.88	0.50	1.08	0.98	1.33	1.09
Cr_2O_3	0.62	0.46	0.13	0.16	0.20	0.16	0.26	0.15	0.56	0.66	0.60	0.48	0.40	0.50	0.28	0.61	0.65	0.70	0.70
FeO*	3.17	3.29	2.06	2.83	3.02	2.22	2.57	2.33	4.03	3.27	3.56	2.86	3.02	3.19	3.21	3.39	3.51	3.39	3.56
MnO	0.14	0.12	0.10	0.09	0.08	0.08	0.12	0.11	0.14	0.12	0.12	0.13	0.12	0.12	0.11	0.14	0.15	0.10	0.07
MgO	17.19	17.08	17.46	17.66	17.40	17.59	17.64	17.49	17.80	17.59	18.43	17.54	17.32	17.24	17.49	17.47	17.62	17.60	17.59
CaO	23.35	23.71	25.03	24.11	24.18	24.67	24.30	24.69	22.34	23.06	22.25	23.43	23.97	23.47	24.03	22.83	22.87	22.38	22.98
Na_2O	0.26	0.22	0.05	0.12	0.13	0.11	0.14	0.12	0.23	0.20	0.21	0.20	0.19	0.18	0.12	0.19	0.23	0.26	0.20
Total	99.61	99.96	99.94	99.71	99.89	99.58	100.00	99.72	100.05	100.16	99.97	99.74	100.21	99.66	100.47	99.99	100.34	99.87	100.41
Cations (p.f.u.)																			
Si	1.957	1.964	1.958	1.958	1.974	1.973	1.961	1.944	1.959	1.962	1.958	1.958	1.962	1.982	1.976	1.976	1.978	1.966	1.970
Ti	0.006	0.006	0.007	0.005	0.004	0.003	0.005	0.004	0.005	0.005	0.005	0.007	0.007	0.002	0.003	0.003	0.003	0.003	0.002
$Al^{[IV]}$	0.043	0.036	0.042	0.042	0.026	0.027	0.039	0.056	0.041	0.038	0.042	0.042	0.038	0.018	0.024	0.024	0.022	0.034	0.030
$Al^{[VI]}$	0.006	0.012	0.010	0.011	0.004	0.000	0.006	0.001	0.000	0.006	0.003	0.009	0.013	0.021	0.011	0.010	0.008	0.002	0.002
Cr	0.016	0.012	0.016	0.012	0.014	0.015	0.020	0.022	0.023	0.021	0.019	0.022	0.020	0.013	0.018	0.020	0.017	0.026	0.028
Fe^{3+}	0.019	0.011	0.013	0.017	0.009	0.014	0.010	0.033	0.017	0.009	0.020	0.007	0.000	0.000	0.000	0.000	0.000	0.010	0.006
Fe^{2+}	0.111	0.111	0.122	0.115	0.080	0.084	0.103	0.059	0.077	0.090	0.070	0.105	0.108	0.072	0.095	0.106	0.100	0.091	0.091
Mn	0.005	0.004	0.003	0.005	0.003	0.001	0.003	0.003	0.004	0.004	0.003	0.003	0.004	0.002	0.003	0.004	0.002	0.005	0.004
Mg	0.950	0.928	0.951	0.956	0.966	0.985	0.942	1.005	0.954	0.953	0.980	0.939	0.933	0.918	0.968	0.966	0.981	0.971	0.974
Ca	0.886	0.912	0.875	0.879	0.917	0.904	0.908	0.880	0.920	0.907	0.902	0.904	0.906	0.955	0.891	0.881	0.880	0.888	0.887
Na	0.011	0.010	0.010	0.008	0.008	0.008	0.008	0.009	0.009	0.009	0.008	0.009	0.008	0.013	0.008	0.008	0.007	0.009	0.009
Total	4.010	4.005	4.007	4.009	4.004	4.015	4.005	4.016	4.009	4.004	4.010	4.004	3.999	3.997	3.998	3.998	3.999	4.005	4.003
End Members (%)																			
Wo	47.1	47.4	49.1	47.6	47.8	48.7	48.0	48.8	44.7	46.0	44.4	46.8	47.6	47.0	47.3	45.9	45.6	45.2	45.8
En	48.2	47.5	47.7	48.5	47.8	48.3	48.5	48.1	49.6	48.9	51.1	48.7	47.9	48.0	47.9	48.8	48.9	49.5	48.8
Fs	4.7	5.1	3.2	3.9	4.4	3.0	3.5	3.2	5.7	5.1	4.5	4.5	4.5	5.0	4.8	5.3	5.5	5.4	5.4
Mg #	0.895	0.894	0.886	0.893	0.922	0.919	0.903	0.942	0.926	0.931	0.905	0.899	0.956	0.929	0.909	0.900	0.905	0.913	0.910

Crystal textural style is abbreviated: cumu. (cumulus), inter. (intercumulus)
Note: Other phases (ol, chr, mt) were also analyzed on certain sections, such that "Cluster" refers to a specific location on each thin section
* Total Fe

Appendix III (continued): Clinopyroxene compositions from clinopyroxene-bearing ultramafic lithologies of the Turnagain intrusion

Rock Type:	Olivine Clinopyroxenite											Olivine Clinopyroxenite							
Sample:	05ES-05-01-01											04ES-01-04-01							
Cluster:	6	1				2			6			2			5			6	
Style:	cumu.	cumu.	cumu.	cumu.	cumu.	cumu.	cumu.	cumu.	cumu.	cumu.	cumu.	inter.	inter.	inter.	inter.	inter.	inter.	inter.	inter.
Zone:	core	rim	mid	mid	core	rim	mid	core	rim	mid	core	rim	mid	core	rim	mid	core	rim	mid
Oxides (wt. %)																			
SiO_2	53.92	53.83	53.96	53.52	53.33	53.57	53.33	53.52	53.91	53.61	53.29	53.84	54.76	54.56	54.27	54.26	54.16	54.39	54.23
TiO_2	0.12	0.22	0.22	0.19	0.24	0.22	0.26	0.22	0.22	0.25	0.18	0.12	0.11	0.12	0.10	0.07	0.12	0.13	0.12
Al_2O_3	0.87	1.13	1.15	0.91	1.13	1.01	1.22	1.14	1.12	1.20	1.23	0.81	0.80	0.71	0.85	0.75	0.78	0.74	0.83
Cr_2O_3	0.61	0.52	0.47	0.40	0.51	0.36	0.60	0.57	0.42	0.54	0.42	0.61	0.71	0.59	0.90	0.98	0.92	0.65	0.78
FeO*	3.32	4.06	4.04	3.85	4.28	3.78	4.11	4.25	3.98	4.43	4.31	3.09	3.51	3.29	3.33	3.19	3.17	3.16	3.26
MnO	0.10	0.16	0.15	0.17	0.12	0.11	0.13	0.15	0.12	0.09	0.15	0.11	0.13	0.06	0.18	0.13	0.09	0.12	0.13
MgO	17.42	17.08	17.33	17.12	17.27	17.13	17.14	17.42	17.09	17.48	17.45	17.70	17.95	18.15	17.98	18.00	18.13	17.95	17.92
CaO	23.01	23.29	23.15	23.31	22.47	23.65	23.00	22.61	23.38	22.35	22.32	22.66	22.77	22.67	22.88	22.80	22.42	23.09	22.60
Na_2O	0.21	0.25	0.31	0.23	0.25	0.25	0.29	0.31	0.29	0.29	0.24	0.22	0.22	0.21	0.25	0.27	0.29	0.24	0.24
Total	99.59	100.53	100.79	99.70	99.61	100.08	100.07	100.20	100.52	100.24	99.59	99.15	100.95	100.37	100.73	100.44	100.08	100.46	100.09
Cations (p.f.u.)																			
Si	1.971	1.973	1.973	1.967	1.971	1.977	1.972	1.972	1.981	1.973	1.978	1.971	1.961	1.972	1.993	1.983	1.986	1.985	1.979
Ti	0.003	0.004	0.003	0.005	0.004	0.004	0.004	0.004	0.003	0.004	0.005	0.005	0.007	0.007	0.002	0.003	0.002	0.003	0.005
$Al^{(IV)}$	0.029	0.027	0.027	0.033	0.029	0.023	0.028	0.028	0.019	0.027	0.022	0.029	0.039	0.028	0.007	0.017	0.014	0.015	0.021
$Al^{(VI)}$	0.004	0.005	0.009	0.009	0.001	0.011	0.003	0.010	0.014	0.007	0.019	0.011	0.011	0.009	0.003	0.000	0.004	0.000	0.000
Cr	0.027	0.019	0.022	0.019	0.013	0.012	0.010	0.017	0.014	0.012	0.016	0.015	0.018	0.013	0.004	0.005	0.006	0.005	0.007
Fe^{3+}	0.002	0.005	0.000	0.003	0.014	0.000	0.014	0.003	0.000	0.009	0.000	0.002	0.006	0.000	0.000	0.010	0.006	0.008	0.009
Fe^{2+}	0.094	0.091	0.099	0.093	0.083	0.087	0.068	0.097	0.099	0.083	0.107	0.106	0.092	0.101	0.063	0.076	0.086	0.059	0.069
Mn	0.003	0.004	0.004	0.004	0.004	0.003	0.005	0.004	0.003	0.004	0.004	0.005	0.004	0.004	0.003	0.003	0.003	0.002	0.004
Mg	0.984	0.971	0.972	0.960	0.942	0.944	0.957	0.955	0.957	0.956	0.952	0.959	0.939	0.930	0.947	0.962	0.947	0.958	0.958
Ca	0.874	0.897	0.881	0.899	0.939	0.932	0.940	0.901	0.896	0.921	0.881	0.886	0.917	0.928	0.975	0.944	0.946	0.966	0.948
Na	0.010	0.008	0.008	0.008	0.007	0.007	0.007	0.011	0.010	0.009	0.010	0.010	0.009	0.008	0.002	0.004	0.005	0.004	0.005
Total	4.001	4.003	3.999	4.002	4.007	3.999	4.007	4.002	3.997	4.005	3.994	4.001	4.003	4.000	3.999	4.007	4.003	4.006	4.005
End Members (%)																			
Wo	46.2	46.6	46.3	46.9	45.4	47.4	46.4	45.5	46.8	44.9	45.1	45.6	45.1	44.9	45.5	45.4	44.8	45.8	45.1
En	48.6	47.6	48.2	47.9	48.5	47.8	48.1	48.8	47.6	48.8	49.0	49.6	49.5	50.0	49.8	49.9	50.4	49.6	49.8
Fs	5.2	5.8	5.5	5.2	6.1	4.8	5.5	5.7	5.7	6.3	5.9	4.8	5.4	5.1	4.7	4.7	4.8	4.6	5.1
Mg #	0.913	0.903	0.910	0.919	0.916	0.933	0.906	0.905	0.918	0.899	0.900	0.969	0.913	0.907	0.939	0.927	0.919	0.942	0.934

Crystal textural style is abbreviated: cumu. (cumulus), inter. (intercumulus)
Note: Other phases (ol, chr, mt) were also analyzed on certain sections, such that "Cluster" refers to a specific location on each thin section
* Total Fe

Appendix III (continued): Clinopyroxene compositions from clinopyroxene-bearing ultramafic lithologies of the Turnagain intrusion

Rock Type:	Hornblende Clinopyroxenite									Hornblende Clinopyroxenite								
Sample:	DDH04-47-7-49									04ES-09-02-02								
Cluster:	6	2			5			8			1		3			5		
Style:	inter.	cumu.	cumu.	cumu.	cumu.	cumu.	cumu.	cumu.	cumu.	cumu.	cumu.	cumu.	cumu.	cumu.	cumu.	cumu.	cumu.	cumu.
Zone:	core	rim	mid	core	rim	mid	core	rim	mid	core	rim	core	rim	mid	core	rim	mid	core
Oxides (wt. %)																		
SiO_2	54.36	49.13	49.95	50.21	49.54	49.73	49.90	49.43	50.05	52.28	53.20	52.98	53.33	52.74	53.79	53.20	53.14	53.88
TiO_2	0.19	0.72	0.62	0.62	0.65	0.53	0.62	0.63	0.59	0.22	0.14	0.22	0.17	0.17	0.04	0.28	0.23	0.12
Al_2O_3	0.98	5.27	4.18	4.19	4.79	4.52	4.48	4.92	4.12	2.12	0.59	1.10	0.68	0.90	0.30	1.22	1.09	0.36
Cr_2O_3	0.67	0.04	0.00	0.00	0.00	0.01	0.03	0.00	0.03	0.00	0.07	0.08	0.04	0.07	0.02	0.13	0.07	0.03
FeO*	3.18	7.85	6.77	6.88	7.73	7.41	7.06	7.26	6.94	6.01	6.30	6.50	6.42	6.90	6.54	6.01	6.16	4.95
MnO	0.13	0.13	0.13	0.22	0.16	0.20	0.15	0.15	0.12	0.15	0.22	0.24	0.22	0.22	0.24	0.21	0.21	0.15
MgO	17.80	13.16	14.17	14.27	13.43	13.41	13.92	13.60	14.09	14.51	15.68	15.56	15.67	15.55	15.32	16.07	16.12	16.03
CaO	23.19	23.55	23.31	23.46	23.37	23.19	23.09	23.34	23.00	25.25	23.26	22.60	23.05	22.30	24.16	22.64	22.36	24.22
Na_2O	0.24	0.26	0.25	0.25	0.24	0.28	0.28	0.27	0.25	0.06	0.10	0.13	0.13	0.13	0.06	0.18	0.12	0.05
Total	100.75	100.12	99.38	100.09	99.91	99.28	99.54	99.58	99.19	100.59	99.55	99.41	99.70	98.97	100.47	99.94	99.51	99.78
Cations (p.f.u.)																		
Si	1.985	1.909	1.921	1.892	1.918	1.897	1.913	1.898	1.904	1.838	1.871	1.869	1.854	1.870	1.867	1.853	1.877	1.930
Ti	0.003	0.012	0.010	0.012	0.010	0.011	0.010	0.012	0.012	0.020	0.017	0.017	0.018	0.015	0.018	0.018	0.017	0.006
$Al^{(IV)}$	0.015	0.091	0.079	0.108	0.082	0.103	0.087	0.102	0.096	0.162	0.129	0.131	0.146	0.130	0.133	0.147	0.123	0.070
$Al^{(VI)}$	0.000	0.043	0.043	0.061	0.047	0.055	0.043	0.037	0.046	0.071	0.055	0.052	0.066	0.070	0.065	0.070	0.059	0.023
Cr	0.004	0.000	0.000	0.001	0.000	0.000	0.000	0.001	0.000	0.001	0.000	0.000	0.000	0.000	0.001	0.000	0.001	0.000
Fe^{3+}	0.008	0.031	0.024	0.030	0.021	0.036	0.031	0.049	0.033	0.059	0.049	0.054	0.052	0.041	0.042	0.052	0.039	0.037
Fe^{2+}	0.063	0.168	0.192	0.206	0.211	0.198	0.175	0.162	0.171	0.187	0.164	0.161	0.190	0.192	0.179	0.175	0.179	0.149
Mn	0.003	0.002	0.006	0.004	0.006	0.005	0.004	0.005	0.005	0.004	0.004	0.007	0.005	0.006	0.005	0.005	0.004	0.005
Mg	0.952	0.826	0.807	0.766	0.775	0.772	0.813	0.825	0.814	0.734	0.791	0.792	0.750	0.752	0.776	0.760	0.788	0.798
Ca	0.966	0.927	0.921	0.925	0.932	0.931	0.933	0.926	0.929	0.944	0.935	0.935	0.937	0.934	0.926	0.937	0.924	0.999
Na	0.004	0.007	0.009	0.009	0.007	0.010	0.007	0.008	0.007	0.009	0.009	0.009	0.009	0.010	0.010	0.010	0.009	0.002
Total	4.004	4.015	4.012	4.015	4.011	4.018	4.015	4.025	4.017	4.030	4.024	4.027	4.026	4.020	4.021	4.026	4.019	4.018
End Members (%)																		
Wo	46.0	50.6	49.5	49.6	49.9	49.7	49.2	50.1	48.9	51.3	46.9	45.9	46.5	45.4	48.1	45.8	45.2	48.2
En	49.2	39.4	41.9	41.9	39.9	40.0	41.3	40.6	41.7	41.0	44.0	44.0	43.9	44.1	42.4	45.2	45.3	44.4
Fs	4.8	10.0	8.7	8.5	10.1	10.2	9.5	9.4	9.5	7.6	9.1	10.1	9.6	10.5	9.4	9.0	9.4	7.4
Mg #	0.939	0.814	0.805	0.794	0.780	0.791	0.816	0.824	0.821	0.810	0.842	0.820	0.818	0.829	0.828	0.832	0.857	0.830

Crystal textural style is abbreviated: cumu. (cumulus), inter. (intercumulus)
Note: Other phases (ol, chr, mt) were also analyzed on certain sections, such that "Cluster" refers to a specific location on each thin section
* Total Fe

Appendix III (continued): Clinopyroxene compositions from clinopyroxene-bearing ultramafic lithologies of the Turnagain intrusion

Rock Type:	Hornblende Clinopyroxenite							
Sample:	DDH05-84-19-104							
Cluster:	2		5			10		
Style:	cumu.	cumu.	cumu.	cumu.	cumu.	cumu.	cumu.	cumu.
Zone:	mid	core	rim	mid	core	rim	mid	core
Oxides (wt. %)								
SiO_2	51.23	51.40	50.74	51.37	50.77	51.77	51.26	51.25
TiO_2	0.43	0.35	0.44	0.35	0.40	0.36	0.42	0.42
Al_2O_3	3.07	2.77	3.83	2.94	3.60	2.98	3.17	3.24
Cr_2O_3	0.00	0.00	0.03	0.01	0.00	0.00	0.03	0.00
FeO*	6.38	6.92	7.56	7.45	7.48	6.64	6.84	6.59
MnO	0.06	0.20	0.13	0.18	0.16	0.14	0.15	0.14
MgO	14.87	14.47	13.78	13.93	13.87	14.76	14.94	14.70
CaO	23.22	22.99	23.15	23.31	23.26	23.55	23.35	23.34
Na_2O	0.19	0.24	0.26	0.19	0.27	0.20	0.23	0.19
Total	99.45	99.34	99.92	99.73	99.79	100.39	100.39	99.86
Cations (p.f.u.)								
Si	1.976	1.969	1.977	1.972	1.985	1.962	1.968	1.986
Ti	0.004	0.006	0.005	0.005	0.001	0.008	0.007	0.003
$Al^{(IV)}$	0.024	0.031	0.023	0.028	0.015	0.038	0.032	0.014
$Al^{(VI)}$	0.002	0.017	0.007	0.011	0.000	0.016	0.016	0.002
Cr	0.002	0.002	0.001	0.002	0.001	0.004	0.002	0.001
Fe^{3+}	0.016	0.004	0.010	0.010	0.015	0.009	0.005	0.006
Fe^{2+}	0.180	0.198	0.189	0.206	0.187	0.176	0.185	0.147
Mn	0.007	0.008	0.007	0.007	0.008	0.007	0.007	0.005
Mg	0.868	0.862	0.866	0.867	0.843	0.884	0.890	0.881
Ca	0.926	0.900	0.916	0.893	0.955	0.895	0.887	0.957
Na	0.004	0.005	0.005	0.005	0.002	0.007	0.004	0.002
Total	4.008	4.002	4.005	4.005	4.011	4.005	4.003	4.003
End Members (%)								
Wo	48.3	48.0	48.8	48.6	49.0	48.6	48.4	48.5
En	43.0	42.0	40.4	40.4	40.6	42.3	43.1	42.5
Fs	8.7	10.0	10.8	11.0	10.4	9.1	8.5	9.0
Mg #	0.824	0.803	0.802	0.790	0.805	0.822	0.817	0.847

Crystal textural style is abbreviated: cumu. (cumulus), inter. (intercumulus)
Note: Other phases (ol, chr, mt) were also analyzed on certain sections, such that "Cluster" refers to a specific location on each thin section
* Total Fe

Appendix IV: Garnet compositions from a serpentinite vein in dunite from the Turnagain intrusion

Rock Type:	Serpentinite							
Sample:	04ES-02-01-01							
Cluster:	3			2		1		
Description:	porph.	porph.	porph.	porph.	porph.	porph.	porph.	porph.
Location	rim	mid	core	rim	core	rim	mid	core
Oxides (wt. %)								
SiO_2	35.15	35.07	35.09	35.07	34.98	35.11	35.18	34.86
TiO_2	0.05	0.23	0.44	0.07	0.44	0.03	0.32	0.58
Al_2O_3	0.00	0.03	0.03	0.01	0.01	0.03	0.01	0.03
Cr_2O_3	4.43	7.66	8.31	3.50	8.21	0.92	8.02	9.17
Fe_2O_3	26.32	22.37	21.52	26.34	21.84	29.35	22.04	20.72
MgO	0.16	0.20	0.24	0.12	0.27	0.08	0.17	0.24
MnO	0.00	0.00	0.00	0.00	0.00	0.01	0.00	0.00
CaO	33.33	33.49	33.51	33.75	33.48	33.53	33.68	33.61
Na_2O	0.02	0.01	0.01	0.15	0.05	0.02	0.03	0.02
Total	99.47	99.06	99.15	99.03	99.29	99.09	99.46	99.22
Cations (p.f.u.)								
Si	2.985	2.984	2.980	2.992	2.970	2.996	2.981	2.961
Ti	0.003	0.015	0.028	0.004	0.028	0.002	0.020	0.037
Al	0.000	0.003	0.003	0.001	0.001	0.003	0.001	0.003
Cr	0.298	0.515	0.558	0.236	0.551	0.062	0.538	0.616
Fe^{3+}	1.682	1.432	1.375	1.691	1.395	1.885	1.405	1.324
Mg	0.021	0.025	0.030	0.016	0.034	0.010	0.022	0.030
Mn	0.000	0.000	0.000	0.000	0.000	0.001	0.000	0.000
Ca	3.032	3.052	3.049	3.085	3.045	3.066	3.057	3.058
Na	0.003	0.002	0.002	0.025	0.008	0.004	0.005	0.003
Sum	8.024	8.028	8.025	8.052	8.032	8.029	8.029	8.032
End Members								
Andradite	0.850	0.735	0.711	0.877	0.717	0.968	0.723	0.683
Uvarovite	0.150	0.265	0.289	0.123	0.283	0.032	0.277	0.317

Crystal textural style is abbreviated: porph. (porphyroblastic)
"Cluster" refers to a specific location on thin section
Andradite: $Ca_3Fe^{3+}{}_2Si_3O_{12}$
Uvarovite: $Ca_3Cr_2Si_3O_{12}$

APPENDIX V: List of X-ray lines and mineral standards for EPMA

Electron-probe micro-analyses of garnet were done on a fully automated CAMECA SX-50 instrument, operating in the wavelength-dispersion mode with the following operating conditions: excitation voltage, 15 kV; beam current, 20 nA; peak count time, 20 s; background count-time, 10 s; spot diameter, 10 μm. Data reduction was done using the 'PAP' $\phi(\rho Z)$ method (Pouchou & Pichoir 1985). For the elements considered, the following standards, X-ray lines and crystals were used: albite, Na$K\alpha$, TAP; almandine, Mg$K\alpha$, TAP; almandine, Al$K\alpha$, TAP; diopside, Si$K\alpha$, TAP; rutile, Ti$K\alpha$, PET; grossular, Ca$K\alpha$, PET; magnesiochromite, Cr$K\alpha$, LIF; synthetic rhodonite, Mn$K\alpha$, LIF; almandine, Fe$K\alpha$, LIF.

Biotite: excitation voltage, 15 kV; beam current, 10 nA; peak count time, 20 s (40 s for F, Cl); background count-time, 10 s (20 s for F, Cl); spot diameter, 10 μm. Data reduction was done using the 'PAP' $\phi(\rho Z)$ method (Pouchou & Pichoir 1985). For the elements considered, the following standards, X-ray lines and crystals were used: synthetic phlogopite, F$K\alpha$, TAP; albite, Na$K\alpha$, TAP; anorthite, Al$K\alpha$, TAP; synthetic phlogopite, Mg$K\alpha$, TAP; synthetic phlogopite, Si$K\alpha$, TAP; scapolite, Cl$K\alpha$, PET; synthetic phlogopite, K$K\alpha$, PET; diopside, Ca$K\alpha$, PET; rutile, Ti$K\alpha$, PET; synthetic magnesiochromite, Cr$K\alpha$, LIF; synthetic rhodonite, Mn$K\alpha$, LIF; synthetic fayalite, Fe$K\alpha$, LIF; barite, Ba$L\alpha$, PET.

Olivine: excitation voltage, 15 kV; beam current, 20 nA; peak count time, 20 s; background count-time, 10 s; spot diameter, 5 μm. Data reduction was done using the 'PAP' $\phi(\rho Z)$ method (Pouchou & Pichoir 1985). For the elements considered, the following standards, X-ray lines and crystals were used: albite, Na$K\alpha$, TAP; kaersutite, Al$K\alpha$, TAP; olivine, Mg$K\alpha$, TAP; olivine, Si$K\alpha$, TAP; orthoclase, K$K\alpha$, PET; diopside, Ca$K\alpha$, PET; rutile, Ti$K\alpha$, PET; synthetic magnesiochromite, Cr$K\alpha$, LIF; synthetic rhodonite, Mn$K\alpha$, LIF; synthetic fayalite, Fe$K\alpha$, LIF; synthetic Ni_2SiO_4, Ni$K\alpha$, LIF.

APPENDIX V (continued): List of X-ray lines and mineral standards for EPMA

Clinopyroxene: excitation voltage, 15 kV; beam current, 20 nA; peak count time, 20 s; background count-time, 10 s; spot diameter, 5 μm. Data reduction was done using the 'PAP' $\phi(\rho Z)$ method (Pouchou & Pichoir 1985). For the elements considered, the following standards, X-ray lines and crystals were used: albite, Na$K\alpha$, TAP; kaersutite, Al$K\alpha$, TAP; diopside, Mg$K\alpha$, TAP; diopside, Si$K\alpha$, TAP; diopside, Ca$K\alpha$, PET; rutile, Ti$K\alpha$, PET; synthetic magnesiochromite, Cr$K\alpha$, LIF; synthetic rhodonite, Mn$K\alpha$, LIF; synthetic fayalite, Fe$K\alpha$, LIF; synthetic Ni_2SiO_4, Ni$K\alpha$, LIF.

Amphibole: excitation voltage, 15 kV; beam current, 20 nA; peak count time, 20 s (40 s for F, Cl); background count-time, 10 s (20 s for F, Cl); spot diameter, 5 μm. Data reduction was done using the 'PAP' $\phi(\rho Z)$ method (Pouchou & Pichoir 1985). For the elements considered, the following standards, X-ray lines and crystals were used: synthetic phlogopite, F$K\alpha$, TAP; albite, Na$K\alpha$, TAP; kyanite, Al$K\alpha$, TAP; diopside, Mg$K\alpha$, TAP; diopside, Si$K\alpha$, TAP; scapolite, Cl$K\alpha$, PET; orthoclase, K$K\alpha$, PET; diopside, Ca$K\alpha$, PET; rutile, Ti$K\alpha$, PET; synthetic magnesiochromite, Cr$K\alpha$, LIF; synthetic rhodonite, Mn$K\alpha$, LIF; synthetic fayalite, Fe$K\alpha$, LIF; synthetic Ni_2SiO_4, Ni$K\alpha$, LIF.

Appendix VI: Original and duplicate whole-rock analyses

Prefix	04ES	05ES				05ES	04ES			
Sample	06-01-01	05-07-01				05-06-01	00-07-01			
	Dunite	Dunite	Ave	2σ	%RSD	Wehrlite	Wehrlite	Ave	2σ	%RSD
Oxide (wt. %)										
SiO2	38.21	37.95	38.08	0.37	0.5	38.95	39.12	39.04	0.24	0.3
TiO2	0.005	0.005	0.01	0.00	0.0	0.086	0.09	0.09	0.01	3.2
Al2O3	0.04	0.05	0.05	0.01	15.7	0.37	0.37	0.37	0.00	0.0
Fe2O3(T)	8.04	10.47	9.26	3.44	18.6	11.43	12.8	12.12	1.94	8.0
MgO	48.74	47.25	48.00	2.11	2.2	43.02	43.17	43.10	0.21	0.2
MnO	0.142	0.145	0.14	0.00	1.5	0.196	0.199	0.20	0.00	1.1
CaO	0.09	0.1	0.10	0.01	7.4	2.91	2.97	2.94	0.08	1.4
Na2O	< 0.01	0.02				0.04	0.05	0.05	0.01	15.7
K2O	< 0.01	0.06				0.11	0.05	0.08	0.08	53.0
P2O5	< 0.01	< 0.01				< 0.01	< 0.01			
LOI	3.55	3.89	3.72	0.48	6.5	1.84	< 0.0100			
Total	98.78	99.94	99.36	1.64	0.8	98.96	99.85	99.41	1.26	0.6
Element (ppm)										
Au	< 1	< 1				6	11	8.5	7.1	41.6
Ag	< 0.5	< 0.5				< 0.5	< 0.5			
As	< 1	< 1				< 1	< 1			
Ba	< 1	< 1				< 1	< 1			
Be	< 1	< 1				< 1	< 1			
Bi	< 0.1	< 0.1				< 0.1	< 0.1			
Br	< 0.5	< 0.5				< 0.5	< 0.5			
Cd	2.6	2.4	2.5	0.3	5.7	2.4	2.4	2.4	0	0
Co	160	160	160	0	0	166	159	163	10	3.0
Cr	2790	2910	2850	170	3.0	3860	3620	3740	339	4.5
Cs	< 0.1	< 0.1				< 0.1	< 0.1			
Cu	17	19	18	2.8	7.9	71	73	72	2.8	2.0
Ga	< 1	< 1				2	1	2	1.4	47.1
Ge	2.5	2	2.3	0.7	15.7	1	1.7	1.4	1.0	36.7
Hf	< 0.1	< 0.1				< 0.1	< 0.1			
Hg	< 1	< 1				< 1	< 1			
In	< 0.1	< 0.1				< 0.1	< 0.1			
Ir	< 1	< 1				< 1	< 1			
Mo	< 2	< 2				< 2	< 2			
Nb	< 0.2	< 0.2				0.2	< 0.2			
Ni	2180	2190	2185	14	0.3	1060	1100	1080	57	2.6
Pb	< 5	< 5				< 5	< 5			
Rb	< 2	< 2				< 2	< 2			
S (wt. %)	0.068	0.066	0	0.003	2.1	0.024	0.026	0.025	0.003	5.7
Sb	< 0.1	< 0.1				0.2	0.2	0.2	0	0
Sc	3.22	3.25	3.24	0.04	0.7	15.2	14.7	15.0	0.7	2.4
Se	< 0.5	< 0.5				< 0.5	< 0.5			
Sn	< 1	1				< 1	2			
Sr	< 2	< 2				7	6	7	1	10.9
Ta	< 0.1	< 0.1				< 0.1	< 0.1			
Th	< 0.05	< 0.05				< 0.05	< 0.05			
U	< 0.05	0.08				< 0.05	< 0.05			
V	< 5	< 5				28	35	32	10	15.7
W	2	2	2	0	0	2	< 1			
Y	< 1	1				1	< 1			
Zn	46	46	46	0	0	56	57	57	1.4	1.3
Zr	< 1	1				< 1	< 1			
La	< 0.05	< 0.05				< 0.05	< 0.05			
Ce	< 0.1	< 0.1				0.1	< 0.1			
Pr	< 0.02	< 0.02				0.02	0.03	0.03	0.01	28.3
Nd	< 0.05	< 0.05				0.2	0.23	0.22	0.04	9.9
Sm	< 0.01	< 0.01				0.09	0.11	0.10	0.03	14.1
Eu	< 0.005	< 0.005				0.038	0.039	0.039	0.001	1.8
Gd	< 0.02	< 0.02				0.13	0.13	0.13	0	0
Tb	< 0.01	< 0.01				0.02	0.02	0.02	0	0
Dy	< 0.02	< 0.02				0.16	0.16	0.16	0	0
Ho	< 0.01	< 0.01				0.03	0.03	0.03	0	0
Er	< 0.01	< 0.01				0.09	0.1	0.10	0.01	7.4
Tl	< 0.05	< 0.05				< 0.05	< 0.05			
Tm	< 0.005	< 0.005				0.013	0.014	0.01	0.001	5.2
Yb	< 0.01	< 0.01				0.08	0.09	0.09	0.01	8.3
Lu	< 0.002	< 0.002				0.015	0.014	0.015	0.001	4.9

Appendix VI (continuted): Original and duplicate whole-rock analyses

Prefix	04ES	05ES				04ES	04ES			
Sample	00-07-04	03-02-01				00-07-01	00-07-01			
	Hblite	Hblite	Ave	2σ	%RSD	Dunite	Dunite	Ave	2σ	%RSD
Oxide (wt. %)										
SiO2	41.95	41.9	41.93	0.07	0.1	39.06	39.18	39.12	0.17	0.2
TiO2	2.154	2.171	2.16	0.02	0.6	0.09	0.09	0.09	0.00	0.0
Al2O3	12.24	12.17	12.21	0.10	0.4	0.36	0.37	0.37	0.01	1.9
Fe2O3(T)	14.23	14.37	14.30	0.20	0.7	11.79	13.8	12.80	2.84	11.1
MgO	11.93	11.97	11.95	0.06	0.2	43.27	43.06	43.17	0.30	0.3
MnO	0.263	0.265	0.264	0.003	0.5	0.199	0.198	0.20	0.00	0.4
CaO	11.52	11.71	11.62	0.27	1.2	2.98	2.96	2.97	0.03	0.5
Na2O	0.77	0.79	0.78	0.03	1.8	0.05	0.05	0.05	0.00	0.0
K2O	0.92	0.86	0.89	0.08	4.8	0.05	0.04	0.05	0.01	15.7
P2O5	0.31	0.3	0.31	0.01	2.3	< 0.01	0.02			
LOI	2.83	2.77	2.80	0.08	1.5	2.09	< 0.01			
Total	99.12	99.28	99.20	0.23	0.1	99.94	99.76	99.85	0.25	0.1
Element (ppm)										
Au	< 1	4								
Ag	< 0.5	< 0.5				< 1	< 1			
As	< 1	< 1				< 1	< 1			
Ba	421	423	422	2.8	0.3	< 0.1	< 0.1			
Be	1	2	1.5	1.4	47.1					
Bi	< 0.1	< 0.1								
Br	< 0.5	< 0.5								
Cd	1.5	1.5	1.5	0	0					
Co	65.7	66.8	66.3	1.6	1.2	< 0.1	< 0.1			
Cr	398	409	404	16	1.9					
Cs	0.6	0.5	0.6	0.1	12.9	1	2	1.5	1.4	47.1
Cu	84	84	84	0	0	1.4	1.9	1.7	0.7	21.4
Ga	20	19	20	1.4	3.6	< 0.1	< 0.1			
Ge	< 0.5	< 0.5								
Hf	2.1	2.1	2.1	0	0	< 0.1	< 0.1			
Hg	< 1	< 1								
In	< 0.1	< 0.1								
Ir	< 1	11				< 0.2	< 0.2			
Mo	< 2	< 2								
Nb	3.6	4.1	3.9	0.7	9.2					
Ni	135	136	136	1	0.5	< 2	< 2			
Pb	35	36	36	1.4	2.0					
Rb	12	12	12	0	0					
S (wt. %)	0.354	0.344	0.349	0.014	2.0					
Sb	0.6	0.6	0.6	0	0					
Sc	72.7	74.6	73.7	2.7	1.8	1	3	2	3	70.7
Se	< 0.5	<0.5				6	6	6	0	0
Sn	6	3	5	4.2	47.1	< 0.1	< 0.1			
Sr	283	284	284	1	0.2	< 0.05	< 0.05			
Ta	0.2	0.2	0.2	0	0	< 0.05	< 0.05			
Th	0.36	0.36	0.36	0	0	37	33	35	6	8.1
U	0.12	0.11	0.12	0.01	6.1					
V	489	495	492	8	0.9	< 1	2			
W	< 1	<1								
Y	39	44	41.5	7.1	8.5	< 1	< 1			
Zn	99	99	99	0	0	< 0.05	< 0.05			
Zr	49	49	49	0	0	< 0.1	0.1			
La	6.61	6.6	6.61	0.01	0.1	0.03	0.03	0.03	0	0
Ce	20.3	20.7	20.5	0.6	1.4	0.23	0.23	0.23	0	0
Pr	3.34	3.36	3.35	0.03	0.4	0.1	0.11	0.11	0.01	6.7
Nd	18.1	18.4	18.3	0.4	1.2	0.041	0.037	0.039	0.006	7.3
Sm	5.97	5.93	5.95	0.06	0.5	0.13	0.13	0.13	0	0
Eu	1.83	1.86	1.85	0.04	1.1	0.02	0.02	0.02	0	0
Gd	7.11	7.25	7.18	0.20	1.4	0.16	0.16	0.16	0	0
Tb	1.31	1.35	1.33	0.06	2.1	0.03	0.03	0.03	0	0
Dy	7.9	7.91	7.91	0.01	0.1	0.1	0.1	0.1	0	0
Ho	1.61	1.63	1.62	0.03	0.9	< 0.05	< 0.05			
Er	4.52	4.55	4.54	0.04	0.5	0.014	0.014	0.01	0	0
Tl	0.1	0.12	0.11	0.03	12.9	0.09	0.09	0.09	0	0
Tm	0.646	0.651	0.649	0.007	0.5	0.013	0.014	0.014	0.001	5.2
Yb	3.84	3.79	3.82	0.07	0.9					
Lu	0.521	0.539	0.530	0.025	2.4					

Appendix VII: Sample Locations

Sample #	Rock Type	*Easting	*Northing	Applicable Table(s)
04ES-00-07-01	Meladiorite	506580	6483611	2.1
04ES-00-07-02	Volc. Wacke	505775	6484455	2.1, 2.4, 4.5
04ES-00-07-03	Wehrlite	509551	6480391	2.2
04ES-00-07-04	Hornblendite	505750	6484462	2.1, 2.2, 2.4, 4.3, 4.5, 4.6
04ES-01-04-01	Ol Cpxite	509390	6481403	3.1, 4.1, 4.2
04ES-02-01-01	Serpentinite	507824	6483614	Appendix IV
04ES-03-01-02	Dunite	508158	6481584	4.5, 4.6
04ES-03-02-01	Dunite	508380	6481497	3.1, 4.1, 4.5, 4.6
04ES-03-04-01	Wehrlite	509052	6481073	4.5, 4.6
04ES-06-01-01	Dunite	507915	6481777	4.1, 4.5
04ES-06-06-01	Ol Cpxite	507735	6481705	3.1, 4.1, 4.2
04ES-07-02-01	Dunite	508610	6481485	4.5, 4.6
04ES-07-02-04	Wehrlite	508559	6481379	4.5, 4.6
04ES-08-01-01	Dunite	508347	6481480	3.1, 4.1, 4.2
04ES-09-01-01	Wehrlite	506444	6484127	4.1, 4.2
04ES-09-02-02	Hbl cpxite	506176	6484247	2.4, 4.2, 4.3, 4.5, 4.6
04ES-10-02-04	Ol Cpxite	506968	6483944	4.5, 4.6
04ES-10-05-01	Dunite	507506	6484333	3.1, 4.1
04ES-10-06-01	Wehrlite	507216	6484294	3.1, 4.1, 4.2
04ES-11-03-03	Wehrlite	506702	6484508	3.1, 4.1, 4.2
04ES-13-01-02	Felsic tuff	513123	6479467	4.7, 4.8
04ES-15-01-05	Wehrlite	511172	6481538	3.1, 4.1, 4.2
04ES-16-08-01	Wehrlite	511636	6481374	3.1, 4.1, 4.2
04ES-19-01-02	Dunite	507690	6481699	3.1, 4.1
05ES-01-01-01	Chromitite	506969	6483816	3.1, 4.1
05ES-01-03-01	Chromitite	507319	6484023	3.1, 4.1
05ES-01-04-01	Chromitite	507440	6484076	3.1, 4.1
05ES-02-01-01	Wehrlite	509393	6481401	4.7
05ES-02-02-02	Dunite	510055	6481749	4.7, 4.8
05ES-02-02-02A	Dunite	510055	6481749	4.7, 4.8
05ES-02-04-01	Dunite	507674	6481706	4.7
05ES-03-01-01	Wehrlite	509551	6480391	4.4, 4.5, 4.6, 4.7
05ES-03-01-02	Ol Cpxite	509542	6480403	2.4, 4.5, 4.6
05ES-04-05-01	Dunite	508875	6480479	4.5, 4.6
05ES-04-06-01	Dunite	510359	6471772	4.5, 4.6
05ES-05-01-01	Ol Cpxite	506839	6483982	2.4, 3.1, 4.1, 4.2, 4.5, 4.6
05ES-05-01-02	Wehrlite	506866	6484017	4.5, 4.6
05ES-05-02-01	Wehrlite	506872	6484246	4.5, 4.6
05ES-05-03-01	Wehrlite	506777	6484487	4.5, 4.6
05ES-05-04-01	Ol Cpxite	506983	6484615	2.4, 4.5, 4.6
05ES-05-05-01	Wehrlite	506153	6484577	4.5, 4.6
05ES-05-06-01	Wehrlite	505878	6484575	4.5, 4.6
05ES-05-06-02	Hornblendite	505917	6484437	2.4, 4.3, 4.5, 4.6

* All UTM coordinates are projected in NAD83, Zone 9

Appendix VII (continued): Sample Locations

Sample #	Rock Type	*Easting	*Northing	Applicable Table(s)
DDH03-03-59-426	Hornblendite	507602	6481902	4.7, 4.8
DDH03-05-8-89	Ol Cpxite	508655	6481467	4.7, 4.8
DDH03-05-45-325	Wehrlite	508655	6481467	4.7, 4.8
DDH03-06-25-181	Wehrlite	508564	6481207	4.7, 4.8
DDH03-07-25-183	Wehrlite	508583	6480856	4.7, 4.8
DDH03-07-54-389	Phyllite	508583	6480856	4.7, 4.8
DDH03-08-13-100	Wehrlite	509447	6481504	4.7, 4.8
DDH03-09-18-134	Ol Cpxite	509447	6481505	4.7
DDH03-12-4-32	Dunite	508730	6481199	4.7
DDH03-16-24-166	Dunite	508691	6481141	4.7, 4.8
DDH03-18-13-85	Dunite	508891	6481302	4.7
DDH04-23-11-76	Wehrlite	508745	6481184	4.7
DDH04-24-31-220	Dunite	508789	6481216	4.7
DDH04-28-6-45	Wehrlite	508729	6481198	4.7, 4.8
DDH04-29-9-64	Dunite	508826	6481132	4.7
DDH04-33-5-38	Wehrlite	508949	6481141	4.7
DDH04-35-5-40	Wehrlite	508790	6481281	4.7
DDH04-36-5-40	Wehrlite	508723	6481260	4.7
DDH04-36-16-108	Dunite	508723	6481260	4.7
DDH04-37-6-40	Dunite	508723	6481260	4.7, 4.8
DDH04-47-7-49	Hbl cpxite	506268	6482843	3.1, 4.2, 4.3
DDH04-47-17-126	Hbl cpxite	506268	6482843	4.7, 4.8
DDH04-57-12-89	Leucodiorite	506263	6482933	2.1, 2.4, 4.5
DDH05-84-19-104	Hbl cpxite	505996	6482358	3.1, 4.2, 4.3, 4.4

* All UTM coordinates are projected in NAD83, Zone 9